USES OF NEAR-INFRARED LIGHT FOR REAL-TIME IMAGE GUIDED SURGERY

Mr Thomas G Barnes MBChB (Hons), MRCS, PGCertMedEd

St Catherine's College

A thesis submitted to the Division of Medical Sciences at the University of Oxford for the Degree of Doctor of Philosophy

Hilary Term 2019

Nuffield Department of Surgical Sciences

For Rebecca and Dylan

ABSTRACT

Fluorescence is a technology where a fluorophore is excited by light at a specific wavelength and light is emitted at a longer wavelength and can be detected. This has been applied for imaging in surgery because in the near infra-red spectrum, light can penetrate through overlying tissue and provide information to the surgeon about underlying structures. Two important applications of fluorescence include identification of critical anatomical structures to prevent injury and guide dissection, and identification of tumours to aid diagnostics. During colorectal surgery, it is essential for surgeons to be aware of the location of the structures in the urinary tract. The ureter is an essential landmark of the correct dissection plane as well as its injury being a devastating complication. To date, fluorescence identification of the ureter has only been described in technical papers. This thesis explores ureteric fluorescence further with a large cohort of patients using methylene blue and a first in man study assessing IRDye 800BK (Chapter 3). Urethral identification with NIR light is also explored from proof of principle to *in-vivo* assessment using methylene blue, ICG and a NIR light emitting device (Chapter 4). During oesophagectomy, the thoracic duct can be injured complicating the post-operative course with chylothorax. Fluorescence of the duct for prevention and identification of intraoperative injuries is, for the first time, described (Chapter 5). Finally, WFA as a target for sugars in the mucus is explored to highlight cancer and dysplasia during colonoscopy and TEMS. Autofluorescence in the colon provides difficulties in fluorescent imaging and is explored as well as the struggles with utilising mucus as a target with WFA. However, an additional potential marker, GPA33, could provide a future for *in-vivo* colonic imaging.

ACKNOWLEDGEMENTS

Completing this thesis would not have been possible without the mentorship and supervision I received from Professor Sir Walter Bodmer and Professor Chris Cunningham. Both have been extremely supportive throughout my time in research, especially during some testing periods where, without their support, I would not have been able to complete this work. Professor Jon Austyn, Director of Graduate Studies has also been extremely helpful and diplomatic throughout my studies DPhil. I am also grateful to Professor Mortensen who has provided guidance and support throughout.

Members of the Bodmer laboratory have provided both scientific and pastoral support throughout my time in their laboratory: Djamila Ouaret, Kamilla Kaprowska, Mustak Ayub, Peter Kalugin, Hani Musa, Jens Puschhof, Haoyu Liu, Laura Colling and Jeff Liu.

The department of Colorectal Surgery at Oxford University Hospitals have been extremely helpful in allowing me to conduct my clinical trials in their department. Oliver Jones, Ian Lindsey, Stephen Boyce, Richard Guy, Bruce George, Richard Gillies, Nick Maynard, Bruno Sgromo and Mark Bignell all allowed me to recruit their patients and take time during their cases to conduct research. Roel Hompes in particular was extremely supportive during his time in Oxford. In addition to the surgeons, without the help of the nursing staff and sterile services department, it would have been impossible to use numerous pieces of equipment in the operating theatres for research purposes, in particular: Mina Somero, Caroline Baker and Jo Nawrocka.

Finally, conducting this DPhil would have been impossible without support from my family, friends and loving partner, Rebecca.

DECLARATION

I, Thomas George Barnes declare that the work on which this thesis is based is my original work and that neither the whole work nor any part of it has been, is being or is to be submitted for another degree in this or any other University. The work is original except where indicated by reference in the text.

Signed: Date:

TABLE OF CONTENTS

List of Tables xiv

List of Figures xvi

List of Abbreviations xx

CHAPTER 1: Introduction 1

CHAPTER 2: Materials & Methods 24

CHAPTER 3: Identification of the ureter during colorectal surgery using fluorescence 30

CHAPTER 4: Near-infrared Light to Highlight the Location of The Urethra During Low Rectal Cancer Surgery 87

CHAPTER 5: Fluorescence identification of the Thoracic Duct during oesophagectomy 112

CHAPTER 6: Molecular Targets to Detect Colonic Dysplasia during Endoscopy and Surgery 137

CHAPTER 7: Discussion and Future Directions 192

References 200

Appendix 1: Adverse events for IRDye 800BK 224

CHAPTER 1: INTRODUCTION 1

1.1. Image guided surgery, augmented reality and virtual reality 2

1.2. Principles of fluorescence 2

1.3. Fluorophores 7

1.3.1. Indocyanine Green 8

1.3.2. Methylene Blue 8

1.3.3. 5-aminolevulinic acid 9

1.3.4. Fluorescein 10

1.3.5. Carbon nanotubes 10

1.3.6. New fluorophores 12

1.3.6.1. Cyanine fluorophores 12

1.4. In-vivo fluorescence enabled devices 12

1.5. Current applications of NIR guided gastrointestinal surgery 13

1.5.1. Anastomosis perfusion during gastrointestinal resections 14

1.5.2. Identifying critical anatomy 15

1.5.2.1. Biliary tree fluorescence 16

1.5.2.2. Critical vessel identification 17

1.5.2.3. Lymphatic mapping 17

1.5.3. Fluorescence mapping of disease using targeted fluorophores 20

CHAPTER 2: MATERIALS & METHODS 24

2.1. Methodology 25

2.2. Capture and quantification of fluorescence 25
2.3. Trial set up 26
2.3.1. Patient recruitment 27
2.4. Statistics 28
CHAPTER 3: IDENTIFICATION OF THE URETER DURING COLORECTAL SURGERY USING FLUORESCENCE 30
3.1. Introduction 31
3.1.1. Anatomy of the ureter 31
3.1.2. Iatrogenic ureteric injury 31
3.1.3. Ureteric stents to protect the ureter 32
3.1.4. Ureteric Fluorescence 34
3.1.5. Aims 35
3.2. Methods 36
3.2.1. Methylene blue clinical trial 36
3.2.1.1. Objectives 36
3.2.1.2. Patients 36
3.2.1.3. Intraoperative methods 37
3.2.1.4. Statistical analysis 38
3.2.2. IRDye 800BK Ureteric Fluorescence Trial 39
3.2.2.1. Objectives 39
3.2.2.2. Patients 41
3.2.3. Assessment of fluorescence with different devices 45
3.3. Results 45

3.3.1. Recruitment....45

1.1.1. Baseline demographics....47

1.1.1. Subjective assessment of ureteric fluorescence with methylene blue..50

3.3.2. Objective assessment of ureteric fluorescence with methylene blue....53

3.4. Ureteric fluorescence with IRDye 800BK....59

3.4.1. Cross-talk between IRDye 800BK and methylene blue....59

3.4.2. Recruitment....62

3.4.3. Baseline demographics....64

3.4.4. Dose optimisation stage....66

3.4.4.1. Optimal dose decision efficacy....67

3.4.4.2. Optimal dose decision - safety....71

3.4.5. Dose Expansion Phase....72

3.4.5.1. Objective measurement of fluorescence – IRDye 800BK....75

3.4.5.2. Safety of IRDye 800BK....76

3.5. Device comparison....78

3.5.1. Comparison of methylene blue versus IRDye 800BK for ureteric fluorescence....79

3.6. Discussion and future directions....83

CHAPTER 4: NEAR-INFRARED LIGHT TO HIGHLIGHT THE LOCATION OF THE URETHRA DURING LOW RECTAL CANCER SURGERY....87

4.1. Introduction....88

4.1.1. Anatomy and clinical significance of the urethra during colorectal surgery 88

4.1.1. Urethral identification during low rectal cancer surgery 92
4.1.2. Aims and objectives 93
4.2. Methods 93
4.2.1. Ex-vivo work 93
4.2.2. ICG Urethra Clinical Trial 95
4.2.3. Clinical trial of NIRCaD 96
4.3. Results 96
4.3.1. Pre-clinical optimisation of urethral fluorescence using direct infiltration 96
4.3.1.1. Methylene blue vs ICG 96
4.3.2. Optimal dose for ICG-Instillagel fluorescence per urethra in human cadavers 99
4.3.3. In-vivo assessment of ICG-Instillagel to identify the urethra.....102
4.3.4. Other methods for urethral fluorescence.....102
4.3.5. NIR light fibre to detect the urethra.....103
4.3.5.1. Cadaveric assessment of NIR light fibre 105
4.3.5.1. NIRCaD Clinical Trial 106
4.4. Discussion and further work 109
CHAPTER 5: FLUORESCENCE IDENTIFICATION OF THE THORACIC DUCT DURING OESOPHAGECTOMY 112
5.1. Introduction.....113
5.1.1. Anatomy.....113
5.1.2. Thoracic duct significance during oesophagectomy.....114

5.1.3. Aims and objectives....116
5.2. Methods....117
5.2.1. Trial Set up....117
5.2.1.1. Protocol....117
5.3. Results....119
5.3.1. Effect of pH and cream on ICG fluorescence....119
5.3.2. ICG thoracic duct clinical trial results....123
5.3.2.1. Recruitment....123
5.3.2.2. Fluorescence results – feeding jejunostomy....125
5.3.2.3. Fluorescence results – mesenteric injection....126
5.3.3. Fluorescence to identify intraoperative chyle leaks....129
5.3.4. Post-operative follow-up....129
5.3.5. Propensity score-matched analysis comparing ICG thoracic duct trial participant with control group....130
5.4. Summary and Discussion....133
CHAPTER 6: MOLECULAR TARGETS TO DETECT COLONIC DYSPLASIA DURING ENDOSCOPY AND SURGERY....137
6.1. Introduction....138
6.1.1. Colonic crypts and goblet cells....138
6.1.2. Lectins as biomarkers....141
6.1.3. Highlighting dysplasia and cancer in the colon....142
6.1.4. Chromoendoscopy....143
6.1.4.1. Absorptive stains....143

6.1.4.2. Methylene Blue *144*

6.1.5. Contrast Stains 145

6.1.5.1. Indigo Carmine *145*

6.1.6. Narrow Band Imaging 145

6.1.7. Autofluorescence Imaging 146

6.1.8. Molecular imaging in endoscopy 147

6.1.9. Aims and objectives 148

6.2. Methods 148

6.2.1. Cell Lines 148

6.2.2. Cell culture condition 148

6.2.3. Passage details 149

6.2.4. Cell Storage and Retrieval 149

6.2.5. Cell Counting 150

6.2.6. Plating of cells 150

6.2.7. Mycoplasma contamination testing 150

6.2.8. Paraffin-Embedded Archived Material 151

6.2.9. Antigen Retrieval for Formalin Fixed Paraffin Embedded Tissue 151

6.2.10. Immunohistochemistry of tissue sections or cultured cells 152

6.2.11. Imaging of whole fresh colonic specimens 152

6.2.12. Microarray analysis 153

6.3. Results 153

6.3.1. Validation of WFA-M 153

6.3.2. In-vivo assessment of WFA-M 159
6.3.3. Validation of WFA-IR800CW 162
6.3.4. In-vivo assessment of WFA-IR800CW 167
6.3.5. Identification of additional targets for identifying early colorectal disease 174
6.3.6. GPA-33 as another marker of colorectal cancer 182
6.4. Discussion and future directions 184
6.4.1. GPA33 as an alternative to WFA 189
6.4.2. Future of molecular endoscopy 190
CHAPTER 7: DISCUSSION AND FUTURE DIRECTIONS 192
7.1. Summary of results 193
7.2. Limitations 193
7.2.1. Difficulties in conducting clinical trials with fluorescence 195
7.3. Future technology 196
7.3.1. NIR-II window 196
7.3.2. Software enhancements 198
7.3.3. Hardware enhancements 198
7.4. Summary 199

LIST OF TABLES

Table 1.1 - Chemical structure and fluorescent properties of clinically approved fluorescent dyes. 11

Table 1.2 - Commercially available laparoscopic systems with their excitation method and excitation and emission wavelengths. 13

Table 1.3 - Current registered trials of targeted fluorescence for colorectal cancer surgery. 23

Table 3.1 Inclusion and exclusion criteria for methylene blue ureter study. 37

Table 3.2 - IRDye Ureter Trial Visual Assessment Scoring System. 40

Table 3.3 IRDye Ureter Trial - Inclusion and Exclusion Criteria 42

Table 3.4 - Breakdown of patients in the study by operation type and indication. The majority of cases were anterior resections for cancer. 49

Table 3.5 - Table comparing mean signal to background ratios between dosing cohorts ... 56

Table 3.6 - Demographics divided by dosing cohort during dose optimisation stage. 65

Table 3.7 - Subjective and safety data from dosing cohorts during dose optimisation stage. 67

Table 3.8 - Reported adverse events during the dose optimisation stage. 72

Table 3.9 - Haematology and biochemistry results from patients in IRDye 800 ureter trial from pre-op to post-op. 77

Table 3.10 - Baseline demographics between methylene blue and IRDye 800BK trial groups. 80

Table 5.1 - ICG thoracic duct and white light visualisation subjective scoring descriptors. 119

Table 5.2 - Comparison of baseline characteristics of patients in the overall population, before the ICG trial and patients in the ICG trial before and after matching. 132

Table 5.3 - Comparison of outcome parameters in all patients, pre-trial patients and participants in the ICG thoracic duct trial. 133
Table 6.1 - Comparison of mucus thickness after different numbers of washings. 172
Table 6.2 – Published phase I/II trials in molecular colonoscopy using both antibody and peptide targets. 187

LIST OF FIGURES

Figure 1.1 - Modified Jablonski diagram outlining the physical process of fluorescence. ...3

Figure 1.2 - Schematic representation of key features to provide fluorescence imaging during surgery. 6

Figure 1.3 - Excitation and emission spectra of fluorescein, ICG and methylene blue. 7

Figure 1.4 - Fluorescence clearly identifying drainage from the splenic flexure to the left branch of the middle colic artery. 20

Figure 2.1 - Method of measuring signal to background ratio of NIR fluorescent image. .25

Figure 3.1 - Dose optimisation decision tree for DSMC in IRDye Ureter Study....43

Figure 3.2: IR800 BK Clinical Trial Application and Approval Process. 44

Figure 3.3 - Patient recruitment flow diagram for methylene blue ureter study. 46

Figure 3.4 - Recruitment graph for the methylene blue ureter study 47

Figure 3.5 - Number of cases recruited to study by surgeon (anonymised)....47

Figure 3.6 - Distribution of BMI and Age across patients in methylene blue trial. 48

Figure 3.7 - Total number of ureteric fluorescence readings per dosing cohort over time. 50

Figure 3.8 - Subjective visualisation of the ureter divided by ureters relevant and irrelevant to the procedure. 51

Figure 3.9 - Assessment of ureteric fluorescence in NIR mode. 52

Figure 3.10 - Proportion of ureteric visualisations by modality over time....55

Figure 3.11 - Signal to background ratio over time by dose. 57

Figure 3.12 - Mean probability of methylene blue being better than white light over time. 58

Figure 3.13 - Assessment of cross-talk between methylene blue and IRDye 800BK at 660nm and 785nm. 61

Figure 3.14 - IR800 BK ureter clinical trial flow diagram. 63

Figure 3.15 - Actual and predicted recruitment during the IR800 ureter study. 64

Figure 3.16 - Graphical representation of age (left) and BMI (right) from IR800 ureter patients. 65
Figure 3.17- Mean signal to background ratio across dosing cohorts in the dose optimisation stage. 68
Figure 3.18 - Background signal across dosing cohorts during the dose optimisation stage. 70
Figure 3.19 - Number of ureteric assessments undertaken over time during IRDye 800BK trial. 73
Figure 3.20 - Summary of subjective fluorescence visualisation of ureters with IRDye 800BK. 74
Figure 3.21 - Graphical representation of signal to background ratio over time and mean signal and background in all patients in IR800 ureter study. 76
Figure 3.22 - Signal to background ratio over time with different devices for IRDye 800BK. 78
Figure 3.23 – Comparison of objective data from IR800 and methylene blue ureteric fluorescence studies. 82
Figure 4.1 - Cadaveric specimen of the midline sagittal section of the male pelvis. 89
Figure 4.2 - Cadaveric model of urethral exposure via perineal dissection. 95
Figure 4.3 – Representative images of intra-abdominal visualisation of the urethra in the pig. 98
Figure 4.4 - Signal and background brightness between ICG and methylene blue in the pig urethra model. 99
Figure 4.5 - Representative images of cadaveric dose optimisation of urethral ICG. 100
Figure 4.6 - Comparison of signal and background across different doses for urethral ICG fluorescence. 101
Figure 4.7 - NIR urinary catheter light source, fibre, and adapter (NIRCaD). 104

Figure 4.8 - Visualisation of NIR Light from NIRCaD in cadaveric TaTME model. 106
Figure 4.9 - In-vivo images of NIRCaD visualisation around the membranous urethra and prostatic regions.....108
Figure 5.1 - Anatomical depiction of thoracic duct location in the saggital plain (left) and coronal plane (right). 114
Figure 5.2: ICG mixed with varying pH solutions and observed under ATG fluorescence imaging camera.....120
Figure 5.3: ICG mixed with cream at pH1 and pH7 and imaged at different time points.122
Figure 5.4 – Recruitment of ICG thoracic duct trial.....124
Figure 5.5- Representative image of fluorescent small bowel following ICG-cream mix infiltrated via a feeding jejunostomy. 126
Figure 5.6 - Graphical representation of data from ICG thoracic duct trial. 128
Figure 5.7 - Representative images of identifying chyle leak under fluorescence in two patients.....130
Figure 6.1 - Schematic representation of the 2 mucus layers over an epithelial surface (left) and the structure of the MUC2 mucin (right). 140
Figure 6.2 - Schematic representation of MUC2 mucus layers in the colon. 141
Figure 6.3 - Comparison of WFA-V and WFA-M at same laser exposure on normal colonic tissue. 155
Figure 6.4 - Comparison of WFA-V with WFA-M on immunostaining of FFPE colonic tissue of different pathology. 156
Figure 6.5 - Comparison of WFA-M at differing storage conditions - quantification of signal to background ratio. 158
Figure 6.6 - In-vivo assessment of WFA-M. 160
Figure 6.7 - Image of 2 whole colonic specimens under fluorescein wavelength without application of WFA. 161

Figure 6.8 - Results of SRB assay comparing WFA-M, WFA-V, WFA-IR800CW, fluorescein and IR800CW with control. 163
Figure 6.9 - Representative images comparing WFA-V to WFA-IR800CW staining in FFPE slides from normal and colorectal cancer. 164
Figure 6.10 - Comparison of pinpoint and ATG devices on imaging WFA-IR800CW at differing concentrations. 166
Figure 6.11 - In-vivo assessment of WFA-IR800CW in three patients undergoing TEMs. 168
Figure 6.12 - WFA-IR800CW on ex-vivo whole colonic cancer resection specimens imaged with IVIS. 170
Figure 6.13 - Ex-vivo biopsy specimens of normal and colorectal tumour samples immersed in WFA-IR800CW. 171
Figure 6.14 - Comparison of the effects of increasing washing on WFA-IR800CW brightness and mucus thickness in fresh frozen sections of normal colon. 173
Figure 6.15 - Representative images of colorectal cancer cell line screening with WFA. 176
Figure 6.16 - Volcano plot of Log_2 Fold change and p-value of differential genes between different groups 178
Figure 6.17 - Comparison of gene expression in CDX-1, GPA33, TFF3 and CDH17 across lumen and non-lumen forming cell lines. 179
Figure 6.18 - RNA Expression from 3 data sets for GPA33, TFF3, CDH17 and CDX1.. 181
Figure 6.19 - Tissue Microarray staining of paired normal and colorectal cancer tissue.. 183
Figure 7.1 - Fluorescent images of cerebro-vasculature in mice in the NIR-I and NIR-II spectrums. 197

LIST OF ABBREVIATIONS

5-ALA	5-Aminolevulinic Acid
ADR	Adenoma Detection Rate
AE	Adverse Event
AFI	Autofluorescence Imaging
ALP	Alkaline Phosphatase
ALT	Alanine Aminotransferase
ANOVA	Analysis of Variance
APER	Abdomino-Perineal Excision of The Rectum
ASGE	American Society for Gastrointestinal Endoscopy
AST	Aspartate Transaminase
ATG	Advanced Technology Group
BMI	Body Mass Index
CBD	Common Bile Duct
CEA	Carcinoembryonic Antigen
CHD	Common Hepatic Duct
CI	Confidence Interval
CIL	Cancer and Immunogenetics Laboratory
CRC	Colorectal Cancer
CRM	Circumferential Resection Margin
CT	Computerised Tomography
CTIMP	Clinical Trial of an Investigational Medicinal Product
DAPI	4′,6-Diamidino-2-Phenylindole
DMEM	Dulbecco's Modified Eagle Medium
DMSO	Dimethyl Sulfoxide

DNA	Deoxyribonucleic Acid
DR	Deep Red
DRE	Digital Rectal Examination
DSMC	Data Safety Monitoring Committee
ECG	Electrocardiogram
EGFR	Epidermal Growth Factor Receptor
λ_{EM}	Emission Wavelength
EMA	European Medicines Agency
ER	Endoplasmic Reticulum
λ_{EX}	Excitation Wavelength
FCS	Foetal Calf Serum
FDA	Food and Drug Agency
FFPE	Formalin Fixed Paraffin Embedded
FITC	Fluorescein Isothiocyanate
HGD	High Grade Dysplasia
HRA	Health Research Authority
ICG	Indocyanine Green
IDEAL	Idea, Development, Exploration, Assessment, Long-Term Follow-Up, Improving the Quality of Research in Surgery
IHC	Immunohistochemistry
IMA	Inferior Mesenteric Artery
IMDM	Iscove's Modified Dulbecco's Medium
IMP	Investigational Medicinal Product
IMS	Industrial Methylated Spirits
IMV	Inferior Mesenteric Vein
IOC	Intraoperative Cholangiography

IQR	Interquartile Range
LED	Light Emitting Diode
LN	Lymph Node
MB	Methylene Blue
MDT	Multi-Disciplinary Team
MHRA	Medicines and Healthcare Regulatory Authority
MRI	Magnetic Resonance Imaging
MUC	Mucin
NBI	Narrow Band Imaging
NHS	National Health Service
NHSLA	National Health Service Litigation Authority
NIR	Near-infrared
ORB	Oxford Radcliffe Biobank
PBS	Phosphate Buffered Saline
PDE	Photodynamic Eye
PFA	Paraformaldehyde
PIL	Patient Information Leaflet
PPIX	Protoporphyrin IX
PSA	Prostate Specific Antigen
PTS	Proline Threonine Serine
PUJ	Ureteropelvic Junction
RCT	Randomised Controlled Trial
REC	Research Ethics Committee
RGB	Red Green Blue
RNA	Ribonuclease Acid
RPM	Revolutions Per Minute

RPMI	Roswell Park Memorial Institute Medium
RR	Risk Ratio
SAE	Serious Adverse Event
SD	Standard Deviation
SEM	Standard Error of The Mean
SLN	Sentinel Lymph Node
SRB	Sulphorhodamine B
TAMIS	Transanal Minimally Invasive Surgery
TEM	Transanal Endoscopic Microsurgery
TMA	Trust Management Approval
TME	Total Mesorectal Excision
UC	Ulcerative Colitis
UK	United Kingdom
ULN	Upper Limit of Normal
USA	United States of America
UTI	Urinary Tract Infection
UV	Ultraviolet
VUJ	Vesicoureteral Junction
WFA	Wisteria Floribunda
WGA	Wheat Germ Agglutinin
WL	White Light
WLE	White Light Endoscopy

CHAPTER 1: INTRODUCTION

1.1. Image guided surgery, augmented reality and virtual reality

Over the last 50 years there has been a movement from open surgery towards minimally invasive techniques. Development of such technology has brought with it a loss of tactile feedback, learning curves, and the dangers of new techniques. There have also been advances in introducing technology to improve visualisation in the operating theatre. Initially, image guided surgery allowed surgeons to use radiological images acquired pre-operatively in the operating theatre which is now standard practice.

More recently, augmented reality has received much attention in surgery. Augmented reality integrates a computer-generated image with a user's view of the real world in real-time and has become the next step to enhance the surgeon's visual information during procedures. Fluorescence and NIR imaging sit under the definition of augmented reality with computer interpretation of the 'invisible light' displayed alongside the operative image. This is the main subject of this thesis. Conversely, virtual reality generates a completely artificial, computer-simulated image and environment with real-time interaction [1].

1.2. Principles of fluorescence

Fluorescence is a type of luminescence (emission of photons or light energy) that involves the detection of light produced by a molecule with fluorescent properties (fluorophore). Any object, when illuminated with white light, will absorb light at some of those wavelengths and reflect the remaining light at wavelengths which gives an object its colour. Fluorescence is very similar to this in that when a fluorophore is exposed to an external light source at a particular wavelength, it absorbs the light and becomes excited from a ground state (S_0) to an excited state (S_1') (Figure 1.1) [2]. Fluorophores stay at their maximal excitation state for a very short amount of time during which the fluorescent molecule undergoes changes where the energy is partially dissipated creating a 'relaxed-excited' state (S_1). Emission of

fluorescent light originates from this stage when the molecules return to the ground state (S_0) [3]. Some of the molecules return to the ground state by other mechanisms including quenching. During emission, as the energies of the photons being emitted are lower, the light is of a longer wavelength than the excitation light. This difference in wavelength is known as the Stokes shift and represented by $h\nu_{EX}$ - $h\nu_{EM}$. The Stokes shift allows selection for only imaging the emitted light wavelengths by blocking or filtering the excitation light [4].

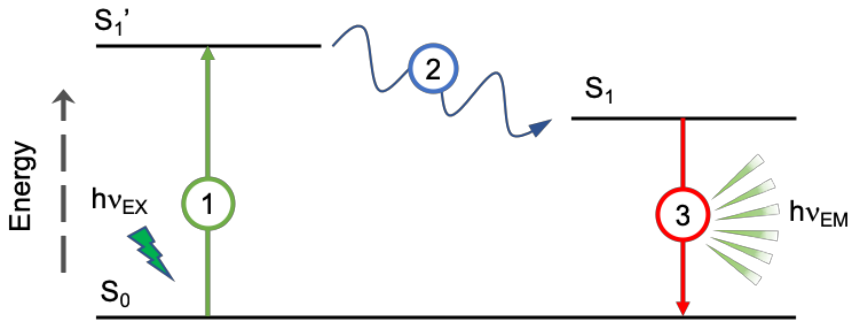

Figure 1.1 - Modified Jablonski diagram outlining the physical process of fluorescence. S_0 represents the ground state, S_1' the excitation state and S_1 the 'relaxed-excited' state. As excitation light ($h\nu_{EX}$) hits the fluorophore (1), the molecule becomes excited. Once the molecule relaxes back to the ground state (3), energy is emitted in the form of light which is at a longer wavelength than the excitation light.

The brightness of a fluorophore is the product of the molar extinction coefficient (ε), which quantifies how readily a molecule absorbs light at a particular wavelength, and the quantum yield (Φ) which is the ratio of the number of photons emitted to the number of photons absorbed [2, 5]. Other factors can affect the brightness of a fluorophore, including quenching of which there are 2 types: static quenching which occurs when individual fluorophores bind together forming dimers or oligomers rendering them unable to emit light [2, 6, 7] and; self-quenching (Förster Resonance Energy Transfer, FRET) where at high concentrations of a fluorophore, energy from one excited fluorophore simply transfers to another adjacent

fluorophore rather than emitting light [8, 9]. Similarly, at lower concentrations of fluorophores, the emitted light from one fluorophore can be absorbed by other adjacent fluorophores [2].

The process of fluorescence is cyclical, i.e. an individual fluorophore can be repeatedly excited and will continue to emit light. When fluorophores are exposed to excitation light, degradation of the fluorophores can occur known as photobleaching [10]. Once excited, a fluorophore may react with oxygen or other molecules and irreversibly generate products that are non-fluorescent. This is an undesirable property of fluorescence guided surgery as the loss of the fluorescent signal is irreversible.

Aside from fluorophores, in 1911, the first form of fluorescence observed under the microscope was autofluorescence from single cells and animal tissues [11]. Autofluorescence occurs from excitation of endogenous fluorophores usually at shorter wavelengths (300-550nm) [2]. In cells, the mitochondria and lysosomes are the responsible organelles with autofluorescent properties whereas in tissues it is the extracellular matrix that contributes over the cellular component due to collagen [12] and elastin [13] being endogenous fluorophores with a high quantum yield. Autofluorescence can be utilised to identify pathology as changes in the collagen and elastin content in pathological tissues have been found in numerous disease states and thus detection of the autofluorescence emitted from these proteins can have significance for *in-vivo* imaging [14-16].

Between 600 and 1000nm, light absorption by biomolecules is at a minimum and thus autofluorescence almost non-existent [17]. Similarly, as the wavelength of light gets longer into the NIR spectrum, the penetration of such light through tissues is up to 5 times greater with the depth being up to 2cm [18]. There are absorbers of NIR light in living tissue which can have a detrimental effect on fluorescence and these include water, lipids,

oxyhaemoglobin and deoxyhaemoglobin [5]. NIR imaging is inherently safe as it does not use ionising radiation. Often, a laser light is used as an excitation light source and provided that this is not at a high energy level where tissue can burn, or fluorophores are irreversibly photobleached, then it remains a safe technology.

For use of real-time fluorescence guided surgery, there are a number of key principles of operation required in the technology (Figure 1.2). Firstly, a fluorescence excitation light source is required of the wavelength that will excite the fluorophore being used. Available sources include filtered light, light emitting diodes (LEDs), and laser diodes [19]. Filtered light sources are often inefficient as they discard the majority of photons produced by the light source to filter the light at the required narrow band and only a small fraction of optical power actually reached the optical field [19]. LEDs are less used in surgical fluorescence devices as they pose significant physical challenges. By far the most commonly used excitation light source are laser diodes which are confined spectrally to the excitation wavelength and at lower power are safe for both the patient and the operator [19]. Secondly, a white light source is required to image the operative field to provide simultaneous colour and NIR imaging. Most standard surgical imaging devices will emit light above 650nm that can interfere with fluorescence imaging, thus, the white light in NIR devices is often filtered between 400 to 650nm [20]. An alternative to this is that the fluorescence imaging modality is separate to the white light mode, thus the white light is inactive during fluorescence visualisation. In addition to the light source, complex collection optics are required which relay NIR and white light emission to the detectors of which there are numerous types.

Finally, as NIR light is invisible to the human eye, an image display monitor and software is required for both the operative white light image and the fluorescence image to be displayed. This software can allow interpretation of the emitted fluorescence light to be

emitted in any colour and allow overlay imaging of the fluorescence onto a white light image, a technology that is currently under patent by Novadaq Technologies Inc [21].

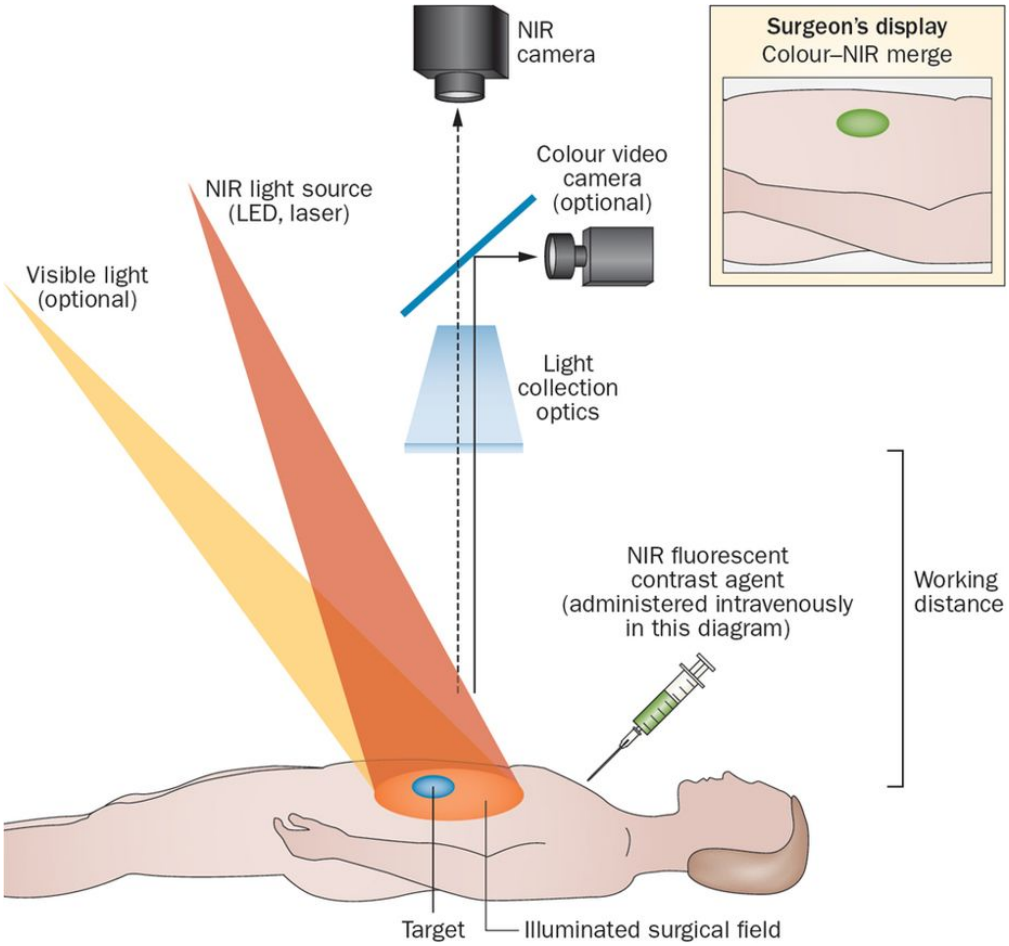

Figure 1.2 - Schematic representation of key features to provide fluorescence imaging during surgery. A fluorophore is administered to the patient and imaged using a fluorescence enabled camera as well as a camera to image the colour image of the operative field. The excitation light source and visible light source are both required, and the cameras often combined into a single hand-held device. NIR, Near-infrared, LED, light-emitting diode. Reproduced with permission from Vahrmeijer *et al* 2013 [22].

1.3. Fluorophores

The majority of fluorophores used in fluorescence guided surgery are organic exogenous contrast agents. There are currently 3 fluorescent dyes approved by the USA Food and Drug Administration (FDA) and European Medicines Agency (EMA): indocyanine green (ICG) [23], methylene blue and 5-aminolevulinic acid (5-ALA). The excitation and emission spectra of these dyes are demonstrated in Figure 1.3 and their chemical structure and fluorescent properties outlined in Table 1.1.

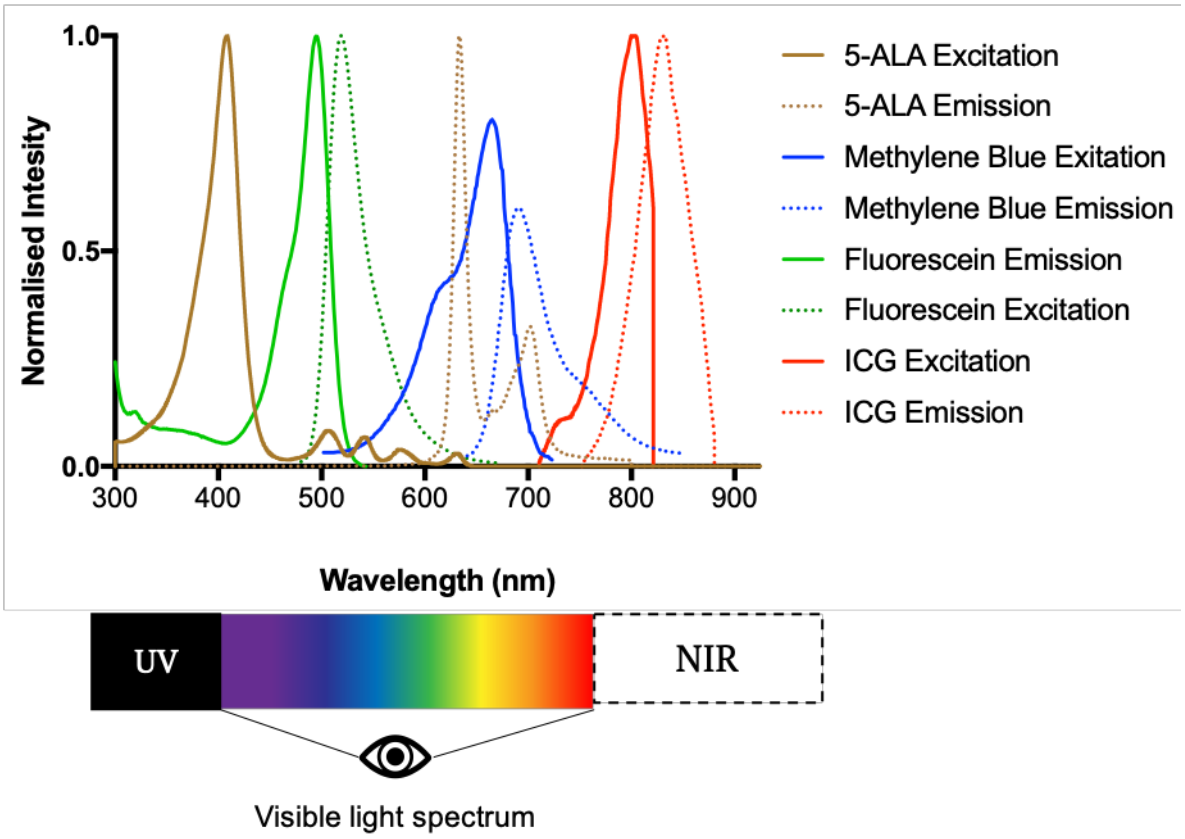

Figure 1.3 - Excitation and emission spectra of fluorescein, ICG and methylene blue. Beneath the graph the light spectrum is demonstrated with the UV light spectra between 100-380nm, the visible light spectra at 380-740nm and at 740-1000nm, the NIR spectrum. UV, ultraviolet, NIR, near-infrared.

1.3.1. Indocyanine Green

The first clinically approved fluorophore was ICG which is a hydrophobic heptamethine cyanine dye with a molecular weight of 776Da and a diameter of 1.2nm [24]. It has long been in use for assessment of hepatic function, ophthalmic angiography and cardiac output assessment. ICG absorbs NIR light at 800-810nm with peak absorption at 806nm (Figure 1.3). When administered to humans it binds to plasma proteins confining it to the intravascular space and is eventually excreted via the hepatobiliary system [25]. These properties make it especially useful for fluorescence angiography, lymphography and biliary tree mapping. ICG is also being used during hepatobiliary surgery to intraoperatively identify liver metastases and hepatocellular carcinomas as the hepatically excreted ICG can extravasate into tumour tissue where the vasculature is leaky. The plasma half-life is 3-5 minutes and it is excreted within 10-15 minutes of administration. Whilst ICG is licensed for use in humans, it is not possible to conjugate it to other antibodies as it loses its fluorescence which therefore limits its use to only non-specific fluorescence. ICG is known to be extremely safe [26] with reports of anaphylaxis being extremely rare only being reported as case reports [27].

1.3.2. Methylene Blue

Methylthioninium chloride or methylene blue has been used for centuries in medical diagnostics and disease therapy [28]. It is currently licensed in the UK for the treatment of methaemoglobinaemia. Its molecular weight and diameter are 320Da and 1.43nm respectively. Most commonly, it is used as a visible blue dye in sentinel lymph node detection especially in breast and melanoma surgery [29-31]. It is also known that methylene blue at low concentrations has NIR fluorescent properties with an excitation peak of 670nm and emission peak of 690nm (Figure 1.3) [32]. When administered intravenously, methylene blue is distributed to tissues and is eventually excreted in the urine. Approximately one third

of methylene blue in the urine is converted to leucomethylene blue which is colourless and does not have the fluorescent properties the non-leucoform has and this varies between patients [33, 34].

The use of methylene blue as a fluorophore has been described for identification of the parathyroid glands during parathyroidectomy and thyroidectomy [35] as well as for sentinel lymph node mapping [36, 37].

Methylene blue is licensed by the EMA [38] and FDA to treat drug induced and genetic methaemoglobinaemia [39] as in low doses, it acts as a cofactor accelerating erythrocytic conversion of methaemoglobin to haemoglobin [40]. Recognised side effects include significant haemolysis in individuals with glucose-6-phosphate dehydrogenase deficiency (G6PD) [40, 41], nausea, vomiting, abdominal pain, headache, hypertension, sweating and dizziness [39, 41]. Of relevance to surgical uses, intravenous use can give a false pulse oximetry reading in the range of 80%-90% [41].

1.3.3. 5-aminolevulinic acid

5-aminolevulinic acid (5-ALA) is an amino acid where its metabolite, protoporphyrin IX (PPIX) exhibits fluorescence with a peak absorption at 405nm and, after a significant Stokes shift, it emits light at a peak of 635nm. The metabolism of 5-ALA to PPIX occurs via the haeme-synthesis pathway in cells with high metabolic activity, therefore its use in cancer guided surgery has received significant attention, particularly for the detection of gliomas with a decrease in R1 resection from 65% to 35% in a randomised phase III trial [42, 43]. 5-ALA has also been assessed in lymph node mapping for colorectal cancer in a feasibility study of 44 patients [44]. Andrew and colleagues assessed oral use of 5-ALA for high risk operable cancer patients and performed a dosing and timing assessment. For lymph node

positive colorectal cancer, 5-ALA was not proven to be sensitive enough to be taken forward for a phase III clinical trial.

1.3.4. Fluorescein

Fluorescein is a xanthine fluorophore and is a clinically used fluorescent agent namely in ophthalmic angiography, corneal staining and for detection of cerebrospinal fluid leaks. It is a well-established medicine in the European Union having been used for over ten years with recognised efficacy and an acceptable safety profile [45]. The maximum excitation and emission are 490nm and 525nm respectively (Figure 1.3). Fluorescein is a bright fluorophore yielding a robust signal even at low concentrations [2]. The major downside of fluorescein is that the excitation and emission spectra lie within the visible light spectrum.

1.3.5. Carbon nanotubes

Single walled carbon nanotubes are molecules are carbon allotropes that are formed into a cylindrical nanostructure. They have numerous physical properties, one of which is their ability to act as fluorophores and, depending on their diameter, have excitation bands from 600-800nm and emission bands from 950-1300nm [46]. Carbon nanotubes have gained interest due to their favourable properties of photostability, low toxicity, and excellent water solubility [47]. However, at present, there are no NIR carbon nanotubes that are ready for human use.

Name	Chemical Structure	Fluorescence properties
ICG	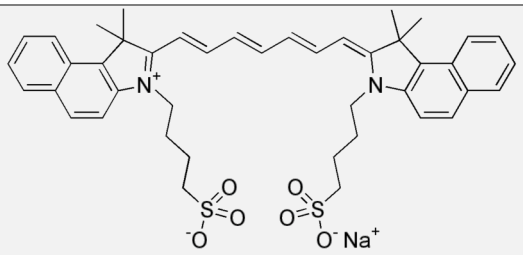	$h\nu_{EX}$: 810nm $h\nu_{EM}$: 822nm Φ: 9.3% (in PBS) ε: 121,000cm^{-1}/M
5-ALA (converted to PPIX)	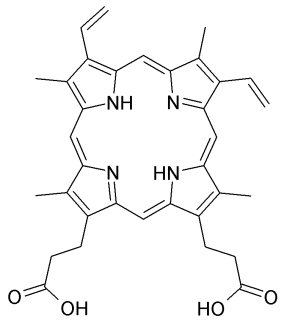	$h\nu_{EX}$: 405nm $h\nu_{EM}$: 635nm Φ: 6% ε: 171,000cm^{-1}/M
Methylene blue	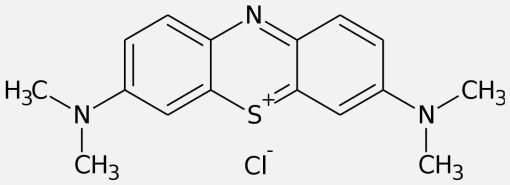	$h\nu_{EX}$: 670nm $h\nu_{EM}$: 688nm Φ: 4.4% **ε**: 32,444cm^{-1}/M
Fluorescein	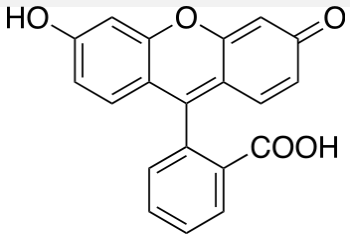	$h\nu_{EX}$: 490nm $h\nu_{EM}$: 525nm Φ: 79% (in ethanol) **ε**: 92,300cm^{-1}/M

Table 1.1 - Chemical structure and fluorescent properties of clinically approved fluorescent dyes. $h\nu_{EX}$, peak excitation wavelength, **$h\nu_{EM}$** peak emission wavelength, Φ, quantum yield, ε, molar extinction coefficient.

1.3.6. New fluorophores

The aforementioned fluorophores have been investigated in non-targeted approaches to fluorescence guided surgery. Their use in cancer specific surgery is limited as knowledge of why in some situations they may highlight tumours is not well understood. There is a lack of tumour targeting potential and ICG, the only potential fluorophore to allow conjugation by using ICG derivatives (e.g. ICG-sOSu), is a complicated process and may not always be successful [19, 48]. Recently, newer NIR fluorophores have been developed that allow easy conjugation, increased stability, and improved tissue depth penetration.

1.3.6.1. Cyanine fluorophores

ICG is a type of cyanine fluorophore and more recently, newer cyanine fluorophores have been manufactured that allow easy conjugation. Their manufacture contains 2 aromatic heterocyclic ring systems which are linked by an extendable polymethine bridge increasing the wavelength of excitation and emission [4, 49]. Such cyanines are available (Cy3, Cy5, Cy7, Cy7.5) with increasing emission excitation into the far-red and NIR ranges but these have poor photostability and low quantum yield in aqueous solution [49]. At present, IRDye 800CW (Li-COR®, Nebraska, USA) has undergone significant safety testing and, because of its ease of conjugation and photostability, an increasing number of studies utilising this fluorophore conjugated to antibodies for molecular targeted images are in progress. Numerous other fluorophores are also in development but are less well characterised and further behind cyanine dyes in their process to clinical use.

1.4. In-vivo fluorescence enabled devices

Numerous devices are available allowing real-time *in-vivo* fluorescence guided surgery. Technology for *in-vivo* fluorescent enabled devices licensed for use intraoperatively can vary slightly. The two main sources of excitation light include laser light or filtered white

light (usually xenon light). NIR fluorescence imaging faces significant challenges requiring optimisation of light sources that can sufficiently excite fluorophores at low concentrations using low-attenuation optics [19, 22]. Table 1.2 outlines the various commercially available fluorescence enabled laparoscopic systems available. There are also numerous other academic systems that are currently undergoing evaluation.

Brand	Excitation Method	$h\nu_{EX}$ (nm)	$h\nu_{EM}$ (nm)	Fluorescence colour
Stryker (1588)	Laser	808	Above 835	Green
Storz (Image 1 SPIES)	Filtered Light	805	Above 835	Blue
Novadaq (Pinpoint)	Laser	805	Above 835	Green
Olympus (VISERA Elite II)	Filtered Light	700-780	Above 800	Green or cyan
Firefly	Laser	803	NA	Green
Photodynamic Eye (PDE)	LED	760	Above 820	White
Fluoptics	Laser	750	Above 800	White
ATG	*Laser*	*805*	*Above 830*	*White*

Table 1.2 - Commercially available laparoscopic systems with their excitation method and excitation and emission wavelengths. $h\nu_{EX}$, excitation wavelength, $h\nu_{EM}$, emission wavelength (wavelength of filter). The advanced technology group (ATG) device has been included for reference but this is not commercially available.

1.5. Current applications of NIR guided gastrointestinal surgery

In fluorescence guided gastrointestinal surgery, there are several applications that have been explored. The following are examples of fluorescence guidance where benefit has been seen and these techniques are starting to become standard practice.

1.5.1. Anastomosis perfusion during gastrointestinal resections

For patients who undergo colorectal resection, a feared postoperative complication is anastomotic leak where healing of the anastomosis fails, causing leakage of colonic content, sepsis and potential multi-organ failure. In the literature, the risk of anastomotic leak is reported as being between 2.7% and 13.3% [50] with higher rates in rectal resection. Over the last 20 years, despite improvements in surgical technology, there has been no change in the leak rate [51]. There are numerous risk factors associated with an increased risk of anastomotic leak including age, male gender, malnutrition, smoking, preoperative chemotherapy and radiotherapy, advanced tumour stage, immunosuppression, blood loss and sepsis [52]. It is essential to have an adequate blood supply to allow the anastomosis to heal [53]. There has been an increasing use of fluorescence angiography to detect colonic ischaemia near the anastomosis intraoperatively by using intravenous ICG. Traditionally, assessment of bowel perfusion during colorectal surgery includes inspection of the serosal colour, palpation of pulsating vessels in the mesentery and pulsatile bleeding at the divided artery [54].

The PILLAR II trial [55] enrolled 139 participants who underwent left-sided colonic resection and observed a leak rate of 1.4% with no leaks being observed in those where ICG angiography altered the surgical plan (n=11). A recent meta-analysis by Blanco-Colino *et al* [56] of studies examined the anastomotic leak rate in at least 30 days of follow up in 1302 patients where 555 underwent ICG angiography and 747 underwent standard care. In the ICG group, a change to the planned anastomotic level was made in 7.4% of cases due to hypoperfusion identified on fluorescence imaging. On performing a subgroup analysis of the 956 cancer patients (382 ICG, 574 control), there was a significant decrease in leak rate in the ICG group (OR 0.34; CI 0.16-0.74; p=0.006). Similar results were demonstrated in those undergoing rectal resection. In a larger study by Ris *et al* not included in this meta-analysis, a leak rate of 2.6% for colorectal anastomoses and 3% following low anterior

resection with 29 patients have an altered surgical plan following fluorescence angiography was observed [57]. Following these promising data, the first multi-centre randomised trial for ICG fluorescence angiography in patients undergoing anterior resection is being conducted with results expected in late 2019 [58].

This technique must use observation of fluorescence in either adjacent small bowel or proximal colon as a visual positive control. The current technology for anastomosis perfusion lacks quantification and the understanding of what is important in the interpretation of the fluorescent signal (e.g. time to signal, time to wash out, maximum signal etc) [57]. Such technology for quantification is already under evaluation where the aim is to give a 'cut-off' level where an anastomosis is less likely to heal [59].

1.5.2. Identifying critical anatomy

During any operative procedure, patient safety and procedural efficiency are key to a successful outcome. This is especially true of laparoscopic surgery which gives major advantages of reduced post-operative pain, decreased length of stay and wound infection. Minimally invasive surgery can sometimes provide a limited field of view, decreased tactile feedback and the loss of three-dimensional imaging occasionally making identification and differentiation of critical anatomical structures difficult. Vessel, bile duct, nerve and ureteric injury are all complications that can occur from anatomical misinterpretation and earlier, clearer identification of these structures may reduce risk of injury [60]. A brief overview of fluorescence identification for critical anatomy is discussed here whilst ureteric imaging will be discussed in Chapter 3.

1.5.2.1. Biliary tree fluorescence

Laparoscopic cholecystectomy is one of the most commonly performed surgical procedures internationally. Bile duct injury during this procedure is one of the most serious complications having a devastating impact on the patient's quality of life and survival [61]. The most frequent biliary injury involves complete transection of the common bile duct when it is mistaken for the cystic duct [62]. During cholecystectomy, it is essential to visualise the critical view of safety where Calot's triangle is clearly visualised. Intraoperative cholangiography (IOC) has been used to assist surgeons in outlining the biliary anatomy, but this requires training, additional equipment and IOC itself can cause ductal injury [63]. As previously mentioned, ICG binds to plasma proteins and is eventually excreted via the liver. This property has been utilised to visualise the bile ducts using fluorescence even before dissection of Calot's triangle. First reports of fluorescence to identify the bile ducts used rolitetracycline and fluorescein as a proof of principle study, replaced over 10 years later, with ICG [64]. Numerous studies have reported on the use of ICG fluorescence during cholecystectomy with a recent meta-analysis identifying 19 studies reporting on visualisation of the common bile duct (CBD) and common hepatic duct (CHD) before and after Calot's dissection as well as 4 studies comparing ICG to IOC [65]. The CBD was visualised under fluorescence prior to Calot's dissection in 78.7% of cases where ICG was given. There was however, no documented comparison to white light visualisation in these studies. In 4 studies, ICG was compared with IOC visualisation of ductal structures with moderate to low quality evidence that visualisation of the cystic duct (RR 1.16; 95% CI 1.00-1.35), CBD (RR 1.00; 95% CI 0.97-1.03) but not the CHD (RR 0.76 95% CI 0.58-1.01) is better with ICG compared to white light visualisation. A large proportion of these studies (14) included patients with uncomplicated gallbladder disease and it is likely that patients who have gallbladder disease complicated by cholecystitis will have a lower fluorescence intensity [66]. A larger multi-centre randomised trial comparing ICG

cholangiography with white light visualisation has completed and due to report by 2020 (NCT02702843) [67].

1.5.2.2. Critical vessel identification

In addition to fluorescence of organ perfusion where intravenous ICG eventually reaches the micro-vasculature, this technique can be employed to visualise critical vessels during surgery. This use of fluorescence has only been reported in two studies. Schols *et al* [68] first described this technique for using ICG as a repeated injection to identify the biliary vasculature, namely the cystic artery which was successful in 87% of patients, although it was also seen clearly under white light. Finally, during oesophagectomy, a report from Sarkaria and colleagues [69] demonstrated visualisation of the short gastric arteries, gastroepiploic arcade and unrecognised small communicating arteries aiding the gastric mobilisation. Although this was an incidental finding in a study primarily assessing conduit perfusion, vessel identification could help in numerous procedures.

1.5.2.3. Lymphatic mapping

For curative resection of solid tumours, the two principles of removing the tumour in its entirety providing an R0 resection along with the draining lymph nodes is essential in providing the maximum recurrence free survival to the patient. In addition, the draining lymph nodes provide essential pathological staging to guide further treatment. In some solid tumours, the concept of the sentinel lymph node (SLN) allows surgeons to stage and stratify patients into those requiring lymphadenectomy. In particular, for melanoma [70] and breast cancer surgery [71], lymph node mapping and SLN biopsy has become the standard of care. The technique for SLN biopsy often involves injection of a visible blue dye (e.g. patent blue-V, isosulfan blue or methylene blue), a radioactive tracer with gamma probe detection, or

both, around the tumour, retroareolarly or periareolarly in breast cancer. During dissection for the SLN, the visible dye or radioactive tracer can then be identified positively in the first lymph node(s) in the lymphatic basin. Utilising these 2 techniques, the SLN detection is high being around 96-99.1% in large trials [72, 73] where it can be 10% lower with the use of a single technique [74]. The use of radioisotopes can provide difficulties for institutions with their handling, disposal, training and legislative requirements being costly as well as the injection needing to be performed by a nuclear medicine department. Similarly, with blue dyes, there is a risk of anaphylaxis and tattooing of the skin with their use. Thus, fluorescent SLN lymphatic mapping has been explored. When comparing ICG to blue dye alone, ICG is significantly better for SLN identification than blue dye (OR 18.37; 95% CI 8.63-39.10) as indicated by Ahmed *et al* in a meta-analysis of 15 studies [75]. When compared with a radiocolloid, there is no consensus on which is superior [75, 76].

In colorectal cancer, the concept of SLN biopsy is less widely adopted because there is variability in the sensitivity of the SLN technique [77]. Therefore, all patients undergoing resection have en-bloc mesenteric resection even for T1 and T2 disease that may be node negative which may provide no additional oncological benefit [78]. However, there is a fear of 'skip-metastases' where lymph nodes of aberrant drainage contain metastatic disease and thus the SLN biopsy would not identify these. The current evidence for fluorescence guided SLN detection in colorectal cancer is limited by its heterogeneity in terms of technique, dose, equipment and timing as well as small patient numbers. Most importantly however, the studies reporting this technique only report their sensitivity and specificity based on positivity by histopathology which does not report its value in identifying a negative SLN. ICG is a non-specific dye and thus reporting the sensitivity according to SLN positivity is perhaps a reasonable explanation for the varying results. Three, well conducted meta

analyses, although stating the technique as promising, fail to reach the same detection rates and quality of evidence seen in fluorescence guided SLN biopsy for breast surgery [79-81].

Aside from SLN biopsy, lymphatic mapping with ICG can be used in colorectal surgery to identify the pattern of the lymph node basin and to recognise aberrant lymph node drainage allowing a tailored colorectal resection [82]. This is perhaps a more important question with important outcomes being visualisation of the lymphatic drainage, identification of aberrant lymph nodes and change to mesenteric resection. In particular, resection of some colorectal cancers including the splenic flexure, are still not standardised due to difficulty in deciding on the appropriate mesenteric resection due to variation in the draining lymphatics from middle colic to left colic arteries [83]. Watanabe and colleagues have demonstrated huge variety in the lymphatic drainage of splenic flexural tumours with 38.7% of their 31 patients having lymphatic drainage to the left accessory aberrant colic artery (LAACA) and of the 61.3% without the LAACA 19.4% drained to the left branch of the middle colic, 25.8% to the left colic and 16.1% to the route of the IMV [84]. The appearance of fluorescence clearly demonstrating the lymphatic drainage is striking (Figure 1.4). More work is required to optimise the dosing, timing and patient selection for fluorescence lymphatic mapping during colorectal cancer surgery.

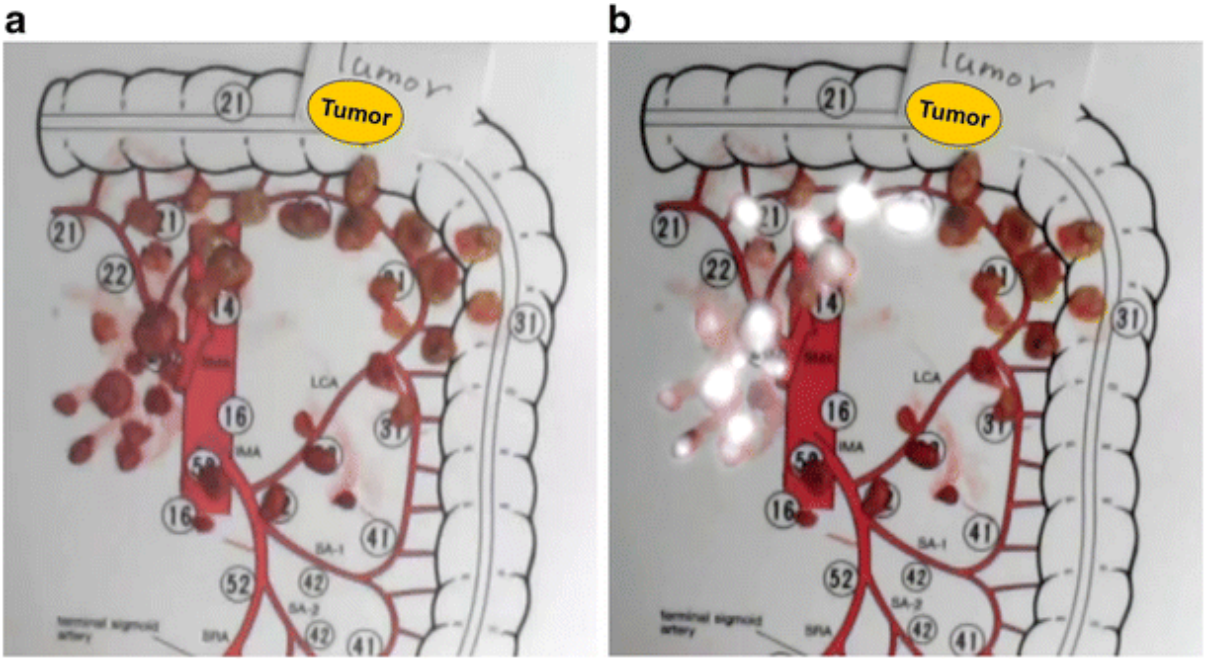

Figure 1.4 - Fluorescence clearly identifying drainage from the splenic flexure to the left branch of the middle colic artery. Reproduced with permission from Watanabe *et al* [84].

1.5.3. Fluorescence mapping of disease using targeted fluorophores

Perhaps a more exciting area of fluorescence guided surgery involves the use of targeted fluorophores towards tumours to identify either tumour margins, positive lymph nodes or metastatic disease. Using fluorophores conjugated to cancer specific agents can increase the sensitivity and specificity for disease detection [85]. This is still a new area of research where there are currently no approved conjugated fluorophores for clinical use but numerous under investigation. Targeted fluorophores can include small molecules, peptides, activatable fluorophores and antibodies, all of which are of varying size and thus differing pharmacokinetic, biodistribution and fluorescent properties [4]. Broadly speaking, targeted fluorophores can be categorised into either: affinity-based which bind to target specific tissue markers (e.g. receptors, ion channels or cell surface antigens) [86] a good example of which is the folate receptor for fluorescence guided ovarian cancer surgery [87] or; activity-based which emit fluorescent signal upon enzymatic localisation and amplification [88, 89].

Some fluorophores can be designed to only emit fluorescence following successful binding to target tissue which substantially decreases the background emitted by non-specific binding [4]. LUM015 has been tested in clinical trials which utilises a mechanism of protease activation via a quencher that is linked by a pan-cathepsin protease cleavable peptide to a Cy5 fluorophore. Cathepsins are overexpressed in tumour cells and cleave the linker which releases the quencher, activating the fluorophore [90].

There is only 1 published phase I/II clinical trial for targeted molecular fluorescence in colorectal cancer which utilises an anti-CEA monoclonal antibody conjugated to a NIR fluorophore (BM104) manufactured by the authors with an excitation and emission of 685 and 700nm respectively [91]. This pilot study included patients with elevated serum CEA levels undergoing resection of a colorectal cancer. In their dose expansion phase, a sensitivity of 98% and specificity of 62% was observed with 19 of 43 lesions detected using fluorescent imaging whilst not being clinically suspected before NIR detection changing the treatment strategy in 35% of patients [91]. Only 3 possibly related adverse events were observed making this a real potential for future investigation although it is only limited to cancers which are CEA positive. There are numerous other targeted fluorescence guided clinical trials, which are all phase I/II, underway with a few completed and awaiting publication of results (Table 1.3).

Study name	NCT	Phase	Drug	Type	Fluorophore	Administration	Detection of	Detection by	Sponsor	Status
Early Detection of Polyps and Colon Cancer by Fluorescence Imaging - a Dose-finding Study	NCT00285701	I/II	(5-ALA)	Fluorescent peptide	PPIX	Oral & topical	Polyps and CRC	Colonoscopy	Photocure	Completed 2010
Study of QRH-882260 Heptapeptide Application in the Colon	NCT03148119	I/II	QRH-882260	Conjugated peptide	Cy5	Topical	Tumour	Colonoscopy	Michigan University	Terminated - used for a new study
Phase I of SGM-101 in Patients with Cancer of the Colon, Rectum or Pancreas [91]	NCT02973672	I/II	SGM-101 (Anti-CEA)	Conjugated antibody	BM104	Intravenous	Tumour	Laparoscopy	Surgimab	Published
Multi-modality Imaging in Peritoneal Carcinomatosis of Colorectal Origin	NCT03699332	I/II	Labetuzumab	Antibody	IRDye800CW	Intravenous	Tumour	Laparoscopy	Radboud University	Not yet recruiting
EMI-137 in Laparoscopic Colonic Resections	NCT03360461	II	EMI-137	c-Met receptor peptide	Cyanine based dye not specified	Intravenous	Tumour and LN metastases	Laparoscopy	Leeds University	Recruiting
FluoFAP	NCT02113202	I	Bevacizumab	Conjugated peptide	IRDye800CW	Intravenous	Polyps	Colonoscopy	Groningen University	Published
An Open Dose-finding Study of Oral Applied HAL Imaging in Patients with Suspicion or High Risk of Neoplasia in the Colon	NCT01344902	I/II	(5-ALA)	Fluorescent peptide	PPIX	Oral	Polyps and CRC	Colonoscopy	Photocure	Terminated - poor efficacy

Study name	NCT	Phase	Drug	Type	Fluorophore	Administration	Detection of	Detection by	Sponsor	Status
Targeted Silica Nanoparticles for Real-Time Image-Guided Intraoperative Mapping of Nodal Metastases	NCT02106598	I	cRGDY-PEG-Cy5.5-C	Conjugated peptide	Cy5.5	Peritumoral	Nodal metastases	Laparoscopy	Memorial Sloan Kettering Cancer Center	Recruiting
Rapido-tract	NCT01972373	I	Bevacizumab	Conjugated antibody	IRDye800CW	Intravenous	Tumour	Colonoscopy	Groningen University	Completed
Feasibility of the LUM Imaging System for Detection of Gastrointestinal Cancers	NCT02584244	I/II	LUM015 (cathepsin)	Cleaved quencher	Cy5	Intravenous	Tumour	LUM 2.6 Imaging Device	Lumicell, Inc	Recruiting

Table 1.3 - Current registered trials of targeted fluorescence for colorectal cancer surgery. NCT, clinicaltrials.gov identifier, 5-ALA, 5-Aminolevulinic acid, PPIX, Protoporphyrin IX, CRC, colorectal cancer, CEA, carcinoembryonic antigen, LN, lymph node, CRC, colorectal cancer.

CHAPTER 2: MATERIALS & METHODS

2.1. Methodology

Methodology for work described in this thesis is outlined in each chapter. Generic methods used throughout the work are described here.

2.2. Capture and quantification of fluorescence

All fluorescent and NIR images were captured using either the ATG, Pinpoint, Stryker or Storz fluorescence enabled laparoscopic systems. For *ex-vivo* work where comparison is being performed, distance from the detector and the subject were kept consistent. Images were taken in the dark to minimise background signal from ceiling lights.

To quantify fluorescent signal, after obtaining images, fluorescence signal to background ratios were calculated using Image J [92]. After image upload, the polygon selection tool was used to delineate the area of interest. The size of the area measured in the region of interest matched the size of the area in the control region. A measurement of brightness was then obtained using the software which converts RGB pixels to brightness values using the formula V=(R+G+B)/3 [93]. Following this, the same area polygon was transferred to a random control area and a further measurement made (Figure 2.1).

Figure 2.1 - Method of measuring signal to background ratio of NIR fluorescent image. A = image before measurement made, B = measurement of signal, C = measurement of background.

2.3. Trial set up

All clinical trials described in this thesis were developed and set up as described hereto. A protocol was written to outline the trial objectives and outcomes, methodology, recruitment, analysis and study closure. These were written to comply with good clinical practice (GCP) guidance [94]. Trial designs were largely to assess proof of principle and were modelled on the IDEAL collaboration stages 1, 2A and 2B [95]. All studies were open-label, unblinded, non-randomised studies. Inclusion and exclusion criteria were listed and specific to each trial which is outlined in the methods of subsequent chapters. Withdrawal of participants occurred only due to safety concerns or if their data could not be used for analysis.

Following completion of the protocol, patient information leaflets (PILs) were written to inform participants of what their involvement would mean. Informed consent forms were designed on a template provided by the University of Oxford. Once the 'document package' was complete, sponsorship was applied from either the University of Oxford or Oxford University Hospitals NHS Foundation Trust (OUH). After document review and amendment from the sponsor team, the research and development (R&D) department of OUH would review and sign off the document package. Study contracts were completed in co-ordination with legal teams at Oxford University and OUH for site-level agreements and for agreements with third parties relating to drug or equipment supply. Study information was simultaneously uploaded onto the Integrated Research Application System (IRAS) (www.myresearchproject.org.uk), to apply for approvals. Once the sponsor and R&D department signed the study off, approval was sought from an ethical committee and the Health Research Authority (HRA) which involved attendance at their meeting to discuss any ethical issues impacting patients or the wider community. Following ethical review, any adjustments were made (if required) prior to obtaining full ethical and HRA approval. At this point, an electronic trial master file (eTMF) was created in accordance with GCP. A

delegation log for each study was created to ensure all staff were GCP trained. All studies only had the author (TGB) and 1 other person working on the study except for IRDye 800BK ureter where a research nurse was provided by the National Institute for Health and Research (NIHR). Training for each trial was developed and performed by TGB and recorded in the training log for each study team member. Standard operating procedures (SOPs) were developed for each trial to cover essential trial management procedures and were stored in the eTMF.

Trial recruitment logs were developed to record all patients approached, their eligibility and whether they declined or accepted to participate. For data collection, a study data matrix was developed to ensure all data points were recorded. From this, an electronic study database was created for data input and recording. Case report forms (CRFs) were largely paper based and designed to match each data point on the database. Once the eTMF was complete with all the aforementioned material, a sponsor review was conducted, corrections made (if required) and green light approval granted.

2.3.1. Patient recruitment

Screening to identify potentially eligible participants was performed using MDT lists, planned operating lists and outpatient appointment lists. This involved assessment of their operation type, previous surgery, BMI, drug allergies, American Society of Anaesthesiologist's Grade (ASA) and blood results obtained pre-operatively as part of their routine care.

For all studies, patients were initially approached either at their outpatient consultation, via telephone, at their pre-operative assessment (POA) appointment, or via a letter and PIL sent by post. The trial was explained to them and any questions answered. All patients were given

at least 24 hours to consider the information provided. The participant personally signed and dated the latest approved version of the consent form before any trial specific procedures were performed. It was clearly stated that the participant is free to withdraw from the trial at any time for any reason without prejudice to future care, without affecting their legal rights and with no obligation to give the reason for withdrawal. Participants were allowed as much time as wished to consider the information, and the opportunity to question the investigator, their GP or other independent parties to decide whether they will participate in the trial. Informed consent was then obtained by means of participant dated signature and signature of the person obtaining consent. A copy of the signed consent form was given to the participant, the original signed form retained within the TMF and a copy held in the participants medical records.

Following consent, baseline assessments were performed, recorded in the CRF and eligibility checked for the final time. Once the patient was positioned for their procedure on the operating table under general anaesthetic, the intervention for the trial (described in each chapter) was conducted.

2.4. Statistics

For clinical trials, as all studies were proof of principle or early phase studies, sample size calculation was not required. The sample size was calculated based on previous published studies of a similar design, feasibility to recruit within the time-constraints of TGB, operating list capacity and predicted recruitment rate.

After assessing for normality, categorical data were analysed using either the chi-squared or, for smaller population sizes, Fisher's exact test. Continuous non-parametric data were compared using the Mann-Whitney U test for 2 groups or the Kruskal-Wallis ANOVA test for multiple groups. Parametric data were assessed with the t-test or one-way ANOVA.

Where multiple comparisons were performed, p-values were corrected using either the Bonferroni or Dunn's method. For analysing change in results over time, linear regression models including generalised linear mixed models and random coefficient models (to assess impact of other factors) were used. Results were deemed significant when the p-value was less than 0.05. Software used for statistical analysis included SPSS (IBM, IBM Corp. Released 2016. IBM SPSS Statistics for Mac, Version 24.0. Armonk, NY: IBM Corp), Prism (version 7.0c for Mac, GraphPad Software, La Jolla California USA, www.graphpad.com) and Microsoft Excel (version 16.18 for Mac, Microsoft).

CHAPTER 3: IDENTIFICATION OF THE URETER DURING COLORECTAL SURGERY USING FLUORESCENCE

Data from this chapter has been published in:

Barnes TG, Hompes R, Birks J, et al. Methylene blue fluorescence of the ureter during colorectal surgery. Surgical Endoscopy. 2018;32:4036-4043.

3.1. Introduction

3.1.1. Anatomy of the ureter

The ureter is a 25-30cm long retroperitoneal structure that runs from the ureteropelvic junction (PUJ) to the bladder. Its abdominal segment extends from the renal pelvis to the pelvic brim where on the right this is just caudal to the descending part of the duodenum. The ureters are crossed by the gonadal vessels just below their origin and run on top of the psoas muscle anterior to the genitofemoral nerve. On the left, the sigmoidal vessels run in the mesentery anteriorly to the ureter. Proximally, the inferior mesenteric artery (IMA) and its branch, the superior rectal artery, follow the ureter closely medial to the gonadal vessels. In the pelvis, the approximately 15cm long ureter crosses the common iliac vessels and runs caudally still covered by peritoneum. It then skirts around the lateral pelvic side-wall crossing the obturator artery, vein and nerve before entering into the trigone of the bladder [96]. In the female, the ureter crosses dorsal to the ovary underneath the broad ligament, close to the uterine vessels where it is most at risk during gynaecological surgery [97].

3.1.2. Iatrogenic ureteric injury

Damage to the ureters during surgery is a feared but uncommon complication amongst surgeons. The nature of injury includes laceration, crush injury, ligation and devascularisation resulting in either ischaemic necrosis or ischaemic strictures [98]. Less than 30% of ureteric injuries are identified intraoperatively [99, 100] and the clinical sequelae of late identification include sepsis, renal failure, ureteral fistulas, urinoma and death [101]. Most ureteric injuries occur in patients without significant risk factors, but the incidence increases in patients with prior pelvic surgery, inflammatory processes including diverticular disease and inflammatory bowel disease, sepsis, large tumours, obesity, pelvic radiation and aberrant ureteric anatomy such as duplication and bifid ureters [97]. Re-operative surgery also comes with increased risk of ureteric injury. Gynaecological procedures account for the

majority of ureteric injuries with colorectal surgery being the second most common cause. In colorectal surgery, the rate of injury has remained at ~0.07% to 1.70% despite the introduction of laparoscopic surgery [97, 102-105]. Injury of the ureter occurs even in experienced hands and the risk is highest during low anterior resection or abdomino-perineal excision of the rectum (APER) [98]. Injury most commonly occurs during ligation of mesenteric vessels and dissection at the sacral promontory [98].

In addition to the devastating effects to the patient, ureteric injury contributes significant costs from both additional treatment, increased length of stay and medicolegal costs. A freedom of information request to the NHS Litigation Authority (NHSLA) in 2016 (unpublished data, Barnes TG) demonstrated that there is a general increase to the number of claims made to the NHSLA following ureteric injury since 2006. The cost of a claim to the NHS averages at £104,091.70 per successful claim and from 2006 to 2016, the cost of successful medicolegal claims has reached over £27,000,000.

Early identification of the ureter, keeping in the correct surgical plane and visualising the hallmark 'vermiculation' of the ureter to confirm its location is essential in reducing risk of ureteric injury [98]. During colorectal surgery, it is not always possible to clearly see the ureter and it may take significant time to identify during difficult cases. As well as identifying the ureter to protect it, it is a key landmark of left sided resections indicating to the surgeon the correct dissection plane between Gerota's and Toldt's fascia [106]. Therefore, early identification may help the surgeon maintain the correct plane of dissection.

3.1.3. Ureteric stents to protect the ureter

Prophylactic ureteral stents are occasionally employed in cases to assist the surgeon in identifying the ureter. In addition to identification of ureteric location, stents potentially

allow intraoperative identification of iatrogenic injury [99], although there is a huge paucity of evidence surrounding ureteric stents for these purposes [107]. Ureteric stents have an obvious benefit in open surgery where they can be easily palpated, and the rigid plastic would be easily distinguishable from any other structure. Despite this, ureteric injury is not completely mitigated with the use of a stent and numerous retrospective studies reporting on their use compared with unstented patients still report unrecognised ureteric injuries [98, 99, 108, 109]. From the limited evidence available, one can conclude that stents are placed entirely under surgeon choice and only for cases where difficulty in identifying the ureter in complex cases, particularly diverticular disease, is predicted [98, 108]. Stent placement itself is not without problems. There is an increased operating time and cost associated with placement. Extra staff are required including a urologist, radiographer as well as additional equipment. Additional time for stent insertion reported in the literature varies from 5 to 55 minutes [99, 110, 111]. Cost of prophylactic stent placement is estimated by Bothwell *et al* to exceed $2000 [112].

In addition to costs and time, ureteral stents are not routinely employed as they are not without their own complications. Complications from stent insertion range from pain, urinary tract infection, urinary retention, haematuria, anuria/oliguria which is often secondary to oedema of the vesicoureteric junction and may require stent re-insertion, and even ureteric perforation. Ureteric perforation is a rare complication and often follows a traumatic and failed catheterisation [112].

Over the last 10 years, the number of colorectal resections performed laparoscopically has increased with most patients now undergoing a minimally invasive approach. Standard ureteric stents are less useful in this situation as the ability to rely on tactile feedback is reduced and the visual appearance of the ureter may not be enhanced. As a result, lighted

ureteral catheters have been introduced. The first case series of 49 patients to describe their use was by Senagore *et al* who reported visualisation of the emitted light in 83% of cases [110]. The only other series reported in the literature by Boyan *et al* describes their 5 year experience of using lighted stents in 402 patients, however, they have only reported on zero ureteric injuries and not commented on whether the stents improved ureteric visualisation or not [113].

3.1.4. Ureteric Fluorescence

The drawbacks outlined above have led to development of a solution providing improved ureteric visualisation that is fast, easy and reliable by using fluorescence. Over the last 10 years, a small number of institutions have investigated ureteric fluorescence with different fluorophores and techniques. Initially, ICG was explored as the potential fluorophore for this modality given that it has well known safety profile and its approval status by the FDA and EMA. However, as it is hepatically excreted, it has to be administered via retrograde injection via the VUJ. These case series are reported for both urological [114-116], and gynaecological surgery [117]. These techniques, although providing good signal to background ratios, still require bladder instrumentation and whilst this is simpler than stent insertion, would still come with potential risks of UTI and ureteric injury. In addition, none of these studies report on the duration of ICG fluorescence nor signal to background ratios over time.

In animals, a number of other fluorophores have been explored including intravenous fluorescein in rats [118] and IR800CW-CA in rats and pigs [119, 120]. In the latter study by Tanaka *et al* [119], it was demonstrated that with intraureteral injection of IR800CW-CA that intraoperative ureteric injury could be identified by leakage of fluorescent contrast in the NIR visualisation mode. IR800CW-CA is a costly manufactured carboxylated form of

IR800CW and has since been abandoned for further development by its manufacturer LI-COR®.

Methylene blue was first explored for its fluorescent properties and ureteric use by Matsui *et al* in 2010 [34] in pigs following intravenous injection. This was taken by the same group to a first in man study where low doses of methylene blue were assessed in patients undergoing open abdominal surgery in which exposing the ureters was a planned part of the procedure [121]. The fluorescence device was an in-house manufactured mini-FLARE™ system that is not for commercial use. A similar study using an in-house device demonstrated that the ureters could be fluoresced in laparoscopic surgery in 6 patients [122]. Both technical papers demonstrate a potential feasibility for methylene blue ureteric fluorescence.

3.1.5. Aims

The aims of the work in this chapter was to further clarify the use of methylene blue ureteric fluorescence and to:

1. Compare methylene blue ureteric fluorescence identification of the ureter with white light
2. Optimise the dosing of methylene blue
3. Assess the safety of methylene blue in a larger cohort of patients
4. Assess use with a commercially manufactured device

3.2. Methods

3.2.1. Methylene blue clinical trial

3.2.1.1. Objectives

A clinical trial was designed to assess methylene blue fluorescence of the ureter during colorectal surgery at Oxford University Hospitals. The study was a phase 1/2a IDEAL [95] design being an open label, non-randomised, prospective cohort study designed to establish the proof of concept, timing, dosing, safety and efficacy. The primary objective was to compare ureteric identification during colorectal resections with white light versus methylene blue fluorescence (where patients acted as their own controls) with outcome measures being the number of ureters identified during surgery under each modality at different time points. Secondary objectives were to ascertain the optimal dose of methylene blue and timing of administration. Quantification of fluorescence over time were the outcome measures chosen to answer these objectives. The tertiary objective of safety was included to record adverse events related to methylene blue. The study was sponsored by Oxford University, fluorescence enabled equipment was provided by NOVADAQ, ethically approved by East Midlands – Derby REC (14/EM/1107) and registered on clinicaltrials.gov (NCT03177070). Advice was sought from the MHRA as to whether this trial would fall under the clinical trial regulations and it was confirmed that the study would not be a clinical trial of an investigational medicinal product (CTIMP).

3.2.1.2. Patients

Participants undergoing open or laparoscopic surgery were eligible to enter the study and were approached sequentially (according to TGB availability) in either their surgical clinic or pre-operative assessment clinic to discuss participation. A PIL was given to the participant to read at least 24 hours prior to their surgical procedure. On the day of admission for their colorectal procedure, patients were approached to consent into the study and then

assessed whether they were eligible according to the inclusion and exclusion criteria (Table 3.1). Exclusion criteria applied were purely due to safety reasons.

Inclusion Criteria	Exclusion Criteria
1. Participant is willing and able to give informed consent to participate in the study 2. Male or female aged 18 years or above 3. Patients undergoing laparoscopic or open colorectal surgery 4. In the investigator's opinion, is able and willing to comply with all study requirements	1. Patient who is unable or unwilling to give informed consent 2. Female participant who is pregnant, lactating, or planning pregnancy during the trial 3. Significant renal or hepatic impairment 4. Known allergy to methylene blue 5. Patient is at risk of serotonin syndrome including those taking serotonin re-uptake inhibitors and with known gluose-6-phosphate dehydrogenase (G6PD) deficiency

Table 3.1 Inclusion and exclusion criteria for methylene blue ureter study.

3.2.1.3. Intraoperative methods

Four dosing cohorts were assessed in the study: 0.25mg/kg, 0.5mg/kg, 0.75mg/kg and 1mg/kg. Following general anaesthetic and patient positioning, methylene blue (Proveblue, Provepharm Life Solutions, Marseille, France) was administered intravenously over 5 minutes, 5-10 minutes prior to the operating surgeon entering 'ureteric territory'. Fluorescence was assessed using the PINPOINT DR system (outlined in section 1.4) under white light followed by fluorescence mode at 5-10-minute time intervals for up to 100 minutes following methylene blue injection. Visualisation under each modality was deemed either 'visible' or 'not visible' according to the surgeon and an additional observer. Visibility was defined as the surgeon or observer being 100% certain that the ureter was visualised,

not another structure. No additional dissection to explore the ureter(s) was performed outside of the standard operative procedure to identify fluorescence. Discretion was given to the operating surgeon as to whether techniques were employed to identify a ureter not identified with white light but with fluorescence.

According to the procedure being undertaken, the ureters were classified as being either relevant or irrelevant to the procedure. Examples of relevant ureters included: left ureter in an anterior resection, both ureters during subtotal colectomy, right ureter during a right hemicolectomy. Irrelevant ureters were those that would not be routinely looked for but were observed under fluorescence for the purposes of this study. Documentation was made as to whether the ureter was visible with white light alone, fluorescence alone, both fluorescence and white light or not visible at all by the operating surgeon (primary observer) and an independent (secondary) observer. Where possible, a final assessment of the ureter(s) was made at the end of the procedure to observe whether fluorescence was still present. The order in which ureters were assessed were as follows: white light only and then fluorescence (including overlay and pure fluorescence modes).

Fluorescence was deemed 'useful to the case' where the surgeon used fluorescence mode without prompting outside of the fixed time points. At 30-days post operatively, patient notes were reviewed to collect any adverse reactions.

3.2.1.4. Statistical analysis

Descriptive statistics were used to present the majority of data arising from the study. Comparison of means across all times points between dosing cohorts from signal to background ratio data were assessed using a one-way analysis of variance. Ureteric visualisation with methylene blue or white light was analysed using generalised linear mixed

models. Random coefficient models were fitted to allow for differences between the change over time between patients, and the change over time was modelled using a second order regression equation. Baseline characteristics including dosing level were included as fixed effects to investigate whether these may explain variation between patients. Intra-observer agreement was assessed using the kappa statistic.

Signal to background ratio over time was assumed to have a normal distribution and linear mixed models were used to analyse this change over time modelled using a second order regression equation. A random coefficient model and random intercept was fitted which allowed for differences in the change over time between patients. Where there was no superiority of either method to fit the data, the random coefficient model was utilised for simplicity. To model the correlation over time within patients, the unstructured covariance matrix was used. Baseline characteristics including dosing level were included as fixed effects to investigate whether these may explain any variation between patients.

3.2.2. IRDye 800BK Ureteric Fluorescence Trial

Following assessment of IRDye 800BK, a single centre, phase 1 study was set up to assess the safety and efficacy of IRDye 800BK in fluorescing the ureter during surgery.

3.2.2.1. Objectives

As this was a phase 1 study, the 2 main objectives to be assessed were efficacy and safety. Efficacy was measured objectively by signal to background measurements over time and subjective assessment using a visual scoring system of ureteric visualisation under fluorescence and whether the ureter was visible under white light or not over time. The

scoring system utilised is outlined in Table 3.2. A score of 2 or above was defined as being positive.

Score	Description
0	No fluorescence observed
1	Weak fluorescence signal observed, not convincingly outlining the ureter
2	Weak fluorescence signal observed, convincingly outlining the ureter
3	Strong fluorescence signal clearly outlining the ureter

Table 3.2 - IRDye Ureter Trial Visual Assessment Scoring System.

A 'dose optimisation' phase in the first 12 participants was designed in order to ascertain the best dose followed by a dose expansion phase with the identified dose. A starting dose of 0.06mg/kg was used based on efficacy in animal testing (unpublished data by LI-COR). Three patients would be given a dose, following which the independent data safety monitoring committee (DSMC) would meet to review the safety and efficacy data and decide as to whether the dose would be increased by 0.03mg/kg or decreased by 0.015mg/kg (Figure 3.1). In addition to the safety and efficacy data, stopping rules for dose escalation were included as:

1. A severe serious adverse reaction (i.e. a serious adverse event considered at least possibly related to the IMP administration) in one subject in this trial or any other trial at a particular dose of the same IMP
2. A severe non-serious adverse reaction (i.e. severe non-serious adverse events considered at least possibly related to the IMP administration) in two subjects in the same cohort independently, within the same system-organ-class.

The optimal dose was defined as:

1. No serious adverse reaction or serious non-severe adverse reaction related to the IMP at that dose in any patient previously being dosed at that level.
2. Highest mean fluorescence score throughout all fluorescent readings amongst all patients in that cohort.
3. Highest signal to background ratio across all readings amongst all patients in the cohort. This will account for possible higher background signals observed in the higher dosing cohorts.

As well as adverse events, renal and liver function of the different dosing cohorts during the dose optimisation phase was also assessed.

3.2.2.2. Patients

Patients were eligible to enter the study if they were undergoing laparoscopic colorectal resection. Inclusion and exclusion criteria are listed in Table 3.3. Potential participants were approached in either the surgical clinic or the pre-operative assessment clinic. After having at least 24 hours to read the information sheet, they were invited to consent to enter the study. Eligibility was confirmed, and baseline assessments were recorded consisting of demographics, medical history, medications, allergies, physical examination, blood tests, ECG and pregnancy test (if applicable).

Inclusion Criteria	Exclusion Criteria
1. Participant willing and able to give informed consent for participation in the trial 2. Male or female aged 18 years or above 3. Undergoing elective laparoscopic colorectal surgery 4. Available laboratory and ECG results within 3 months of enrolment 5. Female participant of child bearing potential and male participants whose partner is of child bearing potential willing to ensure that they or their partner use effective contraception during the trial and for 3 months thereafter [*] 6. In the investigator's opinion is willing and able to comply with all trial requirements	1. Female participant who is pregnant, lactating or planning pregnancy throughout the trial 2. Significant renal impairment (eGFR < 50mL/min/1.73m^2) 3. Significant liver impairment defined as a. AST $\geq$ 3.0 x ULN or b. ALT $\geq$ 3.0 x ULN or c. Total serum bilirubin $\geq$ 1.5 x ULN 4. Involved with any other research trial involving an unlicensed medication in the past 12 weeks 5. Any of significant disease or disorder that may put the participant at risk 6. Known allergy to D-Mannitol or citric acid

Table 3.3 IRDye Ureter Trial - Inclusion and Exclusion Criteria

[*] Women of child bearing potential defined as per the Clinical Trial Facilitation Group guidelines relating to contraception and pregnancy in clinical trials.

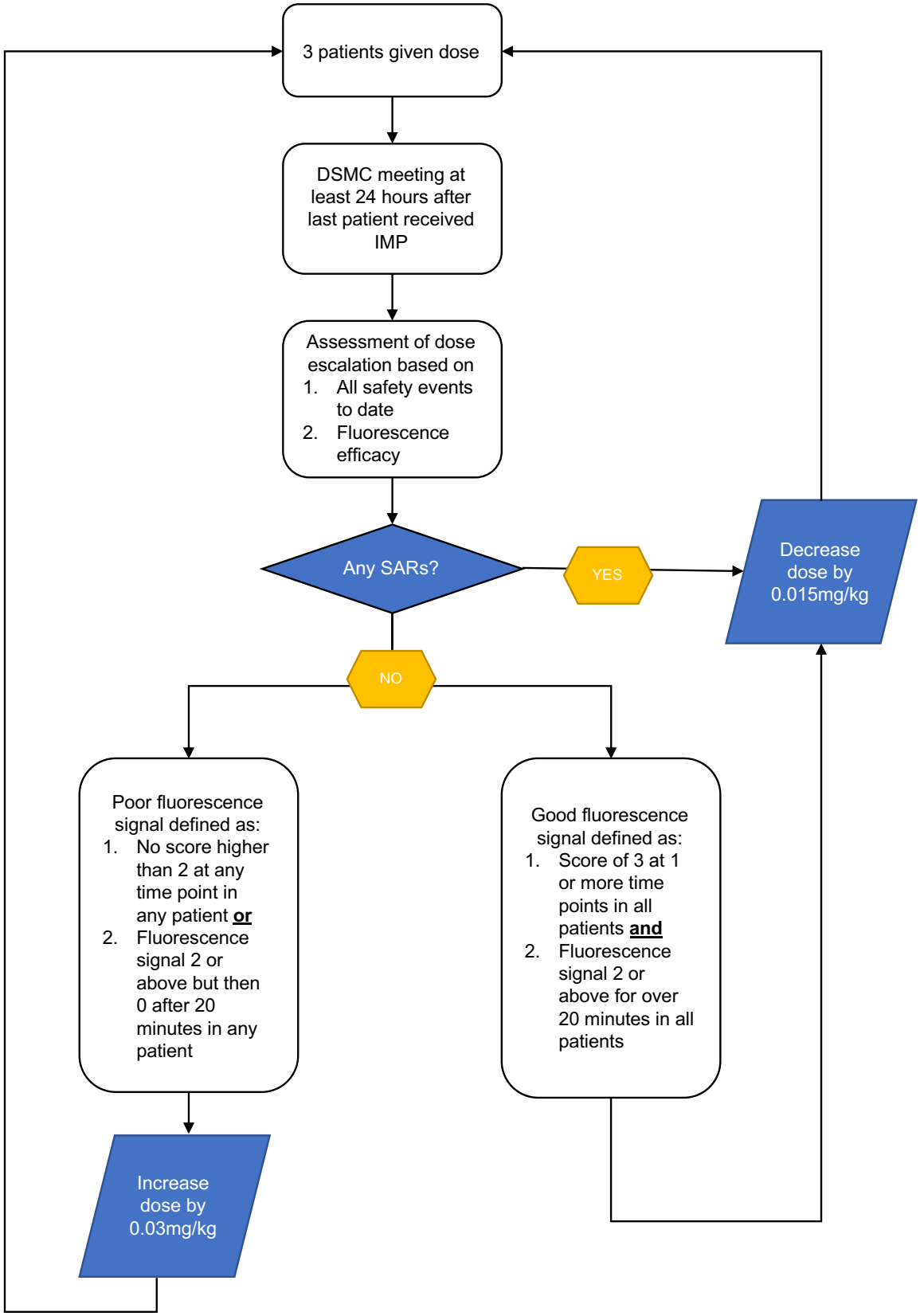

Figure 3.1 - Dose optimisation decision tree for DSMC in IRDye Ureter Study

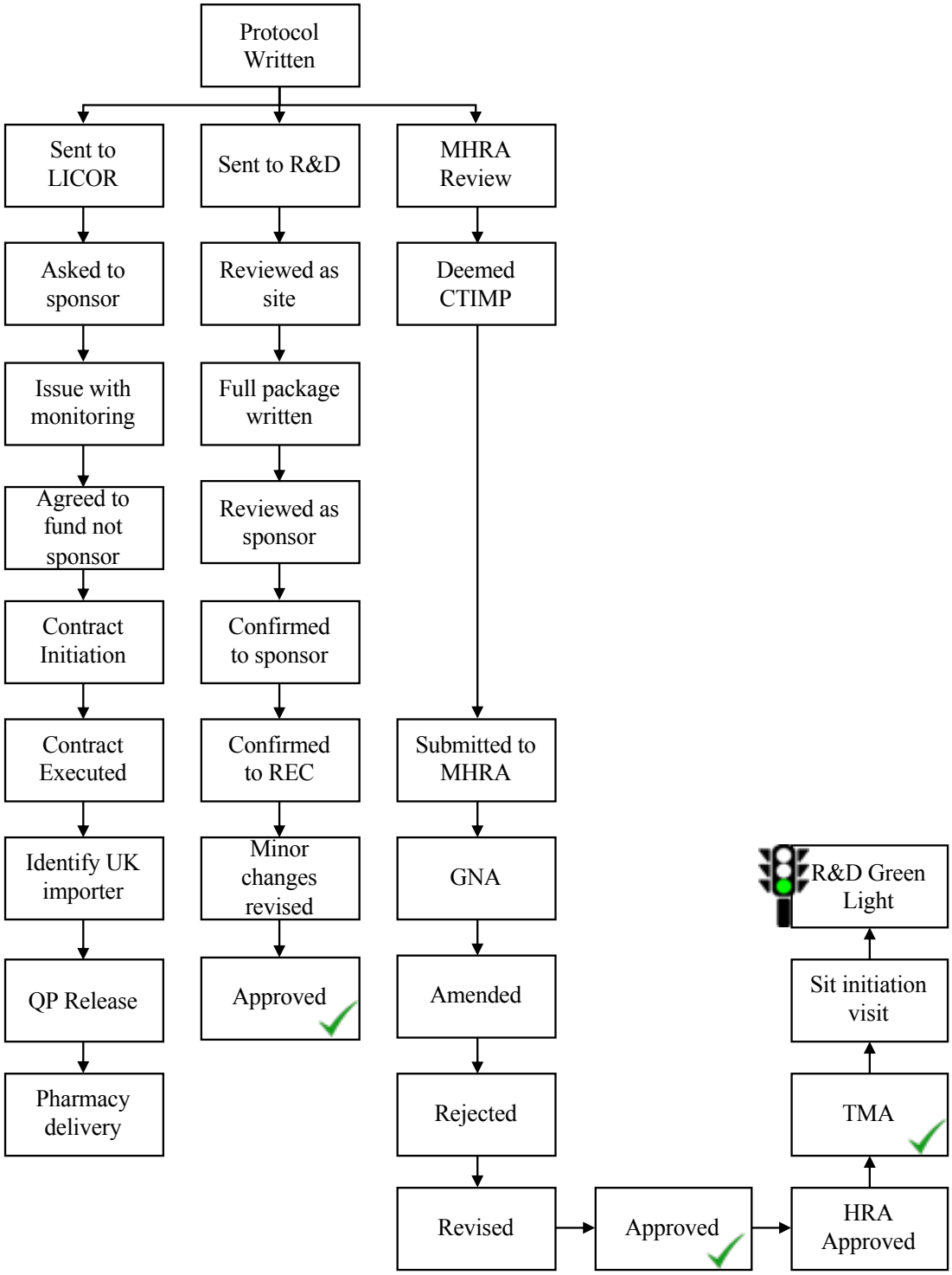

Figure 3.2: IR800 BK Clinical Trial Application and Approval Process. R&D, research & development; MHRA, Medicines and Healthcare Regulatory Authority; CTIMP, Clinical Trial of an Investigational Medicinal Product; QP, Qualified Person; GNA, Grounds for non-acceptance; HRA, Health Research Authority, TMA, Trust Management Approval.

3.2.3. Assessment of fluorescence with different devices

Where time allowed during the procedure, comparison of different devices with IRDye 800BK fluorescence was used. During the trial, 3 different devices were utilised: Pinpoint, Stryker and Storz. Where time during the case permitted, a second device was used to assess the fluorescence and the signal to background ratio recorded as described previously. Comparison of devices were assessed using the aforementioned statistical analyses.

3.3. Results

3.3.1. Recruitment

From August 2016 to April 2017, 56 patients were screened to participate in the study. Only four patients declined to participate, and 6 patients were ineligible as they did not meet the inclusion or exclusion criteria. Of 46 participants consented, the laparoscopes were not sterilised in time for 4 of these cases and therefore methylene blue was not administered. Of the remaining 42 patients receiving methylene blue, 2 were excluded from analysis (Figure 3.3).

In order to recruit at a steady rate, it was estimated that at least 1 patient would complete the study per week from all of the colorectal lists. Initially, the recruitment rate met this target, however, after more surgeons in the department became interested in the technology and patients found it acceptable as there was a safety element to the study, recruitment exceeded the recruitment targets (Figure 3.4). Six surgeons were involved in the study and the number of readings and cases per surgeon is outlined in Figure 3.5.

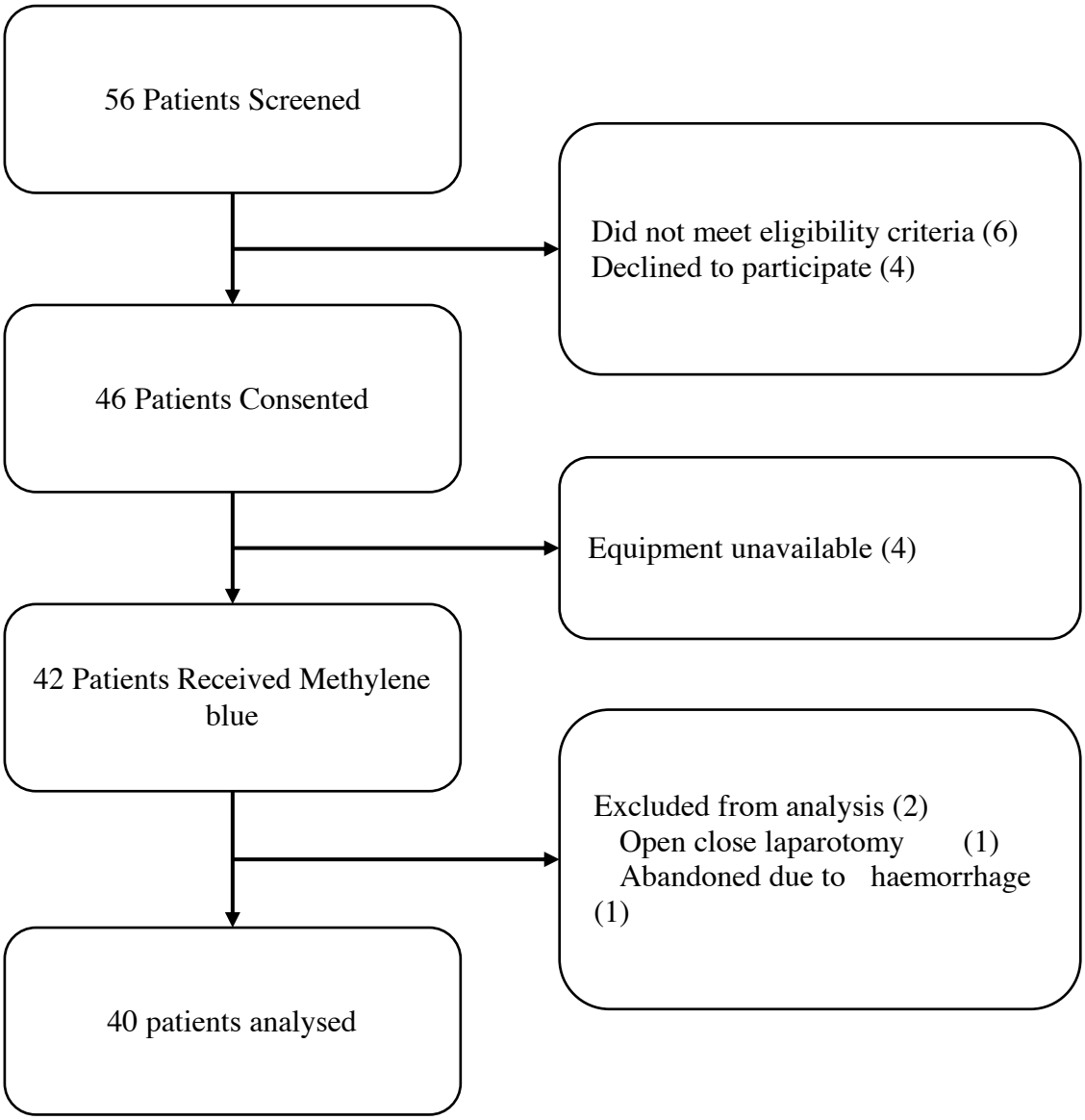

Figure 3.3 - Patient recruitment flow diagram for methylene blue ureter study.

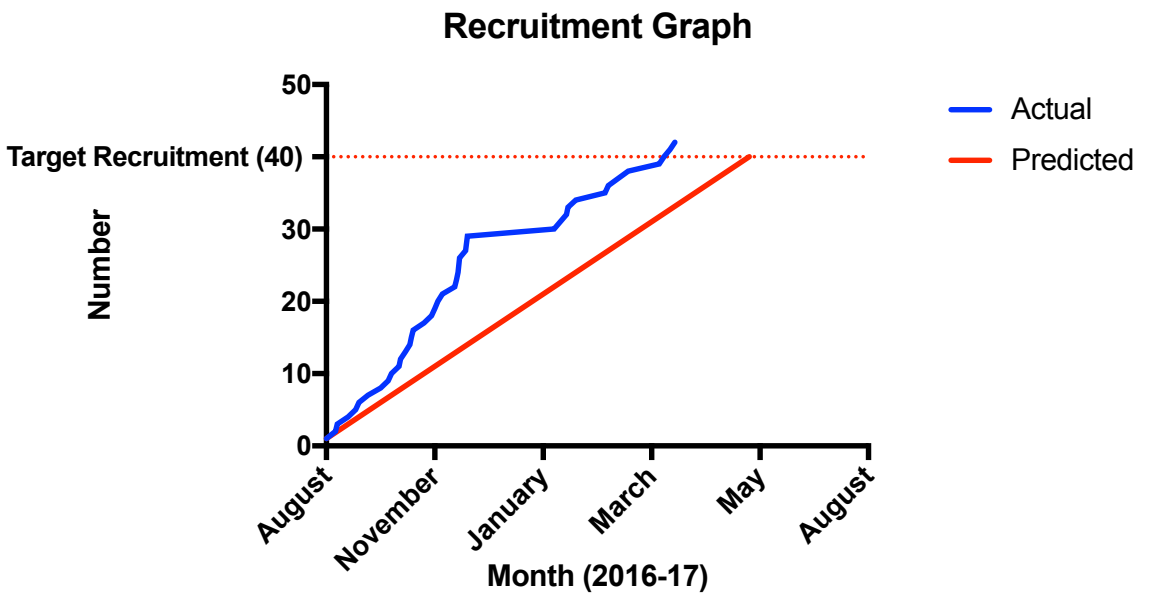

Figure 3.4 - Recruitment graph for the methylene blue ureter study

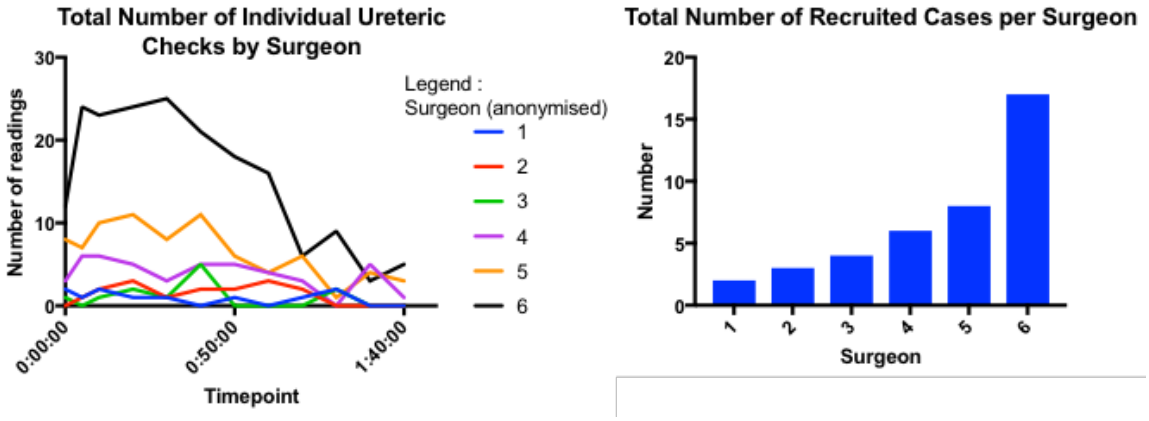

Figure 3.5 - Number of cases recruited to study by surgeon (anonymised)

1.1.1. Baseline demographics

Twenty-one participants were male. Median BMI was 27 (range 13-39) following a normal distribution similar to that of a standard colorectal patient population (Figure 3.6). Median age was 66 (39-91) and most patients were male (21, 52.5%). Table 3.4 outlines the indication for surgery with the majority being anterior resections for cancer (48%). Ureteric

fluorescence was assessed in a variety of different indications for resection including those where the ureter may be more difficult to identify (e.g. endometriosis, Crohn's disease and re-do surgery). Ninety percent of cases were undertaken laparoscopically.

Dosing cohorts were as follows: 4 for 0.25mg/kg; 11 for 0.5mg/kg; 12 for 0.75mg/kg and 13 for 1mg/kg.

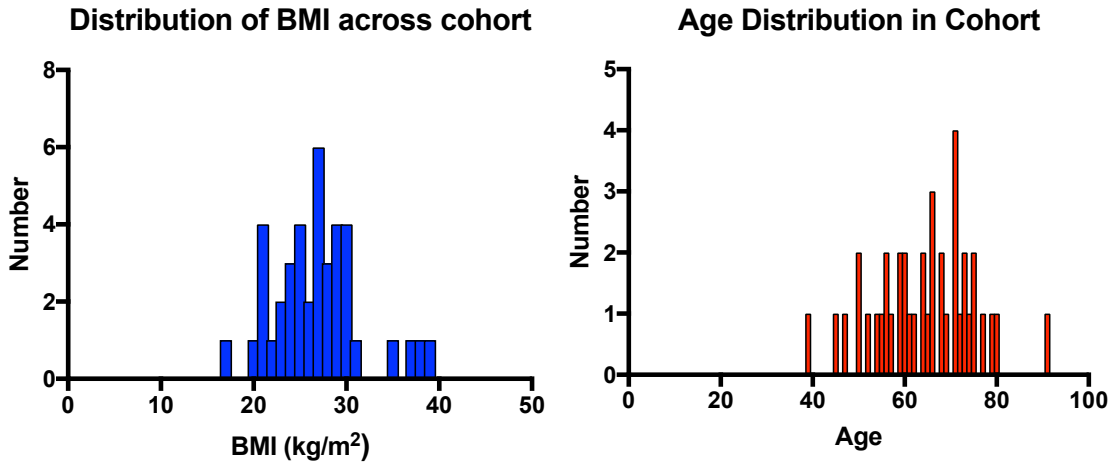

Figure 3.6 - Distribution of BMI and Age across patients in methylene blue trial. BMI appeared to have a normal distribution in keeping with the standard cohort of colorectal patients. Age was positively skewed towards an older age group, similar to the standard colorectal patient cohort.

Procedure *(and indication)*	**n**
Anterior Resection	
Cancer	*19*
Diverticular disease	*3*
Endometriosis	*1*
Right Hemicolectomy	
Cancer	*6*
APER	
Cancer	*2*
Subtotal colectomy	
Cancer	*1*
Ulcerative colitis	*1*
Hartmann's procedure	
Cancer	*1*
Diverticular disease (colovaginal fistula)	*1*
Take down anastomosis & proctectomy	
Anterior resection syndrome	*1*
Re-do proctocolectomy	
Cancer (recurrence)	*1*
Combined right hemicolectomy & anterior resection	*1*
Cancer (+ bilateral oophorectomy)	
Panproctocolectomy	
Crohn's disease	*1*
Reversal of Hartmann's	
Previous diverticular resection	*1*

Table 3.4 - Breakdown of patients in the study by operation type and indication. The majority of cases were anterior resections for cancer.

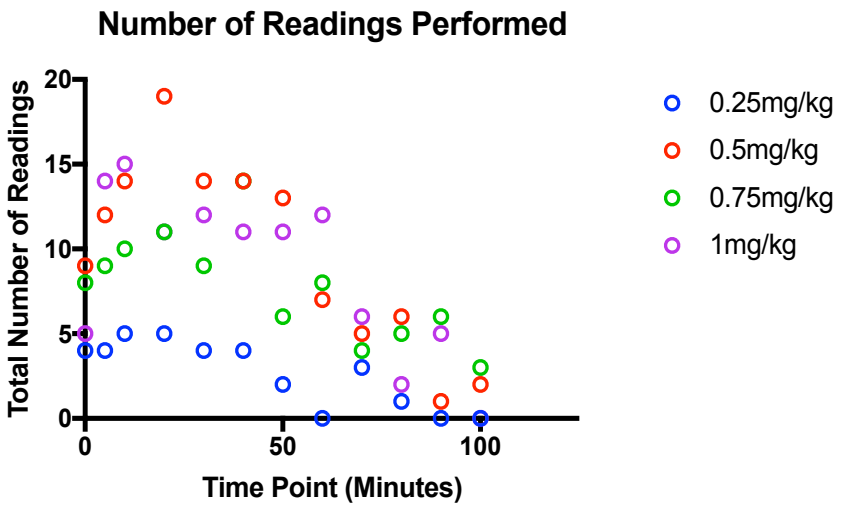

Figure 3.7 - Total number of ureteric fluorescence readings per dosing cohort over time. The majority of readings fell between 0 and 75 minutes across all dosing cohorts.

1.1.1. Subjective assessment of ureteric fluorescence with methylene blue

In the 40 participants, there were a total of 351 ureteric visualisations within 100 minutes with a median of 8.5 assessments per patient (range 1-21) (Figure 3.7). As time progressed, less visualisations occurred with most readings occurring between 0 and 50 minutes.

Sixty-nine ureters were imaged out of the 40 patients recruited in total accounting for a number of patients where both the right and left ureter was assessed within the case (Figure 3.8). Eleven ureters were not assessed which consisted of 6 left ureters during right hemicolectomy, 4 right ureters during a left sided resection and one right ureter during a subtotal colectomy. Nearly all ureters (n=64, 93%) were visualised, at any single point, with methylene blue fluorescence. Of the 43 relevant ureters, the majority (n=33, 76.7%) were seen with both modalities throughout the case, in 16, the ureter was seen initially with both white light and methylene blue at the same time point. A further 12 were seen first with methylene blue (i.e. not initially seen with white light) and were subsequently seen with

white light later in the case (median time of 30 minutes earlier, range 10-70 minutes). Five relevant ureters were seen initially with white light and subsequently with methylene blue a median of 5 minutes later (range 5-50 minutes). In 9 relevant ureters, the ureter was only ever visible with fluorescence throughout the case and was never visualised with white light. No relevant ureters were seen with only white light throughout and 1 relevant ureter was not seen with either modality during the case which was a limited resection right hemicolectomy.

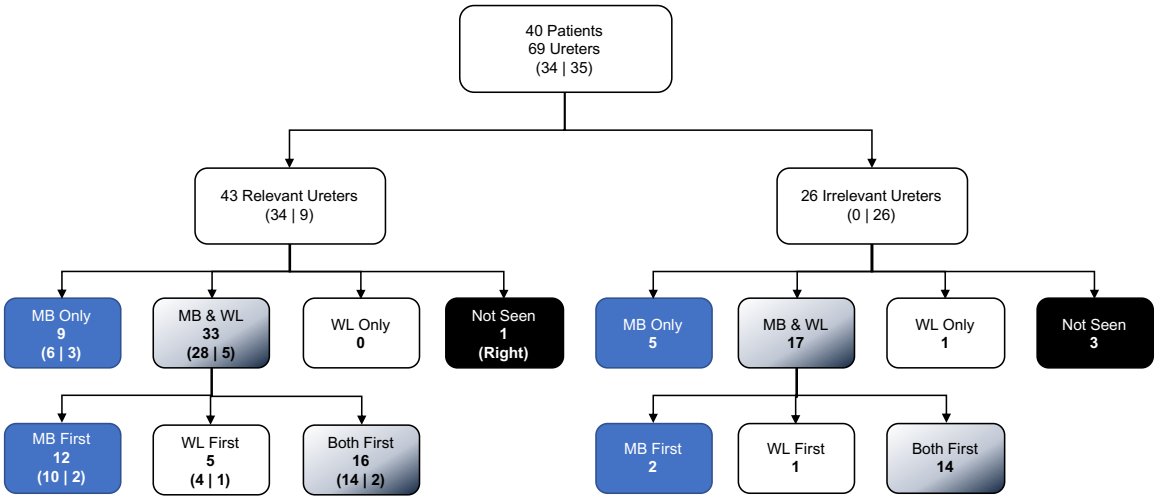

Figure 3.8 - Subjective visualisation of the ureter divided by ureters relevant and irrelevant to the procedure. Numbers in brackets represent laterality of ureter (left | right). Most ureters were seen using both modalities (white light and methylene blue).

Of the irrelevant ureters (n=26), fourteen were visualised initially with both modalities. Two irrelevant ureters were seen initially with methylene blue 35 and 70 minutes prior to visualisation with white light and one irrelevant ureter was seen 20 minutes with white light prior to being seen with methylene blue fluorescence. Five irrelevant ureters were seen only under fluorescence throughout the whole case, 1 was only seen with white light and 3 ureters were not visualised under any modality.

A

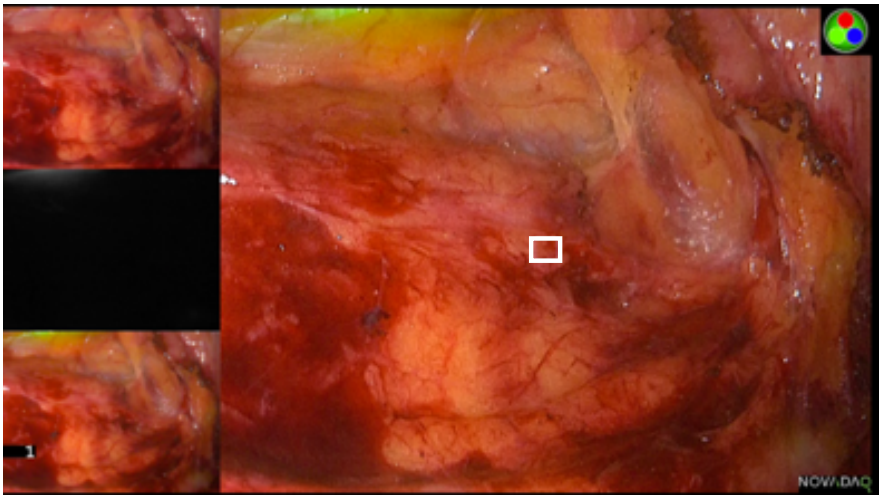

B

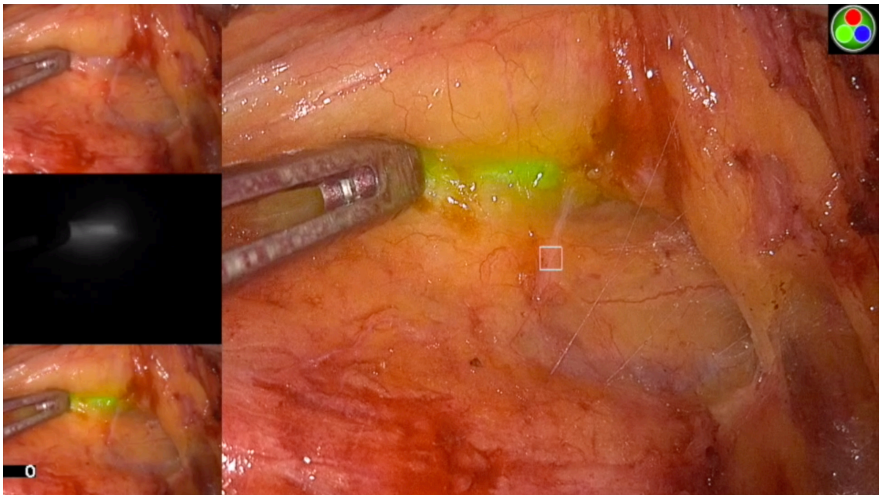

Figure 3.9 - Assessment of ureteric fluorescence in NIR mode. A - The surgeon has been asked to place the centre of the image (white square) where they believe the ureter to lie prior to enabling the fluorescence mode. Note the strong fluorescent signal at the top of the image away from the centre. When moving closer to the area of fluorescence, the ureter is clearly seen (B). Image captured using the PINPOINT DR in 'overlay' mode where the centre image is a colour image with green fluorescent signal in overlay. The three panels on the left from top to bottom are colour image without fluorescence, SPY mode (black and white fluorescence) and overlay mode.

Of the forty patients analysed, in 13 (32.5%) of the operations, the operating surgeon utilised the fluorescence modality outside of the fixed time points indicating that they found it useful to the procedure. In 10 of these, the ureter was revealed to be in a slightly different location

under fluorescence to where it was thought to be in white light (Figure 3.9). In 2 participants, the operative plan was altered. The first was an obese male (BMI 39) undergoing anterior resection where, whilst performing the medial to lateral dissection underneath the IMA, the ureter could not be visualised due to extensive retroperitoneal fat. The urologists were requested to the operating theatre to place a ureteric stent and during the set-up, a strong bolus of fluorescence signal could be seen through the retroperitoneal fat indicating the ureter was in the correct location and not at risk if injury prior to vessel division. The second case was a participant undergoing a Hartmann's procedure for a diverticular colovesical fistula. It was suspected after division of what was thought to be a sigmoidal vessel, that it was in fact the ureter. Urologists were again requested but, as in the previous case, fluorescence subsequently outlined the location of the ureter clearly.

3.3.2. Objective assessment of ureteric fluorescence with methylene blue

For all doses combined, the mean signal to background ratio of methylene blue fluorescence was 4.41 (SD 2.57, 95% CI 4.09 to 4.73). Mean signal to background ratio was significantly different between dosing cohorts ($p < 0.0001$) being lowest in the 1mg/kg dosing cohort at 3.656 (SD 1.89, 95% CI 3.37 to 3.94) and highest in the 0.75mg/kg cohort at 5.294 (SD 2.73, 95% CI 4.84 to 5.75). When comparing mean signal to background ratio of each dosing cohort with every other dosing cohort (Table 3.5), only the lower ratio of 1mg/kg compared with 0.75mg/kg and 0.5mg/kg reached statistical significance ($p<0.0001$ and $p=0.0396$ respectively).

When assessing the different doses on signal to background ratio, a random effects linear regression model was fitted. The signal to background ratio declines at different rates over time with all doses (Figure 3.11) and were statistically significantly different ($p=0.0003$). As the dose increases, the rate of signal to background ratio decline decreases. The 2 lowest

doses significantly decreased in signal to background ratio over time with 0.25mg/kg having the highest rate of decline (slope -0.1165, 95% CI -0.19 to -0.05, p=0.0019) followed by 0.05mg/kg (slope -0.3698, 95% CI -0.05 to -0.02, p<0.0001). X intercepts were calculated for a Y value (signal to background ratio) of 1. The x intercept of the dosing cohorts 0.25mg/kg and 0.5mg/kg was 54.62 minutes (95% CI 41.01 to 103.8) and 130.2 minutes (95% CI 100.7 to 203.6) respectively. 0.75mg/kg and 1mg/kg cohorts had a significantly slower rate of decline (slope -0.01, 95% CI -0.03 to 0.003, p=0.1156) and (slope -0.006, 95% CI -0.017 to 0.005, p=0.3112) respectively. At 0.75mg/kg the x intercept is 376.9 minutes (95% CI 191.7 to infinity) and 251 minutes (95% CI 191.8 to infinity) for 1mg/kg likely to indicate that 100 minutes is not a sufficient amount of time to adequately assess the decay in signal. At the higher doses, the logistic regression equation did not reach significance and would require assessment over a longer period to obtain a narrower 95% CI for the x intercept.

In this trial, visualisation of the ureter is more likely to occur under fluorescence rather than white light (OR 4.5176, 95% 3.33 – 6.133, p<0.0001). To assess the effect of 'ureteric relevance' on fluorescence visualisation, a logistic regression model was utilised. The odds ratio for visibility by methylene blue but not white light comparing relevant with non-relevant ureters, derived from fitting the random intercepts logistic regression model with no covariates was 0.66 (95% CI 0.32, 1.38, p=0.27). The probability for visibility by methylene blue but not white light varies over time with the maximum at 58 minutes from baseline (Figure 3.12).

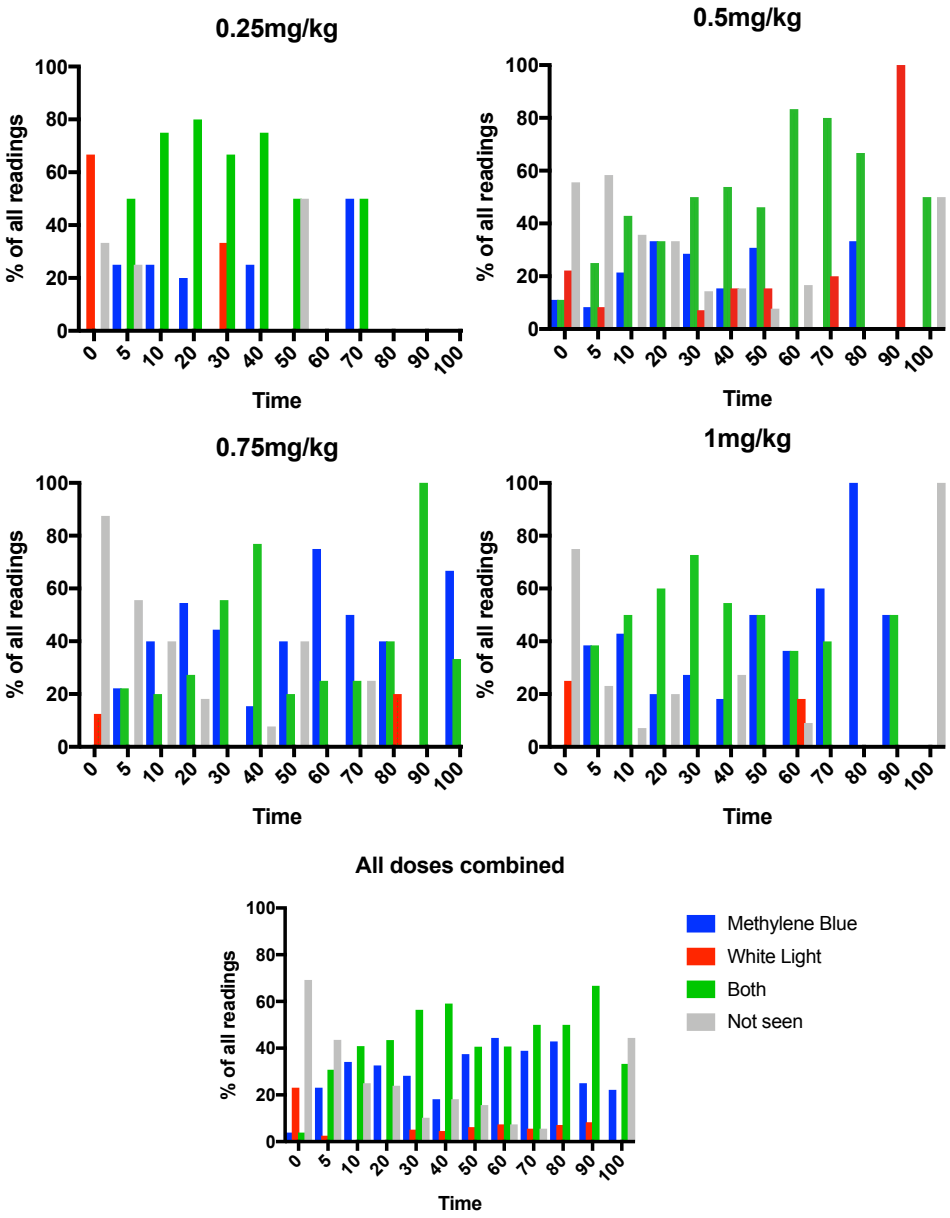

Figure 3.10 - Proportion of ureteric visualisations by modality over time. From clockwise, each figure represents the modality by which the ureter was visualised by proportion over time for 0.25mg/kg, 0.5mg/kg, 0.75mg/kg and 1mg/kg. In the lower doses (0.25mg/kg and 0.5mg/kg), a higher proportion were seen with both modalities, whereas in the higher doses, methylene blue identified the ureter in more cases. When all doses are combined, most of the ureters are seen by both modalities at each time point, followed by methylene blue fluorescence.

Comparison	Mean signal to background ratio 1	Mean signal to background ratio 2	Adjusted p value
1mg/kg vs. 0.75mg/kg	3.656	5.294	<0.0001*
1mg/kg vs. 0.5mg/kg	3.656	4.39	0.0396*
1mg/kg vs. 0.25mg/kg	3.656	4.668	0.1532
0.75mg/kg vs. 0.5mg/kg	5.294	4.39	0.0104
0.75mg/kg vs. 0.25mg/kg	5.294	4.668	0.5758
0.5mg/kg vs. 0.25mg/kg	4.39	4.668	0.9407

Table 3.5 - Table comparing mean signal to background ratios between dosing cohorts. Mean signal to background ratio of each dosing cohort is compared using ANOVA and p-value adjustment for multiple comparisons. Ratio 1 in column 2 refers to the first dosing cohort mentioned in the 'comparison' column and ratio 2 in column3 refers to the second dosing cohort mentioned in the 'comparison' column.

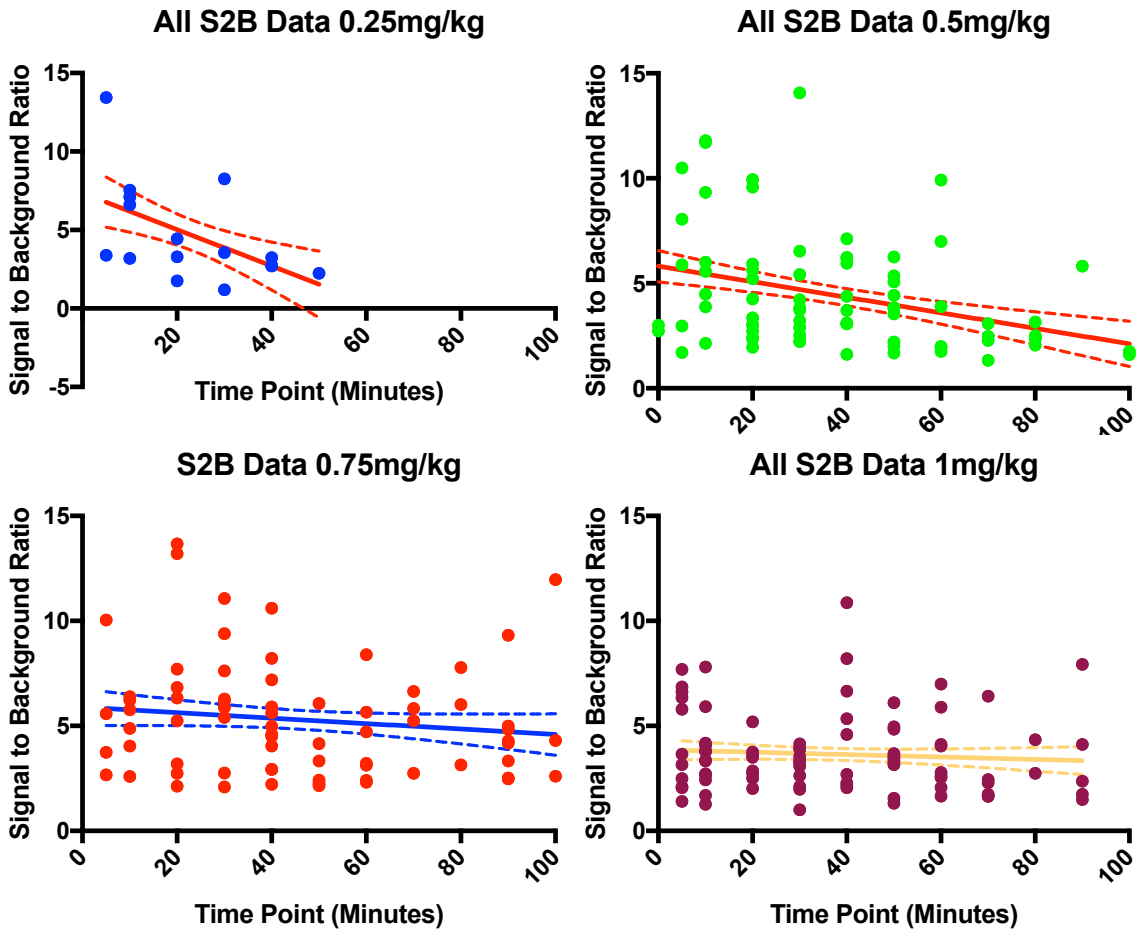

Figure 3.11 - Signal to background ratio over time by dose. Dots represent individual signal to background ratio of a single ureteric visualisation. Solid line represents linear regression line with dotted lines representing 95% confidence intervals.

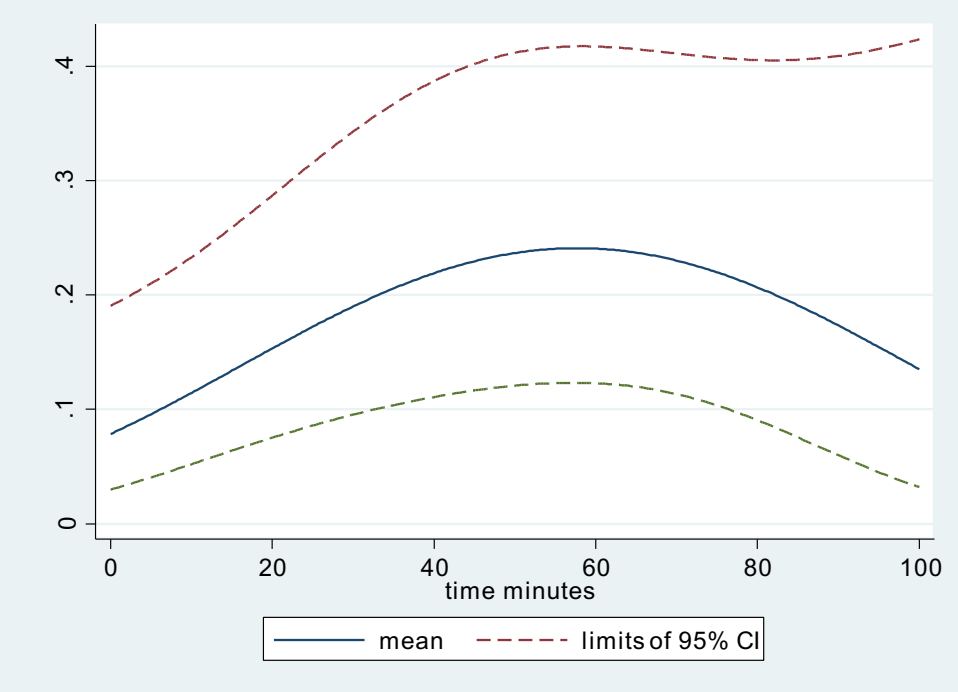

Figure 3.12 - Mean probability of methylene blue being better than white light over time. Fitted using a non-linear regression curve. Dotted lines represent 95% confidence interval.

3.4. Ureteric fluorescence with IRDye 800BK

3.4.1. Cross-talk between IRDye 800BK and methylene blue

Following some success in the methylene blue ureter trial, IRDye 800BK had been manufactured by LICOR to be renally excreted and with similar fluorescent properties to ICG. This was offered to the author to assess for safety and efficacy for a first in man trial following successful animal work undertaken by LICOR. In addition to IRDye 800BK alone, it was important to compare this new dye with methylene blue and two potential trial designs were explored:

1. IRDye 800BK administered at the same time as methylene blue in all participants and to assess ureteric fluorescence using a dual wavelength device, comparing fluorescence strength between each wavelength with white light.
2. IRDye 800BK administered alone.

Initially option 1 was pursued as being the most useful. Concern was explored over whether there would be any effect on fluorescence interpretation between devices using different wavelengths where both methylene blue and IRDye 800BK were present in the region of interest. In order to assess this, increasing doses of IRDye 800BK and methylene blue were visualised under both a 660nm and 785nm fluorescence system in separate Eppendorf tubes, and in combination (Figure 3.13). On two-way ANOVA with p-values corrected for multiple comparisons, there was a significant difference ($p<0.0001$) between all combinations at each concentration in both 660nm and 785nm. The main concern was that whilst there was minimal signal from methylene blue at 785nm, there was significant signal emitted from IRDye 800BK at 660nm at both 1mg/mL, 0.1mg/mL and 0.01mg/mL which would confuse assessments made in vivo at this wavelength.

The decision was therefore made that an in-vivo use of both IRDye 800BK and methylene blue could not be pursued. Therefore, the methodology of choice was to use IRDye 800BK alone and to compare the historic data from the methylene blue trial with the IRDye 800BK trial.

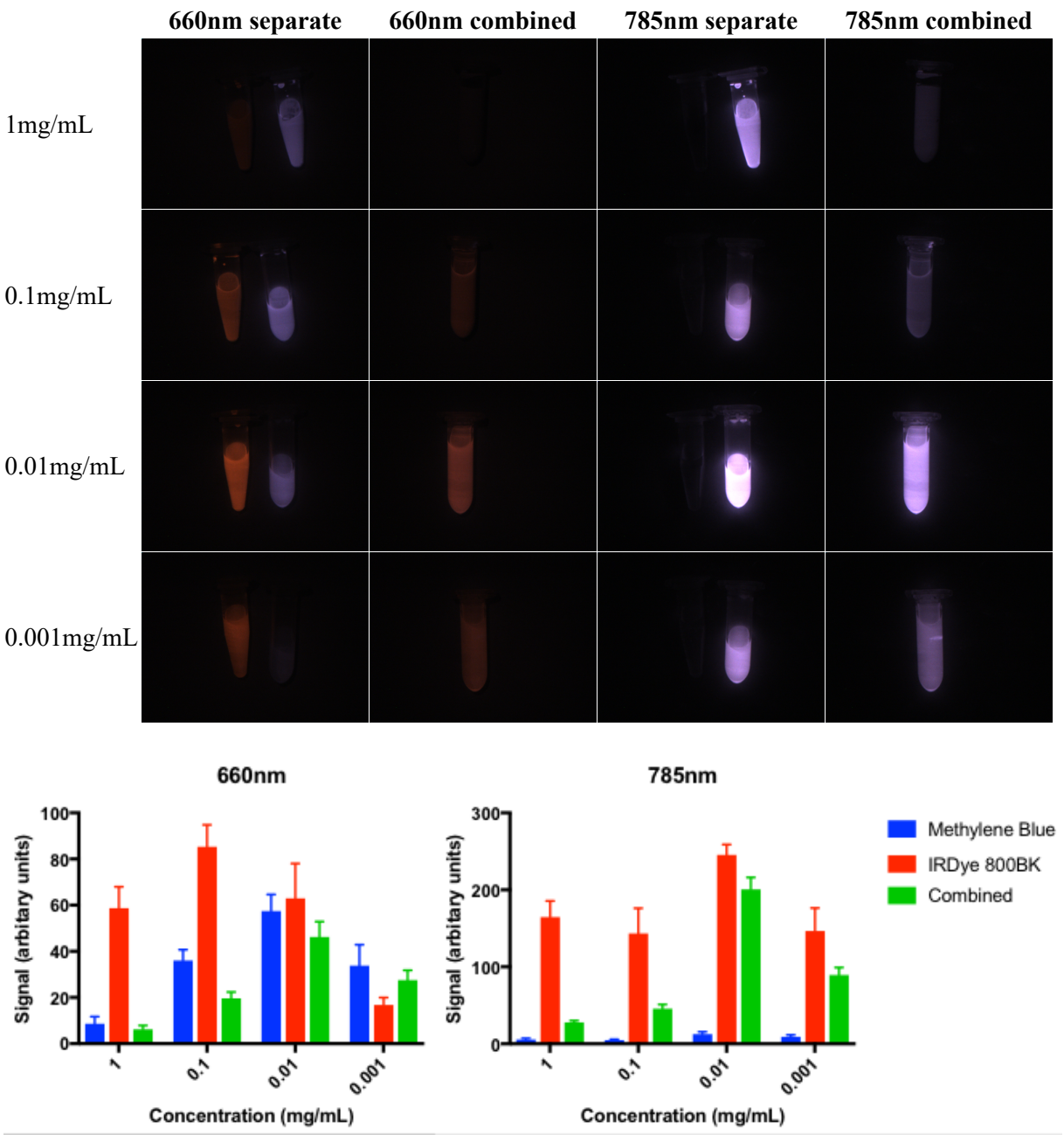

Figure 3.13 - Assessment of cross-talk between methylene blue and IRDye 800BK at 660nm and 785nm. Top table represent images of Eppendorf tubes containing methylene blue and IRDye 800BK either separately or combined at different concentrations. When dyes are shown separately, methylene blue is the Eppendorf tube and IRDye 800BK is the tube on the right. Bottom graphs represent mean signal (bars = standard deviation) of each dye combination at the varying concentration.

3.4.2. Recruitment

From April 2018 to September 2018, 107 patients identified through MDT (n=56) or operating lists (n=51) were screened for eligibility into the study (Figure 3.14). Seventeen patients were ineligible: not offered resection (n=10), eGFR <50 (n=3), ineligible operation (n=3), inappropriate clinical results (n=1). Twenty-two patients met the eligibility criteria but were not approached due to the following reasons: dye not available on operation date (n=7), DSMC required prior to further recruitment (n=2), clash with another patient or less than 24 hours since previous patient during dose optimisation phase (n=10), TGB not present on day of case (n=1) and patient declined discussion (n=2). The remaining 68 patients were consulted regarding trial participation and handed the PIL. Of these, twenty, were not consented due to: clash with other participant (n=5), dye not available on day (n=4), operation date postponed (n=2) and patient declining to consent (n=9), leaving 48 participants recruited to the study. Eight recruited participants were withdrawn due to rescheduling of case (n=3), IMP not being available (n=1), no longer fit for surgery (n=1), patient request to withdraw (n=1), TGB not available for case (n=1) and over recruitment (n=1) leaving 40 participants who received IRDye 800BK as part of the study. Thirty-nine participants were followed up until 30 days for adverse effects. One participant died post-operatively due to necrotising fasciitis unrelated to IRDye 800BK administration.

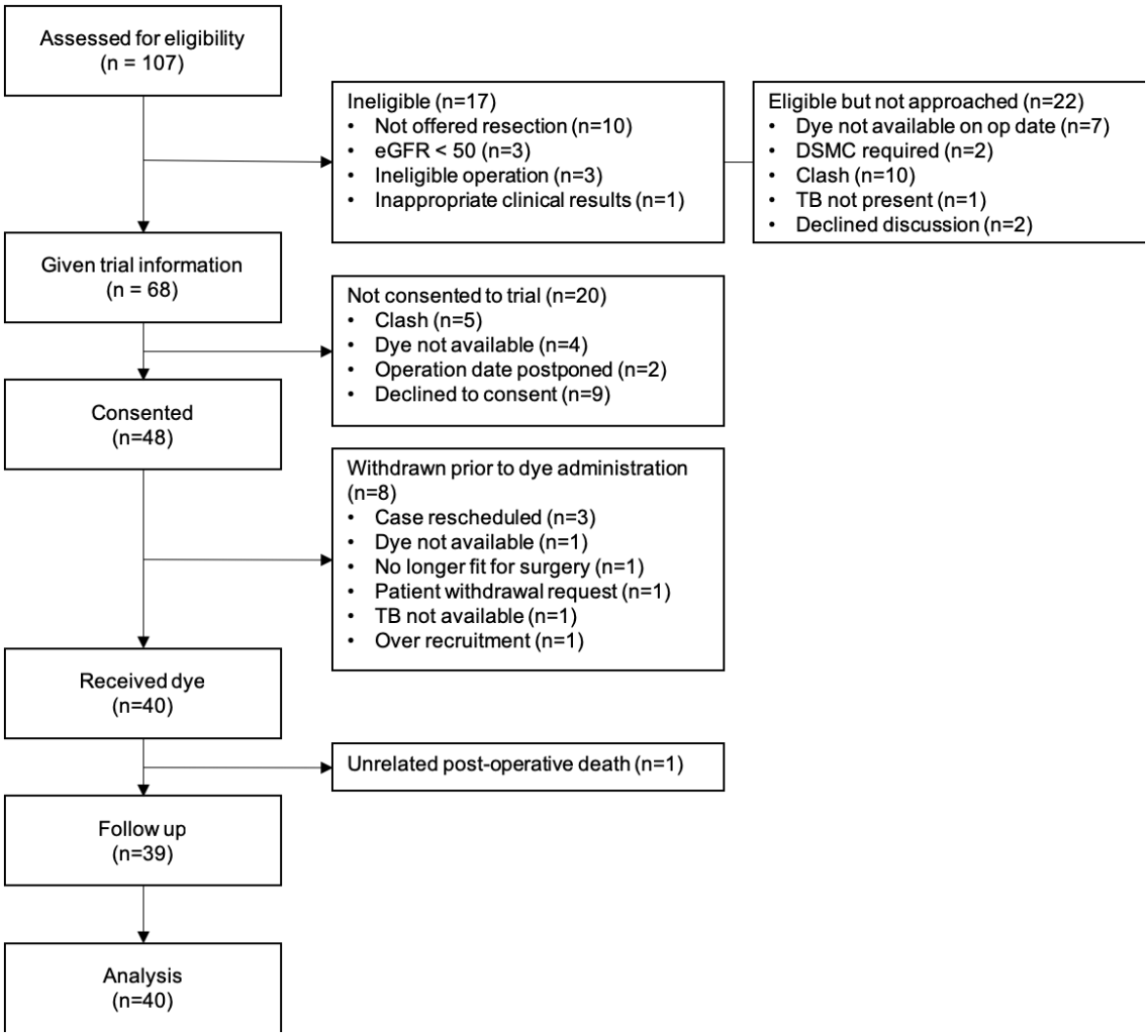

Figure 3.14 - IR800 BK ureter clinical trial flow diagram.

Actual recruitment to the study during the dose optimisation stage was in line with predicted recruitment. During the dose expansion phase, recruitment exceeded the planned recruitment target of 1.5 recruited participants per week (Figure 3.15).

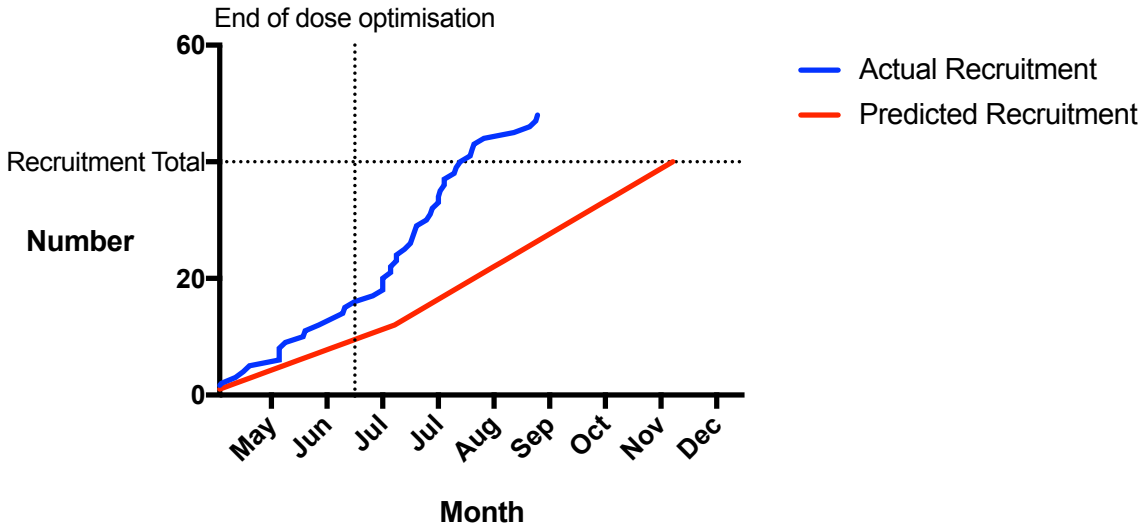

Figure 3.15 - Actual and predicted recruitment during the IR800 ureter study. Recruitment was predicted at 1 participant per week throughout the dose optimisation phase and 1.5 participants in the subsequent dose optimisation phase. Over-recruitment was necessary to replace withdrawals.

3.4.3. Baseline demographics

Twenty-two participants were male. The median age was 65 (IQR 16.75) and BMI ranged from 20 to 42 (median 26.1, IQR 6.4) (Figure 3.16). The majority of cases (n=38) were for cancer being low anterior resections (n=14), high anterior resections (n=13), right hemicolectomy (n=5), APER (n=3), proctocolectomy (n=2) and left hemicolectomy (n=1). Benign cases included a proctocolectomy for ulcerative colitis (n=1) and reversal of Hartmann's procedure (n=1).

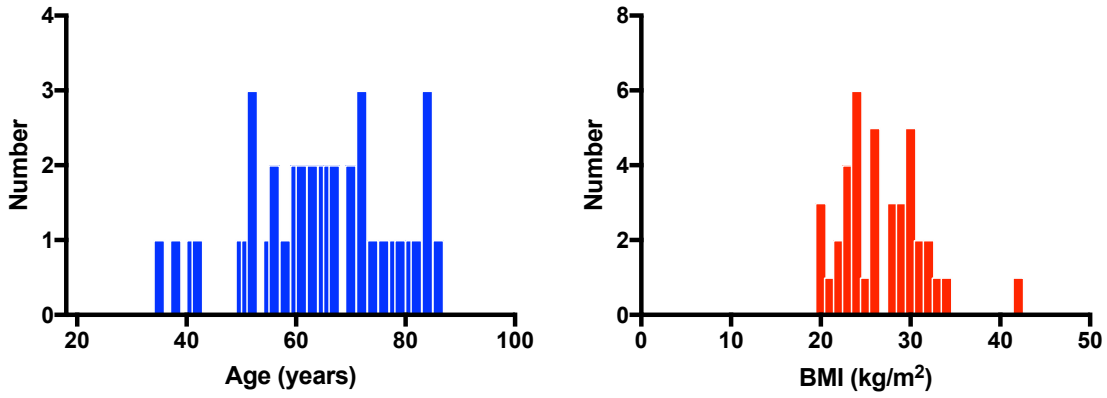

Figure 3.16 - Graphical representation of age (left) and BMI (right) from IR800 ureter patients.

Demographic	Dosing cohort			
	1	2	3	4
Dose (mg/kg)	0.06	0.045	0.075	0.06
Gender				
Male	1	1	3	2
Female	2	2	0	1
Median age (range)	61 (52-79)	52 (51-66)	42 (35-55)	72 (65-84)
Median BMI (range)	24.6 (21-30)	33.8 (26-42)	26.7 (23-31)	23.5 (20-28)
Procedure				
Low Anterior	2	2	1	2
High Anterior	1		1	1
Right		1		
Hemicolectomy			1	
Proctocolectomy				

Table 3.6 - Demographics divided by dosing cohort during dose optimisation stage.

3.4.4. Dose optimisation stage

During the dose optimisation stage, demographics were similar to the entire cohort with 6 male participants and 6 female participants with a median age of 58 (IQR 15.75) and BMI ranging from 19.69 to 42.15 (median 25.71, IQR 8.1). All cases during the dose optimisation phase were cancer resections: low anterior resection (n=7), high anterior resection (n=3), right hemicolectomy (n=1) and proctocolectomy (n=1). A breakdown of these demographics by dosing cohort is outlined in Table 3.6.

Each dosing escalation and de-escalation decision was made by the DSMC as outlined in Figure 3.1. The starting dose was 0.06mg/kg and, following the first 3 participants, a decision to decrease the dose to 0.045mg/kg was made. After a further 3 participants at this dose the dose was increased. Finally, after the penultimate cohort was dosed at 0.075mg/kg a decision to decrease the dose back to repeat the dose of 0.06mg/kg was made (Table 3.7).

ID Number	Dosing Cohort (mg/kg)	Score of 3 at any point?	Score of 2 beyond 20 minutes?	Number of AEs (serious)	Related AEs (related)	Decision
IRU-01	0.06	Yes	Yes	2 (0)	0	Decrease
IRU-02	0.06	Yes	Yes	1 (1)	0	
IRU-03	0.06	Yes	Yes	1 (0)	0	
IRU-05	0.045	No	Yes	1 (0)	0	Increase
IRU-07	0.045	No	Yes	1 (0)	0	
IRU-08	0.045	No	Yes	0	0	
IRU-06	0.075	Yes	Yes	0	0	Decrease
IRU-10	0.075	Yes	Yes	0	0	
IRU-11	0.075	Yes	Yes	0	0	

Table 3.7 - Subjective and safety data from dosing cohorts during dose optimisation stage. Table outlines all three participants in each dosing cohort, the fluorescent score of 3 at any time point and whether the fluorescent score of 2 extended beyond 20 minutes. Adverse events are represented as numbers with serious adverse events in brackets.

3.4.4.1. Optimal dose decision efficacy

Signal to background ratio across the different cohorts (Figure 3.17A) was 1.75 for 0.06mg/kg (95% CI 1.57 to 1.93), 1.97 for 0.075mg/kg (95% CI 1.65 to 2.29), 1.511 for 0.045mg/kg (95% CI 1.37 to 1.65) and 1.49 for the second 0.06mg/kg cohort (95% CI 1.49 to 1.85). As the dosing cohort of 0.06mg/kg was assessed twice, the difference between both data sets were assessed and as no difference was identified ($p>0.9999$), the data was combined. 0.045mg/kg was identified as the cohort with the lowest signal to background ratio being lower than 0.06mg/kg ($p=0.0479$) and 0.075mg/kg ($p=0.013$).

During the longest assessment period in the dosing cohort, neither dosing cohort declined significantly: 0.045mg/kg (slope -0.0089 ± 0.04439, $p=0.8420$); 0.06mg/kg (slope -0.0367

± 0.0598, p=0.3756); 0.075mg/kg (slope 0.159 ± 0.1035, p=0.1447) with no difference between the linear regression lines (p=0.1651).

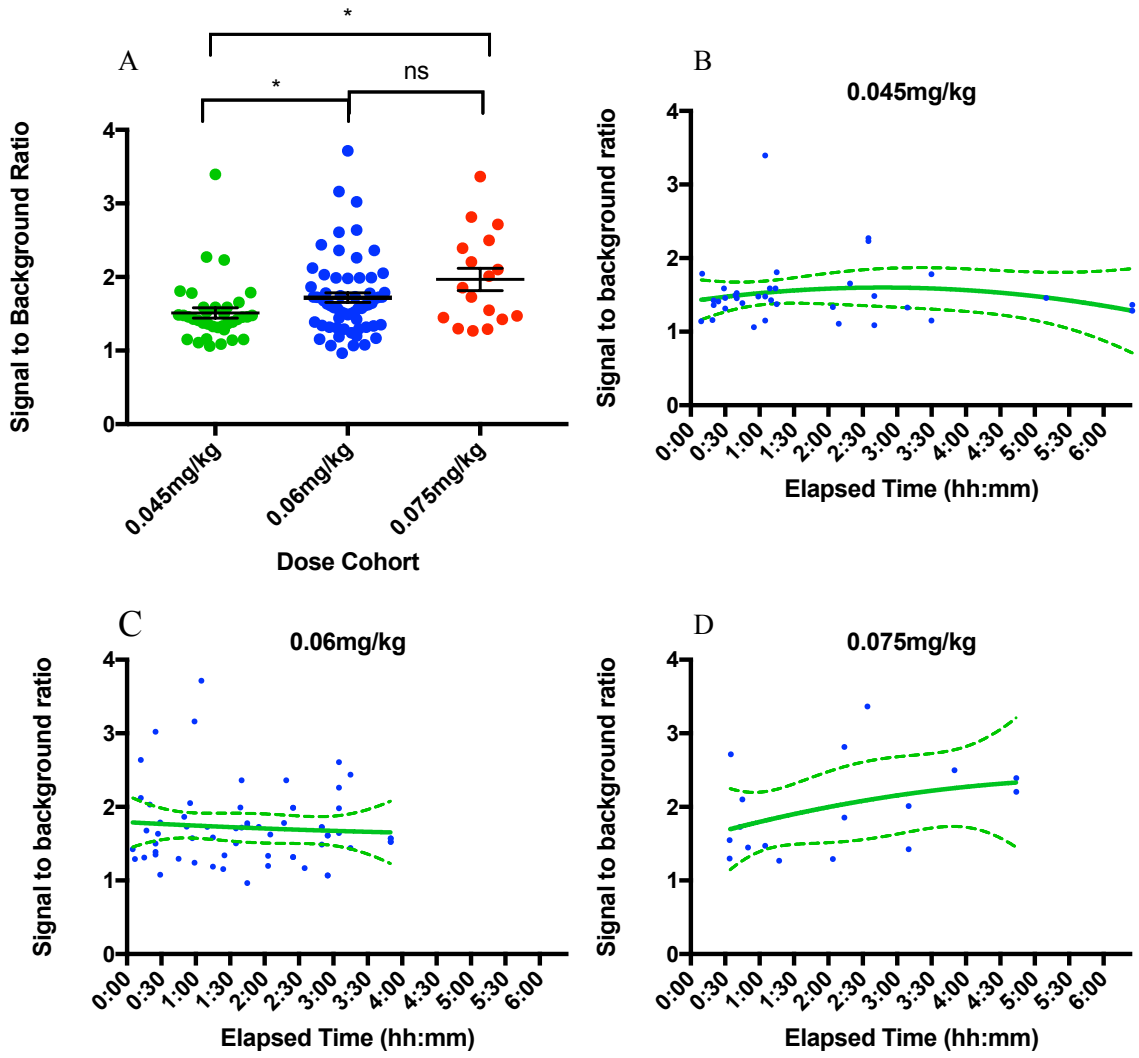

Figure 3.17- Mean signal to background ratio across dosing cohorts in the dose optimisation stage. A = Mean signal to background ratio between dosing cohorts. B-D represent signal to background ratio over time at 0.045mg/kg (B), 0.06mg/kg (C), and 0.075m/kg (D). Solid green line represents non-linear regression fit of curve using second order polynomial quadratic equation inside 95% CI of lines (dotted green). Both 0.075mg/kg and 0.06mg/kg were significantly higher than 0.045mg/kg (p=0.013 and p=0.0479 respectively) and there was no significant difference between 0.06mg/kg and 0.075mg/kg (p=0.6547).

Decision for the optimal dose was unclear based on signal to background ratio as there was no significant difference between the 0.06mg/kg and 0.075mg/kg dosing cohorts. Subjectively, background signal seemed to be a significant drawback in the use of IRDye 800BK. In order to assist in the decision for optimal dose, background signal between dosing cohorts was assessed separately (Figure 3.18). 0.075mg/kg had the highest background signal compared to both 0.045mg/kg (2.47 x greater, $p<0.0001$) and 0.06mg/kg (1.68 x greater, $p<0.0001$) with no significant difference between 0.045mg/kg and 0.06mg/kg ($p=0.2307$). Furthermore, on assessing rate of decay of background signal between the dosing cohorts, 0.075mg/kg had a slower rate of decay although this did not reach statistical significance ($p=0.9982$).

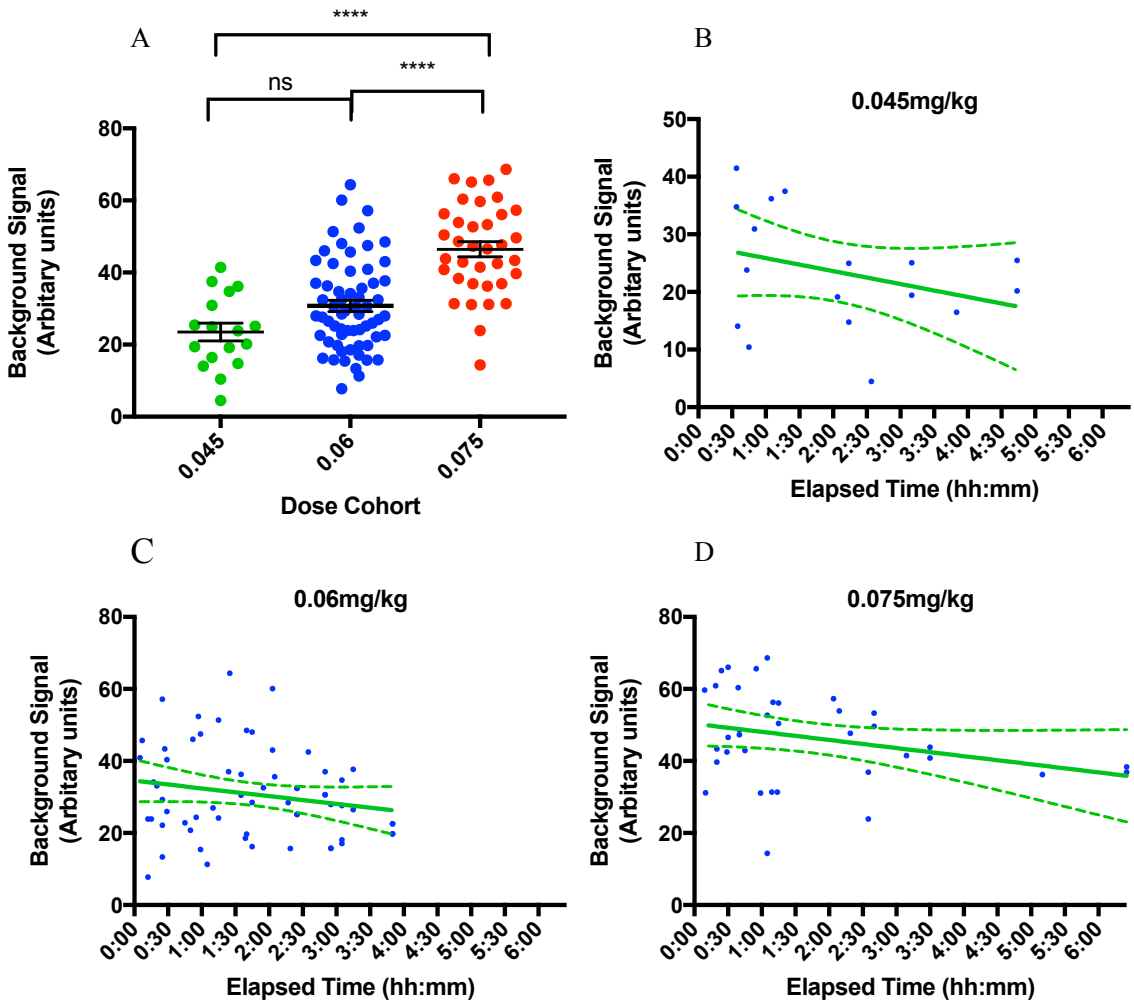

Figure 3.18 - Background signal across dosing cohorts during the dose optimisation stage. A = Mean signal to background ratio between dosing cohorts. B-D represent signal to background ratio over time at 0.045mg/kg (B), 0.06mg/kg (C), and 0.075m/kg (D). Graph A bars represent mean and SEM. Solid green lines represents linear regression fit of line inside 95% CI of lines (dotted green). The 0.075mg/kg dosing cohort had the slowest rate of decline (slope -2.253, 95% CI -4.839 to 0.334, X intercept 22.35) compared with 0.06mg/kg (slope -2.148, 95% CI -4.972 to 0.676, X intercept 16.08) and 0.045mg/kg (slop -2.248, 95% CI -5.928 to 1.432, X intercept 12.51).

3.4.4.2. Optimal dose decision - safety

During the dose optimisation stage, there were 12 adverse events recorded in 9 participants. Only 1 severe adverse event occurred where there was a failure to ventilate the patient after pneumoperitoneum was obtained, however, this was prior to IRDye 800BK administration and was therefore deemed unrelated. Of the 12 adverse events, 9 were deemed unrelated to IMP administration. The remaining 4 were classified as possibly related including vomiting, rash and two participants had mildly elevated liver enzymes (ALT and AST) on discharge but the participant was asymptomatic. The adverse events are summarised in Table 3.8.

Biochemistry was analysed between the participants (using linear regression) in each dosing cohort and there was no significant difference for renal profile biochemistry: urea (p=0.3432), creatinine (p=0.5985), eGFR (p=0.5983) with none of the slopes deviating from 0 except for urea at the 0.045mg/kg cohort which had a downward slope (slope -1.333, 95% CI -2.183 to -0.0833). Liver biochemistry was similar: bilirubin (p=0.991), ALT (p=0.3788), AST (p=0.2566) and ALP (p=0.9602) with all slopes not deviating from 0 except for ALP at the 0.045mg/kg dose, again with a downward slope (slope -7.167, 95% CI -12.71 to -1.624).

It was therefore decided that the optimal dose to take forward into the dose expansion phase was 0.06mg/kg.

AE Number	SAE Criteria	Summary of Event	Severity	Relationship
IRU-01-2	None	Increased stoma output	Mild	U
IRU-01-1	None	Raised liver enzymes AST (150), ALT (140), patient clinically well	Mild	PR
IRU-02-1	Medically Important Event	Failure to ventilate following intubation prior to IMP administration	Severe	U
IRU-02-2	None	Rash over face and arms. Resolved with antihistamine	Mild	PR
IRU-02-3	None	Post-operative ileus	Moderate	U
IRU-03-1	None	Nausea and abdominal pain	Mild	U
IRU-05-1	None	Drowsy and poor respiratory effort with retained CO_2. Probably opioid related.	Moderate	U
IRU-07-1	None	Post-operative ileus	Mild	U
IRU-09-1	None	Drop in blood pressure following IMP administration but abdomen insufflated at same time therefore thought to be cause.	Mild	U
IRU-11-1	None	Temperature spike to 38.2°C. Resolved with no intervention	Mild	U
IRU-11-2	None	Vomiting	Mild	PR
IRU-13-1	None	Mildly elevated liver enzymes on discharge.	Mild	PR

Table 3.8 - Reported adverse events during the dose optimisation stage. U = unrelated; PR = possibly related.

3.4.5. Dose Expansion Phase

Trial results for IRDye 800BK are reported using all patients including those recruited to the dose expansion phase.

In the 40 participants, there were a total of 471 ureteric visualisations from 0 minutes to 6 hours and 25 minutes (median 1 hour 25 minutes) with a median of 12 assessments per patient (range 2 - 21). Nearly all of the readings occurred within the first 2 hours following dye administration (Figure 3.19).

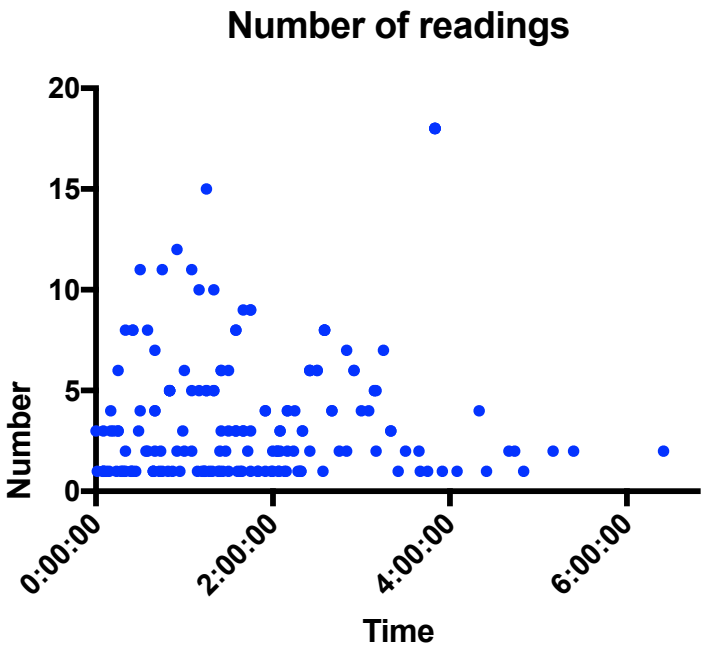

Figure 3.19 - Number of ureteric assessments undertaken over time during IRDye 800BK trial.

Of the 40 patients recruited, 74 ureters (36 left) were assessed for white light and fluorescence (Figure 3.20). Forty-three (35 left) were relevant ureters and thirty-one (1 left) were classified as irrelevant. Four ureters not assessed were left ureters during right hemicolectomy, and the remaining 2 ureters not assessed were right ureters during a left hemicolectomy and a high anterior resection. Seventy-one ureters were visualised at any single point throughout the case with IRDye 800BK at a subjective score at 2 or above by the surgeon (95.9%).

A

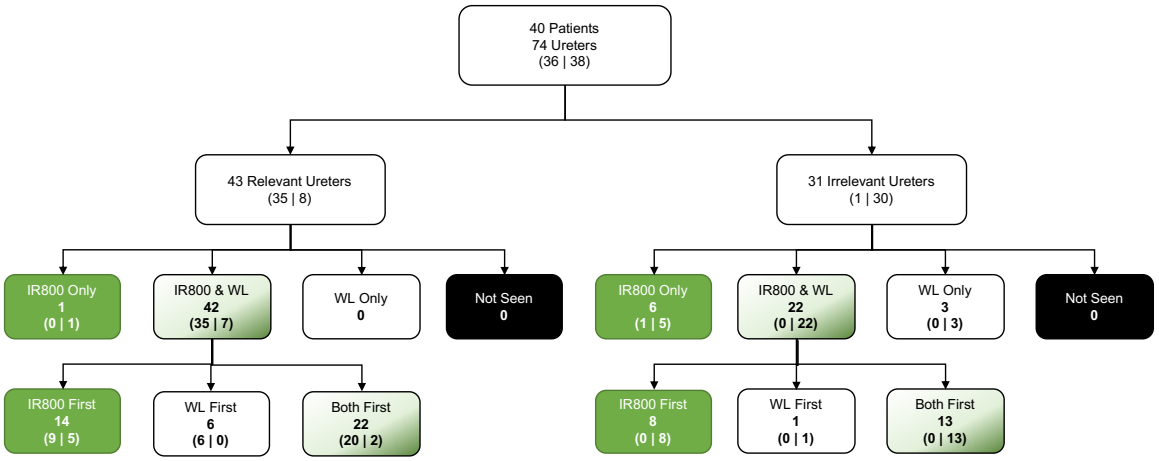

B

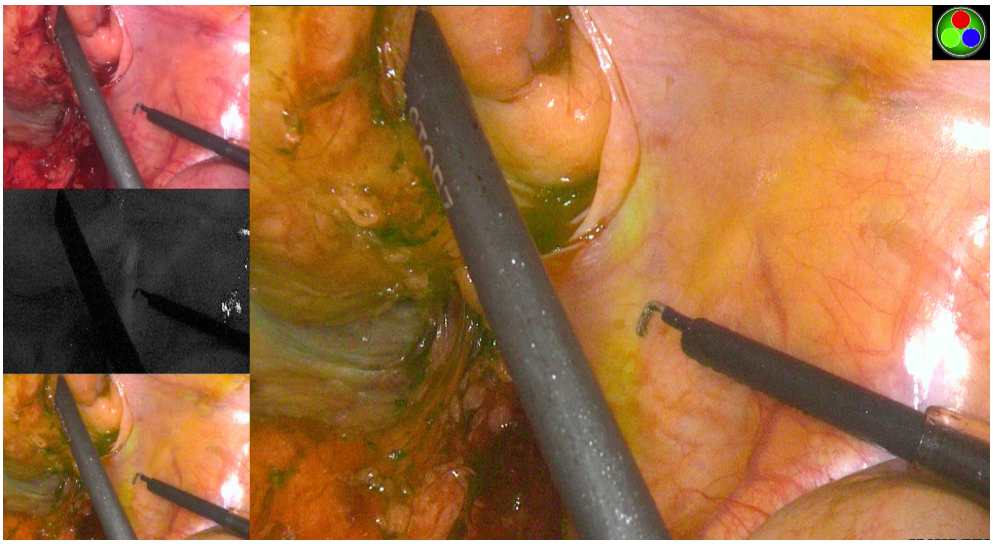

Figure 3.20 - Summary of subjective fluorescence visualisation of ureters with IRDye 800BK. A – Flow diagram of ureteric visualisation: ureters are divided into either relevant or irrelevant to the procedure. Green boxes = ureter only visualised by IR800; green and white = visualised with both white light and IR800; white = visualised with white light only; black = not seen with either modality. B – representative image of ureteric fluorescence with IRDye 800BK.

Only 1 relevant ureter (right sided) was visualised with IR800 fluorescence and not white light throughout the entire case. The remaining 42 relevant ureters (35 left) were visualised

with both modalities throughout with the majority (22) being seen with both white light and IR800 at the first visualisation. Fourteen relevant ureters were seen initially with IR800 and subsequently with white light: 9 were left ureters at a mean of 48 minutes prior to white light (95% CI = 28 minutes) and 5 were right ureters at a mean of 52 minutes prior to white light (95% CI = 15 minutes). The six ureters seen with white light first and subsequently IR800 were all left ureters and were seen a mean of 37 minutes prior to fluorescence (95% CI = 34 minutes).

Six irrelevant ureters (1 left) were see only with fluorescence throughout the whole case and three irrelevant right sided ureters were not seen at all with fluorescence but were visualised with white light. Twenty-two irrelevant ureters were seen with both modalities, again, the majority seen with both fluorescence and white light at the first time-point. Eight right irrelevant ureters were seen first with fluorescence a mean of 19 minutes (95% CI - 19 minutes) prior to being seen with white light. One right irrelevant ureter was first seen with white light 35 minutes prior to being seen with fluorescence.

3.4.5.1. Objective measurement of fluorescence – IRDye 800BK

Across all patients over time, mean signal to background ratio was 1.71 (95% CI – 0.8331 to 0.04434). Mean ureteric fluorescence signal was 51.59 (95% CI 49.57 to 53.61) and mean background signal was 34.54 (95% CI 32.74 to 36.34). Over time, signal to background ratio did not significantly decline (slope 0.01699, 95% CI -0.06004 to 0.09403, p=0.6647) but mean signal (slope -1.732, 95% CI -3.509 to 0.04473, p=0.0560) and mean background (slope -1.33, 95% CI -2.918 to 0.2509, p=0.0988) when analysed separately did decline over time although neither of these reached statistical significance (Figure 3.21A). Subjectively, it was noted that there was a significantly higher background than when methylene blue was

used but the mean background signal was significantly lower than the ureteric fluorescence signal for IR800 ($p<0.0001$) (Figure 3.21B).

3.4.5.2. Safety of IRDye 800BK

Change in haematology and biochemistry profiles were assessed using one-way ANOVA (Table 3.9). A significant decrease was seen in haemoglobin ($p <0.0001$) and platelets ($p<0.0001$) which was attributed to intraoperative blood loss or intravenous fluid administration. Renal function (urea, eGFR and creatinine) had a trend to improving but this was not statistically significant. Bilirubin and liver enzymes (AST & ALT) increased following dye administration but not significantly.

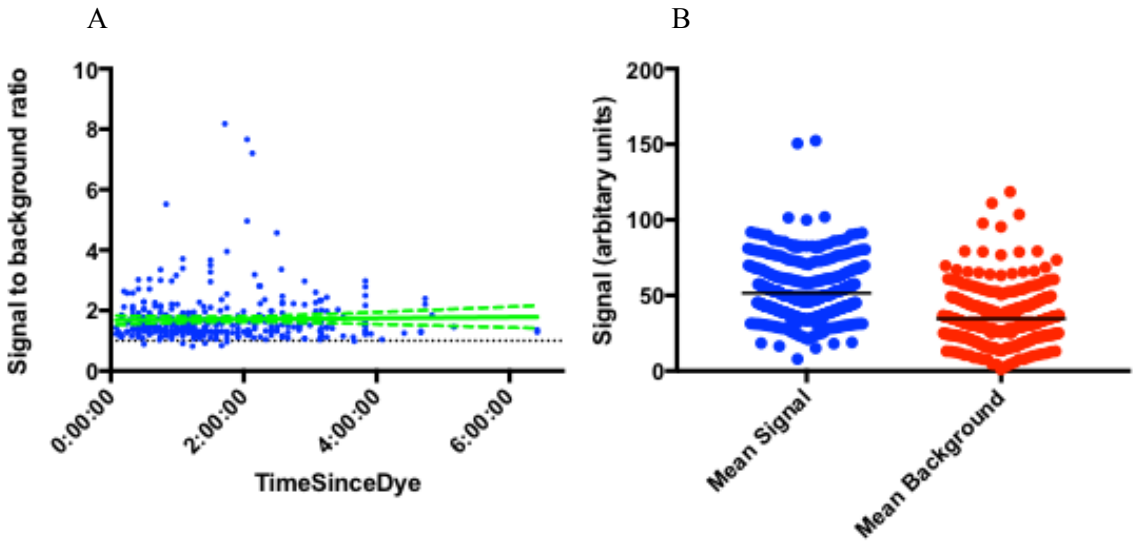

Figure 3.21 - Graphical representation of signal to background ratio over time and mean signal and background in all patients in IR800 ureter study. Graph A represents signal to background ratio over time for all IR800 patients. Blue dots represent individual readings of signal to background ratio, solid green line is linear regression fit with 95% confidence intervals plotted as dotted green lines. Black dotted line represents signal to background ratio of 1 where background would be greater than the signal and therefore not visible. Graph B represents plots of mean signal and mean background. Black lines represent mean with SEM either side (not visible as matching the mean).

Blood result	Pre-op mean	Day 1 mean	Day 2 mean	p-value
Haemoglobin	135.1	118.5	118	<0.0001
Platelets	272.3	228.9	218.4	<0.0001
Sodium	140.1	136.3	137.1	<0.0001
Potassium	3.833	4.195	3.945	<0.0001
Urea	5.458	4.59	4.298	0.0002
Creatinine	73.3	71.78	69.33	0.0136
eGFR	80.73	81.65	83.13	0.1012
Bilirubin	9.225	13.58	15.33	0.0855
ALT	20.53	19.03	22.28	0.3164
AST	22.03	22.45	25.83	0.2398
ALP	84.33	65.53	66.65	<0.0001

Table 3.9 - Haematology and biochemistry results from patients in IRDye 800 ureter trial from pre-op to post-op. Comparative statistics between measurements made using one-way ANOVA. Haematology results, renal function and ALP all had a trend to decrease post operatively. Bilirubin and liver enzymes increased but this did not reach statistical significance. eGFR = estimated glomerular filtration rate, ALT = Alanine aminotransferase, AST = Aspartate aminotransferase, ALP = alkaline phosphatase.

Adverse events collected during participants in-patient stay and up to 30-days are reported in Appendix 1. Briefly, 35 adverse events were recorded throughout the study with three SAEs recorded all of which were deemed unrelated to IRDye 800BK. One subject died during the study period 3 days after their operation from an anastomotic leak which was managed by re-look laparotomy, take down of anastomosis and end-colostomy. Following this, they developed sepsis and multi-organ failure secondary to necrotising fasciitis.

Nine adverse events were deemed possibly related to IRDye 800BK, all of which were mild in severity and included rash (n=1), altered urine colour/smell (n=2) vomiting (n=1). Five participants had deranged liver function tests following IRDye administration none of which required intervention and resolved over time.

3.5. Device comparison

Among the ureteric visualisations, the majority were performed with Pinpoint (196, 46%), 153 were performed using Storz and 53 using Stryker. When comparing signal to background ratio across the devices over time, Stryker gave the highest ratio followed by Pinpoint and then Storz (Figure 3.22). This proved to be statistically significant ($p<0.0001$).

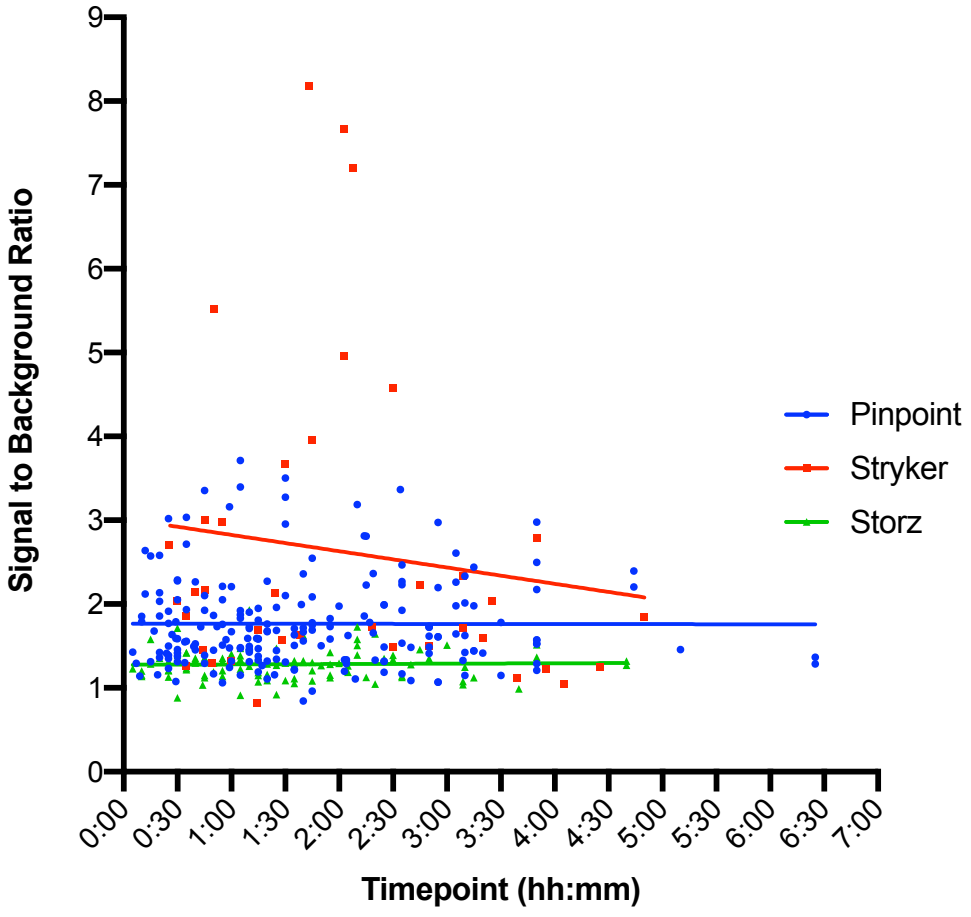

Figure 3.22 - Signal to background ratio over time with different devices for IRDye 800BK. Decrease in Stryker signal to background ratio is likely to be complicated by outlying readings above a ratio of 5. Stryker gave the highest signal to background ratio followed by Pinpoint and Storz.

In 30 time-points, a reading was taken with the Pinpoint and Storz device under the same circumstances (same patient, same time point, same ureter). Similarly, there were 10 time-points for Storz and Stryker but only 4 time-points comparing Pinpoint and Stryker due to both these devices not being available at the same point during the duration of the trial. A comparison of these subsets of data still revealed superiority of the Stryker device and Pinpoint device to the Storz. Thus, it can be concluded for visualisation of IRDye 800BK, the Storz system is inferior compared to Stryker and Pinpoint.

3.5.1. Comparison of methylene blue versus IRDye 800BK for ureteric fluorescence

Both methylene blue and IRDye 800BK can be used for fluorescence identification. Whilst it was not possible to compare both within each patient and a comparative randomised controlled trial was outside the scope of this work, it was decided to compare the data between both trials outlined in this chapter. For purposes of the comparison, the optimal doses for methylene blue and IRDye 800BK of 0.75mg/kg and 0.06mg/kg respectively, were used using only those patients dosed at these levels. Demographics were compared between the IRDye 800BK and methylene blue cohorts. No significant difference between age, sex, BMI, planned procedure and indication were identified (Table 3.10).

Demographic	Methylene Blue (n=14)	IRDye 800BK (n=34)	p value
Mean age (SD)	67 (11.61)	67 (12.21)	0.955 *
Sex			0.317 **
Male	10	19	
Female	4	15	
Mean BMI (SD)	27.57 (5.25)	26.12 (3.81)	0.405*
Indication			0.058**
Cancer	10	32	
Diverticular	3	1	
UC	0	1	
Crohn's	1	0	
Planned procedure			0.440**
APER	0	3	
Low Anterior	7	11	
High Anterior	2	12	
Hartmann's	1	0	
Hartmann's Reversal	1	1	
Proctocolectomy	1	2	
Left hemicolectomy	0	1	
Right hemicolectomy	2	4	

Table 3.10 - Baseline demographics between methylene blue and IRDye 800BK trial groups. No significant difference was identified between both groups in any of the baseline demographic variables. * = unpaired t-test, ** chi-squared.

For the purpose of comparing the objective analysis of signal to background ratio, signal, and background measurements, only readings taken from 0 to 100 minutes were utilised as the methylene blue study only collected imaging data up until 100 minutes.

There was a significantly higher signal to background ratio in the methylene blue trial (mean 5.294, 95% CI 4.646 to 5.942 versus mean 1.645, 95% CI 1.553 to 1.738) ($p<0.0001$). IRDye 800BK had a much higher ureteric fluorescence signal (mean 52.74, 95% CI 49,98 to 55.49 versus mean 36.79, 95% CI 32.89 to 40.69, $p<0.0001$) but the background signal from IRDye 800BK is nearly 5 times higher than the background of methylene blue (mean 35.79, 95% CI 33.21 to 38.38 versus mean 7.817, 95% CI 7.011 to 8.623, $p<0.0001$) (Figure 3.23). The rate of decline in signal to background ratio over time declined slower in the IR800 trial versus methylene blue although this did not reach statistical significance (Figure 3.23C) (slope -0.001526, 95% CI -0.00497 to 0.0019 versus slope -0.013, 95% CI -0.036 to 0.010, $p=0.1457$).

IRDye 800BK fluorescent signal was mostly observed as a static signal (99% fluorescent visualisations) with fluorescence being seen statically with a 'bolus' of fluorescent signal over the top in 1% of cases. There were no observations of fluorescence only occurring during vermiculation. Conversely, with methylene blue, 45% of visualisations were only seen during vermiculation, 44% with static signal and then increased signal during vermiculation and in 11% of cases static signal only was observed.

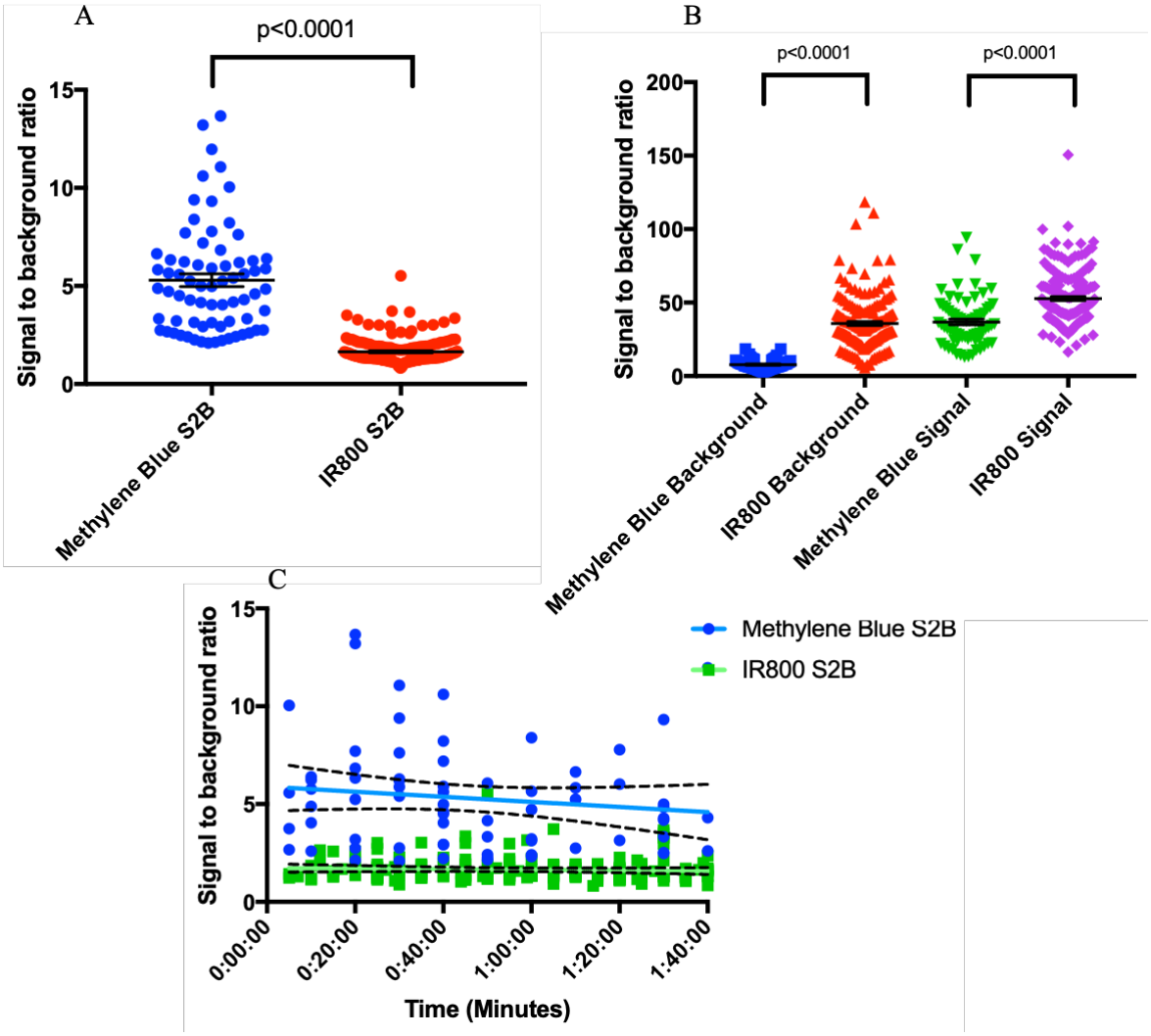

Figure 3.23 – Comparison of objective data from IR800 and methylene blue ureteric fluorescence studies. A represents comparison of signal to background ratio between methylene blue and IR800 trials. B represents individual data for ureteric fluorescence signal and background signals alone. C represents all signal to background ratio measurements over time in each trial with a linear regression line fitted (black dashed line represents 95% confidence intervals).

3.6. Discussion and future directions

This chapter investigates ureteric fluorescence and reports the largest study to date using methylene blue and a first in-man study of IRDye 800BK. In both studies, there were only 3 ureters with IR800 and 1 ureter with methylene blue that were not seen under fluorescence but seen clearly with white light which were both ureters irrelevant to the procedure. In the methylene blue study there were a number of occasions where the ureter was not seen at all with white light for the whole procedure but was clearly seen under fluorescence (20%). Whilst this seems a high rate of non-visualisation with white light it is because discretion was given, in this study, to the surgeon as to whether additional dissection was to be performed to positively identify the ureter under white light. In these cases, the ureteric fluorescence was clear enough to assure the surgeon that the ureter was positively identified and therefore no additional dissection required to identify the ureter under white light. A 'bolus' of fluorescence in a tubal pattern was the clearest indicator that the ureter was fluorescing. For the IR800 study there were no non-visualised ureters as the protocol did not allow this discretion due to it being first in man.

Here, the optimal doses for both methylene blue (0.75mg/kg) and IRDye 800BK (0.06mg/kg) have been demonstrated, largely on signal to background ratio. Whilst it is difficult to compare the 2 dyes due to patient heterogeneity and non-randomisation, it seems that whilst IR800BK provides a brighter signal in the ureter, its background significantly reduces the signal to background ratio well below that of methylene blue. It could be the case that to reduce the background signal, IRDye 800BK should be given much earlier than methylene blue than was given in this study and further work should examine this although it may make it more difficult to use. Over time, methylene blue does decrease slightly quicker than IR800BK, but for colorectal operations in particular, this is unlikely to be detrimental, furthermore, with the dose of 0.75mg/kg, it is likely that a repeated dose could

be given. The only advantage of IRDye 800BK over methylene blue is its predominant signal being a static one rather than a mixed signal. A static signal could be beneficial in that one does not have to wait for a vermiculation, instantly being able to recognise the ureter. However, with a low signal to background ratio, it could potentially be confused for another adjacent structure. Where a 'bolus' fluorescent signal is observed, it is far less likely to be confused with another structure. Another draw-back of IRDye 800BK is the excitation and emission wavelengths being close to that of ICG. As discussed previously, ICG is widely used to assess perfusion and LN identification and where the future is moving to use multiple fluorophores, the cross over between these two may add to confusion to interpretation.

The cost of methylene blue per patient dose is around £70 (~$90), although it is not yet approved for this use by the FDA or MHRA. Whilst the PINPOINT DR system is not currently commercially available, fluorescence enabled laparoscopic systems tuned to ICG cost from £110,000 to £150,000. Dual wavelength systems incorporating compatibility with methylene blue are still under evaluation. IRDye 800BK is yet to be costed for commercial use, however, LI-COR's intentions are to price it competitively against ICG which. The price of laparoscopic systems for ICG/IRDye are similar to the PINPOINT DR and numerous surgical centres now already have a device in place.

Methylene blue is well known to have a good safety profile. IRDye800BK has a similar structure to IRDye800CW which, as discussed, has been used in studies using conjugated antibodies for targeted fluorescence. In this first in man study, IRDye 800BK seemed safe with only deranged LFTs being noticed in a small number of patients as being possibly related to dye administration. Larger studies will allow further accumulation of important safety data.

Both trials recruited a number of patients where the ureter may have been more difficult to identify (e.g. re-operative surgery, high BMI etc). Success of both dyes in these instances indicate that this technology has the potential to benefit patients and surgeons and should be investigated further. The next stage of study is difficult as each dye has its own benefits and could be explored individually or in co-administration with each other. The benefit of co-administration would include both static and 'bolus' fluorescent signal which may increase visibility combined with the high signal to background ratio of methylene blue. This technique could however have high background levels as well as safety implications with the combination of the two dyes. For this to be explored a small development study again with around 40 participants would be appropriate to assess its safety, feasibility and replicability before progressing to a larger trial. For each dye to be taken forward alone, a stage 2B exploration trial [95] would be most beneficial with a large, non-randomised, multi-centre prospective cohort study assessing visualisation with white light and fluorescence as well as subjective outcomes including usefulness and change in operative plan. A final option would be to have a small randomised trial assessing each dye alone and both in combination with the superior being taken forward to the stage 2B study. A limitation with this work is subjective assessment from an operating surgeon which could introduce bias. Careful thought in future trial design must account for this and it may require numerous independent and blinded assessors.

The ideal adjunct to intraoperative ureteric visualisation would be something that is guaranteed to be visualised, penetrates through thick overlying fat or scar tissue, lasts throughout the entire procedure, has minimal background signal and is easy, quick and safe to use. Lighted ureteric stents have been discussed however, the development of NIR-lighted stents would provide guaranteed emission of light, ability to adjust wavelength, intensity and frequency of emission (e.g. pulsation). These would still have the aforementioned cost,

time and resource implications and to date only 1 case report has been published regarding use of the InfraVision NIR ureteral stent by Stryker® [123]. Another alternative that could be used to provide more reliable ureteric imaging would be to have targeted fluorescence using the ureteric urothelium as the target with either antibodies or peptides. Nothing has been published to date but such antibodies to the cytokeratin located in the epithelium exist and could be utilised for this modality [124] bearing in mind there may be unwanted side effects from immunogenicity when using antibodies.

The drawback of background signal with fluorophores is likely due to a mixture of fluorophore metabolism, size, solubility and excretion leading to contrast sitting in unwanted locations. Mahalingam and colleagues have developed UreterGlow which is a cyanine fluorophore, S0456 (λ_{ex} 800nm, λ_{em} 830nm), that has been coupled to glucosamine that cannot be released or metabolised in physiological conditions and is therefore extremely soluble and likely to pass through the kidney into the ureter [125]. Similarly, Cha *et al* synthesised UL-766 [126] to be highly water soluble by using triethylene glycol chains. Both studies in mice and pigs seem to prove reduced background signal in other organs whilst maintaining high signal in the ureter and kidneys. Both dyes now require toxicity testing in animals prior to phase I clinical trials and if successful, should be compared to both methylene blue and IRDye 800BK.

CHAPTER 4: NEAR-INFRARED LIGHT TO HIGHLIGHT THE LOCATION OF THE URETHRA DURING LOW RECTAL CANCER SURGERY

Data from this chapter has been published in:

Barnes TG, Penna M, Hompes R, et al. Fluorescence to highlight the urethra: a human cadaveric study. Techniques in Coloproctology. 2017;21:439-444; and

Barnes TG, Volpi D, Cunningham C, et al. Improved urethral fluorescence during low rectal surgery: a new dye and a new method. Techniques in Coloproctology. 2018;22:115-119.

4.1. Introduction

4.1.1. Anatomy and clinical significance of the urethra during colorectal surgery

The male urethra is an 18-20cm muscular tube that goes from the internal urethral orifice of the bladder to the external urethral orifice at the tip of the glans penis. There are four main parts to the urethra: the pre-prostatic urethra; prostatic urethra; membranous urethra and spongy urethra. The membranous part of the urethra is the shortest and narrowest part beginning at the apex of the prostate and going into continuity with the spongy urethra as it enters the penis. The membranous urethra travels through the deep perineal pouch and is surrounded by the external urethral sphincter and perineal membrane [127]. The close proximity of the distal prostatic and membranous urethra to the anterior rectal wall and the perineal body make the urethra at risk of injury during low rectal cancer surgery (Figure 4.1) [128].

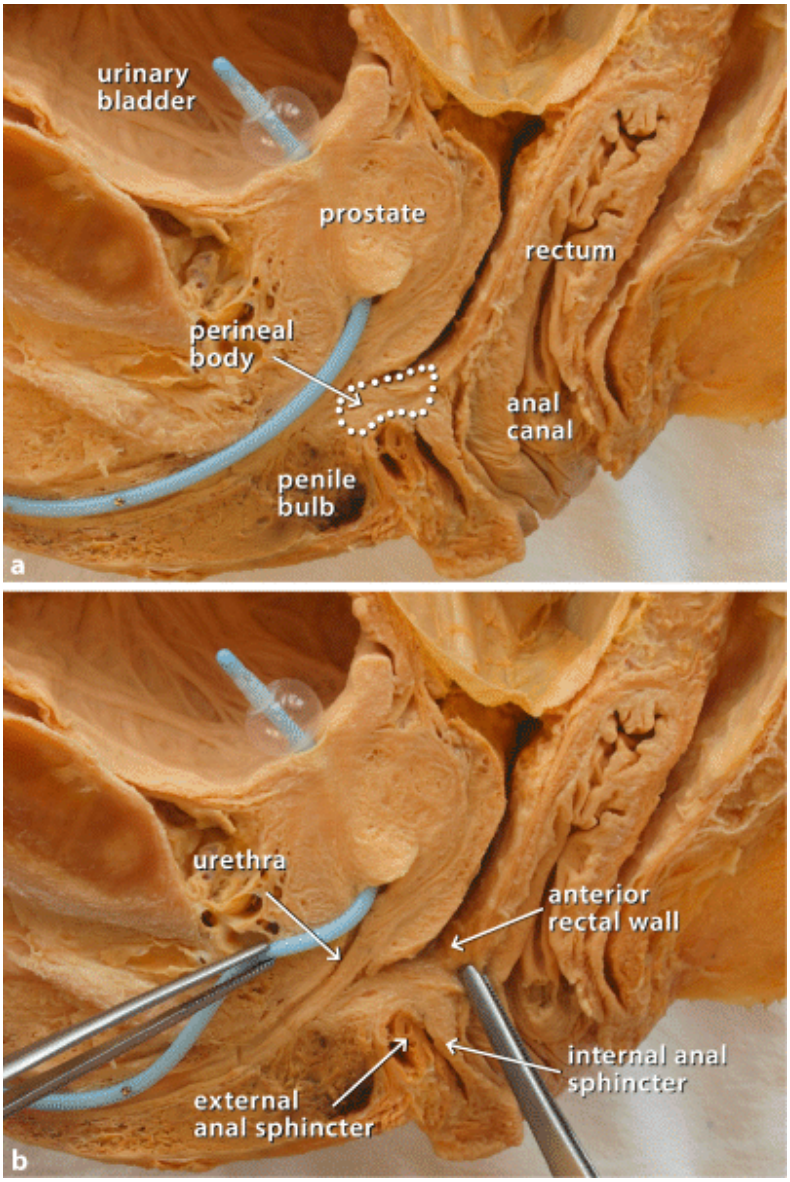

Figure 4.1 - Cadaveric specimen of the midline sagittal section of the male pelvis. The anatomical dissection outlines the course of the urethra as denoted by the urinary catheter. This model demonstrates the proximity of the urethra to the anterior rectal wall where the anterior dissection plane lies and hence why urethral injury occurs. Reproduced with permission from Kneist *et al* 2017 [128].

The preferred surgical approach to very low rectal cancers where sphincter preservation is not possible is an abdominoperineal excision of the rectum (APER). Where the sphincters can be preserved, low anterior resection to perform the total mesorectal excision (TME) is preferred. Since the development of laparoscopic TME, there has been a debate surrounding the oncological outcomes of the laparoscopic technique versus an open approach. The COLOR (Colon cancer Laparoscopic or Open Resection) II [129] and COREAN (Comparison of Open versus laparoscopic surgery for mid and low Rectal cancer After Neoadjuvant chemoradiotherapy) [130] trials reported equivalence of both approaches for 3-year survival and recurrence. Two further trials since have failed to show non-inferiority of the laparoscopic approach compared to open surgery [131, 132]. These studies have largely been questioned within the surgical community because of their methodology [133]. A concern amongst surgeons with the TME procedure is achieving a negative circumferential resection margin (CRM) and distal resection margin. These two factors have provided an impetus for surgical innovators to develop an alternative minimally invasive technique in an attempt to provide an improved oncological outcome [129]. The transanal approach to the TME resection (TaTME) was first performed in 2009 [134]. This new technique involves placing a purse-string suture via a transanal access platform distal to the tumour followed by carbon dioxide insufflation and performing the TME under direct vision [129]. Whilst this technique has received a lot of attention, there have recently been concerns amongst surgeons surrounding complications occurring as a result of wrong plane surgery [129, 135]. The most significant morbidity occurring specifically during TaTME is urethral injury. The prostate cannot be mobilised from an abdominal approach; thus, urethral injury only occurs during perineal approaches to the TME. Whilst the CO_2 insufflation allows excellent visualisation of the TME plane, it may also easily lead surgeons into other areolar planes outside the scope of dissection. One such plane is located anterior to the prostate and in particular in the area of the membranous urethra. Increased risk of urethral injury occurs in the setting of anterior

tumours, previous pelvic radiotherapy, prostatic hypertrophy or previous prostatectomy and the need for partial sphincter resection [136, 137]. Furthermore, in patients with a tight narrow pelvis and bulky pelvic muscles (namely the piriformis and levator muscles), the prostate can be pushed higher and therefore elongate the membranous urethra thus exposing it to potential injury [137].

Urethral injuries occur due to wrong plane surgery where failure to recognise the smooth spherical shape of the prostate within the operative field and the critical landmarks of the neurovascular bundles of Walsh can allow inadvertent mobilisation of the prostate dorsally exposing the urethra [129]. Denonvilliers fascia is another important landmark which defines the rectovesical space and should not be breached during TaTME unless an anterior tumour threatens the CRM. Novice TaTME surgeons will have trepidation about violating the anterior rectal wall and thus may overcompensate by entering an anterior plane. Less commonly reported is injury to the urethra during abdomino-perineal dissection and this is primarily because the urethral catheter can be palpated easily during dissection [97].

Consequences of urethral injury include urinary sepsis, rectourethral or urethrocutaneous fistula or urethral stricture [97, 138], all of which carry significant morbidity for the patient. Urethral fistulae rarely close spontaneously and will require urinary diversion with a suprapubic catheter and, for rectourethral fistulae, enteric diversion is required. If identified at the time of surgery, repair is possible and the patient would need an extended duration of indwelling urinary catheter to allow the repair to heal [97].

The incidence of urethral injury during TaTME was reported by Penna *et al* at 0.7% in the first 720 voluntarily entered cases in the international TaTME registry [139]. It is likely however, that this complication is grossly under-reported with one reported case series of

30 patients having 2 urethral injuries [140] and in another case series, 1 urethral injury in 50 cases [141]. In addition, urethral injury is a gender specific complication and thus reported incidence also includes females in the denominator. Incidence of urethral injury is likely to decrease as surgeons progress along the learning curve and it has been advocated to undergo appropriate cadaver-based training models as well as proctorship of the technique [128, 135]. Urethral injury during APER is estimated to occur in 1.5% - 3.125% of cases and historically is not associated with sphincter preserving surgery [142].

4.1.1. Urethral identification during low rectal cancer surgery

Current strategies to urethral localisation to attempt prevention of urethral injury include recognition of the previously mentioned critical anatomical landmarks, as well as performing a digital rectal examination (DRE) prior to commencing the TaTME dissection. If question is raised as to whether the prostate is being mobilised dorsally then the operation should be paused, the transanal access platform removed and a DRE performed to confirm the position of the prostate. Tactile feedback may still be insufficient and if the prostate location cannot be confirmed then the TaTME dissection should be abandoned and the operation continued abdominally. In addition to tactile feedback, a thorough patient history and review of pre-operative magnetic resonance imaging (MRI) images should be reviewed particularly for the anterior plane with specific reference to the prostate.

Other suggestions to assist the surgeon in identifying the urethra include applying a vibratory stimulus to the urinary catheter and detecting the vibration with a doppler probe [142]. The vibratory device used can simply be a battery-powered hair clipper. Intraoperative ultrasound with doppler colour flow imaging can also be used to identify the urethra when applying retrograde flow of fluid down the urinary catheter. A newly applied technology

using stereotactic technology has been described where a CT or MRI scan is performed after applying skin-fixed markers which allow multiplanar 3D reconstructions with interpretation of the operating instrument providing real-time localisation on a displayed image. Whilst early results of this technology seem promising, it often requires scans being acquired intraoperatively and the surgeon must look at two screens (operating screen and the image displaying the scan) [143].

These urethral-localising techniques often require interruption to the procedure or, in the case of stereotactic navigation, expensive technology and software in order to assess their efficacy. Fluorescence and NIR light are currently an unexplored modality for operative guidance and urethral identification. This chapter aims to explore both for use in low rectal cancer surgery.

4.1.2. Aims and objectives

1. To assess the use of fluorescence using approved fluorophores to highlight the urethra
2. To validate methods of using NIR light guidance to visualise the urethra or prostate intraoperatively

4.2. Methods

4.2.1. Ex-vivo work

Pre-clinical work was conducted using live Yorkshire male pigs and human male cadavers. Animal work was conducted at the University of British Columbia funded by NOVADAQ® with ethical approval granted from the University of British Columbia ethics board. All pigs

were given a general anaesthetic by a veterinary technician and placed supine on an operating table. After the procedure was conducted, the pigs were euthanised with phenobarbital.

Freshly frozen and thawed human male cadavers for the purposes of experimentation and training were obtained from the Department of Anatomy, University of Oxford. All cadavers had given consent at the time of living for use in medical sciences and use of images for scientific publication. Ethical approval was granted by the Department of Anatomy, University of Oxford. All cadavers were being used for cadaveric TaTME training. Urethras were accessed by either a perineal dissection with retraction of perineal skin using a Lone Star® retractor system (Cooper Surgical, CT, USA) (Figure 4.2) or transanally following rectal mobilisation through a GelPOINT Path transanal access platform (Applied Medical, CA, USA). ICG was reconstituted according to the manufacturer's instructions with water. The ICG solution was subsequently mixed with 10mL of Instillagel and infiltrated into the urethra prior to any manipulation. The urethra was then imaged using the PINPOINT device.

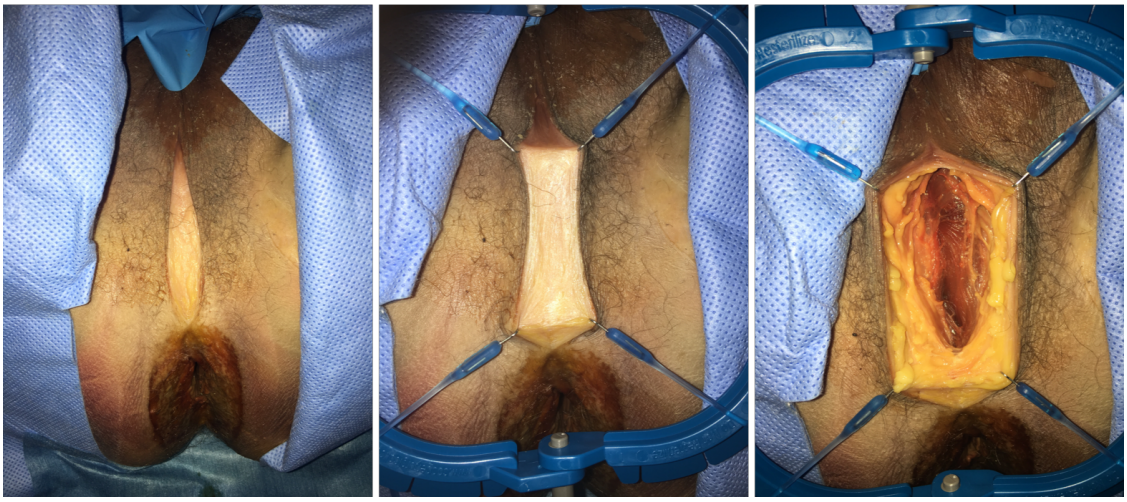

Figure 4.2 - Cadaveric model of urethral exposure via perineal dissection. From left to right: perineal incision through skin only, placement of Lone Star® retractor, dissection through urethral musculature to exposure the urethra.

4.2.2. ICG Urethra Clinical Trial

A proof of principle study was developed to assess the *in-vivo* use of ICG-Instillagel in visualising the urethra under fluorescence. The primary objective to assess the number of urethras identified under white light and fluorescence intraoperatively. Secondary objectives included subjective assessment of the usefulness of the technology, acceptability of the technique, adverse events and signal to background ratio of the fluorescent signal. All participants undergoing TaTME or APER were approached and screened for eligibility. Participants were excluded if they had an allergy to iodine or ICG or known liver failure. Ethical approval was granted by the Oxford B REC committee (17/SC/0299). An interim analysis would be performed every 5 participants for safety and efficacy.

4.2.3. Clinical trial of NIRCaD

Whilst the device did not have CE marking, as it was an in-house, prototype device, MHRA device trial approval was not required. Thus, a first in man open label, IDEAL stage 2A prospective study to assess the device for safety and efficacy was conducted. All male participants undergoing low rectal cancer surgery (TaTME or APER) were eligible and excluded should they have any altered lower urinary tract anatomy, if a urinary catheter could not be inserted or if the participant was part of any other NIR imaging study. Once the patient was positioned on the operating table under general anaesthetic, the NIRCaD was placed inside the urinary catheter under sterile conditions and then placed per urethra into the bladder using the standard technique. The operation continued as per standard care. The sample size was set at 12 based on frequency of procedures and predicted recruitment rate. Ethical approval was granted by the Greater Manchester West REC (17/NW/0479).

Three assessments of urethral visualisation with white light and then NIR light emission were conducted: 1) before any rectal dissection; 2) during TME dissection; 3) following specimen extraction and; 4) in the bladder transabdominally to ensure the NIRCaD was emitting light. Adverse events were assessed using the online patient database and patient notes 30 days following their procedure.

4.3. Results

4.3.1. Pre-clinical optimisation of urethral fluorescence using direct infiltration

4.3.1.1. Methylene blue vs ICG

In order to assess which licensed fluorescent dye to pursue with urethral fluorescence, a live pig model was created to compare ICG with methylene blue mixed with ICG. Eight male pigs (4 for methylene blue and 4 for ICG) were anaesthetised and an open cut-down technique was utilised to enter the abdomen and create a pneumoperitoneum. The male

urethra in pigs is located in the anterior abdominal wall so can be used to fluoresce through overlying peritoneum and fat. Following infiltration of the fluorophore, the PINPOINT device was used to image the urethra in the anterior abdominal wall.

Mean signal in the ICG group was significantly higher than the methylene blue group (97.6 vs 36.0 p=0.0062). As expected, there was minimal background signal in both methylene blue and ICG with no difference between the two (p=0.8455) (Figure 4.3 and Figure 4.4). It was therefore decided that ICG mixed with Instillagel® (ClinMed®, Buckinghamshire, UK) would be the method of choice to pursue for fluorescent identification of the urethra.

Dissection point	White light	Methylene Blue	ICG
1. No dissection		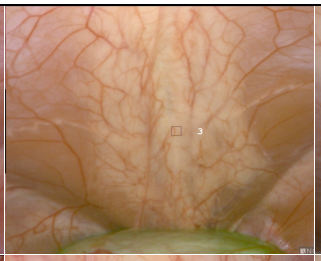	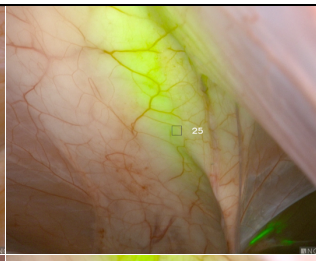
2. Peritoneum	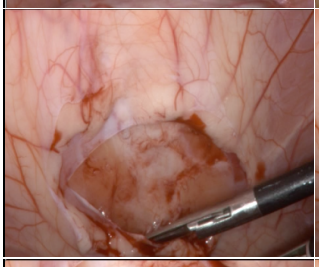	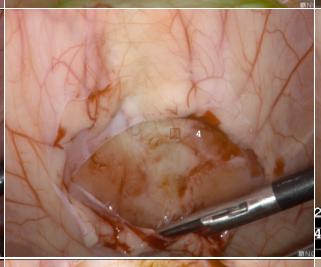	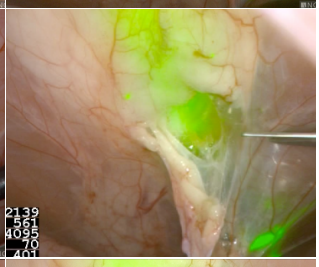
3. Peritoneum & fat	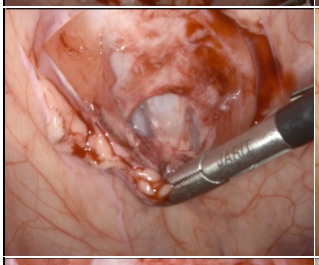		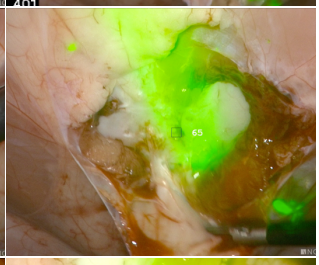
4. Denuded urethra	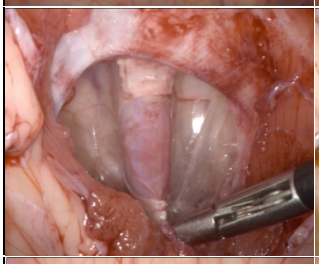	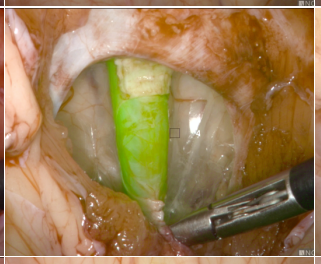	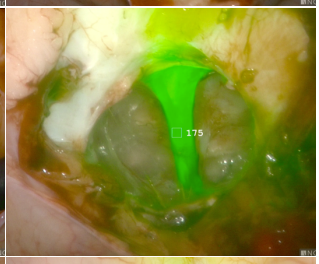
5. Double (MB) or halved (ICG) sensitivity – no dissection	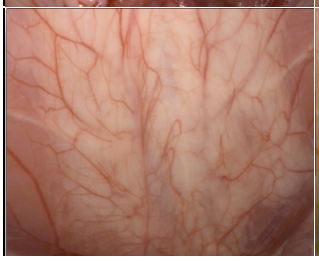	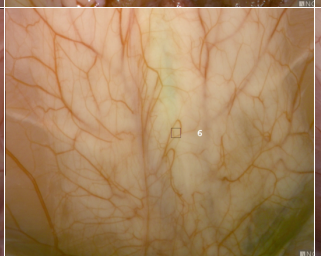	

Figure 4.3 – Representative images of intra-abdominal visualisation of the urethra in the pig. Images are representative and demonstrate fluorescence of the urethra with methylene blue or ICG mixed with Instillagel ® and infiltrated directly into the urethra.

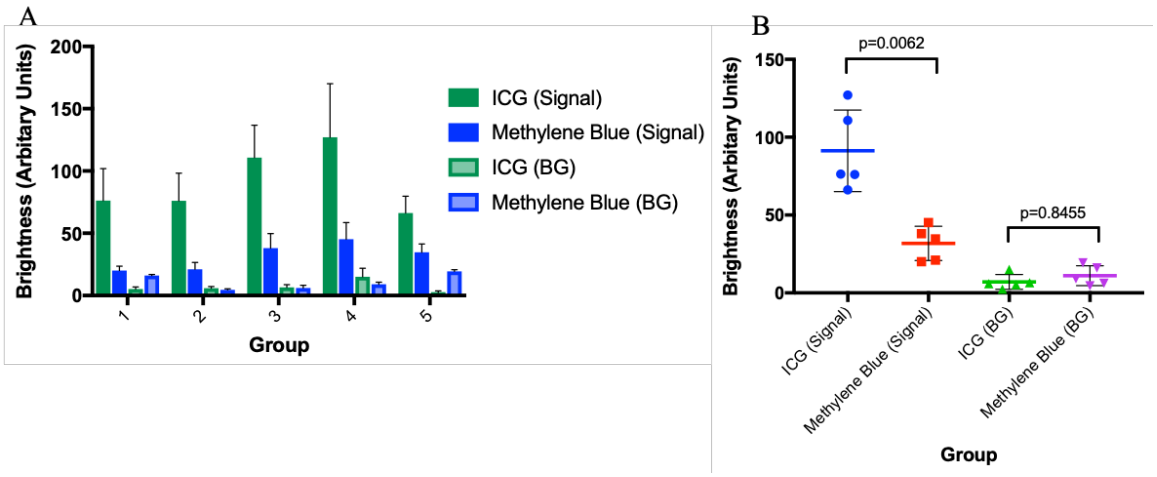

Figure 4.4 - Signal and background brightness between ICG and methylene blue in the pig urethra model. A = mean signal and background brightness (SD in black bars) between ICG and methylene blue across the different dissection points (numbers refer to images in Figure 4.3. B = mean signal and background brightness in ICG and methylene blue over all readings at all dissection levels. Black bars represent mean and standard deviation.

4.3.2. Optimal dose for ICG-Instillagel fluorescence per urethra in human cadavers

For safety, it was decided that the best dose to use *in-vivo* would be the lowest possible dose that gave the best signal. Five dosing cohorts were assessed for urethral fluorescence in 10 cadavers with 2 cadavers at each dose: 2.5mg, 5mg, 10mg, 12.5mg and 25mg. The highest mean signal was identified in the 2.5mg group but there was no statically significant difference between any of the dosing cohorts using a one-way ANOVA (p=0.866) (Figure 4.5 and Figure 4.6). Signal to background ratio was 5.95 for 2.5mg; 3.42 for 5mg, 4.52 for 10mg, 5.05 for 12.5mg and 2.36 for 25mg.

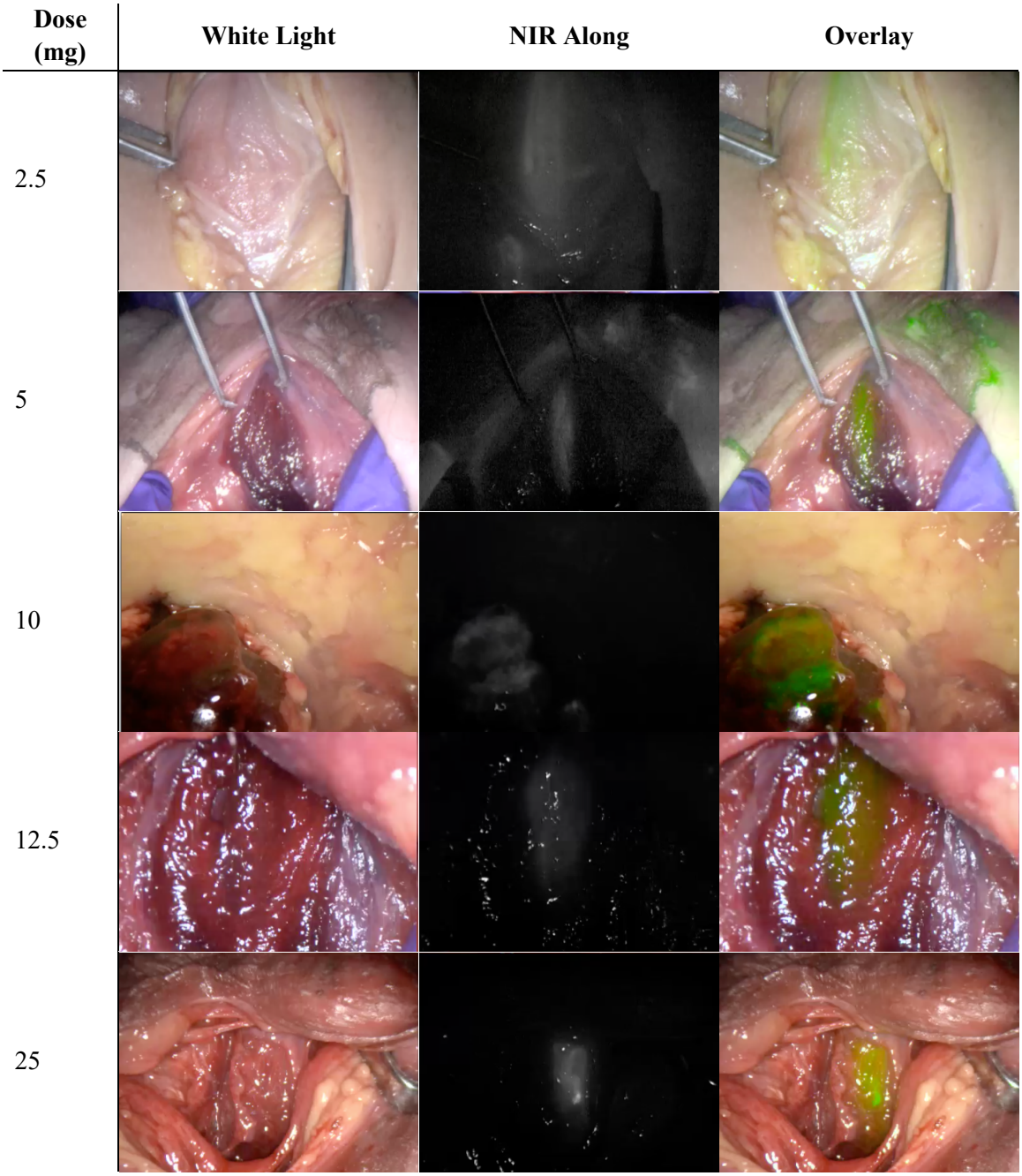

Figure 4.5 - Representative images of cadaveric dose optimisation of urethral ICG.

Doses compared	Mean Difference	95% CI of difference	Significant?	Adjusted P Value
2.5mg vs. 5mg	16.16	-97.13 to 129.5	No	0.9283
2.5mg vs. 10mg	38.16	-75.13 to 151.5	No	0.5050
2.5mg vs. 12.5mg	37.78	-60.34 to 135.9	No	0.4154
2.5mg vs. 25mg	27.86	-64.64 to 120.4	No	0.5808
5mg vs. 10mg	22	-91.29 to 135.3	No	0.8304
5mg vs. 12.5mg	21.62	-76.5 to 119.7	No	0.7708
5mg vs. 25mg	11.7	-80.8 to 104.2	No	0.9507
10mg vs. 12.5mg	-0.382	-98.5 to 97.73	No	>0.9999
10mg vs. 25mg	-10.3	-102.8 to 82.2	No	0.9676
12.5mg vs. 25mg	-9.917	-83.05 to 63.21	No	0.9386

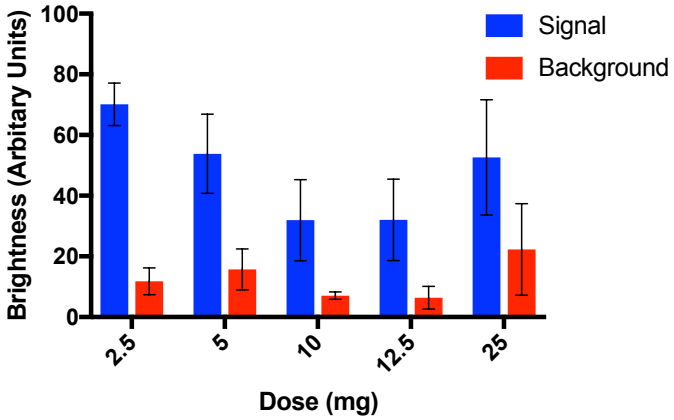

Figure 4.6 - Comparison of signal and background across different doses for urethral ICG fluorescence. Table represents ANOVA comparison between signal in different dosing cohorts. Graph represents signal and background in the different dosing cohorts.

4.3.3. In-vivo assessment of ICG-Instillagel to identify the urethra

Five participants were recruited to the trial from July to September 2017. Two participants were undergoing TaTME and 3 were undergoing APER all for low rectal cancer by a 2-surgeon team. Median BMI was 25.03 (range 21.26 to 28.0). Urethral visualisation under white light and fluorescence was attempted before dissection, during dissection and following specimen removal. In the five patients assessed, no fluorescence was observed at any time-point in the urethra despite the urethral catheter being palpable in all instances although not fully visible under white light. In 2 participants, fluorescence signal was observed in the urinary bladder following administration and in 1 participant, fluorescence signal was seen in the region of the seminal vesicles. During the rectal mobilisation, the seminal vesicle had been injured and fluid with fluorescent signal was seen leaking from the region indicating reflux of ICG-Instillagel into the seminal vesicles. No signal was seen in the region of the urethra despite this being palpable. After 30 days, no adverse events related to ICG administration were observed. Furthermore, in all cases, the technique was difficult as significant volumes of ICG-Instillagel leaked from the penis and occasionally around the operative field resulting in contaminated fluorescence staining.

Following evaluation of the technique in 5 participants, in a live patient, there are numerous variables including alterations in position and operative movements which could affect ICG-instillagel sitting in the urethra throughout the procedure. As no positive signal was observed in any patient despite being palpably close to the urethra, the ICG-instillagel technique was abandoned.

4.3.4. Other methods for urethral fluorescence

As ICG did not work *in-vivo*, 2 new methods were assessed: IRDye 800BK in place of ICG and production of an ICG-silicone catheter. The silicone catheter had the advantage of being

a less difficult technique and no loss of fluorescent material from within the urethra. An ICG-silicone catheter was made by mixing transparent silicone (RS Pro, Northants, UK) was mixed with ICG (Diagnostic Green, Germany) dissolved in 1mL of 100% ethanol and infiltrated down a 10Fr one-way Foley catheter and allowed to set for 1 week.

Further cadaveric work exploring IRDye 800BK mixed with instillagel resulted in a mean signal to background ratio of 5.42 which was no different from use with ICG and therefore not worth exploring further. Similarly, with the ICG-silicone device, the mean signal to background was 5.75 and similarly abandoned.

4.3.5. NIR light fibre to detect the urethra

As using fluorophores as dyes to identify the urethra has proved to be inefficient *in-vivo*, an alternative method of highlighting this critical anatomy was sought. Two main issues with using fluorophores is firstly the fluorophore needs to be administered and kept in the same location of interest for a long period of time for urethral imaging and be resistant to manipulation throughout the operations. When ICG is mixed with a lubricant, whilst some may bind to the epithelial cells in the urethra, significant amounts of ICG may be lost into the bladder through retrograde flow. Secondly, ICG will rely upon penetration through tissue of the laser light emitted from the laparoscope in order to be excited and for the emission light to also penetrate through this tissue. An alternative to ICG is the use of an optical fibre that would emit NIR light. Such a system would firstly have constant emission of NIR light in the desired location and secondly would not rely on excitation light having to penetrate through the tissues. A collaboration was developed with the Advanced Technology Group (ATG), University of Oxford, to design a device that would be tailored to urethral imaging (NIRCaD, NIR Catheter Device). Briefly, the device consisted of a laser light source which emits light at 830nm and is connected to a fibre optic light cable allowing transmission of

the light. These fibres have an insulating jacket and once removed need 'stripping' to emit light along the length of the cable rather than just at the tip. Rather than pass an optical fibre directly through the urethra, a small calibre optical fibre was chosen allowing it to sit inside the drainage channel of a 2-way urinary catheter via the urinary drainage port. As the urinary drainage port would no longer fit a drainage bag, a plastic adapter was manufactured using 3D printing to allow passage of the optical fibre and connection of a drainage bag (Figure 4.7). Thus, this system allowed the simple adaption of a standard urinary catheter to allow passage of a NIR emitting light fibre as well as allowing free drainage of urine which has not been described before.

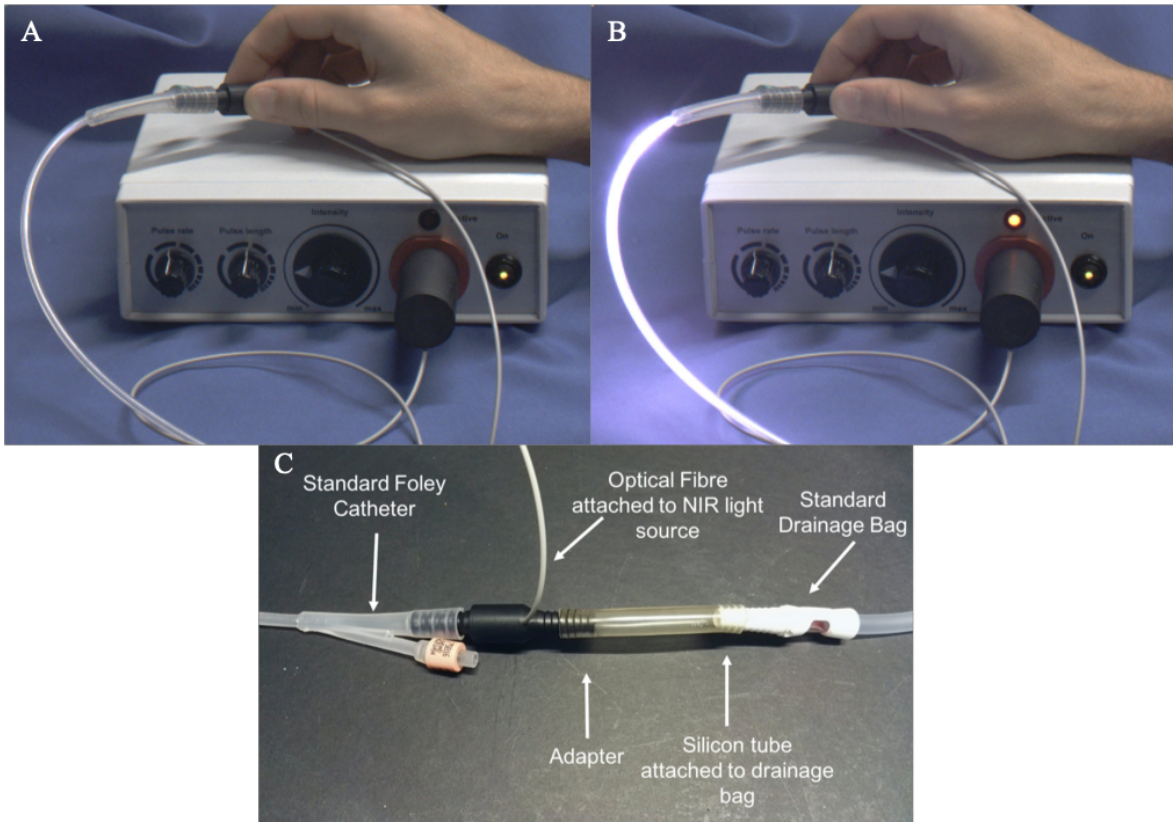

Figure 4.7 - NIR urinary catheter light source, fibre, and adapter (NIRCaD). A&B – Fully connected light source and optical fibre within urinary catheter with light off (A) and light on in NIR mode (B). C – set up of urinary catheter, plastic adapter, optical fibre and drainage bag.

In order to be prepared for patient use, the parts in contact with the urinary catheter (plastic adapter, optical fibre and silicon tubing needed to be sterilised. As the optical fibre and plastic connector would denature in high temperatures, the only method of sterilisation was using the STERRAD®. Both components underwent sterilisation 10 times checking integrity after each run which was successful. The silicon connecting tube was obtained from cutting a length of sterile tubing from a separate urinary drainage bag.

4.3.5.1. Cadaveric assessment of NIR light fibre

The NIRCaD device was tested in 4 human cadavers prior to patient use. In two cadavers, the perineal model described above was used. As expected, the mean signal to background ratio observed in the area of the urethra with minimal dissection was considerably higher than ICG at 10.35. Following this, two further cadavers were assessed during a TaTME simulation. Due to high signal to background observed perineally, it was hypothesised that the emitted NIR light may be able to penetrate through the prostate. Following mobilisation of the rectum in the correct TME plane, in both cadavers, fluorescent signal could be observed clearly outlining a tubal structure in the correct location of the urethra running through the prostate and the seminal vesicles. The incorrect plane of mobilisation anterior to the prostate as described previously was then entered to confirm the urethral location and fluorescence emission from the NIRCaD (Figure 4.8).

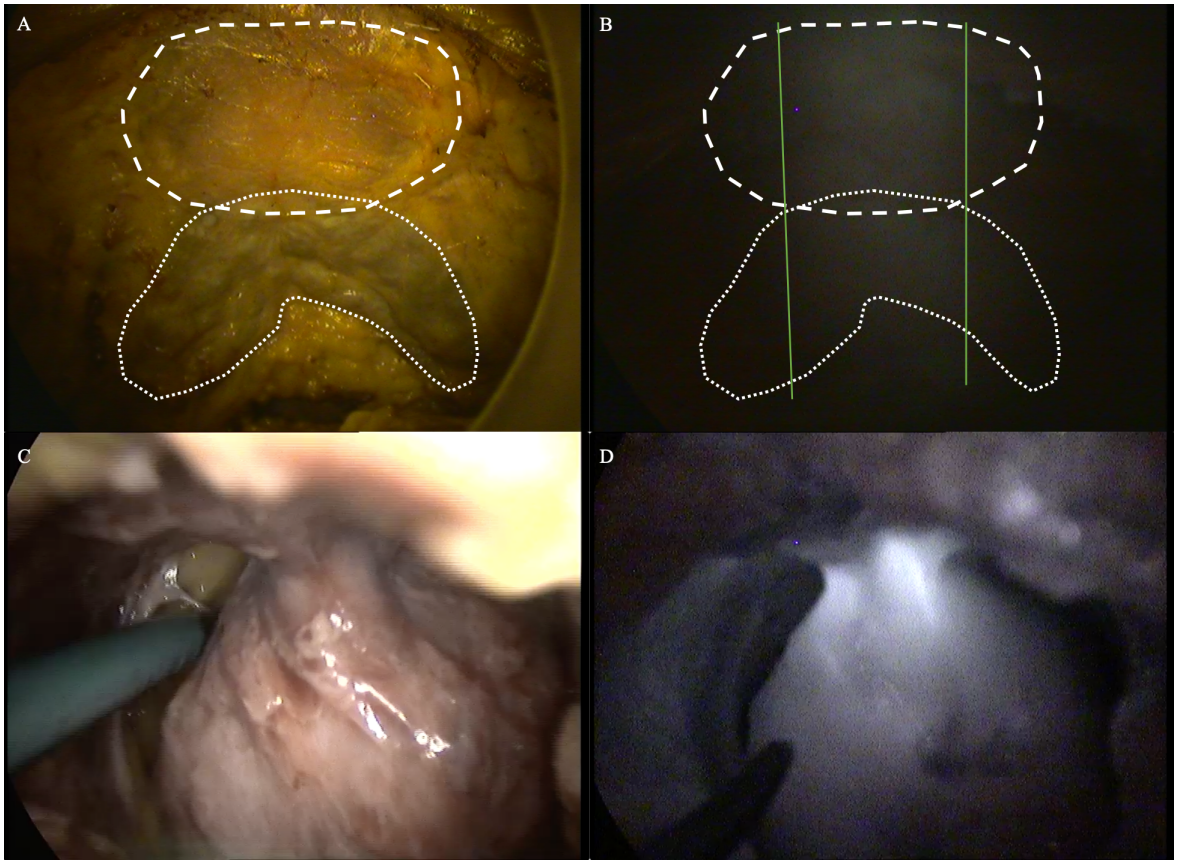

Figure 4.8 - Visualisation of NIR Light from NIRCaD in cadaveric TaTME model. A&B = white light (A) and NIR (B) image of prostate (dashed line) and seminal vesicles (dotted line) with a line of NIR light (green solid lines) being emitted between the 2 structures. C&D = wrong plane mobilisation of the prostate revealing urethral location and bright light emitting from the NIRCaD.

4.3.5.1. NIRCaD Clinical Trial

From November 2017 to June 2018, 12 participants were recruited to the study with a mean BMI of 29.4 (23.8 to 35.0) and mean age of 60 years. Eight participants underwent TaTME with the remainder having an APER. In all participants, NIRCaD insertion to the urinary catheter and urethral placement of the urinary catheter was uncomplicated.

In the first 5 participants, no detectable NIR signal was observed at any point anywhere in the pelvis in either the prostate, area of the membranous urethra or seminal vesicles but the

NIRCaD was confirmed as working through bladder visualisation. The urethral fibre was then reassessed to see if any modification could result in increased light emission. Following inspection, as the optical fibre was stripped along its entire length, loss of light at the proximal end of the fibre could result in reduced emission in the area of interest. Therefore, at this point, a new fibre was constructed to only emit light from the tip of the fibre and through the prostatic and membranous urethra. The length was determined by measuring the pelvic MRI scan from the previous 5 participant which revealed a mean prostatic urethral length of 3.2cm and membranous urethral length of 0.4cm. To account for potential movement an extra 1.5cm was added to the stripped length giving a final stripped length of 5.1cm. To mention about change in signal due to this change.

The following 7 patients were then assessed using the new fibre. Of these, NIR signal was observed in 2 patients. In the first it was seen after specimen removal during APER (S: B 55.9) and in the second it was seen during dissection (S:B 4.09) and post specimen removal (S:B 28.7) during TaTME. In the remaining 5 patients, no signal in the urethral region could be observed despite positive signal emitting from the bladder.

At 30-days there were no adverse events related to use of the NIRCaD device.

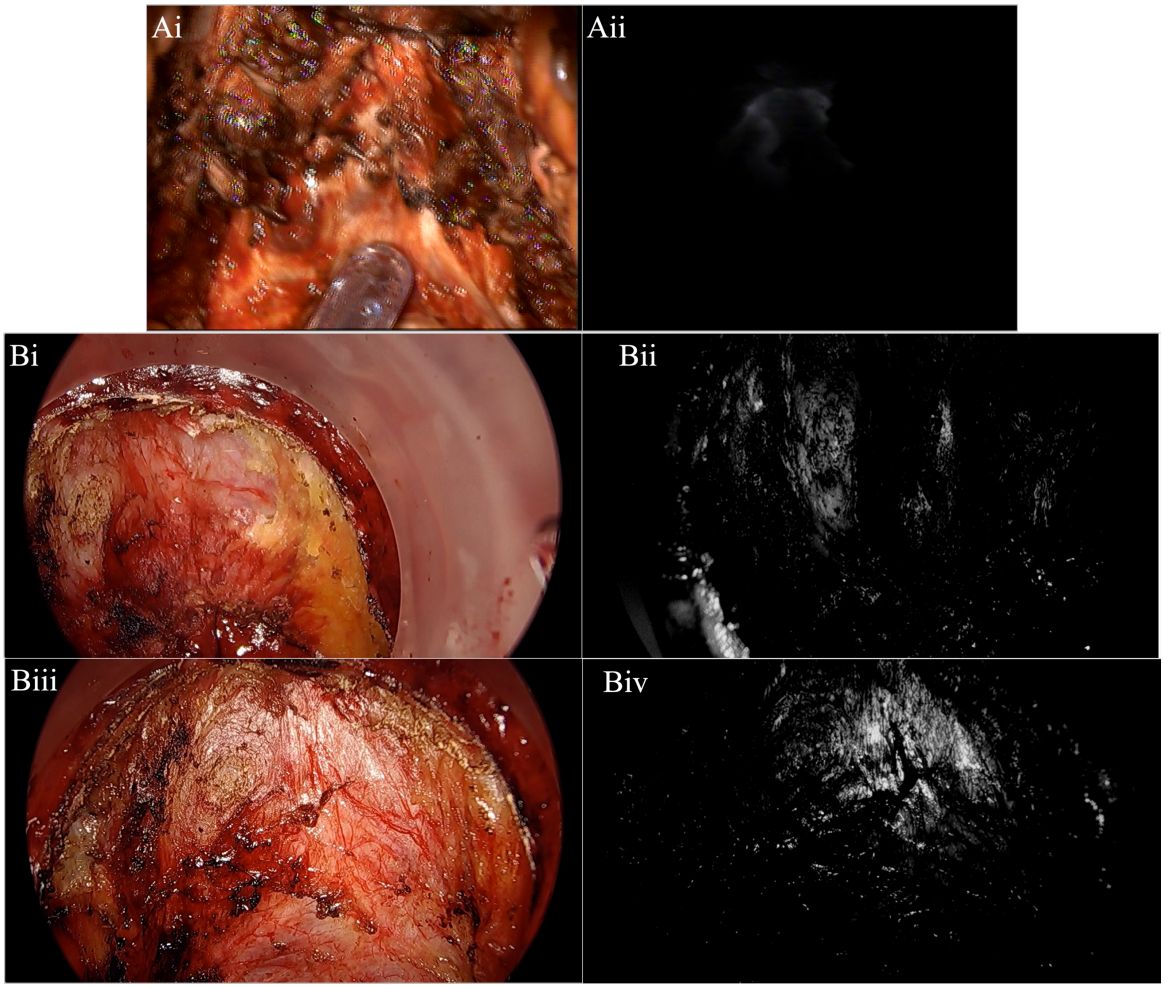

Figure 4.9 - In-vivo images of NIRCaD visualisation around the membranous urethra and prostatic regions. A is following specimen extraction during APER, in the region of the urethra a clear NIR signal (white) is seen with minimal background (i = white light image, ii = NIR image where white is NIR signal). Bi (white light) and Bii (NIR) are during the TaTME dissection where NIR signal is seen just right of the midline in a tubular shape assumed to be the urethra and a broader signal is seen after specimen extraction (Biii and Biv) outlining the prostate.

4.4. Discussion and further work

This chapter has experimented with different methods of visualising the urethra during low rectal cancer surgery with the use of both NIR fluorophores mixed with Instillagel and the manufacture of a NIR emitting light source that can be used with a standard urinary catheter. *Ex-vivo* pig and human cadaver work proved the principle that ICG-Instillagel could be successful in highlighting the urethra and was superior to methylene blue. On moving this into human use, difficulties in the method of application were experienced including loss of volume, contamination, and patient movement. These may have contributed to the failure of this technique. In all 5 patients, the urinary catheter was palpable without any NIR signal, thus the technique merely added time to the procedure in checking for NIR signal without any benefit and hence why it was abandoned. Still using ICG, an ICG-silicon catheter was made to overcome issues of leakage. This offered no benefit in cadavers in signal to background ratio and to take this into human use would require moulding of a hollow-tubed catheter which, after talking to numerous manufacturers is difficult to do without breaching existing patents and issues over fluorescence decay with storage cannot be overcome.

Another reason for failure of fluorescence in this setting but success in cadavers is probably due to the differences in cadaveric versus living bodies. There is significantly more water content in living bodies than cadavers as well as the circulating blood and blood products. It is well known that NIR light is absorbed by both blood and water [144] and could be responsible for the reduced visibility seen *in-vivo*. NIR imaging here is also relying on excitation as well as emission and therefore absorption of NIR light for both excitation and emission may reduce efficacy.

The NIRCaD was designed to provide a fixed, constant level of emitted NIR light without relying on excitation. Again, cadaveric results were extremely promising with very high

signal to background ratios compared with ICG and methylene blue. *In-vivo*, there was slightly more success than with the other techniques but certainly not enough to pursue to a larger trial in its current state. A drawback of this study was it being undertaken in a tertiary centre with surgeons who are experienced in low rectal cancer surgery thus, the risk of wrong plane surgery and visualising the urethra during any procedure is low. The next investigative stage of the NIRCaD device is to go back a step and review its efficacy rather than proceed with studies of larger numbers. Two potential study avenues could be pursued. Firstly, validation of the device in urological surgery where mobilisation and visualisation of the urethra occurs as part of the procedure (e.g. prostatectomy or urethral reconstruction). Such a study should be conducted under stage 1 of the IDEAL framework with a small number of patients. Following this, returning to colorectal surgery should include its use for urethral and prostate identification on cadavers for TaTME simulation as described above but assessed with several different surgeons and different levels of training. To return to *in-vivo* use, a stage 2a study should be conducted with surgeons early in their adoption of the TaTME or APER procedures rather than experienced surgeons as done in this study. If both are successful, then assessment of the NIRCaD in a larger number of non-randomised patients should be performed.

As mentioned previously, stereotactic navigation has been utilised in TaTME surgery, using recent or intraoperative scans and body markers to provide real-time navigation [143]. This technology could be combined with markers on a fibre similar to the NIRCaD adding localisation of the urethra.

Outside of the light spectrum, other theoretical concepts within the electromagnetic spectrum for urethral localisation could be investigated. To the right of the visible light spectrum lies longer electromagnetic wavelengths including microwaves and radio waves.

Wavelengths in this spectrum range from 1cm to 100km and at low levels do not ordinarily pose a risk hazard to humans but can penetrate much deeper than NIR light and transmit through fat and bone much easier [145]. Utilisation of these wavelengths through a similar optical fibre to that used in the NIRCaD and an appropriate detector which could visualise the signal and overlay an operative image could be a promising alternative to NIR light [142]. Care should be taken if investigating these frequencies as if focussed at high frequency, heat damage could occur.

Finally, additional future directions of urethral localisation have been postulated to include laser doppler vibrometry [146], accelerometers with a vibrating catheter [147], passive millimeter-wave imaging [148] and magnetic and radioisotope impregnated catheters [142]. All this technology could utilise the basic framework of the NIRCaD construction emitting the various wavelengths described in this already available technology. Difficulties would be in providing appropriate detection systems small enough to be placed in an operating theatre as well as software engineering to provide real-time overlay operative images.

CHAPTER 5: FLUORESCENCE IDENTIFICATION OF THE THORACIC DUCT DURING OESOPHAGECTOMY

5.1. Introduction

5.1.1. Anatomy

The thoracic duct is the largest vessel of the lymphatic system draining three quarters of lymph from the body. Its main role is to transport the products of fat digestion and is therefore rich in triglycerides, cholesterol, proteins and T-lymphocytes. It originates from the descending intercostal trunks, the right and left lumbar trunks and the gastrointestinal trunks. The cisterna chyli is often described as where these trunks meet located at the level of L2 to T12 between the azygos vein and aorta. The thoracic duct then runs upwards towards T5 where it crosses to the left side posterior to the oesophagus and then enters the base of the neck to terminate at the junction of the left internal jugular vein and the left subclavian vein [149, 150]. There are however, numerous anatomical variations including in nearly half of patients having multiple channels especially in the mid thorax [150, 151]. In length it ranges from 36 to 45cm with a diameter from 2 to 5mm which varies according to its level and physiology but is narrowest in the thoracic region [150].

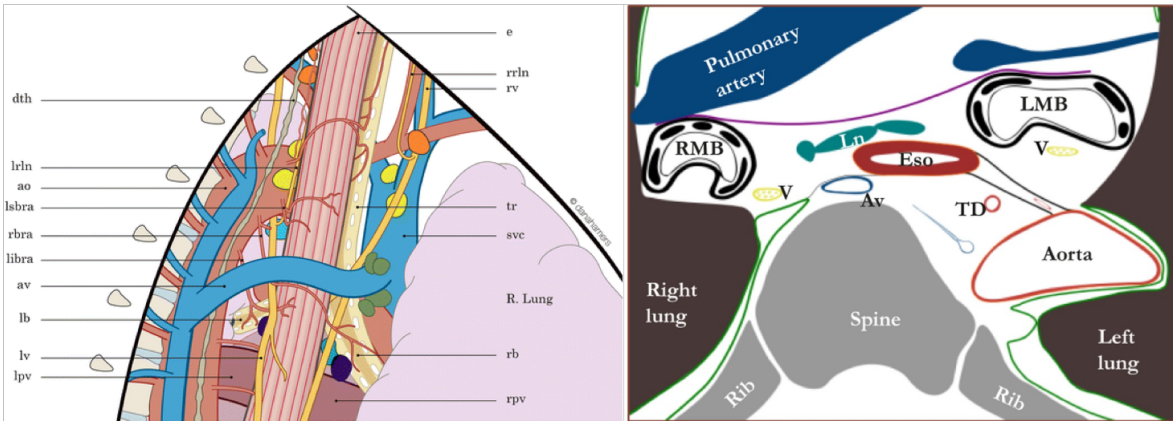

Figure 5.1 - Anatomical depiction of thoracic duct location in the saggital plain (left) and coronal plane (right). Left image depicts a thoracoscopic viewpoint adapted from Cuesta *et al* [152] with permission. DTH, ductus thoracicus; LRLN, left recurrent laryngeal nerve; AO, aorta; LSBRA, left superior bronchial artery; RBRA, right bronchial artery; LIBRA; left inferior bronchial artery; AV, azygos vein; LB, left bronchus; LV, left vagus nerve; LPV, left pulmonary vein; E, esophagus; RRLN, right recurrent laryngeal nerve; RV, right vagus nerve; TR, trachea; SVC, superior vena cava; RB, right bronchus; RPV, right pulmonary vein. Right image is a coronal cross section demonstrating the aorto-oesophageal ligament which is divided as part of the mobilisation during oesophagectomy. Av, azygos vein; LMB, left main bronchus; Ln, lymph node; RMB, right main bronchus; TD, thoracic duct used with permission from Weijs *et al* [153].

5.1.2. Thoracic duct significance during oesophagectomy

Surgical treatment of oesophageal cancer in the UK entails oesophagectomy be it a 2-stage procedure (Ivor-Lewis), hybrid procedure (laparoscopic abdomen and right thoracotomy), a left thoracoabdominal oesophagectomy or, for proximal tumours, a 3-stage oesophagectomy which includes neck dissection. As well as removing the oesophagus, lymphadenectomy should be undertaken but practice varies as to how radical surgeons are in targeting lymph node groups [154]. There is also variation in what surgeons do with the thoracic duct. Some surgeons advocate resection of the thoracic duct as it has been demonstrated that there are lymph nodes in the fatty tissue surrounding the thoracic duct [155, 156] although Udagawa and

colleagues found no significant difference in survival when these were resected. A study comparing thoracic duct dissection to non-thoracic duct dissection showed that when resecting the duct, there is a significantly higher yield of lymph nodes and this may have an improvement on recurrence free survival although more patients in the thoracic duct resection arm received chemotherapy [157]. Opponents to thoracic duct resection fear for complications including chylothorax and an increased operating time and blood loss.

A frustrating complication of oesophagectomy is chylothorax which arises from injury to the thoracic duct. Reported incidence of this complication is around 1% but has been reported as high as 9% [158-160]. Chyle leak is associated with considerable morbidity namely from chest complications including pneumonia and respiratory failure. High volumes of fluid can be lost from a thoracic duct injury resulting in long durations of indwelling chest drains, hypovolaemia and malnutrition from the loss of fat-soluble vitamins, proteins and electrolytes. There is also a risk of sepsis and even death following thoracic duct injury [160] with mortality reported as high as 75% [161]. Management is usually non-operative with pleural drainage and total parenteral nutrition to allow resolution of the chylothorax which can last several weeks and when unsuccessful, operative intervention is required. Large volume chylothorax may require return to theatre to localise and repair the leak by ligating the thoracic duct. Re-operation is difficult as localising the duct in the post-operative setting can be impossible.

The variation in thoracic duct anatomy and its accessory channels can make its identification difficult whether it is for resection as mentioned previously or to avoid injury. A technique employed by some to visualise the thoracic duct intraoperatively is to use enteral administration of cream which gives a white appearance of the duct [161]. Similarly, methylene blue has been used as a visible blue dye in the setting of diagnosing chylothorax [162]. A

difficulty with this technique is that light reflected from the cream will not penetrate the covering fat and fascia and therefore would only be visible once the thoracic duct is dissected free from surrounding structures. NIR fluorescence imaging of the duct could allow better visualisation.

To date, thoracic duct fluorescence has been demonstrated by Ashitate *et al* [163] who demonstrated in rats and pigs that NIR visualisation is possible with IRDye 800CW-CA and IRDye 800CW conjugated to albumin following subcutaneous groin, thigh or shin injection. They also developed a porcine model of thoracic duct injury where it was possible to visualise a leaking duct as well as clearly outlining accessory channels. In humans, there have only been 4 unconvincing case reports where ICG has been attempted to identify a chyle leak at re-look thoracotomy [164-167]. There have been no reports of *in-vivo* human use of fluorescence to both highlight the duct or to identify chyle leakage at the end of oesophagectomy and therefore prevent post-operative chylothorax. Whilst IRDye 800CW has proven successful in the pig, it is an unlicensed drug and thus would require clinical trial authorisation to assess in man, therefore ICG was pursued for this study as an easier alternative.

5.1.3. Aims and objectives

The aims of this chapter are to:

1. Assess the feasibility of ICG fluorescence of the thoracic duct during oesophagectomy using 2 different methods
2. To assess whether intraoperative chyle leaks can be identified at the end of oesophagectomy using fluorescence
3. To compare a thoracic duct fluorescence with a historical cohort of patients for surgical outcomes

5.2. Methods

5.2.1. Trial Set up

5.2.1.1. Protocol

This study was an open label prospective feasibility study assessing ICG to fluoresce the thoracic duct during oesophagectomy. Two methods were compared: infiltration of ICG mixed with double cream administered enterally via a feeding jejunostomy and; subcutaneous injection of ICG into the small bowel mesentery during the abdominal phase of the operation. In each administration method, ICG was given in the operating room following induction of anaesthesia. ICG fluorescence was assessed using a commercially available fluorescence enabled laparoscope compatible with ICG (PINPOINT or Stryker). The study was approved by Wales REC 7 (17/WA/0295) and confirmed by the MHRA that clinical trial approval was not required.

All participants over 18 years of age undergoing elective oesophagectomy were eligible to enter the study. Participants were excluded if they had a known allergy to iodine or ICG, lactose intolerance, significant liver failure (ALT and AST > 1.5 ULN) or female patients who were pregnant, planning pregnancy or breastfeeding. Participants were identified at their outpatient appointment or through planned operating lists and were approached by phone call or at their clinic visit and given a PIL. After being assessed for eligibility, informed consent was taken on the day of surgery. It was decided to perform ICG fluorescence on 3 participants with each method and assess both techniques and take forward the most successful approach.

Baseline assessments were performed on the day of surgery including BMI and past medical/surgical history. Following induction of anaesthesia and entering the abdominal cavity, ICG was administered in the following methods:

ICG Cream: 50mL of double cream mixed with 2.5mL of reconstituted ICG (10ml in 25mg of ICG).

Small bowel mesentery: 1.5-2mL of reconstituted ICG (as above) injected into the small bowel mesenteric root.

Following administration, the operation proceeded as per the standard of care. During the thoracic part of the procedure, attempts were made at numerous unfixed timepoints to visualise the thoracic duct under white light and then fluorescence. The time point (following administration) as well as a subjective score was recorded (Table 5.1). Finally, following removal of the oesophageal specimen, observation for any chyle leakage was undertaken with white light and fluorescence. Following these assessments, the participant returned to standard care. At 30 days following surgery the participant's clinical notes were reviewed for any adverse events and recorded chest drain output.

Score	White Light Scoring	Fluorescence Scoring
0	TD or branches not visible at all	No fluorescence signal
1	In area of thoracic duct but not clearly visible	Weak fluorescence signal not convincingly in TD / branches
2	TD/ branches partially visible	Weak fluorescence signal convincingly in TD / branches
3	TD / branches clearly visible	Strong fluorescence signal convincingly in TD / branches

Table 5.1 - ICG thoracic duct and white light visualisation subjective scoring descriptors.

A historical group of patients were obtained from a prospectively collected database of patients who underwent oesophagectomy was used as a control group for a propensity score matched analysis. Data collected included baseline demographics (BMI, weight, ASA, pre-operative albumin, tumour and nodal staging). Propensity score-matched analysis was performed to minimised selection bias and all the baseline demographics listed were used in the regression model. The dependent variable for grouping was the use of ICG. A matching ratio of 1:1 was used with a nearest neighbour matching protocol and a caliper of 0.2 using IBM SPSS for Mac (version 24.0, Armonk, NY). Cases were not reusable after matching. The outcome parameters were analysed by the Mann-Whitney *U* test and differences were considered statistically significant when the p value was less than 0.05.

5.3. Results

5.3.1. Effect of pH and cream on ICG fluorescence

Options for administration included enteral administration or mesenteric injection. It was important to ensure that fluorescence of ICG was not destroyed by the acidic conditions in the upper gastrointestinal tract. Under controlled conditions, ICG, at a concentration of 1mg/mL was mixed with increasing pH solutions (from pH 1-7) and imaged using the ATG fluorescence camera. As pH decreases, the signal to background ratio also decreases (Figure

5.2). Signal to background ratio increased significantly as pH increased assessed by linear regression (slope 2.949+/- 0.412, R^2 statistic 0.911, p=0.0008).

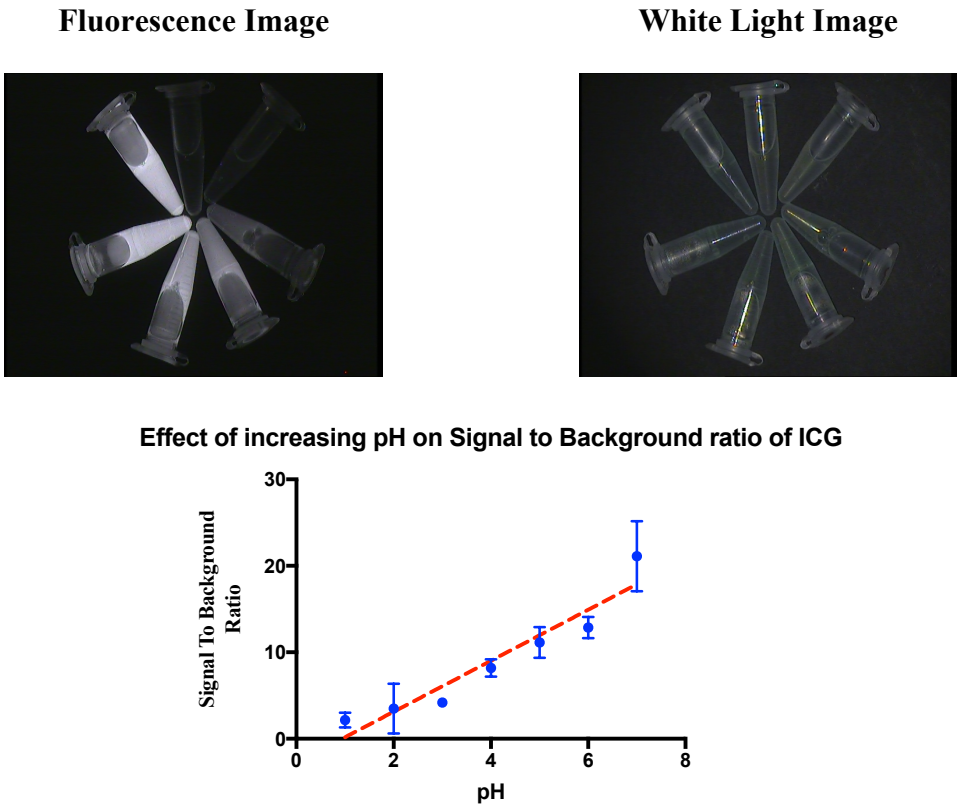

Figure 5.2: ICG mixed with varying pH solutions and observed under ATG fluorescence imaging camera. Eppendorf at 12 o'clock is pH 1 then increasing in a clockwise direction to pH 7. Note the visible increase in fluorescence signal as the pH increases. Dotted line represents fit of linear regression equation.

ICG directly infiltrated into the gastrointestinal tract either via a feeding jejunostomy or nasogastric tube is therefore unlikely to fluoresce as expected. If mixed with cream, the ICG may buffer the acidic conditions and therefore, investigation into signal changes of pH 1 versus 7 in cream was investigated (Figure 5.3). In a pH of 1, the signal to background ratio decreases over time (slope -0.001445 +/- 0.00018, R^2 0.984, p=0.0009), whereas in a pH7 of 7, the signal to background ratio slightly increases which only just reached statistical

significance (slope 0.00089 +/- 0.0003, R^2 0.7766, p=0.048). In pH1 conditions, the signal to background ratio significantly reduced out of time compared to pH7 (p=0.0002).

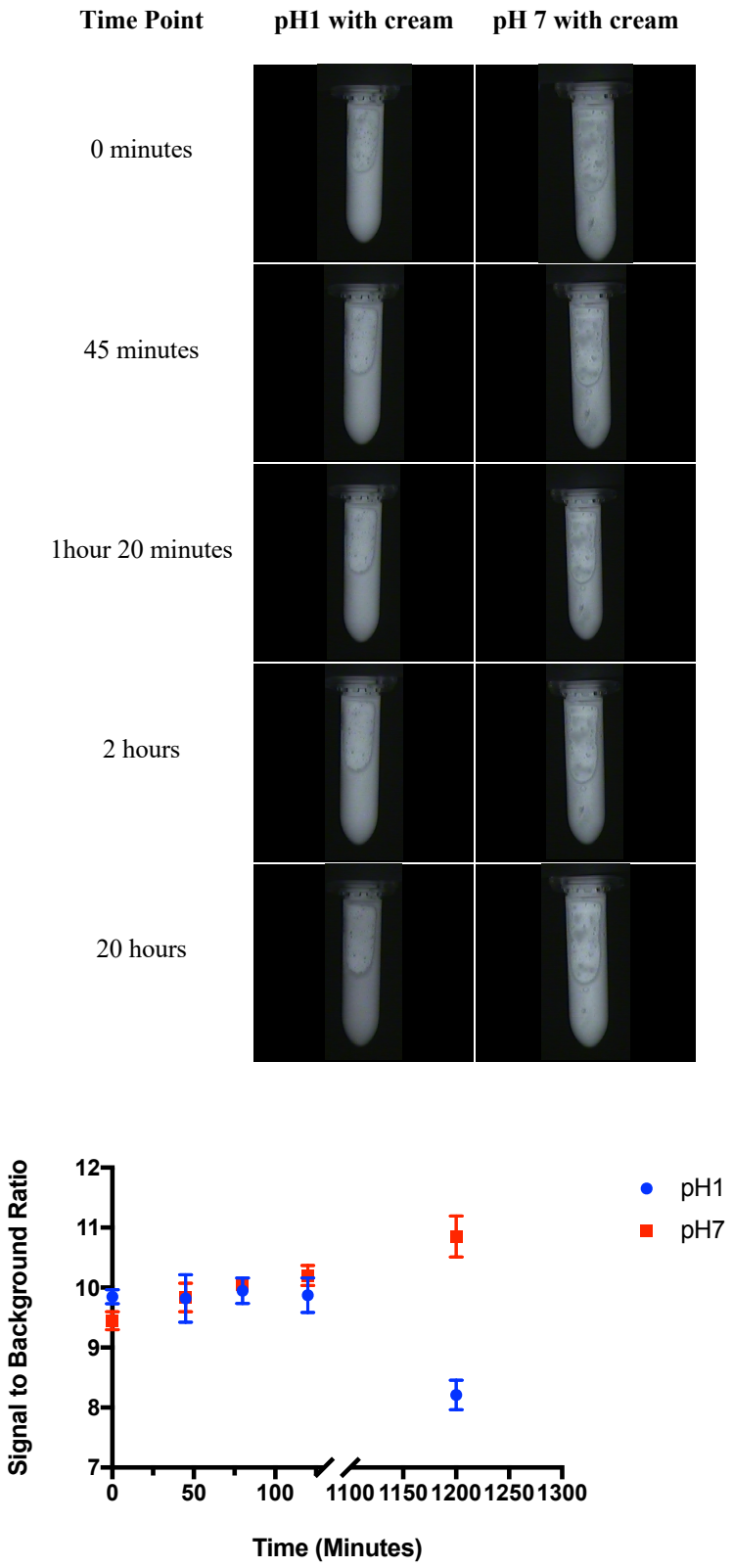

Figure 5.3: ICG mixed with cream at pH1 and pH7 and imaged at different time points. Visualised fluorescence in Eppendorf tubes with graphical representation of signal to background ratio.

5.3.2. ICG thoracic duct clinical trial results

5.3.2.1. Recruitment

As this was a proof of principle study, it was decided that 20 participants would adequately assess whether the technique worked and to provide data for a phase 2 study as well as being able to recruit this number of participants in the time constraints throughout the authors research period. Assessing operative capacity and planned operating lists, it was estimated that for 3 operating surgeons there would be around 1 patient undergoing oesophagectomy per week and allowing for ineligibility and patients declining participation, it was likely that 2 patients would be successfully recruited per month.

Thirty-one patients were screened for eligibility to enter the trial, all of whom met the eligibility criteria. Four were not approached as the author would not be present on their day of surgery (n=3) and there was a clash with another fluorescence trial (n=1). Of the 27 patients approached to consider participation, 2 patients had a planned 'chest first' procedure, for 2 patients there would be no fluorescence enabled laparoscope available on the day, one participant had their operation postponed and the author was not available for 1 other participant. Twenty-one participants were consented to the trial from December 2017 until July 2018 (Figure 5.4). Three participants received ICG-cream mix via feeding jejunostomy and 17 received ICG injection into the small bowel mesentery.

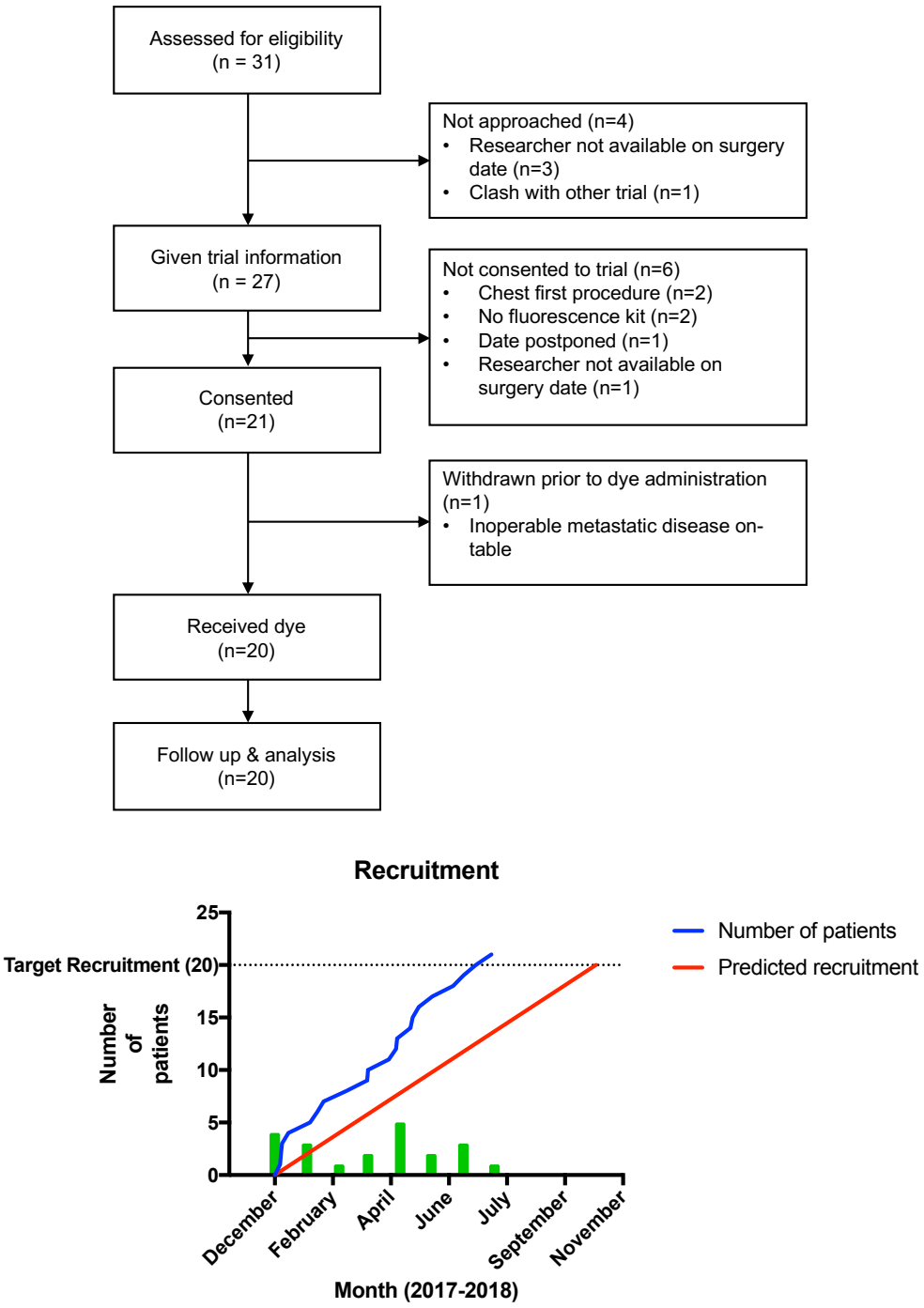

Figure 5.4 – Recruitment of ICG thoracic duct trial. Top represents CONSORT flow diagram of patient recruitment. Bottom represents predicted and actual recruitment. Blue line is the cumulative actual number of patients recruited, red line is the predicted recruitment rate and green bar charts represent the number of patients recruited on a monthly basis.

Seventeen participants were female with a median age of 62 years (range 37 to 78) with a median BMI of 25.7 (range 16.95 to 35.33). All patients were undergoing planned curative oesophagectomy for cancer with either an open procedure (n=12), a hybrid procedure with laparoscopic abdomen and open thorax (n=6) or minimally invasive oesophagectomy (n=3). Of the open procedures, 8 were left thoracoabdominal resections and 4 were Ivor-lewis oesophagectomies. All cases were performed by three different operating surgeons.

5.3.2.2. Fluorescence results – feeding jejunostomy

Three participants received ICG-cream via the feeding jejunostomy. No fluorescent signal was seen at any point in the region of the thoracic duct or in any location throughout the chest during the procedure, despite visualisation of the thoracic duct under white light. It was evident, that the ICG-cream mix fluoresced clearly in the small bowel but was not being absorbed into the lymphatics up to 6 hours and 59 minutes following administration (Figure 5.5). Furthermore, the administration technique of feeding jejunostomy proved lengthy as it took between 10 and 16 minutes to injection the 100mL of cream-ICG into the feeding jejunostomy. It was therefore decided that the feeding jejunostomy technique would be abandoned and subsequent participants would receive ICG via small bowel mesentery injection.

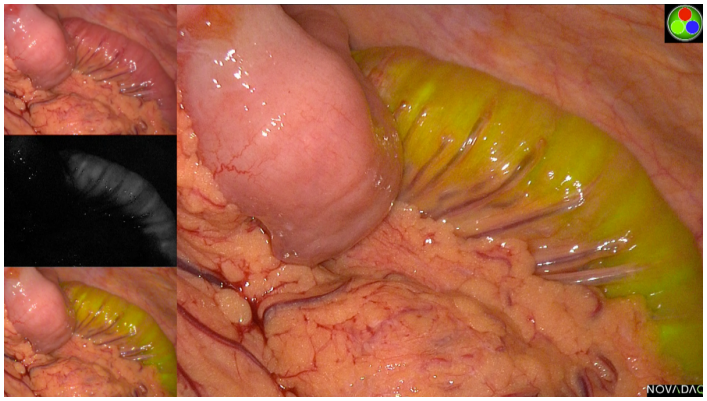

Figure 5.5- Representative image of fluorescent small bowel following ICG-cream mix infiltrated via a feeding jejunostomy.

5.3.2.3. Fluorescence results – mesenteric injection

In 17 patients, ninety observations for fluorescence in the thoracic duct were performed from 4 minutes to 5 hours and 30 minutes (median 2 hours 31 minutes) following ICG administration (Figure 5.6A). The thoracic duct was visualised with both white light and fluorescence in 12 patients, in 8 of these, the thoracic duct was seen with fluorescence prior to being seen with white light (median = 84 minutes, range 10 to 185 minutes), in 1 patient, the thoracic duct was seen with white light 25 minutes before fluorescence and in the remaining three the thoracic duct was seen at the first visualised time point with both modalities. In 2 patients, the thoracic duct was seen with only fluorescence and not white light and vice-versa in a further 2. The thoracic duct was not visible with either modality in 1 participant.

Of the 90 assessments made, the thoracic duct was not visible with any modality in 50% (n=45). In 20% (n=18), the thoracic duct was seen with both modalities and in 23% (n=21) the thoracic duct was only seen under fluorescence. In the remaining 6 observations (6.6%), the thoracic duct was visible under white light but not under fluorescence. Of the 18 seen with both modalities, the subjective score was higher under fluorescence in 11 observations,

scored the same in 7 (6 with a score of 3, 1 with a score of 2), and there were no instances where white light scored higher than fluorescence.

Mean thoracic duct signal was 75.12 (95% CI 62.66 to 87.58) and mean background signal was 24.18 (95% CI 23.34 to 3.404) with the signal being significantly higher than the background (P<0.0001) (Figure 5.6B). Mean signal to background ratio was 5.354 (95% CI 3.91 to 6.80) ranging from 1.064 to 24.37. Over the time assessed in this study, the rate of decline was zero (slope 0.4225, 95% CI -0.678 to 1.523, p=0.443) (Figure 5.6C). Mean probability of thoracic duct visualisation being better with fluorescence was 0.42 (95% CI 0.302 to 0.538) which was significantly higher than visualisation being better with white light (mean 0.147, 95% CI 0.06 to 0.23) (p=0.0003). Over-time, ICG seemed to be better than white light from 1 hour to 5 hours 30 minutes (Figure 5.6D).

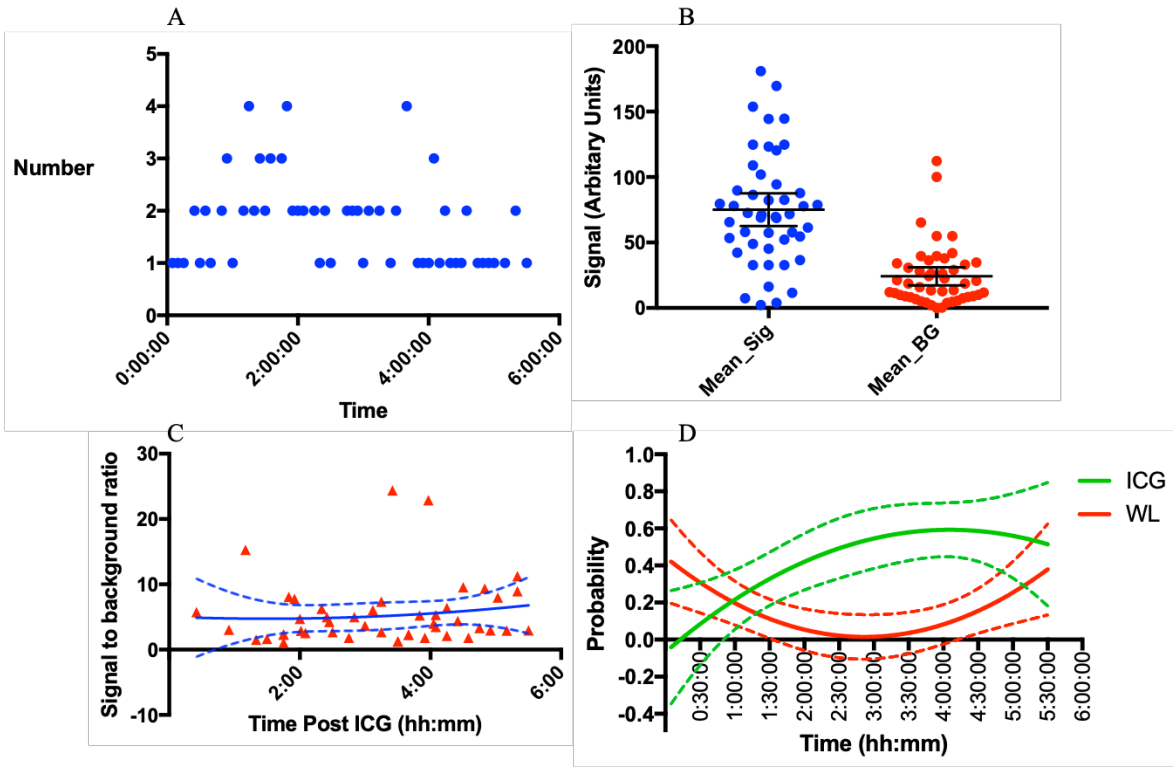

Figure 5.6 - Graphical representation of data from ICG thoracic duct trial. A = graphical representation of number of individual readings over time. B = ICG signal in thoracic duct (blue) versus background signal (red) with 95% confidence interval (black). C = signal to background ratio over time with non-linear regression line of best fine and 95% confidence intervals (dotted line). D = probability of ICG being better than white light (WL) over time (green) and white light being better than ICG (red) – line generated by non-linear regression analysis using second order polynomial equation.

5.3.3. Fluorescence to identify intraoperative chyle leaks

A further subjective assessment of thoracic duct fluorescence was to assess whether active chyle leak could be observed at the end of the oesophagectomy and whether a source could be identified to prevent post-operative chyle leaks. In 6 of the 17 participants receiving ICG via mesenteric injection, fluorescent fluid was identified over the operative field following specimen removal. These were all identified by fluorescence only. Of these, fluorescent fluid was seen all over the operative field with 1 resulting in no further action and another where a small leaking branch was identified and clipped. The remaining 4 patients with an identified leak had fluorescent fluid emerging from a fluorescent tubal structure identified as the thoracic duct. In all four of these participants the main thoracic duct was further clipped, wash applied to the thorax and re-imaging of fluorescence revealing no further leak. Five of these participants were discharged without any complications within 10 days. One patient suffered an anastomotic leak and remained in hospital for 40 days post-operatively.

5.3.4. Post-operative follow-up

All patients were followed up for 30 days following ICG administration. No participants suffered adverse reactions related to ICG. Median length of stay was 10 days (range 7 to 40 days) with one participant having a possible small chyle leak identified with chylous appearing liquid in the drain, however their drain was removed after 5 days with no further complications and the patient was discharged on day 8 post-operatively.

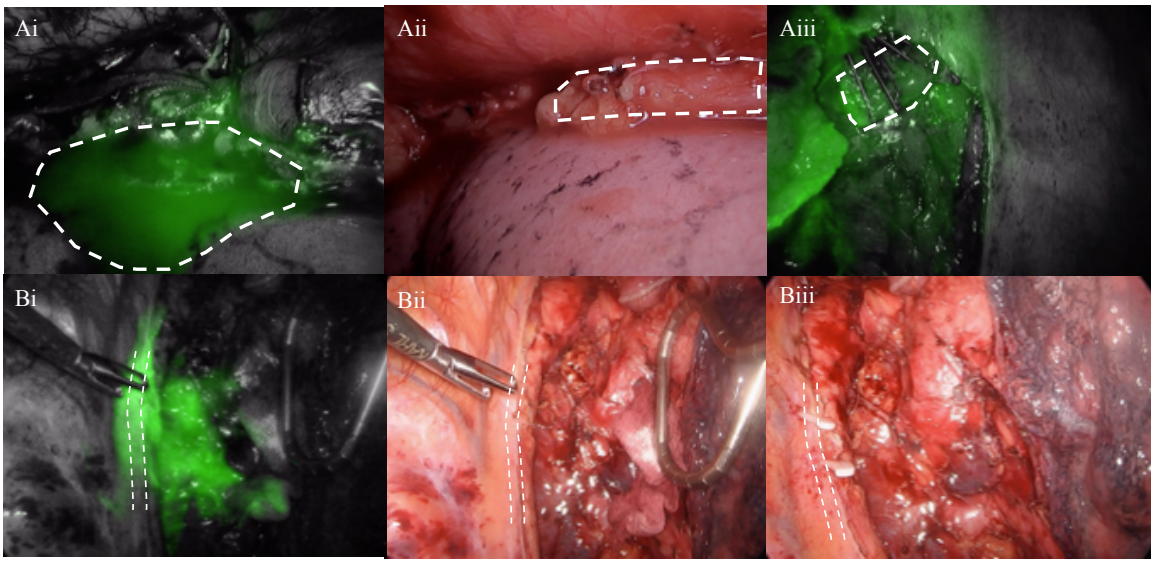

Figure 5.7 - Representative images of identifying chyle leak under fluorescence in two patients. A and B represent two separate participants. Ai – image under fluorescence identifying fluorescent 'pool' of fluid (white line). Aii – image with white light outlining area of thoracic duct. Aiii clipped thoracic duct under fluorescence. Bi = fluorescent image outlining (white line) thoracic duct and adjacent to this fluorescent fluid. Bii – white light image of Bi. Biii – white light image following clipping of thoracic duct.

5.3.5. Propensity score-matched analysis comparing ICG thoracic duct trial participant with control group

Following the ICG thoracic duct trial a potential difference for length of stay, duration of indwelling chest drains and total drain output between the trial cohort and a preceding control group was investigated. Four hundred and fifteen patients were identified as having an oesophagectomy from October 2010 to October 2017 (before the ICG trial commenced). Of these, 137 were coded incorrectly and did not undergo oesophagectomy. Data was missing for 147 patients that was essential for the propensity score-matching (BMI, albumin, ASA, tumour and node stage) resulting in 131 patients used for propensity score matching.

Before matching, no difference between the 2 groups were identified in age, gender, ASA grade, pre-operative albumin, tumour stage, node stage or metastases stage (Table 5.2). All

patients had an M stage of 0 and this was therefore removed from the comparison. BMI was significantly higher in the thoracic duct group (30.75 vs 27.66, p = 0.0001). After propensity score matching, 34 patients remained to be evaluated (17 in each group). After matching, no differences in baseline characteristics remained, although there was still a higher BMI in the trial group but not reaching statistical significance (p=0.485).

Data for whether a chyle leak occurred was not available for all patients in the pre-ICG group but was collected retrospectively in the case-matched control group and therefore was only included in the post propensity score matching analysis. It was decided that outcomes of interest should include length of stay, total chest drain output and duration of indwelling chest drain would be compared. Before and after matching, no difference in length of stay, total drain output and drain duration was observed (Table 5.3). Length of stay was shorter in the ICG group both before (2 days, p=0.55) and after matching (0.9 days p=0.74) but not reaching statistical significance. Total drain output was slightly higher in the trial group after matching by 33mL and did not reach statistical significance. Duration of indwelling drain was 24 days longer in the non-ICG trial group and again did not reach statistical significance (p = 0.35). It is likely that the differences observed in this comparison are not significant due to a type II error. Furthermore, in the non-ICG group, there was a high standard error of the mean for drain duration (25.66).

		Before Matching			After Matching		
Variables	**All Patients (n=148)**	**Pre-trial (n=131)**	**ICG TD (n=17)**	***P***	**Pre-trial (n=17)**	**ICG TD (n=17)**	***P***
Age mean / SEM	64.7 (0.734)	65.03 (0.756)	62.53 (2.633)	0.292	65.24 (1.53)	62.53 (2.63)	0.381
BMI mean / SEM	28.0 (0.581)	27.66 (0.412)	30.75 (3.97)	**0.001**	27.81 (1.135)	30.75 (3.98)	0.483
Sex				0.354			0.485
Male	118	103 (78.6%)	15 (88.2%)		17 (100%)	15 (88.2%)	
Female	17	15 (11.4%)	2 (11.8%)		0 (0%)	2 (11.8%)	
ASA Grade				0.090			0.879
ASA 1	87	83 (63.4%)	4 (23.5%)		3 (17.6%)	4 (23.5%)	
ASA 2	47	38 (29.0%)	9 (52.9%)		11 (64.7%)	9 (52.9%)	
ASA 3	13	9 (6.9%)	4 (23.5%)		3 (17.6%)	4 (23.5%)	
Albumin mean / SEM	28.9 (0.264)	28.81 (0.286)	29.47 (0.642)	0.241	30.0 (1.04)	29.5 (0.642)	0.668
Tumour Stage				0.883			0.982
T0	2	2 (1.5%)	0 (0%)		0 (0%)	0 (0%)	
T1	15	13 (9.9%)	2 (11.8%)		2 (11.8%)	2 (11.8%)	
T2	33	28 (21.4%)	5 (29.4%)		4 (23.5%)	5 (29.4%)	
T3	84	76 (58.0%)	8 (47.1%)		9 (52.9%)	8 (47.1%)	
T4	14	12 (9.2%)	2 (11.8%)		2 (11.8%)	2 (11.8%)	
Node Stage				0.967			0.655
N0	63	56 (42.7%)	7 (41.2%)		10 (58.8)	7 (41.2%)	
N1	45	39 (29.8%)	6 (35.3%)		5 (29.4)	6 (35.3%)	
N2	31	28 (21.4%)	3 (17.6%)		1 (5.9)	3 (17.6%)	
N3	9	8 (6.1%)	1 (5.9%)		1 (5.9)	1 (5.9%)	

Table 5.2 - Comparison of baseline characteristics of patients in the overall population, before the ICG trial and patients in the ICG trial before and after matching. ICG = Indocyanine green; TD = thoracic duct; SEM = standard error of the mean.

		Before Matching			After Matching		
Variables	**All Patients (n=148)**	**Pre-trial (n=131)**	**ICG TD (n=17)**	***P***	**Pre-trial (n=17)**	**ICG TD (n=17)**	***P***
Length of stay mean/SEM	14.18 (13.24)	14.2 (1.20)	12.34 (1.944)	0.545	11.59 (1.08)	12.34 (1.94)	0.736
Total drain output (mL) mean/SEM	659.1 (367.3)	669.47 (32.27)	578.8 (85.05)	0.34	546.18 (51.3)	578.82 (85.05)	0.745
Drain duration (days) mean/SEM	15.47 (59.07)	16.7 (5.47)	6.06 (1.29)	0.487	30.35 (25.66)	6.06 (1.29)	0.352
Chyle leak (number)	NA	NA	NA	NA	1	0	0.50

Table 5.3 - Comparison of outcome parameters in all patients, pre-trial patients and participants in the ICG thoracic duct trial. ICG = indocyanine green; TD = thoracic duct; SEM = standard error of the mean.

5.4. Summary and Discussion

This proof of principle study is the first to report the use of fluorescence in thoracic duct visualisation and identification of chyle leak intraoperatively during oesophagectomy. Two techniques were evaluated: enteric administration using ICG-cream mixture and small bowel mesentery injection. Enteric administration was not successful in thoracic duct identification. In 17 patients the thoracic duct was visualised in 15 with 2 of these being only visible under fluorescence. Failure of the technique was only observed in 2 patients. Fluorescent signal was seen over 5 hours after administration indicating that repeat administration is unlikely to be required. The S2B ratio was always over 1 and an average of 5. This high signal to background ratio indicates that the thoracic duct would be clearly visible and distinguishable from the minimal background signal observed in the study. Fluorescent signal was seen in patients with a BMI from 16 to 33 and it is known that a BMI <25 or >25 increases the risk of chylothorax 9 fold [168].

The comparison with a control cohort of participants was well matched before and after propensity score matching. Prior to propensity score matching the only significant difference was in BMI with the ICG trial group having a higher average BMI than the control group. Comparison of the outcomes of length of stay, chest drain output and chest drain duration were not statistically significant although it is likely that the propensity matching is underpowered. The control group had a very high length of drain duration and this is likely to represent a heterogeneous group of participants who may have had a longer drain duration for other reasons (e.g. anastomotic leak). One patient in the matched control group suffered a chyle leak which was managed conservatively compared with no chyle leaks in the ICG group (p=0.50). It is likely that a difference cannot be inferred here due to type II error.

Since this work was completed, there have been two published reports of ICG fluorescence in the thoracic duct. Steffey *et al* use a technique of ICG injection into either a popliteal LN, mesenteric LN or mesenteric route in 15 dogs and achieved optimal visibility with mesenteric LN or root injection [169]. They also identified a tear in the thoracic duct which was only highlighted by NIR imaging. In humans, Yang and colleagues utilised ICG fluorescence in 4 patients who underwent re-operative surgery for chyle leak and in all of these patients the location of the leak was identified with fluorescence prior to white light [170]. This study differed in that ICG was injected bilaterally into the inguinal region as they do not have access to the abdomen, a method not evaluated in this chapter and a potential advantage as, if re-operating for chylothorax, the abdomen would not be easily accessible. These studies together with the findings in this chapter clearly demonstrate that there is a potential clinical use for this technology during thoracic surgery be it oesophagectomy, cardiac or pulmonary surgery.

The study presented here represents completion of both an IDEAL stage 1 (innovation) and stage 2a (development) study having reported a new technique with use in patients as well as the completion of a planned procedure in an initial small group of patients to refine and modify the precise technique. Here the dosing has been demonstrated as well as injection technique. As recommended by IDEAL, the protocol was developed prospectively and registered prior to patient recruitment and ethically approved. The next stage of development of thoracic duct fluorescence could be 2b (exploration) or by-passing 2b to stage 3 (assessment) trial. The IDEAL statement is a set of recommendations geared towards new surgical procedures. Thoracic duct fluorescence is conducted as part of well recognised intervention and no change is made to the oesophagectomy itself. There is also likely to be a very limited learning curve in this technique which is unlikely to require further exploration. Trial design could include a randomised controlled trial (RCT) or a large prospective cohort study. A difficulty with an RCT in this setting is deciding the outcomes of interest to power the study. For an RCT, proposed outcomes and their study sizes could include:

1. Post-operative chyle leak: this binary outcome would be of major importance to both patients and surgeons however, it would need careful definition and measuring post-operatively to ensure the diagnosis is appropriate. To power the study, if the incidence was estimated at 3% and a reduction to 1% is advantageous, with a power of 80% and significance (α level) of 5%, 1532 participants would be required. This would require a multi-centre study over a long period of time and would be associated with significant cost.
2. Post-operative drain output, duration and length of stay: a reduction in these outcomes could potentially be cost saving to departments undertaking oesophagectomy. These outcomes would require smaller sample sizes: to detect a

reduction in the mean length of stay by 1 day at 90% power, 5% α, 380 participants would be required. Matching for pre-operative co-morbidities such as those listed in Table 5.2 would be required as well as adjusting for confounders such as other post-operative outcomes (e.g. anastomotic leak, pneumonia). Whilst this is easier to conduct as an RCT, it is likely that a difference is these outcomes are unlikely to provide enough evidence to allow surgeons to adopt this technology. If patient reported outcomes such as an improvement in quality of life was associated with these outcomes, then it may be more beneficial.

3. Subjective outcomes on usefulness and decision changing: subjective outcomes are difficult to power, however, an important feature of a future trial should asses how useful the technology was during each case. If any technology such as this is to be implemented, it must be beneficial and easy to use without adding significant time. Decision changing would be essential in any study namely whether the use of fluorescence led to further operative intervention on the thoracic duct (e.g. identification of additional leak, accessory branches or ligation of the thoracic duct).

Given the difficulty with the above options, a further possibility is to skip stages 2b and 3 in the IDEAL framework and proceed with a stage 4 long-term study [95]. A safety of the technique and ICG is well known, a long-term study could be implemented in a number of studies by way of a registry which allows larger numbers of cases being available for analysis.

CHAPTER 6: MOLECULAR TARGETS TO DETECT COLONIC DYSPLASIA DURING ENDOSCOPY AND SURGERY

6.1. Introduction

6.1.1. Colonic crypts and goblet cells

The colonic lumen is lined with a specialised epithelial layer designed to digest passing substances, absorb nutrients and water and form a barrier against luminal pathogens. In the colon, the epithelium is organised into millions of crypts that increase the functional surface area and is made up of three differentiated epithelial cells: enterocytes which primarily are involved with absorption; goblet cells which secrete mucus; and enteroendocrine cells which secrete hormones [171]. Turn-over within the crypts is rapid and three days after terminal differentiation, cells will reach the top of the crypt, undergo spontaneous apoptosis and shed into the lumen of the colon [171, 172].

The terminally differentiated epithelial cells are thought to arise from either a secretory lineage (goblet and enteroendocrine cells) via Wnt signalling dependent on ATOH1 [173]; or absorptive lineage (enterocytes) via the notch pathway [174]. Goblet cells form around 16% - 20% of the population of cells within the colonic crypt [175]. Fully differentiated goblet cells are located in the parts of the colonic crypts where they are characterised by large and numerous mucous granules within the theca giving a typical goblet cell appearance with the nuclei being located at the bottom of the cell [176]. The mucins produced by goblet cells are either gel-forming mucins (MUC2, MUC5AC, MUC6 and MUC5B), or transmembrane mucins (MUC1, MUC3, MUC4, MUC12, MUC13 and MUC17) [177]. No morphologically identifiable goblet cells in the colonic epithelia are identified in the MUC2 deficient mouse primarily because the theca, no longer containing mucus, are collapsed despite other goblet cell products being present [178]. Thus, the bulk of mucus produced by the colon consists of MUC2, whereas in the stomach it is MUC5AC [177-181].

The human MUC2 is a protein of around 5100 amino acids long. The MUC2 monomer domain structure consists of central tandem repeat regions rich in proline, threonine and serine (PTS domain) [182]. The MUC2 product is rapidly dimerised by forming C-terminal disulfide bonds within the endoplasmic reticulum (ER) then leaving the ER and becoming densely O-glycosylated by the golgi apparatus where the PTS domains become saturated with glycans extending like brush bristles [183, 184] (Figure 6.1). This complex process is initiated by a family of up to 20 GalNAc transferases and after the addition of GalNAc, the sugar chain is extended in a stepwise manner to higher order glycans [185, 186]. The fully glycosylated, mature MUC2 is then densely packed and stored into the secretory vesicles and secreted into the lumen via calcium dependent exocytosis and is triggered by numerous pathways including cholinergic agonists, hormones, microbes and microbial products and toxins [179, 187]. Once the granules are released, the MUC2 mucin dramatically expands in volume organising a net-like network of mucin underneath the inner mucus layer [180, 184].

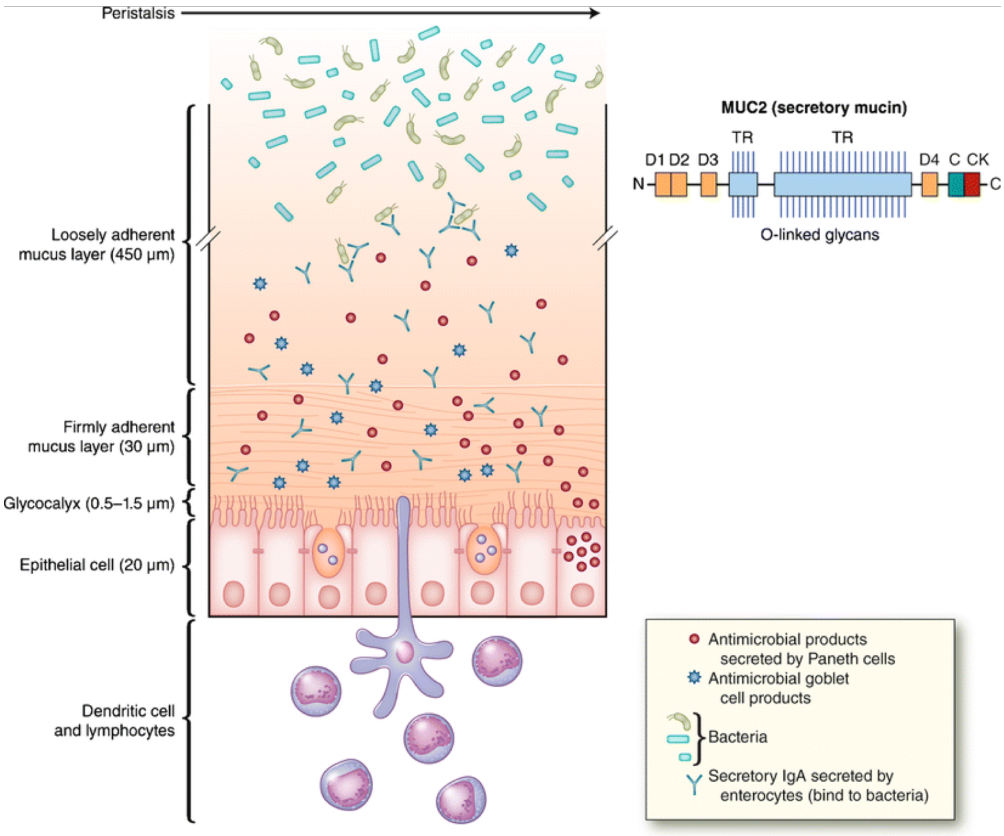

Figure 6.1 - Schematic representation of the 2 mucus layers over an epithelial surface (left) and the structure of the MUC2 mucin (right). The glycosylated MUC2 shows the N terminal region rich in disulphides followed by 2 tandem repeats (TR) which consist of the Proline, Threonine and Serine (PTS) domains. Following the two TR regions is a C-terminal region. Image reproduced from Kim *et al* [187] (2010).

The mucus layer covering the colonic epithelium is a firmly adherent insoluble layer that measures between 30 and 100µm (data from mice and rat colon) which can only be removed by gentle scraping [180, 183, 188]. This densely packed inner layer is completely devoid of bacteria thus building a mucus barrier separating the colonic epithelia from bacteria and defects in this mucus layer can cause colonic inflammation [180]. By comparison, the outer mucus layer at around 450µm, is readily soluble and non-adherent being removed by gentle suction. This loose layer is thought to arise from proteolytic cleavages taking place allowing the mucus to expand 4 times in volume whilst still maintaining the structure of the MUC2 polymer (Figure 6.2). It is thought that the outer mucus layer contains the commensal

colonic bacteria which enzymatically digest the large number of glycans, releasing monosaccharides as their energy source [189]. Glycans, the process of glycosylation, and thus glycoproteins, change in certain disease processes including cancer and inflammation. Numerous serological biomarkers target glycoproteins that are altered as part of a malignant process including prostate-specific antigen (PSA) [190], carcinoma antigen 125 (CA125: also known as mucin-16) [191] in ovarian cancer, CA15-3, also known as MUC1 in breast cancer [192, 193], CA19-9 in gastric and pancreatic cancer [194] and carcinoembryonic antigen (CEA) in colorectal cancer [195, 196]. The changes in colonic mucin expression and glycosylation are associated with colorectal cancer [197, 198] and can indicate a poor prognosis [199].

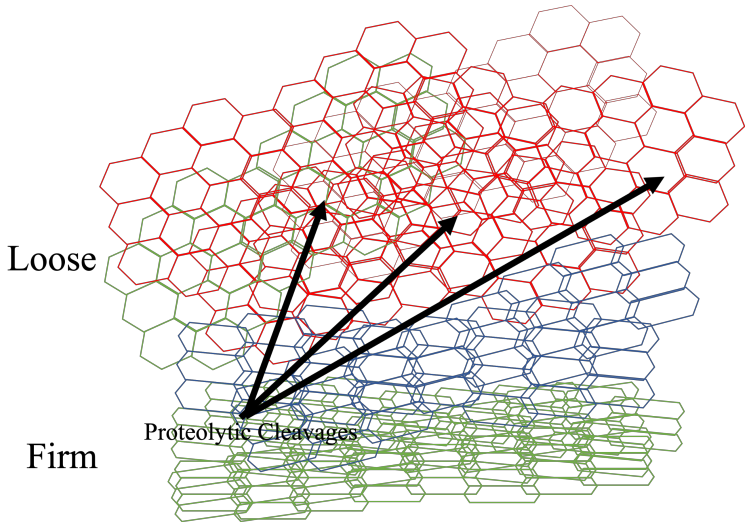

Figure 6.2 - Schematic representation of MUC2 mucus layers in the colon. The lower, firmly adherent layer undergoes proteolytic cleavages to allow the mucus to expand in volume to become a loose layer. The firm layer is non-soluble and after expansion, becomes soluble but still maintaining its polymeric structure. Adapted from Johannson *et al* 2011 [184].

6.1.2. Lectins as biomarkers

The term 'lectin' originates from *legere,* which in Latin means to select or choose, were originally utilised in blood grouping [200, 201]. Lectins, of which there are hundreds, are proteins that bind to carbohydrates and are found naturally largely originating from plants.

Most lectins bind to different glycan structures which have been classified as containing either *N*-acetylglucosamine (GlcNAc), *N*-acetylgalactosamine (GalNAc), galactose, mannose, maltose, sialic acid, or glucose [202]. The abundance of glycosylated MUC2 in the colonic mucus, makes this a potential *in-vivo* imaging molecular target to aid diagnostics with endoscopic imaging. The relatively large size of lectins (20-200kDa) makes them suitable for fluorescent conjugation as their molecular structure is unlikely to be altered during this process. They are also stable at low pH, heat stable and resistant to proteolysis [203]. Lectins are also abundant in fruits and vegetables that are part of human diets and thus, at low concentrations are unlikely to have toxicity [204]. In the Bodmer laboratory, analysis of a selected set of genes related to glycosylation in a panel of 30 colorectal cancer cell lines and 22 normal tissue specimens suggested B3GALT4 and ST6GalNac6, which encode enzymes acting on GalNAc, were significantly up-regulated in normal tissue compared to colorectal cancer (unpublished work, Yeung 2014). After screening a panel of GalNAc specific lectins, Wisteria Floribunda (WFA) was identified as having the most clinical potential and validated *ex-vivo* for clinical use to identify colonic dysplasia and cancer. Similarly, *ex-vivo* use of the lectin *Tritiicum vulgare* agglutinin or wheat germ agglutinin (WGA) conjugated to Alexa Fluor 488 has been demonstrated to be specific in identifying oesophageal dysplasia on a background of Barrett's oesophagus [204].

6.1.3. Highlighting dysplasia and cancer in the colon

White light endoscopy (WLE) has long been considered the gold standard in surveillance, screening, and diagnostic colonoscopy [205]. The importance of detecting adenomas at endoscopy is vital as it has been shown that polypectomy during colonoscopy reduces the risk of colorectal cancer [206]. Despite technical advances in endoscopic equipment there remains a plethora of evidence surrounding miss-rates of lesions during colonoscopy. [207-210] Lesion miss rates during colonoscopy, even in experienced hands, have been documented

to be between 10-26% [207-209, 211]. Adenoma detection rate (ADR) is a primary quality indicator of effective colonoscopy according to the American Society for Gastrointestinal Endoscopy (ASGE) [212]. The ADR has been shown to significantly influence the clinical outcomes of colorectal cancer screening [213-215] and endoscopists with ADRs below 20% have been shown to have higher rates of interval colorectal cancer development [208, 216].

6.1.4. Chromoendoscopy

Chromoendoscopy is a technique which consists of application of dye to the gastrointestinal tract to improve the visualisation of the microstructure and vascular patterns of areas of concern. It also aims to improve the recognition of minute changes in the mucosa to help identify flattened or depressed lesions.

The stains used can be divided into: absorptive stains which are absorbed into the tissue; non-absorptive (contrast) stains that pool into mucosal tissue or; reactive stains based on chemical reactions indicating special functions of the underlying tissue. [217]

The substances used to stain tissue are generally inexpensive and readily available. Disposable spraying catheters are available to apply the dyes onto the gastrointestinal mucosa. An essential pre-requisite to the use of dye spray in the colon is good bowel preparation. [217]

6.1.4.1. Absorptive stains

Absorptive or 'vital' stains are absorbed into cells which varies according to cell type and dye used. [218] The most commonly used absorptive stain in chromoendoscopy is Lugol's iodine which was first applied to the cervix to diagnose cervical cancer (Schiller's test). [219] In 1966 Voegeli used Lugol's solution to diagnose oesophageal cancer. [220] The potassium

iodine in Lugol's solution reacts with glycogen in normal epithelium and is stained brown, and so in the presence of abnormal mucosa no staining occurs due to low glycogen levels in the tissue. [218] Side effects can include oesophageal irritation, allergic reaction and thyrotoxicosis.

6.1.4.2. Methylene Blue

Methylene blue is absorbed by small intestinal and colonic epithelial mucosa but not by non-absorptive mucosa including squamous or gastric epithelium. Therefore, when used in the small intestine and colon it is used as an absorptive stain. When used in the oesophagus and stomach it is as a non-absorptive contrast stain. In Barrett's oesophagus, methylene blue is absorbed by dysplastic cells and some specialised intestinal metaplastic cells [221]. A meta-analysis of 9 trials showed no significant difference in diagnostic yield of dysplasia when compared with standard four-quadrant biopsies in Barrett's oesophagus [221].

Methylene blue in colonoscopy has primarily been used for surveillance endoscopy in inflammatory bowel disease patients. In a randomised trial, 174 patients with long-standing ulcerative colitis were allocated to chromocolonoscopy with methylene blue versus conventional colonoscopy with random biopsies. There was a significantly better correlation using chromocolonoscopy between the degree and extent of inflammation with histopathological findings compared with the conventional endoscopy group. More intraepithelial neoplastic lesions were identified with chromoendoscopy and there was a 93% sensitivity and specificity when differentiating non-neoplastic and neoplastic lesions [222]. Methylene blue for colonic staining in tablet form has been proposed as an alternative to dye spray. An initial randomised, open-label safety study concluded that it is a possible application technique, but further studies are awaited [223].

6.1.5. Contrast Stains

Contrast stains accumulate in the pits and valleys between cells, highlighting the surface profile of lesions. Indigo carmine is the most commonly used contrast stain.

6.1.5.1. Indigo Carmine

Indigo carmine is a contrast dye that simply pools in the mucosal grooves and pits allowing better topographical definition. This is the most common staining method used [218].

The use of indigo carmine in both polyp detection and characterisation is promising. The Cochrane review in 2010 identified five randomised trials comparing chromoendoscopy (all used indigo carmine) with standard endoscopy. Chromoendoscopy gave a higher yield of patients with one neoplastic lesion (OR 1.67, CI 1.29-2.15) [224].

6.1.6. Narrow Band Imaging

Narrow band imaging (NBI) enhances the endoscopic images using contrast enhancement and is one of the most widely studied virtual chromoendoscopy techniques. NBI utilises a white light filter system placed at the front of the endoscope light source allowing only blue and green light (415nm and 540nm) to reach the mucosa [218]. The 2 wavelengths are chosen to enhance the appearance of blood vessels with the 415nm wavelength penetrating capillaries in the superficial mucosa, creating a brown appearance and the 540nm wavelength penetrating the deeper vessels in the mucosa and submucosa appearing green [225]. This therefore provides information on inner structure and vasculature of the tissue [226].

NBI has been investigated for both polyp detection and classification in the colon as well as its use in surveillance of patients at risk of developing CRC. However, four meta-analyses have demonstrated no benefit in detection of colorectal polyps with NBI when compared to

standard colonoscopy [227-230], one of which was a Cochrane review performed in 2012 [228]. The most recent randomised controlled trial randomised 898 patients to either NBI or WLE examination of the colon. [231] NBI was found to have equal detection rates in both serrated (204 vs 158, p=0.085) and adenomatous polyps (438 vs 434, p=0.894) proximal to the sigmoid compared with WLE. However, there was a significant increase in serrated lesions over 5mm being detected on NBI (134 vs 79, $p<0.05$).

A large randomised controlled trial of 122 patients comparing magnified NBI with non-magnified NBI demonstrated no difference in identifying mean size, location, morphology and histology of the polyps [232].

6.1.7. Autofluorescence Imaging

Autofluorescence imaging (AFI) works by detecting the natural tissue fluorescence emitted by endogenous molecules induced by short-wavelength light excitation. Collagen has been identified as a natural fluorophore in human colorectal tissue and therefore a reduced autofluorescence in the colon is seen in neoplastic tissue as there is an increased mucosal thickness in the abnormal tissue [233].

The AFI endoscope system works by emitting white light from a xenon lamp and separating this with a rotary filter into excitation light (390-470nm) and green light (540-560nm). A barrier filter blocks light from 500-630nm thereby removing excitation light reflected from abnormal colonic tissue. A false colour image is then produced through a monochrome CCD enhancing autofluorescent tissue through an amplifying green channel and reflected green light through a red/blue channel. Therefore, areas of low fluorescence (abnormal tissue) are displayed as purple and high fluorescence tissue is displayed as green. AFI technology is

used in the Olympus system in the combination of NBI, AFI and WLE known as endoscopic tri-modal imaging (ETMI).

Whilst the AFI technology seems to have a promising concept, there is conflicting evidence to support its use. A recent meta-analysis identifying 6 randomised studies reported no significant difference in adenoma detection rate (OR 1.01; 95% CI 0.74 – 1.37; p=0.96) or polyp detection rate (OR 0.86; 95% CI 0.57 – 1.30; p=0.71) between AFI and WLE with no obvious heterogeneity in the data [207]. Conversely the same study demonstrated AFI as having a lower adenoma miss rate (OR 0.62; 95% CI 0.44 – 0.86; p=0.004) and polyp miss rate (OR 0.64; 95% CI 0.48 – 0.85; p=0.002) again with no obvious heterogeneity.

6.1.8. Molecular imaging in endoscopy

Due to the non-specificity of colonoscopic techniques previously mentioned, there has been a drive of research into targets for molecular imaging in endoscopy. The advantage of molecular targets is that they can be specific to the molecular changes within the colon rather than macroscopic appearances [234, 235]. Combining advanced imaging technology and targeted molecular imaging could improve polyp detection.

Molecular targeted colonoscopy has been investigated using numerous different targets and fluorophores in both the mouse and human. Both colitis associated dysplasia and cancer and sporadic colorectal cancer have been utilised as targets for molecular imaging in both mouse models and humans. Antibodies against CEA [236] and EGFR [237-239] have been assessed in the green light range using either fluorescein or Cy5.5. Difficulties with fluorescently labelled antibodies include a long clearance half-life after injection and concerns around immunogenicity [240]. These issues can often make it difficult to gain approval for phase I studies. Lower molecular weight peptides for molecular imaging are potentially

advantageous due to favourable pharmacokinetics, tissue distribution patterns, increased permeability, lower toxicity, lower immunogenicity and flexibility in chemical modification [241]. A number of studies have investigated the use of fluorescently conjugated peptides as markers of cancer and dysplasia in the colon [239, 242, 243].

6.1.9. Aims and objectives

1) To obtain a WFA suitable for human use
2) To validate the human use WFA against the existing WFA *ex-vivo*
3) To assess WFA in humans in identifying dysplasia and cancer during colonoscopy or TEMS
4) To identify additional potential genetic markers associated with WFA positivity

6.2. Methods

6.2.1. Cell Lines

Cell lines were obtained from the cryogenic storage of the Cancer and Immunogenetics Laboratory (CIL) at the Weatherall Institute of Molecular Medicine (WIMM), Oxford, UK.

6.2.2. Cell culture condition

All cell lines were grown in either 25cm^2 or 75cm^2 vented tissue culture flasks (Corning) filled with 5ml or 15ml of medium respectively. Cell lines were cultured in Dulbecco's Modified Eagle Medium (DMEM), Roswell Park Memorial Institute (RPMI) medium, or Iscove's Modified Dulbecco's Medium (IMDM). All medium used was supplemented with

10% foetal calf serum (Bioclear, UK) and 1% penicillin/streptomycin. Cells were incubated at 37^{o}C in an atmosphere containing 95% humidity and 10% CO_2.

6.2.3. Passage details

Cell lines were passaged approximately weekly when they were 70-80% confluent. Old medium was removed, and the cells were washed with phosphate-buffered saline (PBS). 1-2ml of trypsin was used to disaggregate the cells for 5 minutes or until most of the cells were detached from the culture flask. The trypsin was deactivated using medium and the cell suspension gently pipetted up and down multiple times to break up cellular clumps into a cell suspension which was then transferred to a Falcon tube. Suspension cell lines simply had the medium placed into a Falcon tube. Cell suspensions were centrifuged at 1000 revolutions per minute (RPM) and re-suspended in medium for continued culture. According to cell line growth rates they were divided into new culture flasks in ratios from 1:3 to 1:20.

6.2.4. Cell Storage and Retrieval

To prepare cells for cryogenic storage, cells from 70-80% confluent culture flasks were trypsinised, centrifuged and the cell pellet re-suspended in 1ml of FCS containing 10% dimethyl sulfoxide (DMSO) before being transferred into sterile cryogenic vials (Corning, USA). Cryogenic vials were then placed into a Mr Frosty container (ThermoFisher) filled with isopropyl and placed in a -80^{o}C storage freezer for 24 hours. This was to achieve a rate of cooling close to -1^{o}C per minute. For long-term storage, the cryogenic vials were transferred into cryogenic tanks containing liquid nitrogen at -170^{o}C.

Cells were thawed from frozen cryogenic vials by incubation at 37ºC for around 1 minute. After defrosting, the cells were re-suspended into 3-5ml of medium and then centrifuged at 1000rpm for 5 minutes. Cell pellets were then re-suspended into tissue culture flasks.

6.2.5. Cell Counting

In all experiments, cells were counted using a haemocytometer. The cell count was determined using a Cellometer Auto T4 (Nexcelom Biosciences, USA) allowing an automated cell count using 20µl of cell suspension loaded onto a disposable cell counting chamber. The software captures eight areas of the chamber and approximates the concentration of cells per millilitre.

6.2.6. Plating of cells

Cells from culture flasks were trypsinised and re-suspended as described above. After counting, 2500 cells were transferred in 200µl of medium per well in a 96-well plate (Corning, USA). Cells were grown until 70-80% confluent and then fixed with 4% paraformaldehyde (PFA), permeabilised with 0.1% Triton and washed in-between stages with wash buffer (PBS + 2% FCS).

6.2.7. Mycoplasma contamination testing

In the Bodmer laboratory, cell cultures are routinely tested for mycoplasma contamination using the MycoAlert® assay (Lonza, Rockland, Maine, USA). Briefly, 1mL of medium is withdrawn from cells that have been in culture for at least 72 hours and centrifuged into a pellet at 1,200 RPM for 5 minutes. 100µl of supernatant is transferred into a 96-well white-walled microplate with 100µl of MycoAlert reagent and incubated at room temperature for 5 minutes. Background fluorescence was then measured (Reading A) using a FLUOstar

OPTIMA Luminometer (Offenburg, Germany). 100µl of MycoAlert substrate was then added into each well and incubated for a further 10 minutes and a repeated fluorescence measurement taken (reading B). The ratio of reading B to reading A was calculated and a ratio of less than 1 indicates a negative test for mycoplasma contamination. If the ratio was between 1 and 2, cells would be cultured for a further 7 days and re-tested. A ratio greater than 2 was considered contaminated and all cell lines cultured in the same incubator were discarded and the incubator decontaminated.

6.2.8. Paraffin-Embedded Archived Material

Archived Formalin-Fixed Paraffin Embedded Tissue (FFPE) tissue slides were obtained from the Oxford Radcliffe Biobank (ORB). Paired samples (normal and cancer) were obtained from patients diagnosed with colorectal cancer. Use of the material was approved under the ORB blanket ethical approval process. Slides were also stained for haematoxylin and eosin (H&E).

6.2.9. Antigen Retrieval for Formalin Fixed Paraffin Embedded Tissue

For immunohistochemistry (IHC) staining, FFPE slides were deparaffinised in Histoclear II (National Diagnostics) for 5 minutes and then rehydrated in 100% industrial methylated spirit (IMS) for 5 minutes, 90% IMS for 5 minutes, 70% IMS for 5 minutes and finally 30% IMS for 5 minutes. Slides were washed in PBS for a further 5 minutes. Dako target retrieval solution (Dako, pH6.1) was used for antigen retrieval at 100^{o}C for 20 minutes using a microwave. Slides were cooled to room temperature for 1 hour then washed with PBS for 5 minutes. The tissue specimen was encircled using a hydrophobic ImmEdge pen (Vector labs). Non-specific binding was blocked with wash buffer (PBS + 2% FCS) for 1 hour at room temperature. The FFPE slides were then ready for antibody incubation.

6.2.10. Immunohistochemistry of tissue sections or cultured cells

The following methods were used when staining cultured cells or FFPE slides after preparation as described above. All samples for staining were blocked using 2% FBS in PBS for 30-60 minutes at room temperature. Samples were incubated with a primary antibody diluted in blocking solution for 1 hour at room temperature followed by wash with blocking solution twice for 5 minutes. Secondary antibodies were then applied and incubated for 1 hour at room temperature followed by a repeated wash step. 4',6-diamidino-2-phenylindole (DAPI) was applied to stain the nuclei with incubation of at least 10 minutes. Following this, a cover slip was mounted onto the FFPE slides. Tissue microarray (TMA) sections were stained in the same fashion as described. On imaging, H&E and DAPI pictures were reviewed to ensure epithelial surfaces were included and those without were excluded from analysis.

6.2.11. Imaging of whole fresh colonic specimens

Whole colonic specimens were obtained from patients undergoing surgery with ethical approval granted from ORB. Immediately following the procedure, the specimen was retrieved and opened along the antimesenteric border. After washing the specimen, an image under white light was obtained.

WFA conjugated to fluorescein (Medicago, Sweden) was applied using a 20ml syringe and 21-gauge needle to spray across the mucosal surface. The specimen was incubated for 5-10 minutes at room temperature and then imaged with the IVIS® SpectrumCT in vivo imaging system (Perkin Elmer). The specimen was then returned to the pathologist for routine histopathological assessment. After obtaining images, signal to background ratios were calculated using Image J [92].

6.2.12. Microarray analysis

For the cell line microarray data used in this thesis, the methodology of how these data were obtained by the Bodmer laboratory is described here. Briefly, 10μg of RNA was extracted from each colorectal cancer cell line and analysed using Affymetrix U133 Plus 2.0 microarrays at the Paterson Institute, Manchester with data analysis conducted in the Bodmer Laboratory. mRNA from each cell line was converted to cDNA by reverse transcription and then labelled with biotins. 10μg of fragmented cDNA was then hybridised to the probes (more than 54,612 transcripts) on the Affymetrix U133 Plus 2.0 oligonucleotide arrays. The microarray expression data was normalised using the Robust Multichip Analysis algorithm.

Analysis was performed using Python™ and Prism (GraphPad, California, USA) using multiple t-tests to determine significance between mean levels of expression in each probe set between the groups of comparison. p-values of <0.05, corrected for multiple testing, were considered significant and genes with a fold change difference which was not significant were not included in the analysis.

6.3. Results

6.3.1. Validation of WFA-M

The original WFA conjugated to fluorescein validated as described in section 6.1.2 was manufactured by Vector laboratories in the USA (WFA-V) and contained azide as a preservative agent. Prior to utilising the WFA-V, validation ensuring that the newly imported WFA-M (Medicago, Sweden) bound to the same target as the WFA-V *ex-vivo* was carried out. Two cell lines were selected as either goblet cell rich (LS180) or goblet cell negative (HCT116) from the colorectal cancer cell lines. Cells were co-stained with WFA from vector laboratories and PR5D5. PR5D5 is an in-house mouse monoclonal antibody

found to react specifically with only cells of goblet morphology [244]. Further validation reveals it to bind to a glycoprotein of around 70kDa in size [245] which is likely to target a form of glycosylated MUC2 [246]. In the negative cell line (HCT116), no immunofluorescent signal was observed when stained with PR5D5 and similarly both WFA-V and WFA-M were both negative. In LS180, PR5D5 demonstrated positivity in 18% of cells. With both WFA-V and WFA-M, the positive cells matched 100% of those that stained positive with PR5D5. In addition to this, an SRB assay was performed on the cell line LS180 at different doses comparing WFA-M, WFA-V and fluorescein with an untreated, control sample. Results from this are shown in 6.3.3 and Figure 6.8 to avoid repetition.

On human FFPE slides stained with WFA for both WFA-V and WFA-M, two outcomes were assessed: overlapping of staining in normal tissue specimens and a decrease in signal in pathological specimens. Paired specimens (normal with abnormal) were assessed from 8 patients. In normal colonic tissue from adjacent microtome sections in the same specimen, WFA-V and WFA-M had almost exactly overlapping staining within each imaged specimen (Figure 6.4A, normal images) located within the goblet cells and the mucus. When exposed to the same laser exposure time, signal from the WFA-V was 2.34 times brighter than WFA-M (91.78 vs 39.22, p=0.0286) (Figure 6.3).

On imaging additional pathology, differences between signal and background between WFA-V and WFA-M were compared amongst varying colorectal pathology types (Figure 6.4B). Comparison was made at optimal laser exposure times with both WFA-V and WFA-M to compare the same area on an FFPE specimen. In all specimens, there was no significant difference between WFA-V or WFA-M indicating that the WFA from each manufacturer maintains the same target on a cellular level.

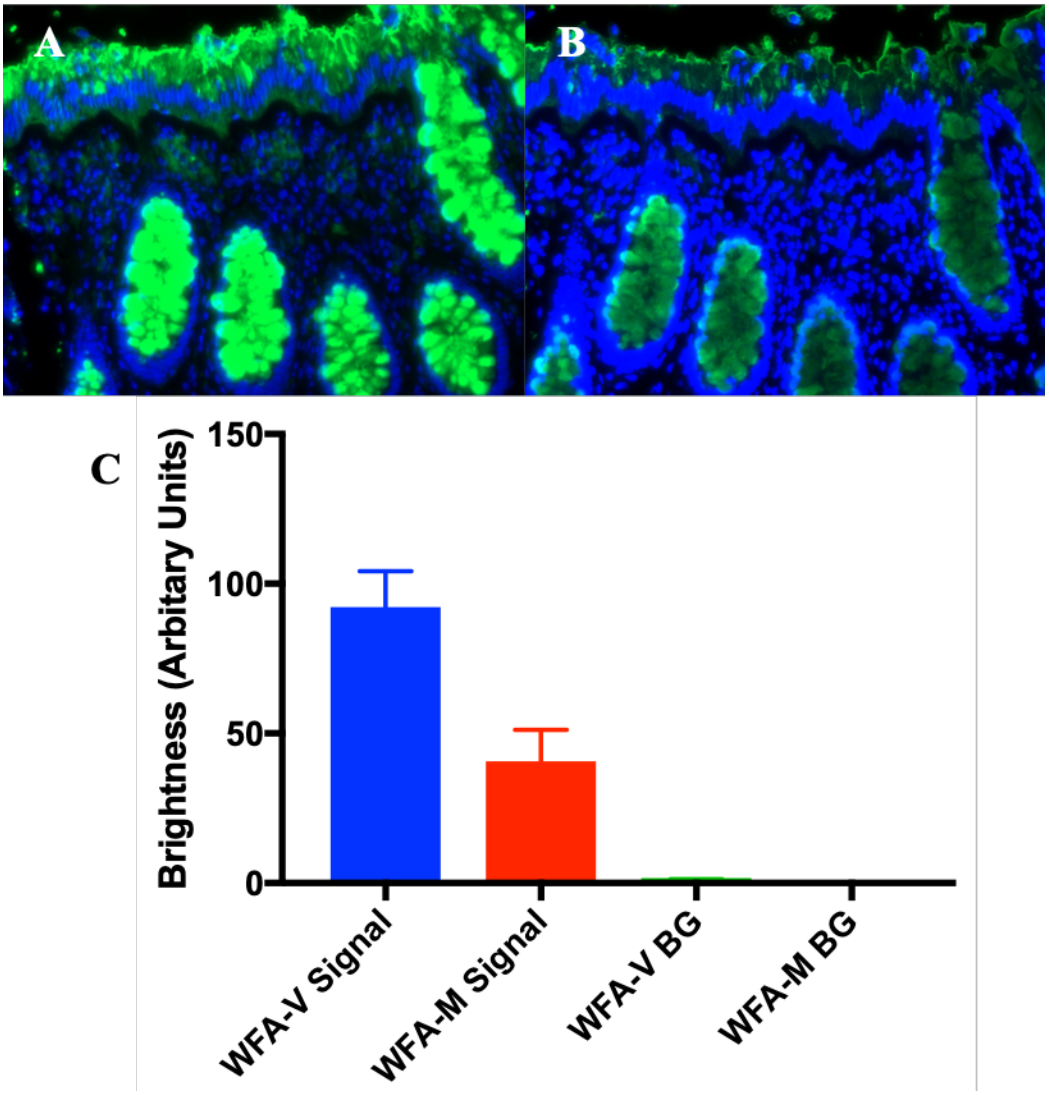

Figure 6.3 - Comparison of WFA-V and WFA-M at same laser exposure on normal colonic tissue. A is a representative FFPE slide of normal colonic tissue stained with WFA-V (green); B is another representative FFPE slide of normal colonic tissue in the adjacent microtome slice from the same specimen stained with WFA-M (green) at the same exposure as the image in A. Note that subjectively figure A is significantly brighter in the green channel and on measuring brightness, the signal in A was 2.34 times brighter as seen in the graphical representation of this data in C. No difference in background signals were observed. Negative control not included however, no background fluorescent signal was observed when staining with fluorescein alone.

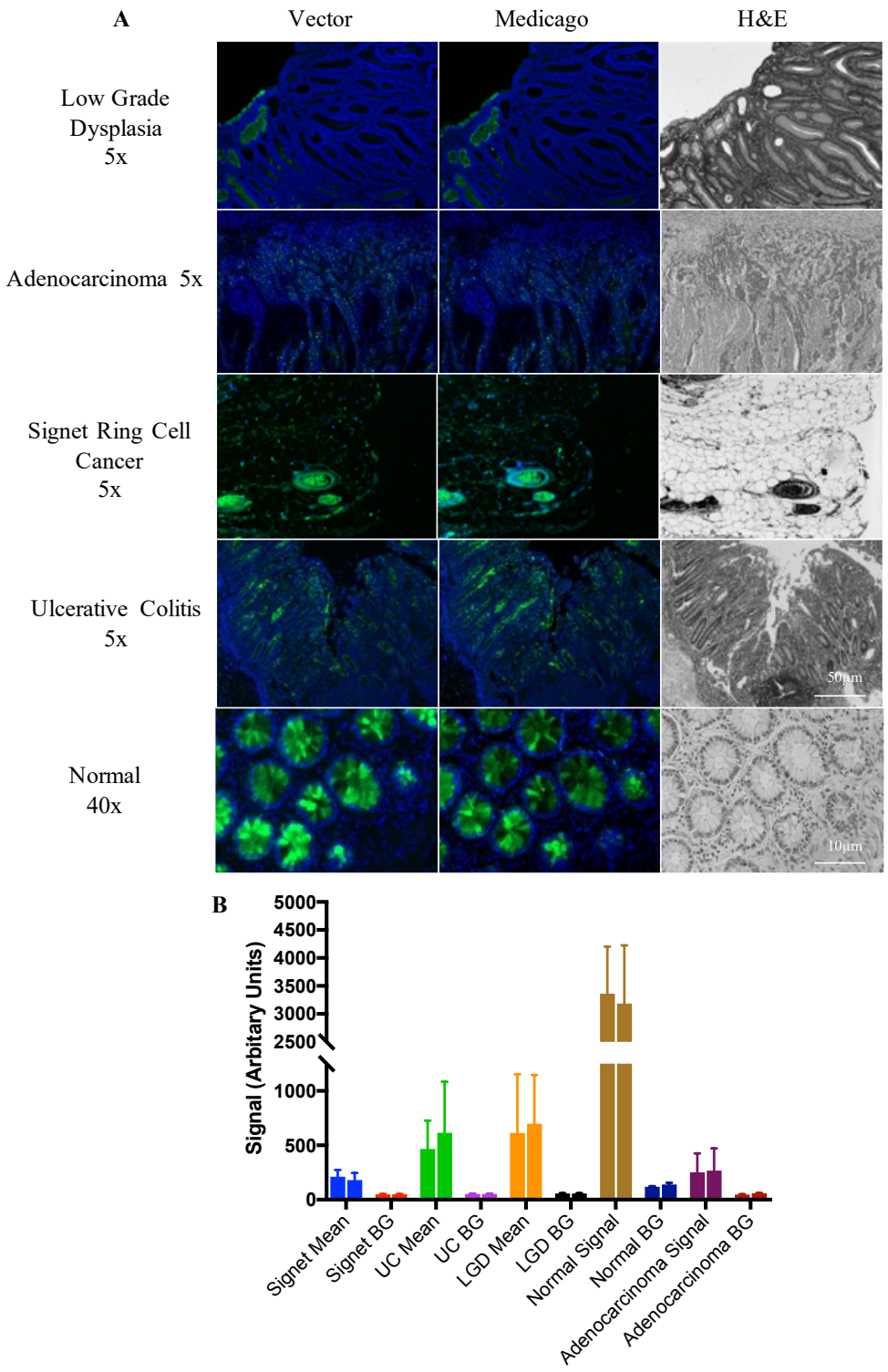

Figure 6.4 - Comparison of WFA-V with WFA-M on immunostaining of FFPE colonic tissue of different pathology. A = representative images of differing colonic pathology of FFPE slides. B = mean (and SD) signal and background brightness of immunostained specimens. Left columns represent WFA-V and right represent WFA-M.

During the validation stage prior to patient recruitment, the WFA-M product was divided into aliquots and kept at differing storage conditions (-20^{o}C, 4^{o}C and room temperature) for a period of 12 months to assess the impact on binding and fluorescent signal as WFA-M does not contain azide and may lose its fluorescence over time. Two different dilutions were assessed: 1:100 and 1:200. The cell line LS180 was used to assess the fluorescent signal and signal to background ratio across the different cohorts was assessed over time. Subjectively, the immunostaining in the room temperature aliquots seemed to be decreased as well as a lower proportion of positive staining cells compared to other storage conditions (Figure 6.5, table). On comparing signal to background ratio across the different storage conditions, no significant difference was observed between 4^{o}C versus -20^{o}C and -20^{o}C and room temperature at both 1:100 and 1:200 dilutions. However, the standard deviation in the -20^{o}C was much broader than the other storage conditions and therefore may vary significantly. Signal to background ratio at 4^{o}C was significantly higher than at room temperature at both the 1:200 (difference 25.46, p=0.0086) and 1:100 (difference 23.59, p=0.0158) dilutions (Figure 6.5 graph). Therefore, the optimal storage condition for WFA-M is at 4^{o}C.

Comparison	Mean rank diff.	Adjusted P Value
4ºC 1:200 vs. 4ºC 1:100	-1.429	>0.9999
4ºC 1:200 vs. -20ºC 1:200	6.27	>0.9999
4ºC 1:200 vs. -20ºC 1:100	13.83	0.8229
4ºC 1:200 vs. Room Temperature 1:200	25.46	**0.0086**
4ºC 1:200 vs. Room Temperature 1:100	22.16	**0.0313**
4ºC 1:100 vs. -20ºC 1:200	7.698	>0.9999
4ºC 1:100 vs. -20ºC 1:100	15.25	0.5122
4ºC 1:100 vs. Room Temperature 1:200	26.89	**0.0041**
4ºC 1:100 vs. Room Temperature 1:100	23.59	**0.0158**
-20ºC 1:200 vs. -20ºC 1:100	7.556	>0.9999
-20ºC 1:200 vs. Room Temperature 1:200	19.19	0.0855
-20ºC 1:200 vs. Room Temperature 1:100	15.89	0.2749
-20ºC 1:100 vs. Room Temperature 1:200	11.64	>0.9999
-20ºC 1:100 vs. Room Temperature 1:100	8.333	>0.9999
Room Temperature 1:200 vs. Room Temperature 1:100	-3.306	>0.9999

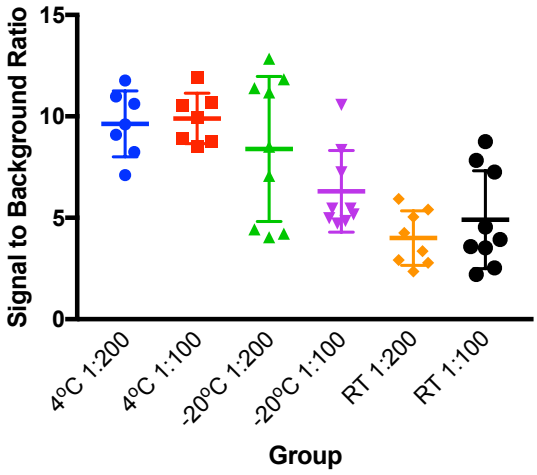

Figure 6.5 - Comparison of WFA-M at differing storage conditions - quantification of signal to background ratio. Table gives individual comparison of each storage condition with corrected p-values. Graphical representation of each assessment is outlined in the figure beneath. RT = Room temperature

6.3.2. In-vivo assessment of WFA-M

Two patients undergoing colonoscopy for assessment of polyp suitability for TEM were recruited to the study. It was decided to validate *in-vivo* using patients with known pathology so an area of pathological colonic tissue and adjacent normal tissue could be assessed. One patient was male, the other female at ages of 69 and 82 respectively. The pathology of the lesions assessed were both rectal tubular adenomas of low-grade dysplasia (sized at 10 x 15mm and 50 x 40mm). Lesions were assessed under white light and then under AFI mode before the WFA was applied (incubation for 5 minutes), after WFA application pre- and post-wash with 50mL of saline using the CF-FH260AZL/I AFI video colonoscope (Olympus). Subjectively, before the WFA was applied, a clear signal could be seen in the normal colon with absence of signal over the polyp in both patients in AFI mode. Once the WFA was applied, no increase in signal was seen subjectively over the normal colonic tissue. After incubation, the polyp and adjacent normal colon were re-assessed with no significant change in signal on the normal colon or background from the polyp either pre- or post-wash after WFA application (Figure 6.6). No adverse effects were observed in the 30-days following WFA-M administration.

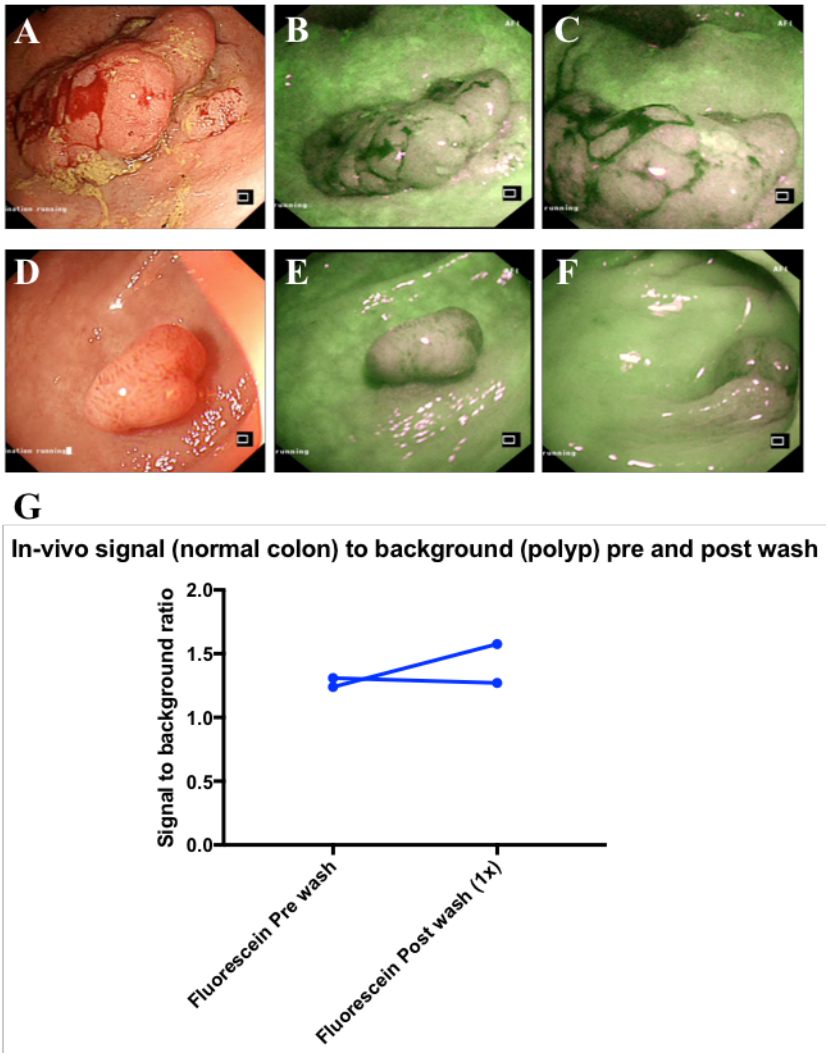

Figure 6.6 - In-vivo assessment of WFA-M. A-C = patient 1, D-F = patient 2, G = graphical representation of pre- and post-wash signal to background ratio. A&D = white light image without WFA, B&E = pre-WFA-M application under AFI mode, C&F = assessment in AFI mode following WFA-M application, incubation and wash.

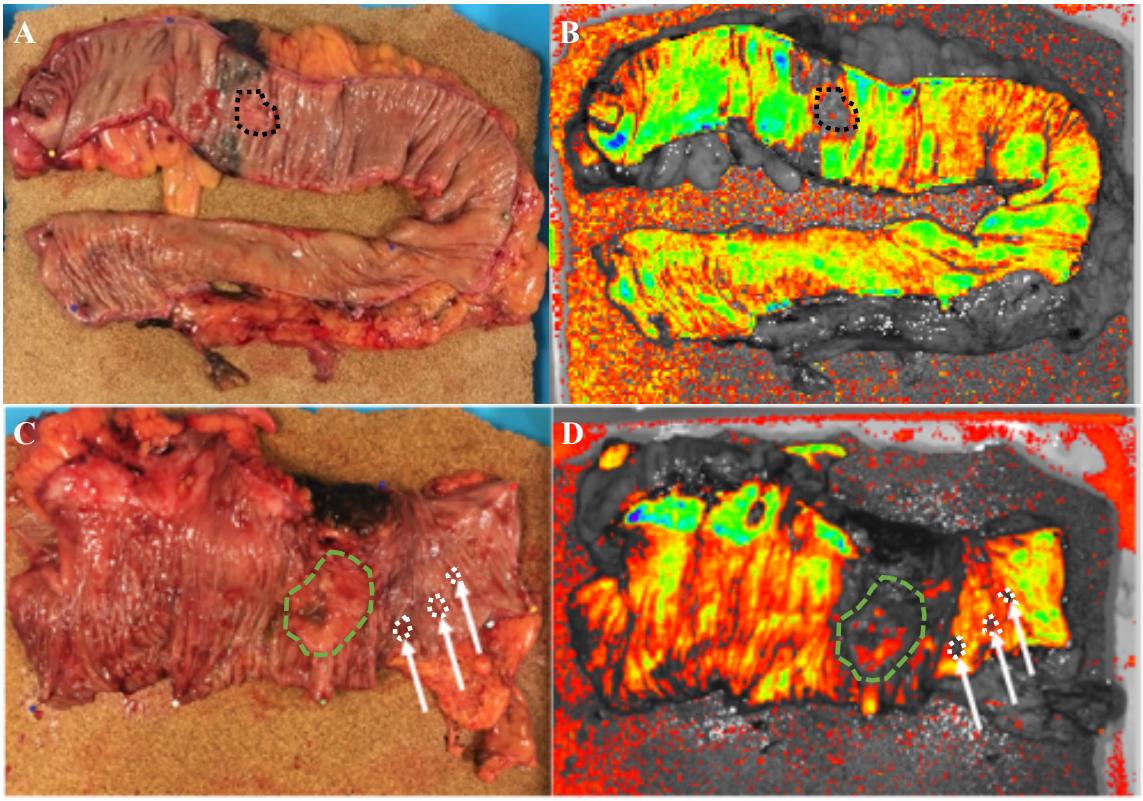

Figure 6.7 - Image of 2 whole colonic specimens under fluorescein wavelength without application of WFA. A&B = right hemicolectomy specimen with adenocarcinoma in the ascending colon (black dotted line); C&D = anterior resection specimen with adenocarcinoma in the rectum (green dotted line) and 3 sessile serrated polyps adjacent to the tumour (white dotted lines). A&C = white light image, B&D = IVIS image under 465nm excitation and 520nm filter.

Following this *in-vivo* assessment, it was apparent that the autofluorescent signal from the colon in AFI mode, would prevent assessment of WFA conjugated fluorescein. Access was sought to visualise whole colonic specimens from cancer resections in an IVIS imager (Figure 6.7). Two specimens (right hemicolectomy and anterior resection for adenocarcinoma) were assessed for autofluorescence under similar excitation/emission wavelengths to the AFI colonoscope. High signal was observed over the normal colonic surface and over the pathological areas (confirmed by histopathological assessment), no fluorescent signal was observed. Pathological areas assessed included adenocarcinoma and

3 incidentally identified SSPs. It would thus prevent any assessment of the effect of WFA *in-vivo* with autofluorescence being the background.

In addition to the difficulty of autofluorescence, the loan period for the AFI colonoscope from Olympus had ended and no further loan extension was possible and therefore no further patients could be assessed using fluorescein conjugated WFA. It was therefore decided that a fluorophore outside of the autofluorescent spectrum be conjugated to WFA. After discussions with chemists at LI-COR®, a WFA conjugated to IR800CW using the same raw WFA product as used WFA-V.

6.3.3. Validation of WFA-IR800CW

Once this was manufactured, validation of WFA-IR800CW was again required. Firstly, a repeated SRB assay was conducted to assess for toxicity on cell lines. Compared to the control assay, WFA-V significantly decreased cell growth in both 4 and 5 days of treatment. WFA-IR800CW had some impact on cell growth compared to WFA-M, fluorescein and IR800CW but this difference was not seen at 5 days post treatment (Figure 6.8).

For imaging assessment of WFA-IR800CW, no microscope was available that would image with the appropriate excitation lasers and emission filters other than a Nikon eclipes (Ni-E) which only had an imaging platform capable of imaging glass slides rather than tissue culture plates and therefore one could only image FFPE slides from colonic tissue rather than cell lines. The Ni-E microscope has a maximum excitation wavelength of 750nm which was used with a custom-made filter dichroic filter (Semrock, New York) allowing light above 815nm. This filter was optimised for imaging ICG and would image IRDye 800CW but would not have the optimal excitation and may not detect some emitted light.

FFPE slides were imaged from normal and adenocarcinoma colorectal specimens with WFA-IR800CW and WFA-V. As the fluorophores were different, they could not objectively be compared and therefore a subjective assessment only was utilised to verify the binding target of WFA-IR800CW. As the WFA was the same in both products, only samples of normal and adenocarcinoma were assessed. Both WFA-IR800CW and WFA-V bound to the same target in adjacent sections of tissue (representative images in Figure 6.9).

A

		Corrected p-value					
	Day 4	**WFA-M**	**WFA-V**	**WFA-IR800CW**	**Fluorescein**	**IR800CW**	**Control D4**
Concentration (µg/200ul)	1	0.0269	0.0001	0.0725	0.9767	0.8976	0.0001
	2	0.055	0.0001	0.102	0.8818	0.0136	0.0001
	3	0.0068	0.0001	0.0243	0.4749	0.0142	0.0001
	4	0.0083	0.0001	0.0497	0.9999	0.9996	0.0001
	5	0.2191	0.0001	0.0381	0.9997	0.3277	0.0001
	6	0.0066	0.0001	0.0368	0.8076	0.6892	0.0001
	7	0.3263	0.0001	0.0008	0.7883	0.966	0.0001
	8	0.1053	0.0001	0.2815	0.0069	0.0001	0.0001
		Corrected p-value					
	Day 5	**WFA-M**	**WFA-V**	**WFA-IR800CW**	**Fluorescein**	**IR800CW**	**Control D4**
Concentration (µg/200ul)	1	0.9769	0.033	0.2801	0.7565	0.6094	0.0001
	2	0.9898	0.0003	0.1055	0.9995	0.9869	0.0001
	3	0.2205	0.0001	0.0845	0.0141	0.5522	0.0001
	4	0.95	0.0001	0.9611	0.2408	0.4738	0.0001
	5	0.9857	0.0001	0.993	0.5148	0.8649	0.0001
	6	0.5549	0.0001	0.9999	0.9917	0.7742	0.0001
	7	0.9941	0.0001	0.0254	0.9999	0.9997	0.0001
	8	0.9979	0.0001	0.3628	0.7398	0.0904	0.0001

B **C**

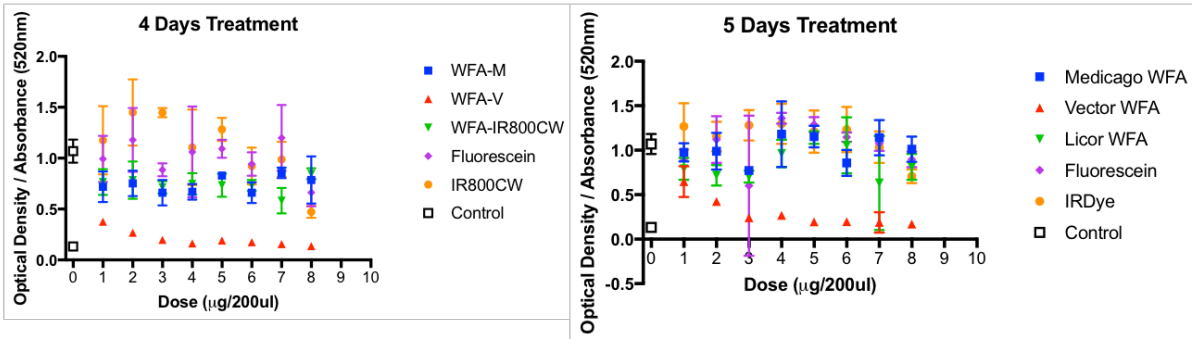

Figure 6.8 - Results of SRB assay comparing WFA-M, WFA-V, WFA-IR800CW, fluorescein and IR800CW with control. A = tabular results of SRB assay with corrected p-values displayed at varying concentrations when comparing with control sample. Red = significantly lower cellular growth, green = significantly higher cell growth. B&C = graphical results of SRB assay after 4 (B) and 5 (C) days treatment.

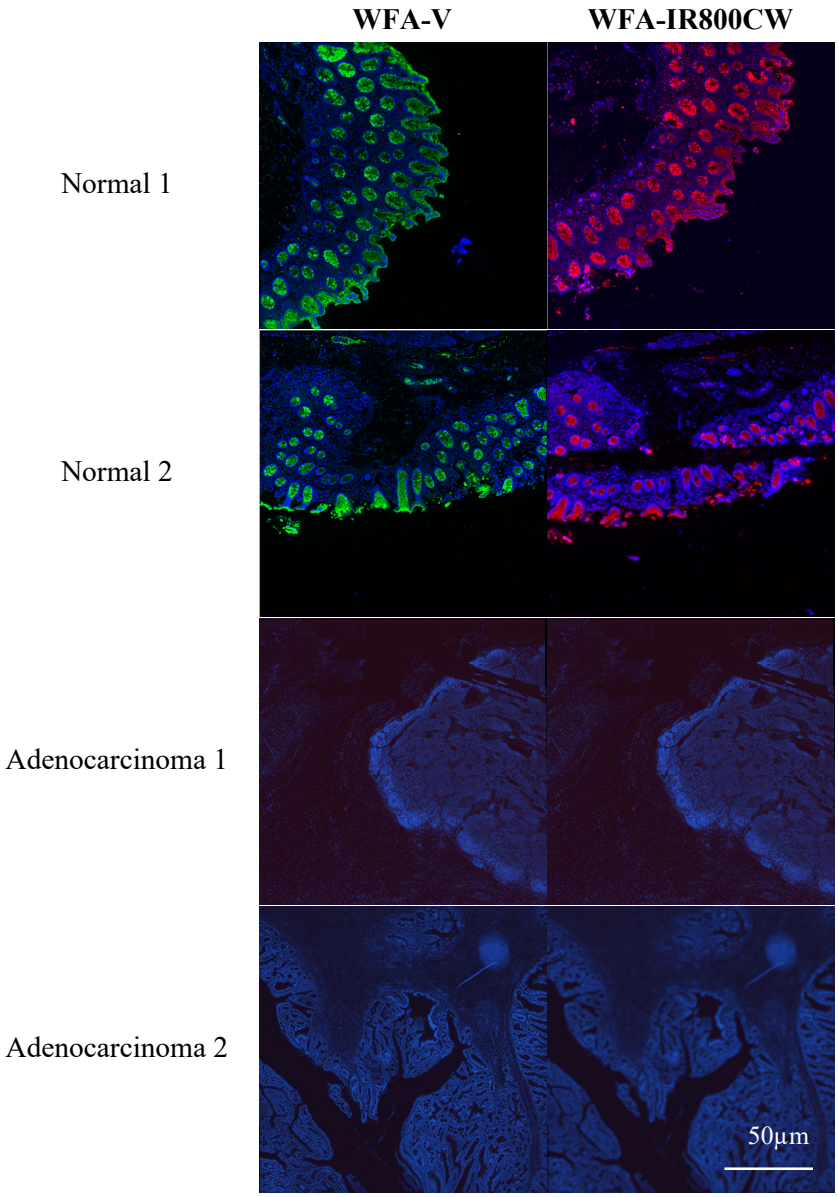

Figure 6.9 - Representative images comparing WFA-V to WFA-IR800CW staining in FFPE slides from normal and colorectal cancer. Staining was observed within the goblet cells and mucus layer within the normal colonic tissue, and no staining was observed in adenocarcinoma tissue slides. Blue = DAPI, red = WFA-IR800CW, green = WFA-V.

Prior to testing *in-vivo*, as IRDye800CW does not have exactly the same excitation and emission spectra as ICG, equipment usually used for imaging ICG needed to be assessed for visualising WFA-IR800CW. To proceed under the approved protocol, an imaging device was sought to assess patients undergoing TEMS/TAMIS or endoscopy. No commercially available endoscope is currently available that has fluorescent capabilities in the NIR range. Discussions with Karl Storz ® (Germany) were commenced for a potential collaboration and their technical team commenced development of adapting an existing colonoscope to contain emission filters for IR800CW as well as an additional light source that could be manually activated to emit the excitation light. Unfortunately, after discussions over a period of 5 months, it was decided by Storz that such a device would take years to manufacture and meet device regulations. At this point, there was no other option than to abandon the endoscopy arm of patients in the protocol and proceed with TEM/TAMIS participants with a rigid laparoscope. Two devices for rigid laparoscopy were available at the point of WFA-IR800CW being available, PINPOINT (Novadaq/Stryker®, USA) and the ATG in-house device. Eppendorf tubes containing increasing concentrations up to the maximum allowed in the protocol (20μg/mL) were imaged under both devices and measured for brightness. Using the ATG device, signal could be observed at the lowest dose 2.5μg/mL, exponentially increasing to the maximum dose. Using the PINPOINT device, no signal could be observed at any concentration as well as the signal for the highest dose being no different to that of the control sample (Figure 6.10). Therefore, the ATG device was the only device that could be utilised to assess WFA-IR800CW for this trial.

A

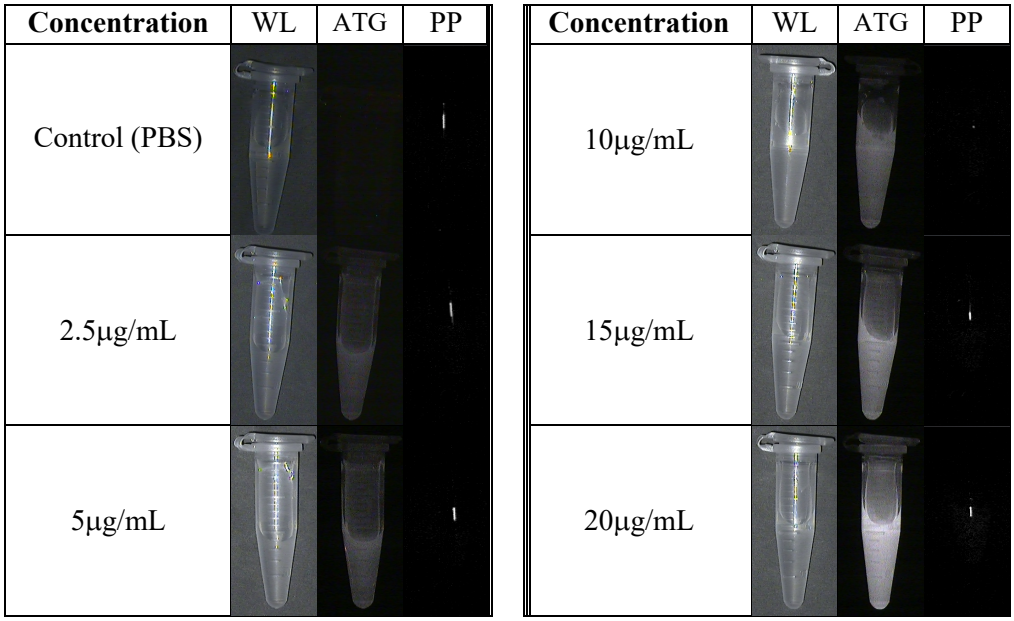

B

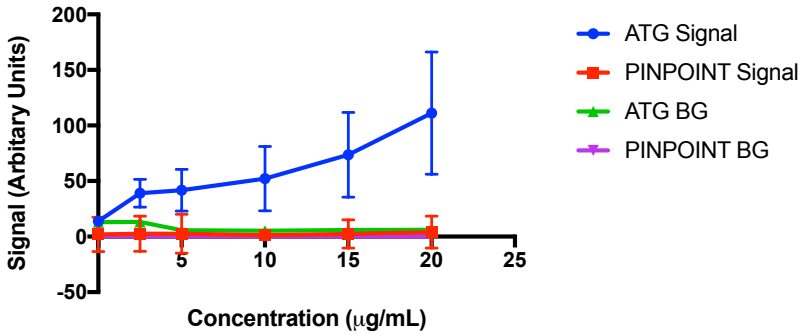

Figure 6.10 - Comparison of pinpoint and ATG devices on imaging WFA-IR800CW at differing concentrations. A = images of WFA-IR800CW in Eppendorf tubes imaged with each system. B = signal across each concentration up to the maximum allowed in the protocol (20µg/mL).

6.3.4. In-vivo assessment of WFA-IR800CW

Between April and July 2018, 4 patients were approached to enter the study, 1 declined and the remaining 3 participants were recruited (1 male, 2 females aged 56-74) all undergoing TEMS for rectal polyps. The maximum concentration (20mL of 20μg/mL) and volume of WFA-IR800CW allowed in the protocol was applied to the lesion and adjacent normal colon in all 3 participants. Incubation time was 5-7 minutes with incubation in the final participant being performed with a deflated rectum to see if there was any change in binding to the normal colon. In 2 of the patients there was a significant decrease in signal emitted from the adjacent normal colon versus pathological area after washing, (patients 3 & 4, Figure 6.11) with a visible remaining signal over the tumour in patient 3. In patient 4 there was no significant difference in the signal to background before or after washing.

A

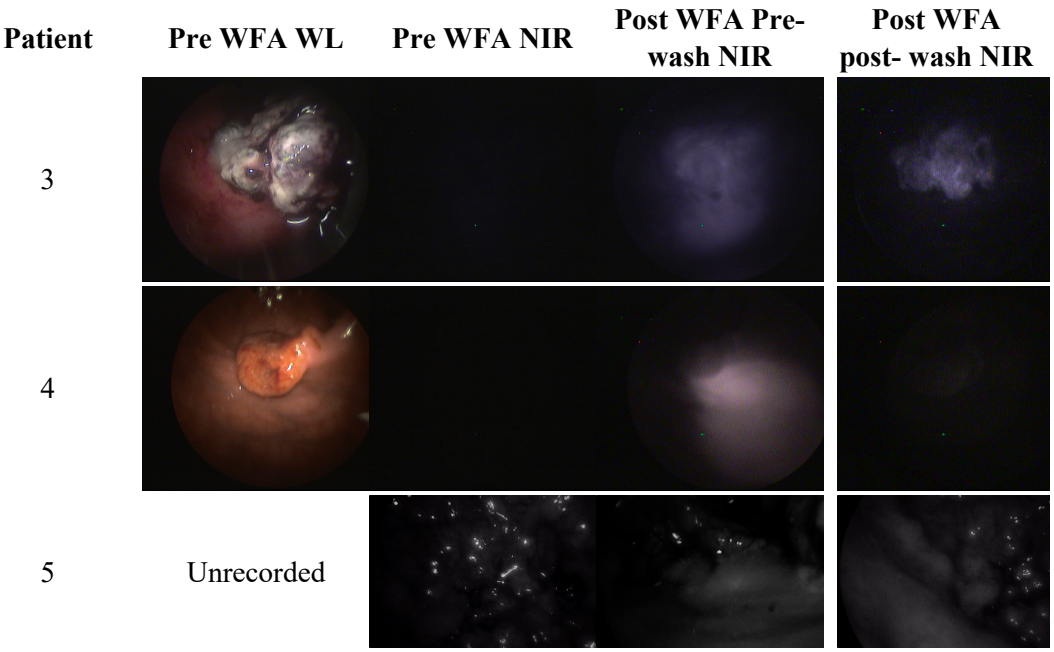

B

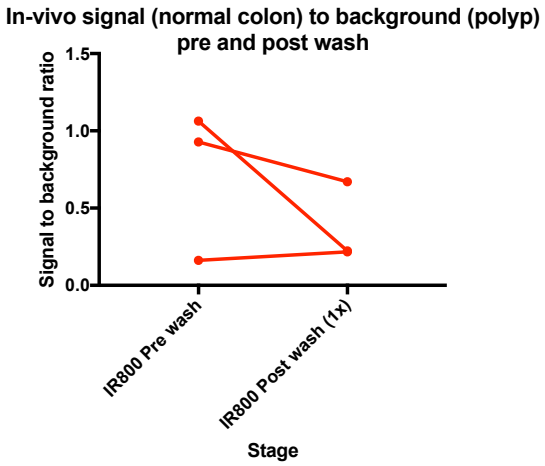

Figure 6.11 - In-vivo assessment of WFA-IR800CW in three patients undergoing TEMs. A = images of procedure in each patient pre-WFA with white light, pre-WFA under NIR and before and after washing. B = graphical representation of signal to background ratio of each patient. Pre-WFA WL image was unrecorded in patient 5 due to fault with recording device. WL = white light, NIR = near-infrared.

Failure in the WFA-IR800CW to bind to even normal colon *in-vivo* seemed to be following a washing step where no WFA was bound to even normal colonic tissue. Longer incubation times *in-vivo* would prove difficult due to time constraints, prolonged anaesthetic time and as such, were outside of the approved protocol. In order to assess whether WFA would work *in-vivo* with longer incubation times and minimal washing, specimens were imaged *ex-vivo* using the IVIS. Three whole-colonic specimens resected for adenocarcinoma we opened and washed with saline to remove faecal material. WFA-IR800CW was applied for 30 minutes at room temperature and imaged before and after washing with differing techniques. Unwashed WFA could be clearly be visualised on the specimen prior to washing in all cases (Figure 6.12a). Three different methods of WFA application were attempted. Direct application on a specimen that had hypertrophic muscle and thus had a 'cupping' shape allowing pooling of the WFA solution (Figure 6.12ci); direct application on the second specimen failed (Figure 6.12cii) and a 'paper towel wrap' incubation was attempted (Figure 6.12civ); and immersion of the entire specimen into a container of WFA solution (Figure 6.12ciii). Neither of these methodologies worked as no specific binding of WFA to the normal colonic surface was observed (Figure 6.12D).

In addition to whole colonic specimens, paired normal and colorectal cancer 5mm size biopsy specimens were obtained and incubated at room temperature for 1 hour followed by a single dip in normal saline without any additional manipulation. Samples were imaged under IVIS at each stage. Following specimen submersion in WFA solution, bright signal was observed in both normal and tumour specimens. Following a single dip in saline, all signal was removed (Figure 6.13).

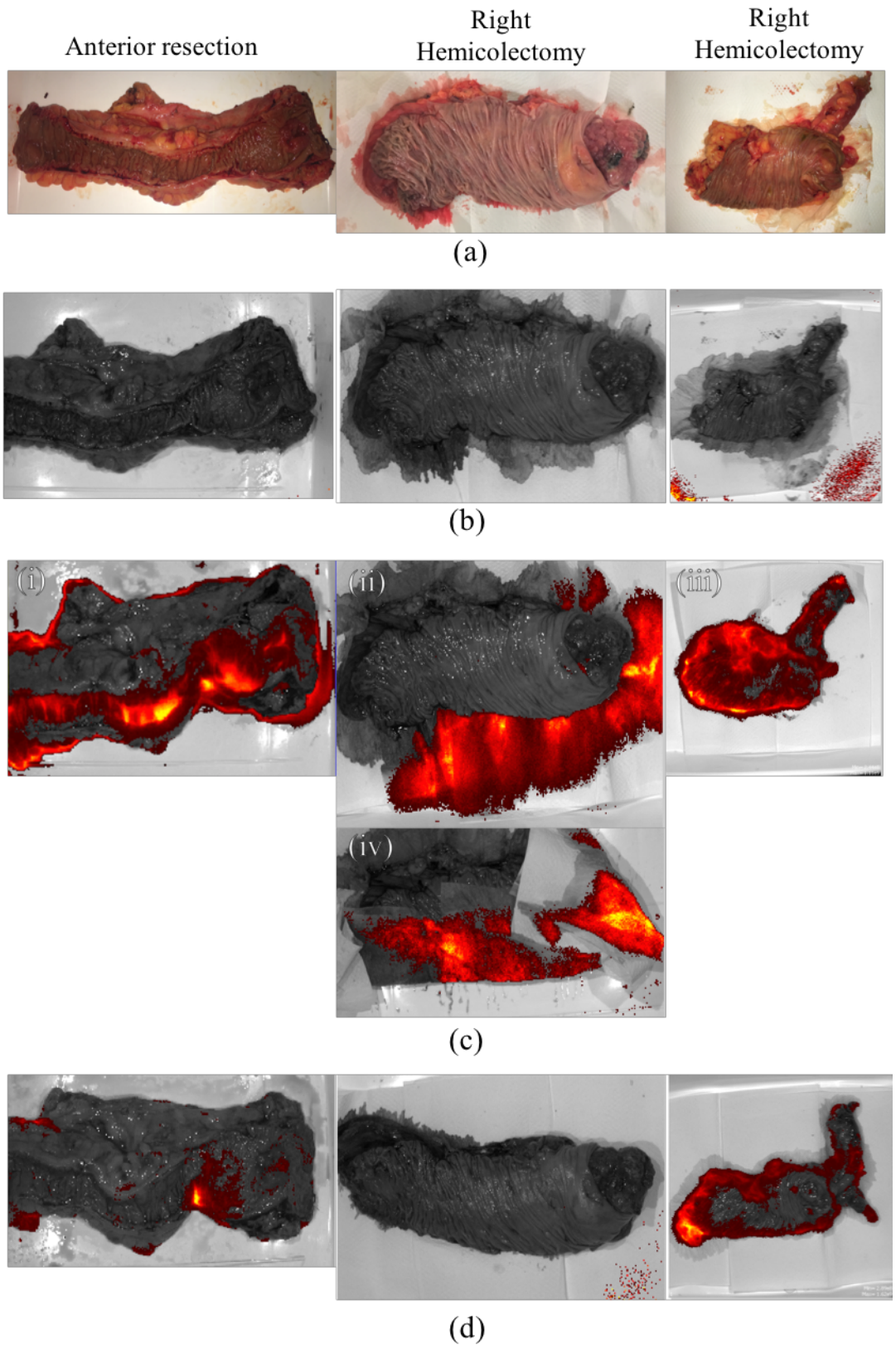

Figure 6.12 - WFA-IR800CW on ex-vivo whole colonic cancer resection specimens imaged with IVIS. (a) = white light image; (b) = pre WFA NIR image; (c) = WFA applied, no wash: (i) = application with syringe to pool in colon, (ii) application with syringe – on

imaging, all the WFA solution had fallen off the colon on to the adjacent paper towel, a 'towel wrap' incubation technique was attempted to apply WFA onto the colonic surface (iv), (iii) whole colonic specimen immersed in WFA solution; (d) = image of specimen after single wash with 10mL of saline.

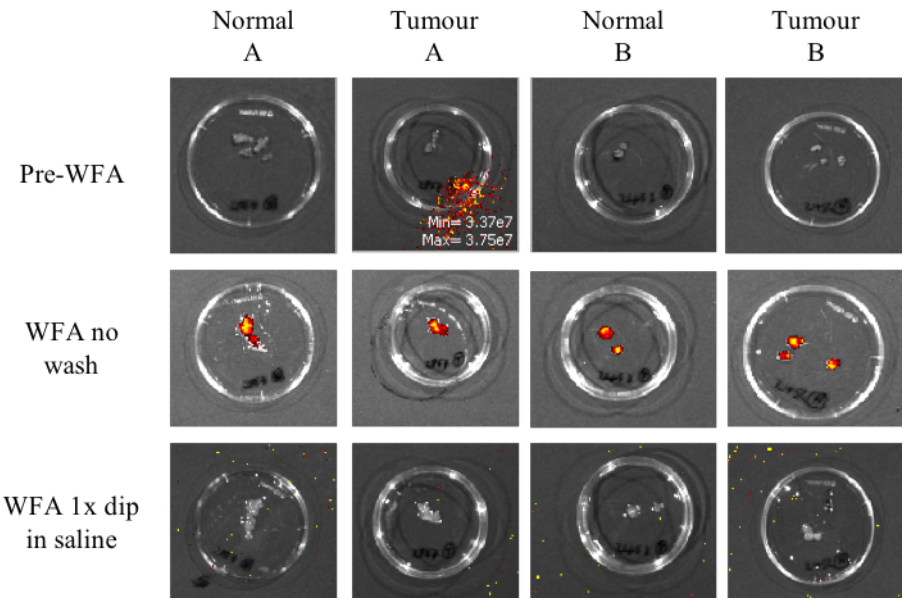

Figure 6.13 - Ex-vivo biopsy specimens of normal and colorectal tumour samples immersed in WFA-IR800CW. Specimens from 2 different patients are displayed imaged under the same conditions prior to WFA application, following WFA application without wash and after 1x dip in saline. Note that no signal difference can be seen following WFA application and wash when compared with the pre-application images.

It was therefore hypothesised that it may not be the WFA that is washed from the colon preventing its application, but the actual mucus layer on the colon that gets washed away. Presently, WFA has only successfully seen to work in FFPE specimens and not in fresh tissue. To further explore this, fresh frozen specimens were placed onto tissue slides and exposed to differing washing conditions. Measurements were made on the thickness layer of mucus as well as fluorescent signal with increased amount of washing. As number of washings increased, there was a trend to decreasing mucus thickness from a mean thickness of 26.36μm without any washing to 7.46μm when washing 4 times. With only 1 washing, the thickness of the mucus layer significantly decreased (p=0.0327). After washing once, the difference in mucus thickness between washing steps generally decreased (Table 6.1). Although mucus thickness decreased, fluorescent signal from the WFA-IR800CW did not (p=0.5328) (Figure 6.14G).

Comparison	Mean difference of mucus thickness (μm)	95.00% CI	Adjusted P Value
2x Wash vs. 1x Wash	-7.057	-15 to 0.883	0.1044
3x Wash vs. 1x Wash	-11.33	-19.27 to -3.387	**0.0015**
4x Wash vs. 1x Wash	-10.5	-17.98 to -3.01	**0.0019**
No Wash vs. 1x Wash	8.41	0.4692 to 16.35	**0.0327**
3x Wash vs. 2x Wash	-4.27	-12.64 to 4.1	0.6084
4x Wash vs. 2x Wash	-3.439	-11.38 to 4.501	0.7413
No Wash vs. 2x Wash	15.47	7.097 to 23.84	**<0.0001**
4x Wash vs. 3x Wash	0.831	-7.109 to 8.771	0.9983
No Wash vs. 3x Wash	19.74	11.37 to 28.11	**<0.0001**
No Wash vs. 4x Wash	18.91	10.97 to 26.85	**<0.0001**

Table 6.1 - Comparison of mucus thickness after different numbers of washings. Multiple t-test are displayed with adjusted p-values.

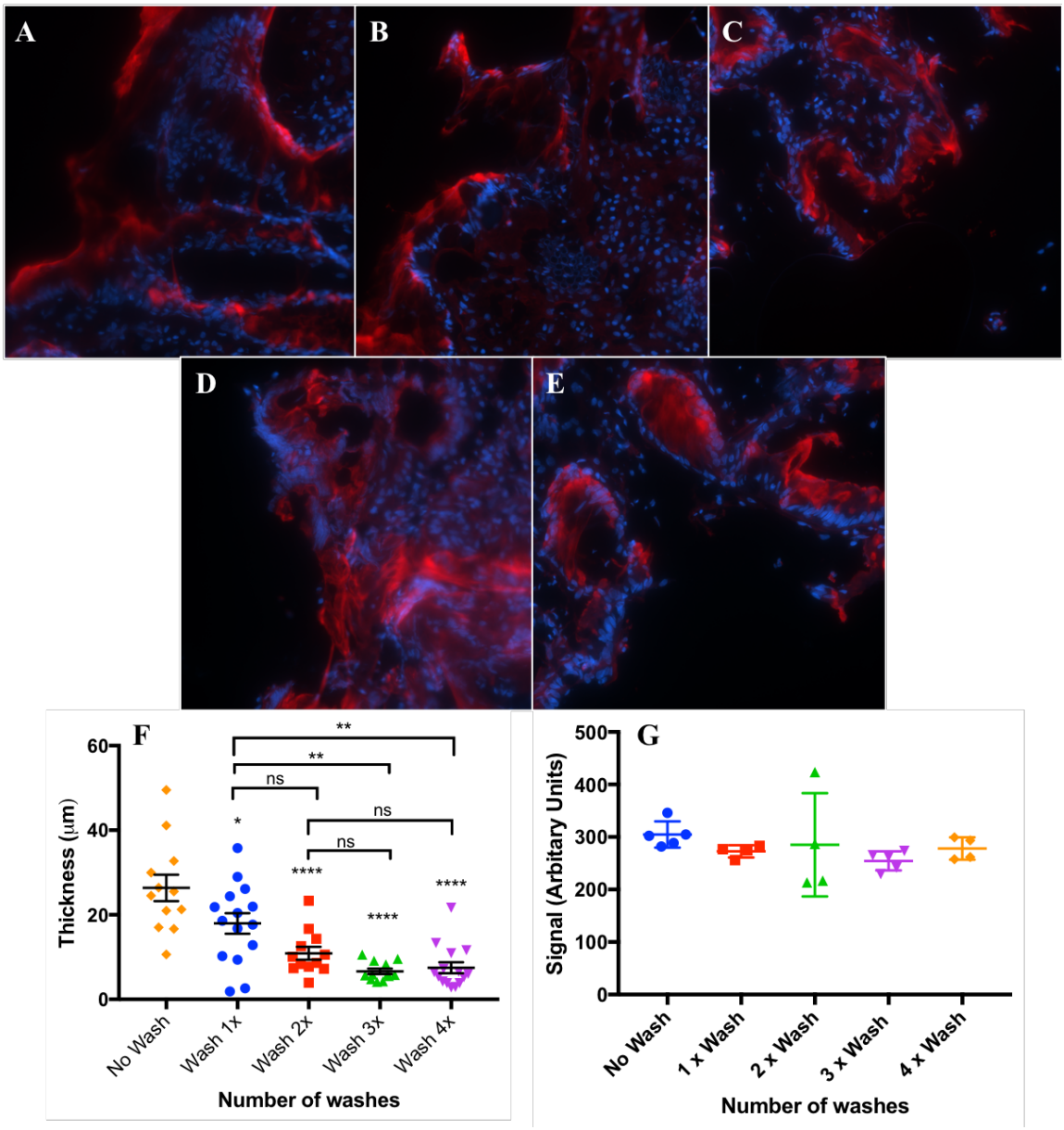

Figure 6.14 - Comparison of the effects of increasing washing on WFA-IR800CW brightness and mucus thickness in fresh frozen sections of normal colon. A= no wash, B= 1x wash, C= 2x wash, D= 3x wash, E = 4x wash, F = thickness of mucus layer following increasing number of washes, G = brightness of WFA-IR800CW after different number of washes. Whilst washing reduces the thickness of the mucus layer, it does not reduce the intensity of intracellular staining.

It is likely that these data show that the use of WFA *in-vivo* to identify colonic dysplasia and cancer is not possible. WFA clearly does not bind to normal colonic tissue – either the mucus layer or any exposed goblet cells on the surface of the epithelium. This may be due to 2 potential issues: firstly, the surface mucus may be extensively washed away by either bowel preparation solution, surgical washing to aid visualisation prior to WFA application or once the WFA has bound to the mucus this is easily washed away as shown above; secondly, there may be a large amount of free GalNAc in digested or broken-down mucus which prevents binding to a mucus layer on the epithelial surface. The latter problem would involve significant work to identify components of the colonic mucus using immunoprecipitation and mass spectrometry of glycoproteins and sugars which is outside the remit of this thesis. As WFA seemed to be a sensitive marker of early dysplasia, it was decided to attempt to identify different markers that may identify but may bind to a different target that is not mucus.

6.3.5. Identification of additional targets for identifying early colorectal disease

As WFA was well characterised in the Bodmer laboratory to discriminate normal from even early dysplasia in the colon, an additional marker was sought utilising WFA by to screening a panel of 51 colorectal cancer cell lines available. All cell lines were immunostained with WFA and imaged and assessed as either negative, partially positive or strongly positive (Figure 6.15). Eighteen (35%) of cell lines were negative for WFA staining including HCT116, RKO and SW480, which are well-known, poorly differentiated cell lines that do not contain goblet cells. Eleven cell lines were strongly positive for WFA staining including LS180 and SW1222 which are well known to be goblet cell rich cell lines; and, RW7213 and NCIH508 which are also goblet cell rich and thought to have been cultivated from signet ring cell carcinomas.

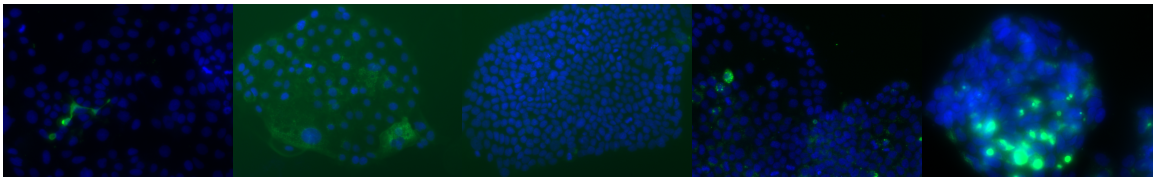

C2BBe1	**C10**	**C32**	**C80**	**C99**
1	0	0	1	2

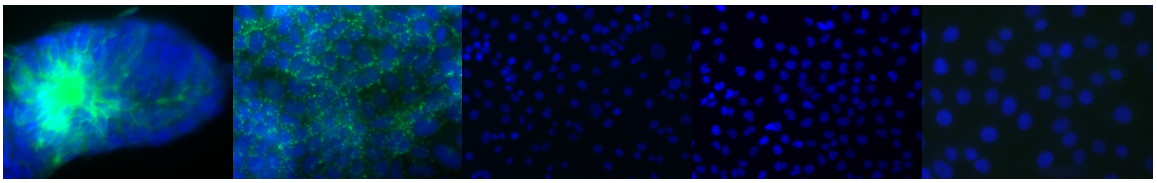

C106	**CaCO2**	**CC07**	**CC20**	**Colo678**
1	0	0	0	0

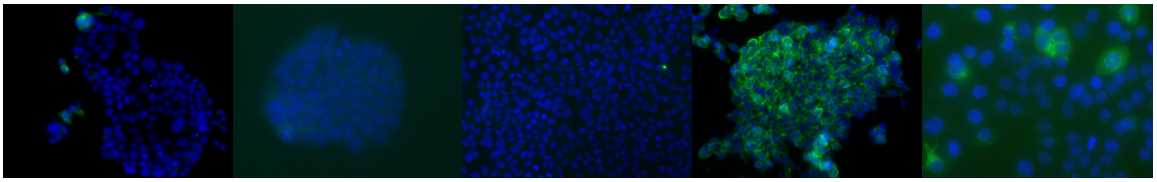

SW1116	**CX1**	**DLD1**	**GP2D**	**HCC2998**
1	0	0	2	2

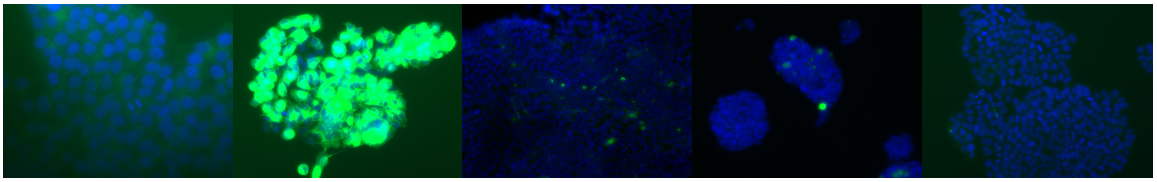

HCT116	**HDC9**	**HDC111**	**HDC114**	**HT29**
0	2	1	1	0

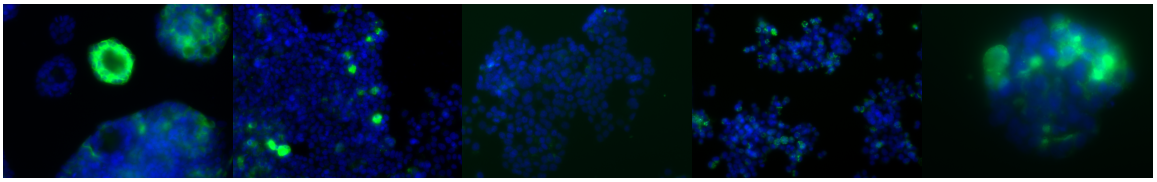

HT55	**LS180**	**LS411**	**LS513**	**NCIH508**
2	2	0	1	2

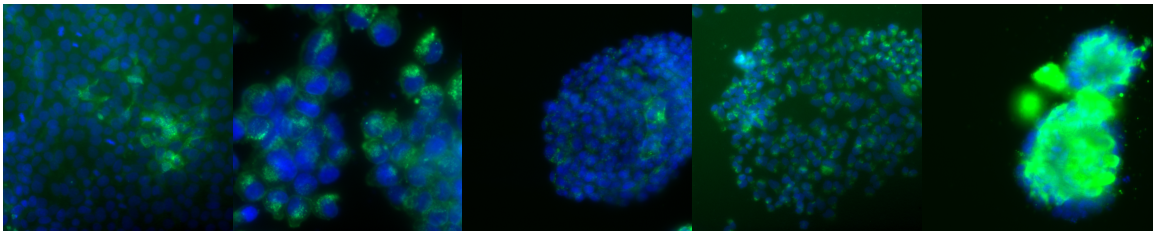

OUMS23	**OXCO1**	**PMFKO14**	**RW2892**	**RW7213**
1	1	1	1	2

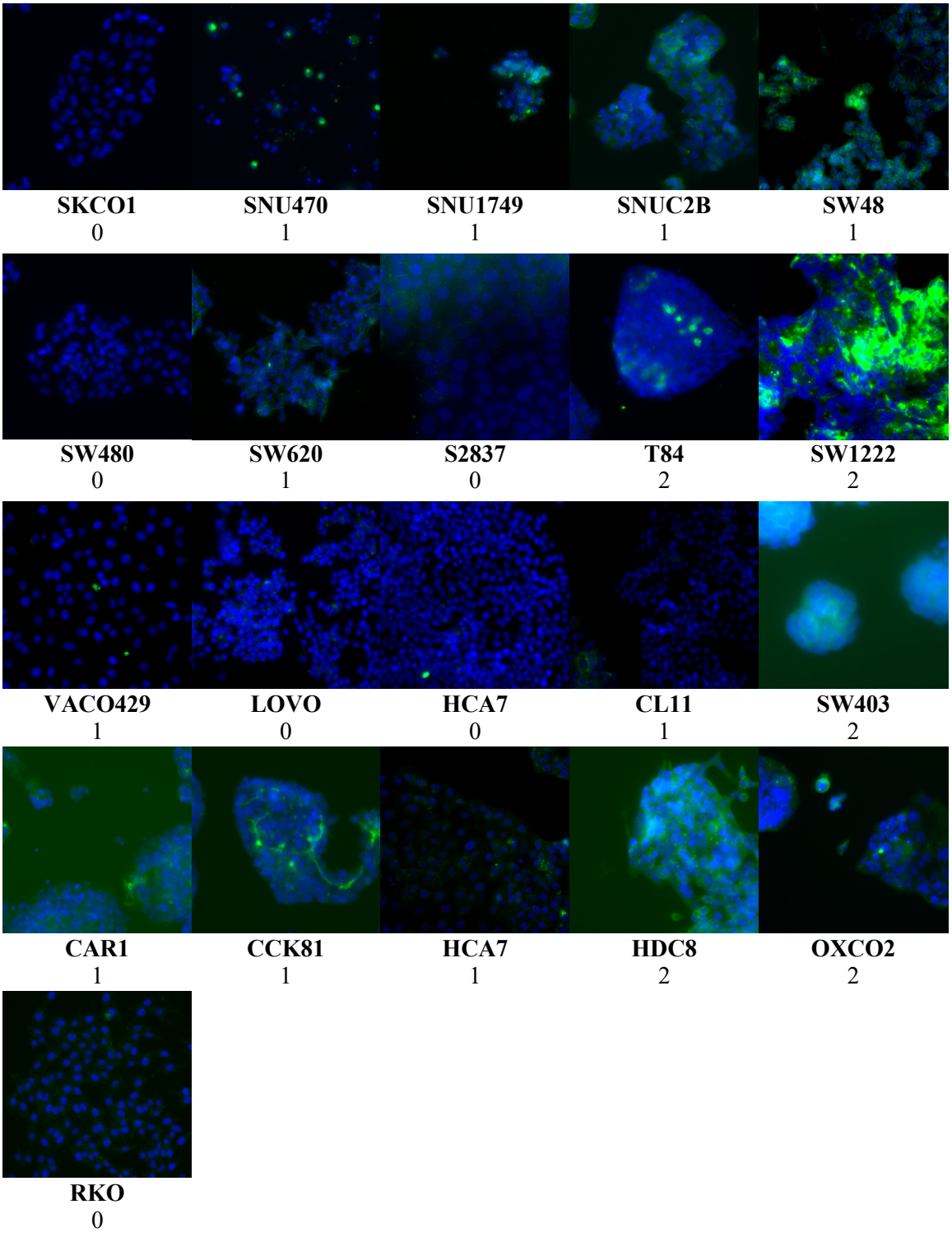

Figure 6.15 - Representative images of colorectal cancer cell line screening with WFA.

0 = negative stain, 1 = partially positive, 2 = strongly positive.

Following the assessment of screened cell lines, the micro-array data for each of the cell lines was interrogated and multiple t-tests were performed between each group for all genes in the micro-array giving fold change and p-value for the difference in gene expression between the groups (Figure 6.16). The groups compared were: 0 vs 1, 0 vs 2, 1 vs 2, 0 vs 1 & 2. Volcano plots were used to visualise the microarray analysis between groups. The top 50 genes in each comparison were reviewed for relevance and further investigation. When comparing the mildly positive with strongly positive (1 vs 2), the fold change of differential genes was much lower than that of the other group comparisons and, the top 50 differentially expressed genes were not relevant to either goblet cells, mucus production or colorectal cancer.

Particular genes of interest that arose from the microarray analysis included CDX1 which is a homeobox that is an intestine-specific target of oncogenic pathways [247] as well as being a key regulator of differentiation in the colon [248, 249]. TFF3 (Trefoil Factor 3) has been shown in the Bodmer laboratory to be another potential marker of the goblet cell [246] but also may be involved in the pathogenesis, progression and invasiveness of colorectal cancer [250-252]. Cadherin 17 (CDH17), regulated by another homeobox gene, CDX-2, has shown to be a useful marker of colorectal carcinomas [253, 254]. Most interestingly, glycoprotein A33 (GPA33) is an epithelial cell surface marker of transmembrane glycoproteins with expression reported in over 95% of colorectal cancers but has much stronger staining in normal epithelium and well differentiated tumours [255-258]. These four markers were taken forward to assess for their potential in being markers for early disease.

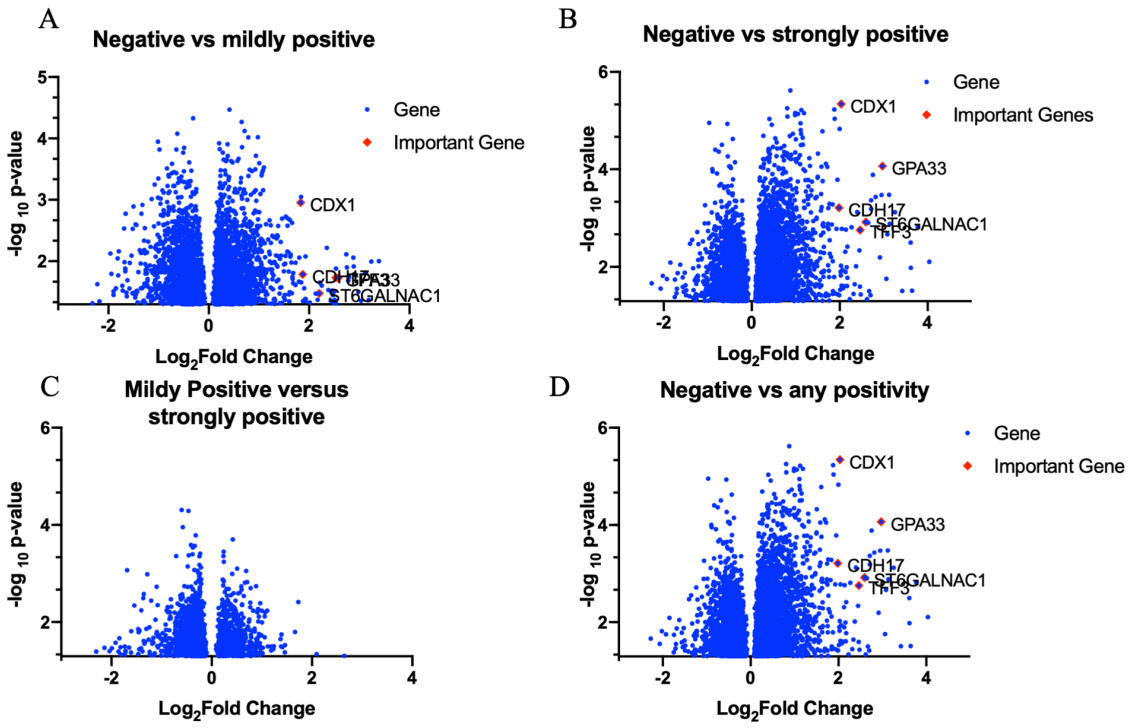

Figure 6.16 - Volcano plot of Log_2 Fold change and p-value of differential genes between different groups. A = negative vs mildly positive, B = negative vs strongly positive, C = mildly positive versus strongly positive, D = negative vs any positivity. Note that similar genes involved with glycosylation (TFF3, ST6GalNac1 and GPA33) are differentially expressed in every comparison as well as CDX1 involved with colonic epithelial cell differentiation.

To investigate the genes of interest, the cell line data from the Bodmer laboratory was further interrogated. All cell lines within the panel have been categorised into lumen forming or non-lumen forming [259] when grown in 3D culture using Matrigel. Lumens have been demonstrated to represent and share characteristics between well and poorly differentiated colorectal epithelium [260] so this was used as a model for comparison. Each of the genes of interest were compared between lumen forming and non-lumen forming cell lines with GPA33 being the only gene with a higher mean expression in lumen forming cells lines than non-lumen cell lines (3466 vs 1679, p=0.0284). CDX1, CDH17 and TFF3 all had higher expression in lumen forming cell lines but did not reach statistical significance (CDX1: 1230

vs 727.8, p=0.9849), (CDH17: 3659 vs 2446, p=0.3549), (TFF3: 1623 vs 1445, p>0.9999) (Figure 6.17).

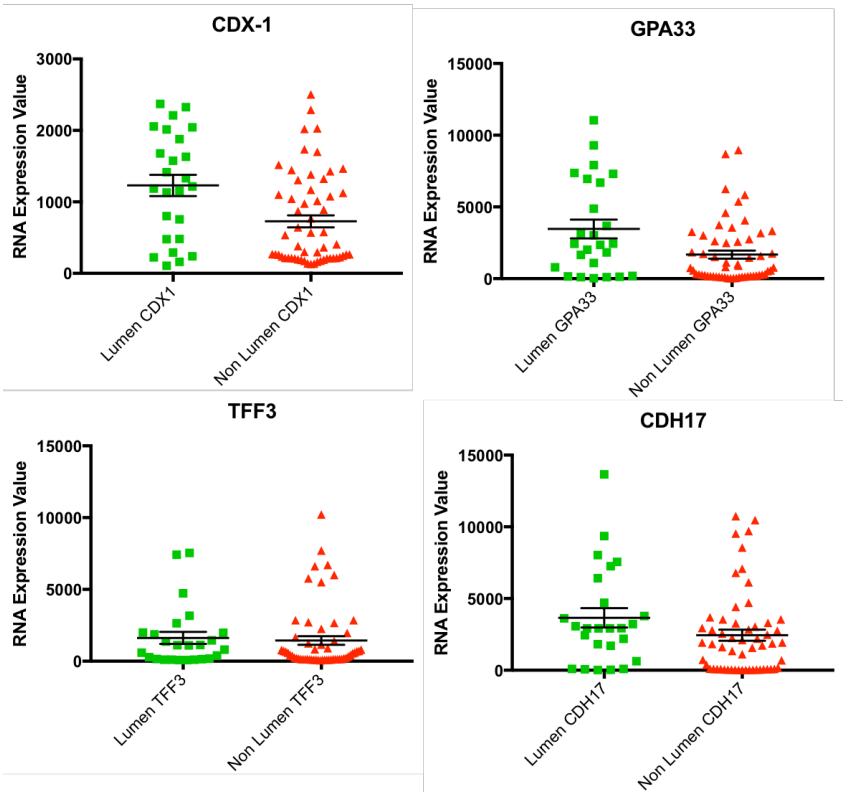

Figure 6.17 - Comparison of gene expression in CDX-1, GPA33, TFF3 and CDH17 across lumen and non-lumen forming cell lines.

Three publicly available datasets publishing transcriptome profiling of human colorectal tissue samples were interrogated for change in expression between the different pathologies in the genes of interest listed above. The datasets interrogated included GDS2947: paired samples of normal and adenomatous polyps [261], GSE41258 [262] and GSE68468 [263]: samples of normal, adenoma, adenocarcinoma, liver metastases and lung metastases. Where more than 2 tissue types in a dataset existed, multiple t-tests were performed comparing pathological tissue against the normal tissue, otherwise, a single t-test was performed comparing 2 groups within the dataset.

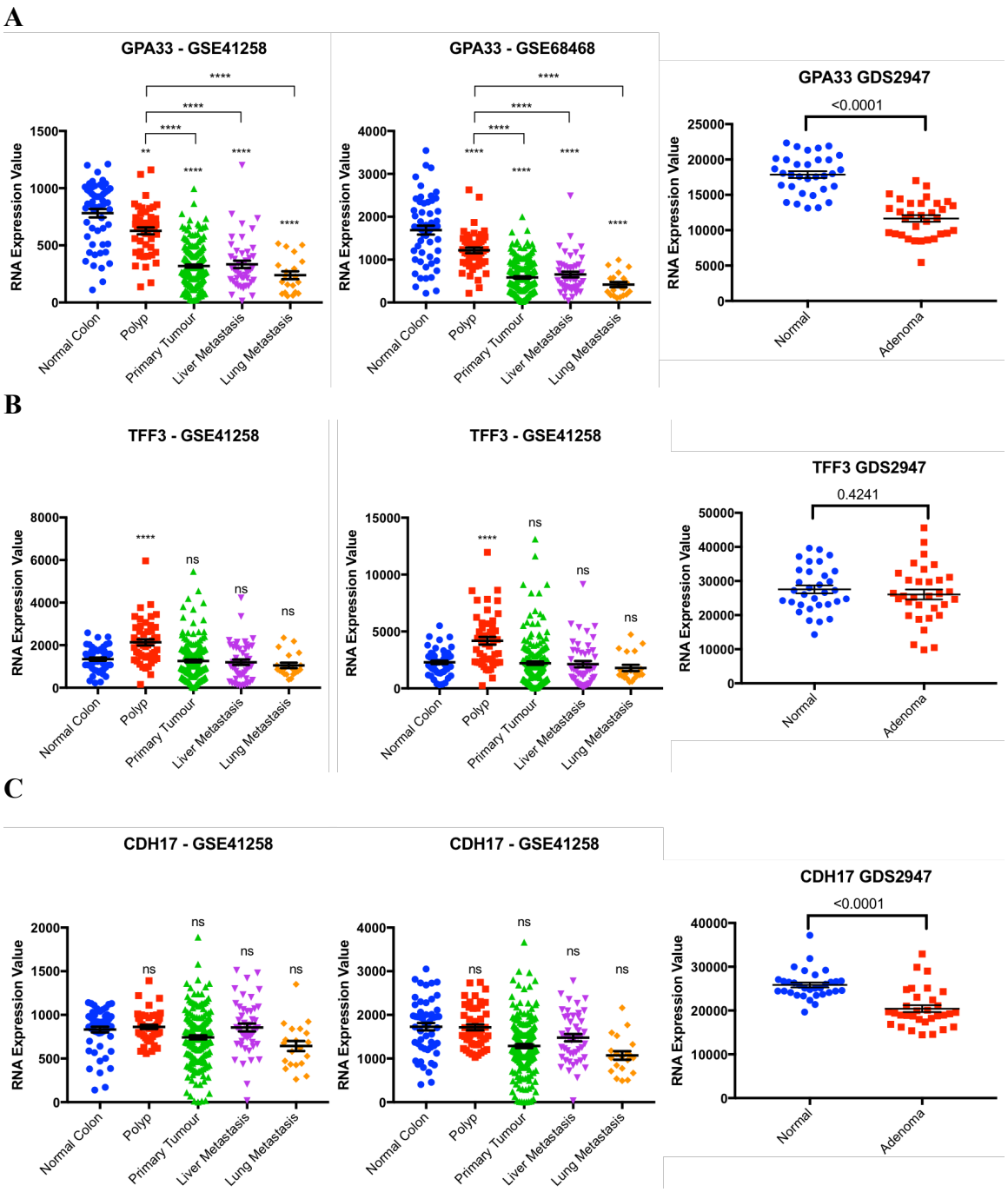
A
GPA33 - GSE41258
RNA Expression Value
Normal Colon
Polyp
Primary Tumour
Liver Metastasis
Lung Metastasis
GPA33 - GSE68468
GPA33 GDS2947
<0.0001
Normal
Adenoma
B
TFF3 - GSE41258
TFF3 - GSE41258
TFF3 GDS2947
0.4241
C
CDH17 - GSE41258
CDH17 - GSE41258
CDH17 GDS2947
<0.0001

D

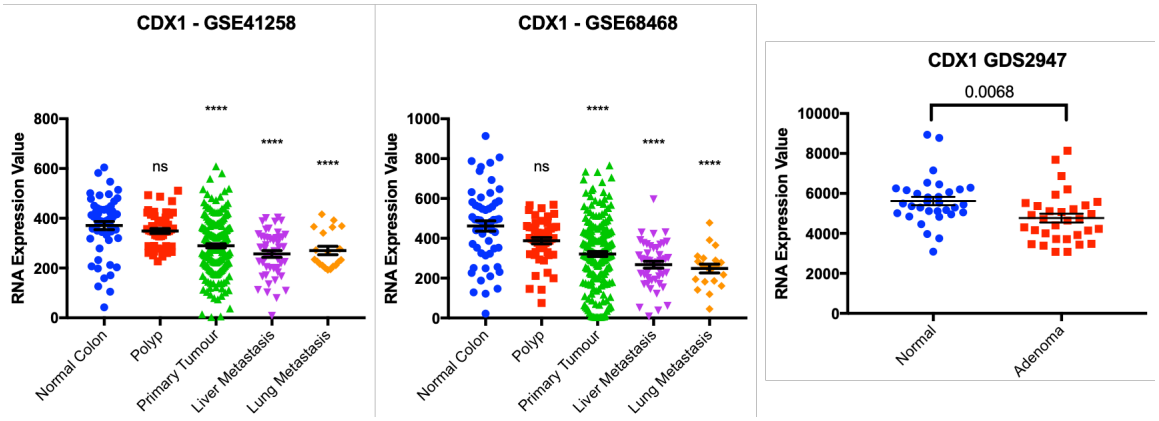

Figure 6.18 - RNA Expression from 3 data sets for GPA33, TFF3, CDH17 and CDX1. Data were from the publicly available datasets GSE41258, GSE68468 and GDS2947. Black bars represent mean and SEM.

From the RNA expression of these genes of interest, TFF3, CDH17 and CDX1 all demonstrated no true correlation with progression of disease from normal colon, adenomatous polyp, primary tumour and metastatic tissue in datasets GSE41258 and GSE68468. In GDS2947 where smaller numbers of fresh tissue were used for sequencing, both CDX1 and CDH17 showed a decrease in expression in the adenomatous polyp versus normal tissue (fold change 1.18, $p=0.0068$) and (fold change 1.27, $p<0.0001$) respectively. GPA33 demonstrated a more striking difference with a fold change of 1.53 ($p<0.0001$) in GDS2947 but in both GSE41258 and GSE68468 significant differences were seen in its expression in progressing pathology.

6.3.6. GPA-33 as another marker of colorectal cancer

To screen GPA-33 as a diagnostic fluorescent marker for colorectal cancer, a TMA slide containing 46 paired normal and cancer punch biopsies was stained with the antibody. Fluorescent signal in the normal colonic biopsies was 1.264 times brighter than in cancer samples and was significantly higher ($p=0.0009$) (Figure 6.19). When analysing subsets of paired tumours according to differentiation, well and moderately well differentiated tumours displayed no significant difference (mean GPA33:DAPI 0.425 vs 0.345, $p = 0.3456$) as well as poorly differentiated tumours, (mean GPA33:DAPI 0.460 vs 0.358, $p = 0.128$) although the poorly differentiated set only consisted of 4 patients, 3 of which had a significant decrease in signal to cancer. For moderately differentiated tumours, mean GPA33:DAPI was significantly higher in the normal tissue ($p = 0.0022$).

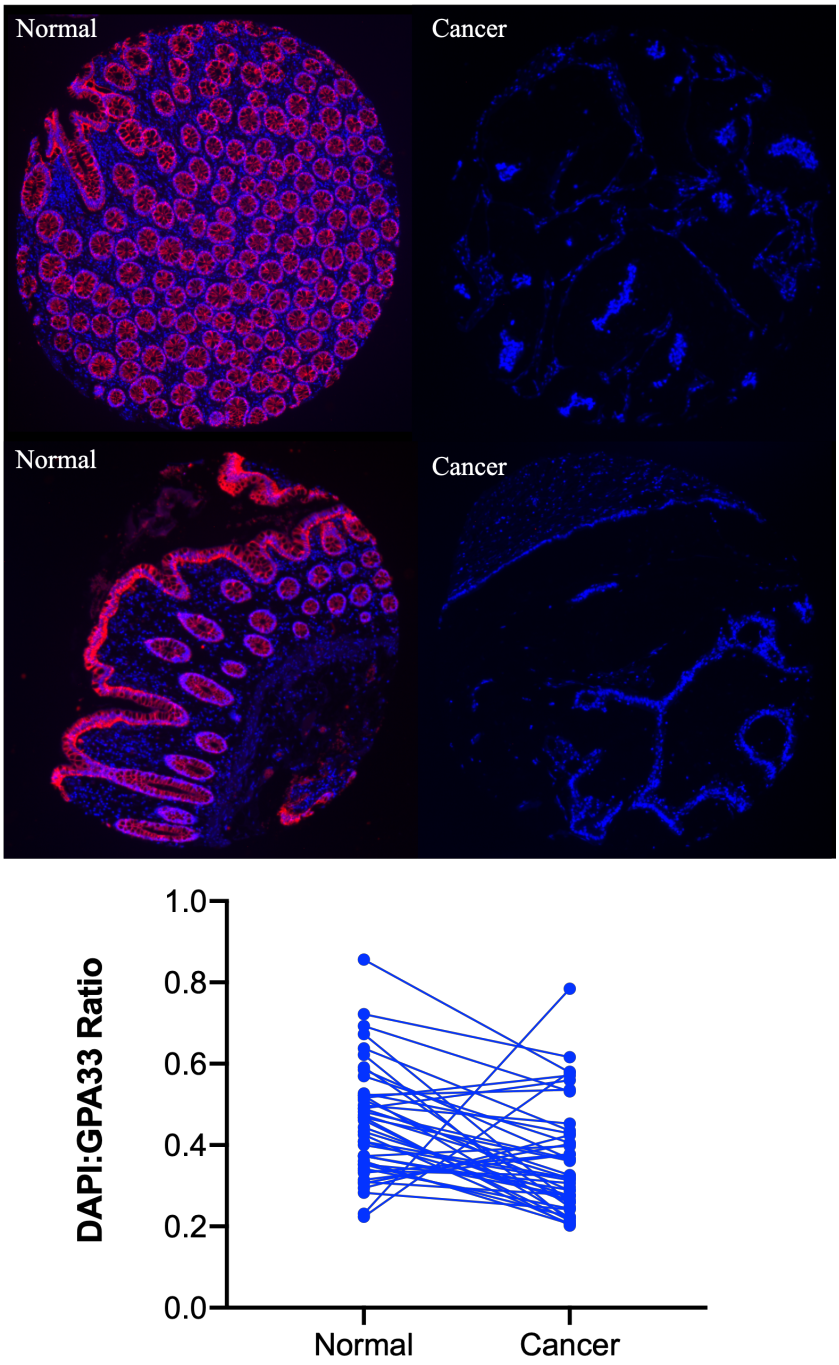

Figure 6.19 - Tissue Microarray staining of paired normal and colorectal cancer tissue. Top immunofluorescent images are the 2 samples on the TMA that showed the greatest difference between normal tissue and cancer. Beneath is graphical representation of difference in DAPI:GPA33 signal ratio.

6.4. Discussion and future directions

The results in this chapter have failed to demonstrate success with WFA as a negative fluorescent marker *in-vivo* to identify dysplasia or cancer. The hope of this application of fluorescence was to improve sensitivity of white light endoscopy especially for proximal colonic lesions where endoscopy has failed to reduce mortality benefit compared to distal colonic lesions [264]. *Ex-vivo* work that compared WFA manufactured by different commercial companies clearly demonstrates that it can successfully identify normal mucus within the goblet cells and mucus layer and does not bind to areas of even low-grade dysplasia. WFA seems to be a replicable peptide with a consistent binding target despite conjugation to different fluorophores.

Initial *in-vivo* assessment of WFA-FITC failed due to competitive autofluorescence at that wavelength. WFA is a 'negative marker' as it detects normal colonic mucus and therefore competes with AFI imaging which detects the increased autofluorescence signal emitted from normal colonic mucosa. Detecting any positive binding by an increase in S:B ratio would be extremely difficult as the difference is likely to be minimal. Thus, FITC as the fluorophore was abandoned in favour for the NIR IR800CW. Disappointingly, WFA-IR800 also failed *in-vivo*. Although this was only in 2 patients, the complete absence of binding to normal colonic mucosa where it has been shown to be extremely sensitive *ex-vivo*, questioned its efficacy. In both whole colonic and biopsy size specimens, WFA-IR800 failed to bind, being easily washed off. As described previously, the colonic mucus has been described in 2 layers, a lose outer layer and more adherent inner layer. WFA should bind to both as the sugars on the glycosylated MUC-2, do not change with dimerisation. However, minimal washing steps seem to easily remove the mucus layer and with the bowel

preparation that patients undertake and washing intraoperatively, it may be that the mucus layer was completely absent in these patients thus explaining the reason for lack of success.

To date, seven phase I/II studies have been published investigating the use of molecular endoscopy (Table 6.2). All studies have used a positive marker of abnormality. Three studies have assessed antibody targeted imaging using anti-CEA in wide-field colonoscopy [236], anti-EGFR in confocal laser endoscopy [238] and bevacizumab in wide-field endoscopy [265]. For the wide-field applications, impressive results were observed with 19/25 adenocarcinomas being positive for fluorescence with a 10-minute incubation of anti-CEA and with IV use of bevacizumab-IR800CW 3 days prior to endoscopy, all lesions even as small as 3mm including flat lesions in 17 patients were seen clearly under fluorescence. Similarly, Liu *et al* described signal being seen in the majority of cancers and in 66% of adenomas using CLE. CLE in the setting of molecular endoscopy is less about polyp detection but can allow real-time molecular classification of polyps aiding decision making [235, 266]. Use of antibodies in molecular endoscopy can be limited by immunogenicity especially if the antibodies are raised in another species, longer binding times and higher manufacturing costs [235, 266, 267]. However, these risks can be mitigated by restricting use to high-risk patients.

Year	Author	Probe	Target	Wavelength	Device	Application	Patient Number	Incubation time	Results
2002	Keller [236]	Anti-CEA	CEA	FITC	Prototype adapted olympus	Topical + mucilago tylose	27	10 min	19/25 adenocarcinomas positive
2004	Endlicher [268]	HAL	5-ALA	390-405nm	Prototype adapted olympus	Topical enema + N-acetylcysteine	10	30-60 min	7 patients had higher signal in pathological area, problems with background
2008	Hsuing [243]	VRPMPLQ	Peptide against dysplasia	FITC	CLE Cellvizio-GI	Topical	ns	5 min	S:B 9.3 +/- 0.9 for TA or TVA. Sensitivity 81% , specificity 82%
2013	Liu [238]	Anti-EGFR	EGFR	AF488	CLE Pentax system	Topical	37	10 min	Signal seen in 18/19 cancers and 12/18 adenomas.
2015	Burggraaf [242]	GE-137 peptide	c-MET	648nm	Custom built	Intravenous	15	120-180 min	9 of 43 lesions visible only under NIR. Mean S:B 2.3 +/- 1.1
2017	Joshi [267]	KCCFPAQ peptide	V600E mutation in BRAF	FITC	Olympus CF-Y0012 (prototype)	Topical	38	6 min	S:B of 1.16 = sensitivity 89%, specificity 92% for SSA. 19 SSAs visualise that were poorly seen with WL

Year	Author	Probe	Target	Wavelength	Device	Application	Patient Number	Incubation time	Results
2018	Hartmans [265]	Bevacizumab	VEGF-A	IR800CW	Prototype adapted olympus	Intravenous	17	3 days	100% detection of visible lesions

Table 6.2 – Published phase I/II trials in molecular colonoscopy using both antibody and peptide targets. CEA, carcinoembryonic antigen, FITC, fluorescein isothiocyanate, hexaminolevulinate, 5-ALA, 5-aminolevulinic acid, EGFR, epidermal growth factor receptor, CLE, confocal laser endoscopy, VEGF-A, Vascular endothelial growth factor A.

Another difficulty with antibody-based targets is that it relies on expression of the gene of interest to be sensitive enough and as such will never be 100% reliable [235, 266]. Keller *et al* observed no fluorescence in ulcerated mucosal areas presumably as they also demonstrated no CEA activity in areas of tumour necrosis on immunohistochemistry. More recently peptides have been investigated for molecular endoscopic imaging. The three studies referenced in Table 6.2 have all successfully used M13 phage display technology to produce conjugated peptides against specific targets.

Joshi [267] and Burggraaf [242] used phage display against known targets (V600E mutation in BRAF present on HT29 cells and c-Met). These studies demonstrated lesions that were not visible under white light on wide field endoscopy. Hsiung and colleagues [243] developed a peptide sequence specific to dysplasia by clearing a phage library by incubating it with non-malignant epithelial cells and normal colonic mucosa. The cleared library was then incubated with dysplastic polyp tissue and bound phage was then used to clone, sequence and synthesis for in human use. Their peptide (VRPMPLQ) thus has an unknown molecular target and showed preferential binding to dysplastic colonocytes versus adjacent normal cells on CLE. Its benefit in wide-field endoscopy has not been demonstrated. This method of producing peptides to unknown targets may allow detection of surface targets that may otherwise not be known but can be limited as it cannot account for the huge heterogeneity of adenomas and cancers. Nonetheless, phage display technology could be used to produce multiple conjugated peptides to increase sensitivity [267] and is an alternative to screening cell lines.

A limitation realised with WFA-FITC was the background from autofluorescence. All except one of the studies outlined in Table 6.2 have used either FITC, AF488 or fluorophores within the visible light spectrum. Joshi *et al* [267] were the only authors to publish control

images of the colon under fluorescence without their fluorescent peptide or antibody. This demonstrated minimal background converse to what was demonstrated in this chapter both using the AFI colonoscope and IVIS to image the colon. An explanation for limited background signal in these studies may be that their in-house made devices had a narrower excitation light than the AFI system used here. This may therefore produce less autofluorescence. In addition, the targets used are positive targets and any signal produced is likely to be higher than background signal from normal colon. This further demonstrates the difficult of WFA as a negative target for colonic imaging.

6.4.1. GPA33 as an alternative to WFA

GPA33 (or A33) was identified as another potential marker of colonic cancer from assessing microarray data in cell lines categorised as either being positive or negative for WFA staining. GPA33 is a membrane-bound glycoprotein with a molecular weight of 43kDa. Its function is not completely understood but has been associated with immunological processes, proliferation, and colonic mucosal repair in an animal model of colitis [255, 269]. Of the identified potential genes of interest, GPA33 seemed the most promising in both publicly available datasets of human samples, cell lines and a tissue microarray. GPA33 is a membrane-bound glycoprotein and has been shown to be expressed on the basolateral surfaces of the stomach, small intestine, colon and rectal epithelial cells [255, 257]. The results from TMA staining presented here demonstrated significantly stronger staining in the normal colon when compared with colorectal cancer. Three studies have investigated the staining pattern of GPA33 in colorectal tissue. The first reported paper reported 96% of colorectal tumours being positive for GPA33 [257]. Similarly, later studies by Baptisella [255] and Wong [256] also demonstrated similar positivity in colorectal studies. None of these reports included paired normal tissue as a comparison. Garinchesa and Baptisella both observed strongly positive staining in well differentiated tumours but as tumours progressed to poorly

differentiation, staining decreased and was even absent in poorly differentiated tumours. Similar results were seen here except the data in this chapter compares abnormal with normal tissue.

GPA33 has not been assessed as an *in-vivo* imaging tool but could be evaluated given the increased staining pattern in normal colonic tissue and as tumours become less differentiated staining becomes increasingly absent. The next stage of work would involve using fresh *ex-vivo* tissue to assess its efficacy as described with WFA in this chapter. A number of groups have attempted to test the effects of GPA33 in colorectal cancer. A xenograft mouse model using SW1222 was evaluated and demonstrated tumour regression after treatment with ^{125}I-labelled or ^{131}I-labelled GPA33 which was taken to phase I and II clinical studies using murine antibodies demonstrating some anti-tumour effects without bowel toxicity [270, 271]. A further phase I study using the humanised monoclonal antibody KRN330 to GPA33 failed as they did not achieve the prespecified response rate [272]. A possible explanation for the mixed results with GPA33 for treatment may be the heterogeneity seen in tissue staining both here and the previously mentioned studies.

6.4.2. Future of molecular endoscopy

This chapter has demonstrated the difficulties with using mucus as a target for molecular imaging. Another difficulty with this technology is application of the substance onto the mucosal surface by using a spray. Numerous authors describe the difficulties with this technique and one can never ensure that the mucosal surface is fully covered [235, 242, 266]. The obvious route of administration would be intravenous however, distribution, higher doses and other side effects then can become difficulties which must be overcome. The antibodies and peptide surface markers described in this section prove promising and, avoiding the use

of antibodies, phage display of peptides towards the pathology of interest should be investigated in larger numbers of patients.

CHAPTER 7: DISCUSSION AND FUTURE DIRECTIONS

7.1. Summary of results

This thesis has explored new applications of using NIR by fluorescence and emitted NIR light for real-time surgical guidance. The two explored themes have been anatomy delineation and molecular fluorescence to highlight tumour. Anatomical guidance for the ureters has shown success with both methylene blue and the first-in-man study of IRDye 800BK. The results presented demonstrate likely superiority of methylene blue in terms of signal to background ratio with IRDye 800BK giving a constantly bright signal that is hampered by background. Highlighting the urethra during low rectal cancer surgery has proven successful *ex-vivo*, however, difficulties arose when taking this application into humans. ICG-Instillagel was a difficult technique which also failed to highlight the urethra *in-vivo*. Similarly, an NIR emitting fibre constructed to be compatible with a standard urethra had limited success and reasons for this area not being have been discussed in depth in section 4.4. The most successful application of fluorescence for anatomical delineation presented has been the use of ICG to highlight the thoracic duct and intraoperative chyle leaks during oesophagectomy. This was the first description of using fluorescence in this modality in the literature. Real-time molecular imaging was explored using WFA conjugated to both FITC and IR800CW in section 6.3. Sadly, failure of this fluorescent peptide and technique was likely due to the mucus which was the primary target being easily removed with washing. As discussed, for tumour specific identification, other compounds such as fluorescent antibodies or peptides manufactured by phage display are likely to become more advantageous in the future.

7.2. Limitations

One of the major drawbacks with work presented here is that all the results are produced from feasibility studies. By nature, these are small numbered studies still in an ‘experimentation’ phase, thus it is difficult to draw conclusions as to whether the technology

is useful on a subjective level. These studies merely provide evidence of working as well as important steps including timing and dose optimisation to inform future work.

In principle, to have the optimal fluorescent signal, there should be minimal depth for both excitation and emission light to penetrate, limited distance between the excitation light, emission detector and the fluorophore to reduce light scatter and the fluorophore should be at the optimal concentration. The *in-vivo* work makes it extremely difficult to make comparisons between patients and cohorts of different dyes as it is almost impossible to fix the distance of a laparoscopic camera to the subject and the covering tissue depth is extremely variable. These confounding factors become less relevant once the technology is validated in a higher number of patients and therefore, dictates that future non-randomised trials assessing these applications in a more heterogeneous population.

For anatomy delineation, there is no validated method by which to score success for fluorescence having a positive outcome for both the patient and the surgeon. The obvious patient outcome of 'structural injury' is unlikely to be useful due to the low incidence. Whilst signal to background ratio has provided information on the fluorescent signal, in order to assess the usefulness in future studies, this is unlikely to provide a persuasive argument in favour of the technology. Similarly, a crude yes/no identification scoring system is also unlikely to be informative in future studies. As explored in this thesis, the likely outcomes for anatomy delineation are: reduction in operative time or time to complete a sub-step of an operation; subjective assessment of surgeon reassurance or for use as a training tool. Molecular imaging is slightly easier to assess as histopathological analysis can be used as the gold standard.

7.2.1. Difficulties in conducting clinical trials with fluorescence

There are numerous difficulties in conducting clinical trials using fluorescence that have been experienced during this work and should be borne in mind when developing future protocols. Fluorescence often requires equipment additional to that used in the primary procedure. This additional equipment required additional space, training to theatre and surgical staff, clinical engineering assessment prior to use and may add on additional time during the procedure. This can often limit how much data is obtained under fluorescence as a slight interruption in operative flow can cause avoidance of multiple use. On a similar note, fluorescence technology currently does not allow continuous visualisation in the NIR modality. Even in NIR mode, the difference in frame display rates reduces the 3D perception from the 2D image and can often be difficult to interpret. Thus, the NIR modality is only ever used when visualising fluorescence. This can lead to variability in when a structure is identified, for example, as fluorescence mode is not continuously displayed.

Currently, fluorescence enabled laparoscopes are bespoke devices with filters fitted according to the fluorophore they are targeting. Therefore, additional laparoscopes are required and need to be sterilised for every case. Fluorescence laparoscopes look identical to standard laparoscopes and can and have been easily mislabelled by theatre staff and sterile services which can lead to last minute delays or even trial withdrawals due to loss of equipment. This seemingly minor logistic issue can make such a trial difficult and lengthy to run efficiently.

When assessing fluorescence technology, it is essential to allow enthusiasts as well as sceptics to use the technology even at an early stage to get an indication of usability and generalisability. With the latter group of surgeons, patience and persistence is required to obtain the essential data. Similarly, in most institutions there is a training element to every

operation and as a trainee often feels slightly stressed and is primarily interested in the operative steps, it can be difficult to ask for a pause to capture the fluorescence data.

As mentioned previously, all devices require training for theatre staff and, in the current climate, the changeover of NHS staff is rapid and multiple training sessions are required and can be quite time consuming. Furthermore, it requires a research member to be present until the very end of the procedure to ensure equipment is correctly labelled and sent for sterilisation.

7.3. Future technology

Fluorescence requires a fluorophore, an excitation and imaging device, and software in order to provide real-time visualisation. Each of these technologies are continuously advancing and will improve signal to background ratios as well as sensitivity and specificity.

7.3.1. NIR-II window

NIR fluorophores have been experimented with in this thesis. Fluorescence imaging in the second near-infrared window (NIR-II, 1000 – 1700nm) is also possible and some argue, more desirable than NIR-I (650-900nm) owing to a reduction in photon scattering, much less tissue autofluorescence and deeper tissue penetration improving imaging quality and signal to background ratio [273-277] (Figure 7.1).

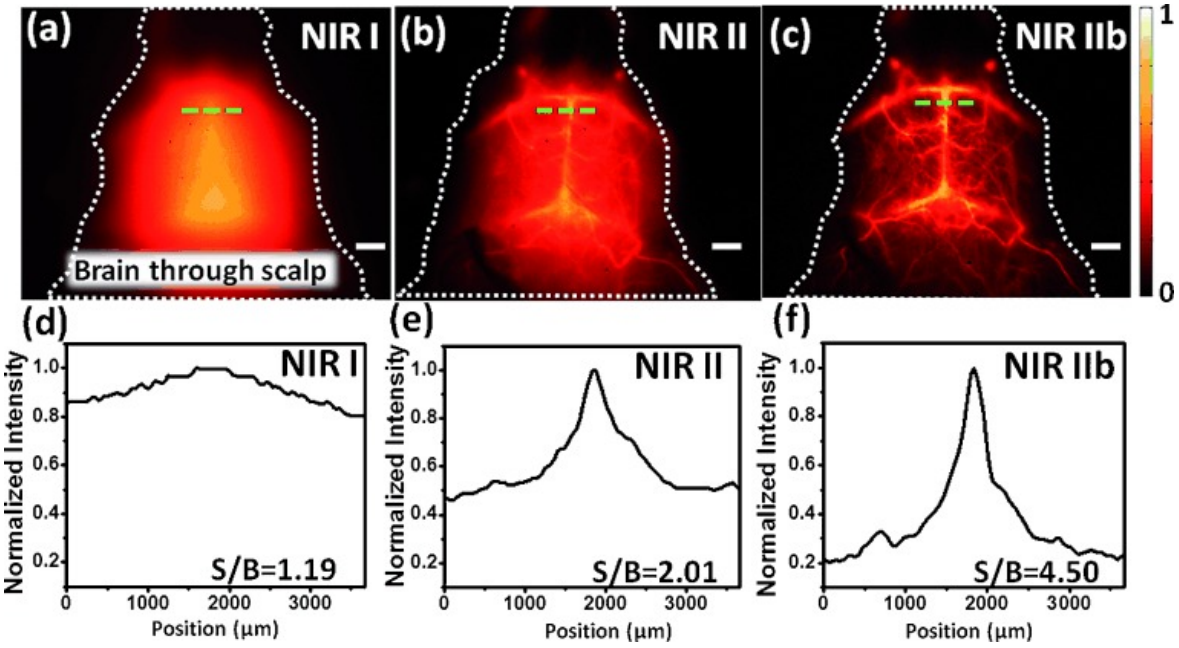

Figure 7.1 - Fluorescent images of cerebro-vasculature in mice in the NIR-I and NIR-II spectrums. The NIR-I image demonstrates significant tissue scatter and therefore less enhancement compared with the NIR-II images. This is also reflected by the broad peak in the signal to background ratio. Reproduced with permission from Diao *et al* [273].

Until recently, the only NIR-II fluorescent agents for *in-vivo* imaging at present are inorganic including carbon nanotubes, quantum dots and nanoparticles. Toxicity concerns over these molecules have arisen as they have extremely long circulation times and are retained in the liver and spleen [278]. Organic fluorophores are much preferred for clinical imaging as they have a rapid metabolism and low toxicity, however the design and manufacture of these are extremely difficult hence why organic NIR-II dye synthesis is further behind the inorganic dyes [274, 278]. Similarly, difficulties with constructing imaging equipment for the NIR-II window for *in-vivo* use is costly and lengthy and as a result, no commercial entities are developing such devices.

7.3.2. Software enhancements

As fluorescence technology is now fully integrated into laparoscopic devices without the need for any additional equipment, software must become more advanced to improve signal to background ratios and overlay real-time image display. Novadaq (Stryker) currently hold the patent for providing simultaneous overlay display of real-time fluorescent images [21]. This aspect of software enhancement greatly improves the applicability, but further developments are required to improve the frame-rate discrepancy as well as reducing the display of background signal through contrast enhancement.

7.3.3. Hardware enhancements

Whilst the fluorescence technology outlined in this thesis is mainly laparoscope and endoscope based, open surgery is an avenue of fluorescence surgery that is rapidly developing. A major barrier to fluorescence guided open surgery is the need to switch off the operating lights as the NIR light emitted from these completely flood the image. Stryker have recently marketed the Spy-PHI portable handheld imaging system which allows fluorescence visualisation in the open field without the need for all operating lights to be off. A step beyond this is to have fluorescence enabled goggles which at present are bulky and unsightly but will no doubt progress to small devices that do not interfere with the surgeon's vision but provide real-time overlaid fluorescence images [279].

As briefly mentioned in section 4.4, stereotactic navigation is another technology enhancement for fluorescence imaging. The combination of detectors of emitted light and information from pre- and peri-operative imaging could improve anatomy delineation of critical structures and identification of tumour.

7.4. Summary

In conclusion, this thesis has demonstrated successful use of real-time NIR guidance to provide anatomical delineation of the ureter during colorectal surgery and the thoracic duct during oesophagectomy as well as the principle of urethral delineation. Highlighting the urethra *in-vivo* has proven to be more difficult however and advances in technology and perhaps the use of the NIR-II window in this area would improve its visualisation. Molecular imaging has been explored using WFA to highlight dysplasia and cancer in the colon and whilst this has worked *ex-vivo*, it failed to behave as expected *in-vivo*. Despite this, GPA33 was identified as another potential marker for diagnostics with suggestions for future work using this antibody. Fluorescence guided surgery is still very much in its infancy with expected enhancements in software, hardware and perhaps a dive into the NIR-II window is coming.

REFERENCES

1. Khor WS, Baker B, Amin K, Chan A, Patel K, Wong J. Augmented and virtual reality in surgery-the digital surgical environment: applications, limitations and legal pitfalls. Ann Transl Med. 2016;4(23):454.
2. Zhang DY, Singhal S, Lee JYK. Optical Principles of Fluorescence-Guided Brain Tumor Surgery: A Practical Primer for the Neurosurgeon. Neurosurgery. 2018.
3. Jablonski A. Efficiency of Anti-Stokes Fluorescence in Dyes. Nature. 1933;131:839.
4. Zhang RR, Schroeder AB, Grudzinski JJ, Rosenthal EL, Warram JM, Pinchuk AN, et al. Beyond the margins: real-time detection of cancer using targeted fluorophores. Nat Rev Clin Oncol. 2017.
5. Frangioni JV. In vivo near-infrared fluorescence imaging. Curr Opin Chem Biol. 2003;7(5):626-34.
6. Landsman ML, Kwant G, Mook GA, Zijlstra WG. Light-absorbing properties, stability, and spectral stabilization of indocyanine green. J Appl Physiol. 1976;40(4):575-83.
7. Schaafsma BE, Mieog JS, Hutteman M, van der Vorst JR, Kuppen PJ, Lowik CW, et al. The clinical use of indocyanine green as a near-infrared fluorescent contrast agent for image-guided oncologic surgery. J Surg Oncol. 2011;104(3):323-32.
8. Lakowicz JR. Principles of frequency-domain fluorescence spectroscopy and applications to cell membranes. Subcell Biochem. 1988;13:89-126.
9. Yuan B, Chen N, Zhu Q. Emission and absorption properties of indocyanine green in Intralipid solution. J Biomed Opt. 2004;9(3):497-503.
10. Zheng Q, Lavis LD. Development of photostable fluorophores for molecular imaging. Curr Opin Chem Biol. 2017;39:32-8.
11. Croce AC, Bottiroli G. Autofluorescence spectroscopy and imaging: a tool for biomedical research and diagnosis. Eur J Histochem. 2014;58(4):2461.
12. Fujimoto D. Isolation and characterization of a fluorescent material in bovine achilles tendon collagen. Biochem Biophys Res Commun. 1977;76(4):1124-9.
13. Deyl Z, Macek K, Adam M, Vancikova O. Studies on the chemical nature of elastin fluorescence. Biochim Biophys Acta. 1980;625(2):248-54.
14. DaCosta RS, Andersson H, Cirocco M, Marcon NE, Wilson BC. Autofluorescence characterisation of isolated whole crypts and primary cultured human epithelial cells from normal, hyperplastic, and adenomatous colonic mucosa. J Clin Pathol. 2005;58(7):766-74.

15. McCallum AL, Jenkins JT, Gillen D, Molloy RG. Evaluation of autofluorescence colonoscopy for the detection and diagnosis of colonic polyps. Gastrointest Endosc. 2008;68(2):283-90.
16. Zonios GI, Cothren RM, Arendt JT, Wu J, Van Dam J, Crawford JM, et al. Morphological model of human colon tissue fluorescence. IEEE Trans Biomed Eng. 1996;43(2):113-22.
17. Lakowicz JR. Principles of fluorescence spectroscopy. In: Lakowicz JR, editor. Principles of fluorescence spectroscopy. 3rd ed: Springer; 2006.
18. Stolik S, Delgado JA, Perez A, Anasagasti L. Measurement of the penetration depths of red and near infrared light in human "ex vivo" tissues. J Photochem Photobiol B. 2000;57(2-3):90-3.
19. Gioux S, Choi HS, Frangioni JV. Image-guided surgery using invisible near-infrared light: fundamentals of clinical translation. Mol Imaging. 2010;9(5):237-55.
20. Troyan SL, Kianzad V, Gibbs-Strauss SL, Gioux S, Matsui A, Oketokoun R, et al. The FLARE intraoperative near-infrared fluorescence imaging system: a first-in-human clinical trial in breast cancer sentinel lymph node mapping. Ann Surg Oncol. 2009;16(10):2943-52.
21. Westwick PR, Potkins D, Fengler J, inventors; Novadaq Technologies Ulc, assignee. Imaging systems and methods for displaying fluorescence and visible images. United States patent US20170064257A1. 2006.
22. Vahrmeijer AL, Hutteman M, van der Vorst JR, van de Velde CJ, Frangioni JV. Image-guided cancer surgery using near-infrared fluorescence. Nat Rev Clin Oncol. 2013;10(9):507-18.
23. U.S. Food and Drug Administration. FDA Approved Drug Products 2018 [Available from: https://www.accessdata.fda.gov/scripts/cder/daf/index.cfm?event=overview.process&applno=011525.
24. Polom W, Markuszewski M, Rho YS, Matuszewski M. Usage of invisible near infrared light (NIR) fluorescence with indocyanine green (ICG) and methylene blue (MB) in urological oncology. Part 1. Cent European J Urol. 2014;67(2):142-8.
25. Cahill RA, Ris F, Mortensen NJ. Near-infrared laparoscopy for real-time intra-operative arterial and lymphatic perfusion imaging. Colorectal Dis. 2011;13 Suppl 7:12-7.

26. Hope-Ross M, Yannuzzi LA, Gragoudas ES, Guyer DR, Slakter JS, Sorenson JA, et al. Adverse reactions due to indocyanine green. Ophthalmology. 1994;101(3):529-33.
27. Chu W, Chennamsetty A, Toroussian R, Lau C. Anaphylactic Shock After Intravenous Administration of Indocyanine Green During Robotic Partial Nephrectomy. Urol Case Rep. 2017;12:37-8.
28. Chu M, Wan Y. Sentinel lymph node mapping using near-infrared fluorescent methylene blue. J Biosci Bioeng. 2009;107(4):455-9.
29. Polom K, Murawa D, Nowaczyk P, Rho YS, Murawa P. Breast cancer sentinel lymph node mapping using near infrared guided indocyanine green and indocyanine green--human serum albumin in comparison with gamma emitting radioactive colloid tracer. Eur J Surg Oncol. 2012;38(2):137-42.
30. Polom K, Murawa D, Rho YS, Spychala A, Murawa P. Skin melanoma sentinel lymph node biopsy using real-time fluorescence navigation with indocyanine green and indocyanine green with human serum albumin. Br J Dermatol. 2012;166(3):682-3.
31. Polom K, Murawa D, Rho YS, Nowaczyk P, Hunerbein M, Murawa P. Current trends and emerging future of indocyanine green usage in surgery and oncology: a literature review. Cancer. 2011;117(21):4812-22.
32. Selvam S, Sarkar I. Bile salt induced solubilization of methylene blue: Study on methylene blue fluorescence properties and molecular mechanics calculation. Journal of Pharmaceutical Analysis. 2017;7(1):71-5.
33. Peter C, Hongwan D, Kupfer A, Lauterburg BH. Pharmacokinetics and organ distribution of intravenous and oral methylene blue. Eur J Clin Pharmacol. 2000;56(3):247-50.
34. Matsui A, Tanaka E, Choi HS, Kianzad V, Gioux S, Lomnes SJ, et al. Real-time, near-infrared, fluorescence-guided identification of the ureters using methylene blue. Surgery. 2010;148(1):78-86.
35. Traynor S, Adams JR, Andersen P, Everts E, Cohen J. Appropriate timing and velocity of infusion for the selective staining of parathyroid glands by intravenous methylene blue. Am J Surg. 1998;176(1):15-7.
36. Cousins A, Thompson SK, Wedding AB, Thierry B. Clinical relevance of novel imaging technologies for sentinel lymph node identification and staging. Biotechnol Adv. 2014;32(2):269-79.

37. Laios A, Volpi D, Tullis ID, Woodward M, Kennedy S, Pathiraja PN, et al. A prospective pilot study of detection of sentinel lymph nodes in gynaecological cancers using a novel near infrared fluorescence imaging system. BMC Res Notes. 2015;8:608.
38. European Medicines Agency. Methylthioninium chloride Proveblue 2018 [Available from: Methylthioninium chloride Proveblue.
39. Medicines and Healthcare Regulatory Authority. Summary of procuct characteristics - methylthioninium chloride 2015 [Available from: http://www.mhra.gov.uk/home/groups/spcpil/documents/spcpil/con1501220853887.pdf.
40. McDonagh EM, Bautista JM, Youngster I, Altman RB, Klein TE. PharmGKB summary: methylene blue pathway. Pharmacogenet Genomics. 2013;23(9):498-508.
41. National Library of Medicine: Toxnet. Methylene Blue 2009 [Available from: https://toxnet.nlm.nih.gov/cgi-bin/sis/search2/r?dbs+hsdb:@term+@rn+@rel+61-73-4.
42. Stummer W, Pichlmeier U, Meinel T, Wiestler OD, Zanella F, Reulen HJ, et al. Fluorescence-guided surgery with 5-aminolevulinic acid for resection of malignant glioma: a randomised controlled multicentre phase III trial. Lancet Oncol. 2006;7(5):392-401.
43. Chohan MO, Berger MS. 5-Aminolevulinic acid fluorescence guided surgery for recurrent high-grade gliomas. J Neurooncol. 2018.
44. Andrew H, Gossedge G, Croft J, Corrigan N, Brown JM, West N, et al. Next Generation intraoperative Lymph node staging for Stratified colon cancer surgery (GLiSten): a multicentre, multinational feasibility study of fluorescence in predicting lymph node-positive disease. Efficacy and Mechanism Evaluation. Southampton (UK): NIHR Journals Library; 2016.
45. Medicines and Healthcare Regulatory Authority. Public Assessment Report Fluorescein Sodium 100 mg/ml, Solution for Injection 2015 [Available from: http://www.mhra.gov.uk/home/groups/par/documents/websiteresources/con500348.pdf.
46. Pansare V, Hejazi S, Faenza W, Prud'homme RK. Review of Long-Wavelength Optical and NIR Imaging Materials: Contrast Agents, Fluorophores and Multifunctional Nano Carriers. Chem Mater. 2012;24(5):812-27.

47. Ko HY, Chang YW, Paramasivam G, Jeong MS, Cho S, Kim S. In vivo imaging of tumour bearing near-infrared fluorescence-emitting carbon nanodots derived from tire soot. Chem Commun (Camb). 2013;49(87):10290-2.
48. Zhou Y, Kim YS, Milenic DE, Baidoo KE, Brechbiel MW. In vitro and in vivo analysis of indocyanine green-labeled panitumumab for optical imaging-a cautionary tale. Bioconjug Chem. 2014;25(10):1801-10.
49. Yi X, Wang F, Qin W, Yang X, Yuan J. Near-infrared fluorescent probes in cancer imaging and therapy: an emerging field. Int J Nanomedicine. 2014;9:1347-65.
50. Park JS, Huh JW, Park YA, Cho YB, Yun SH, Kim HC, et al. Risk Factors of Anastomotic Leakage and Long-Term Survival After Colorectal Surgery. Medicine (Baltimore). 2016;95(8):e2890.
51. Paun BC, Cassie S, MacLean AR, Dixon E, Buie WD. Postoperative complications following surgery for rectal cancer. Ann Surg. 2010;251(5):807-18.
52. McDermott FD, Heeney A, Kelly ME, Steele RJ, Carlson GL, Winter DC. Systematic review of preoperative, intraoperative and postoperative risk factors for colorectal anastomotic leaks. Br J Surg. 2015;102(5):462-79.
53. Rutegard M, Rutegard J. Anastomotic leakage in rectal cancer surgery: The role of blood perfusion. World J Gastrointest Surg. 2015;7(11):289-92.
54. Hirst NA, Tiernan JP, Millner PA, Jayne DG. Systematic review of methods to predict and detect anastomotic leakage in colorectal surgery. Colorectal Dis. 2014;16(2):95-109.
55. Jafari MD, Wexner SD, Martz JE, McLemore EC, Margolin DA, Sherwinter DA, et al. Perfusion assessment in laparoscopic left-sided/anterior resection (PILLAR II): a multi-institutional study. J Am Coll Surg. 2015;220(1):82-92 e1.
56. Blanco-Colino R, Espin-Basany E. Intraoperative use of ICG fluorescence imaging to reduce the risk of anastomotic leakage in colorectal surgery: a systematic review and meta-analysis. Tech Coloproctol. 2018;22(1):15-23.
57. Ris F, Liot E, Buchs NC, Kraus R, Ismael G, Belfontali V, et al. Multicentre phase II trial of near-infrared imaging in elective colorectal surgery. Br J Surg. 2018;105(10):1359-67.
58. Armstrong G, Croft J, Corrigan N, Brown JM, Goh V, Quirke P, et al. IntAct: intra-operative fluorescence angiography to prevent anastomotic leak in rectal cancer surgery: a randomized controlled trial. Colorectal Dis. 2018;20(8):O226-O34.
59. Diana M, Agnus V, Halvax P, Liu YY, Dallemagne B, Schlagowski AI, et al. Intraoperative fluorescence-based enhanced reality laparoscopic real-time imaging

to assess bowel perfusion at the anastomotic site in an experimental model. Br J Surg. 2015;102(2):e169-76.

60. Schols RM, Bouvy ND, van Dam RM, Stassen LP. Advanced intraoperative imaging methods for laparoscopic anatomy navigation: an overview. Surg Endosc. 2013;27(6):1851-9.
61. Giger U, Ouaissi M, Schmitz SF, Krahenbuhl S, Krahenbuhl L. Bile duct injury and use of cholangiography during laparoscopic cholecystectomy. Br J Surg. 2011;98(3):391-6.
62. Branum G, Schmitt C, Baillie J, Suhocki P, Baker M, Davidoff A, et al. Management of major biliary complications after laparoscopic cholecystectomy. Ann Surg. 1993;217(5):532-40; discussion 40-1.
63. Flum DR, Dellinger EP, Cheadle A, Chan L, Koepsell T. Intraoperative cholangiography and risk of common bile duct injury during cholecystectomy. JAMA. 2003;289(13):1639-44.
64. Ishizawa T, Bandai Y, Ijichi M, Kaneko J, Hasegawa K, Kokudo N. Fluorescent cholangiography illuminating the biliary tree during laparoscopic cholecystectomy. Br J Surg. 2010;97(9):1369-77.
65. Vlek SL, van Dam DA, Rubinstein SM, de Lange-de Klerk ESM, Schoonmade LJ, Tuynman JB, et al. Biliary tract visualization using near-infrared imaging with indocyanine green during laparoscopic cholecystectomy: results of a systematic review. Surg Endosc. 2017;31(7):2731-42.
66. van den Bos J, Wieringa FP, Bouvy ND, Stassen LPS. Optimizing the image of fluorescence cholangiography using ICG: a systematic review and ex vivo experiments. Surg Endosc. 2018.
67. Clinicaltrials.gov. Fluorescent Cholangiography vs White Light for Bile Ducts Identification 2018 [Available from: https://clinicaltrials.gov/ct2/show/NCT02702843?term=ICG+cholangiography&rank=10.
68. Schols RM, Bouvy ND, van Dam RM, Masclee AA, Dejong CH, Stassen LP. Combined vascular and biliary fluorescence imaging in laparoscopic cholecystectomy. Surg Endosc. 2013;27(12):4511-7.
69. Sarkaria IS, Bains MS, Finley DJ, Adusumilli PS, Huang J, Rusch VW, et al. Intraoperative near-infrared fluorescence imaging as an adjunct to robotic-assisted minimally invasive esophagectomy. Innovations (Phila). 2014;9(5):391-3.

70. Morton DL, Wen DR, Wong JH, Economou JS, Cagle LA, Storm FK, et al. Technical details of intraoperative lymphatic mapping for early stage melanoma. Arch Surg. 1992;127(4):392-9.
71. Giuliano AE, Kirgan DM, Guenther JM, Morton DL. Lymphatic mapping and sentinel lymphadenectomy for breast cancer. Ann Surg. 1994;220(3):391-8; discussion 8-401.
72. Straver ME, Meijnen P, van Tienhoven G, van de Velde CJ, Mansel RE, Bogaerts J, et al. Sentinel node identification rate and nodal involvement in the EORTC 10981-22023 AMAROS trial. Ann Surg Oncol. 2010;17(7):1854-61.
73. Kuehn T, Bauerfeind I, Fehm T, Fleige B, Hausschild M, Helms G, et al. Sentinel-lymph-node biopsy in patients with breast cancer before and after neoadjuvant chemotherapy (SENTINA): a prospective, multicentre cohort study. Lancet Oncol. 2013;14(7):609-18.
74. Goyal A, Newcombe RG, Chhabra A, Mansel RE, Group AT. Factors affecting failed localisation and false-negative rates of sentinel node biopsy in breast cancer--results of the ALMANAC validation phase. Breast Cancer Res Treat. 2006;99(2):203-8.
75. Ahmed M, Purushotham AD, Douek M. Novel techniques for sentinel lymph node biopsy in breast cancer: a systematic review. Lancet Oncol. 2014;15(8):e351-62.
76. Qiu SQ, Zhang GJ, Jansen L, de Vries J, Schroder CP, de Vries EGE, et al. Evolution in sentinel lymph node biopsy in breast cancer. Crit Rev Oncol Hematol. 2018;123:83-94.
77. Tsioulias GJ, Wood TF, Morton DL, Bilchik AJ. Lymphatic mapping and focused analysis of sentinel lymph nodes upstage gastrointestinal neoplasms. Arch Surg. 2000;135(8):926-32.
78. Currie AC, Brigic A, Thomas-Gibson S, Suzuki N, Moorghen M, Jenkins JT, et al. A pilot study to assess near infrared laparoscopy with indocyanine green (ICG) for intraoperative sentinel lymph node mapping in early colon cancer. Eur J Surg Oncol. 2017;43(11):2044-51.
79. Yuasa Y, Seike J, Yoshida T, Takechi H, Yamai H, Yamamoto Y, et al. Sentinel lymph node biopsy using intraoperative indocyanine green fluorescence imaging navigated with preoperative CT lymphography for superficial esophageal cancer. Ann Surg Oncol. 2012;19(2):486-93.
80. Emile SH, Elfeki H, Shalaby M, Sakr A, Sileri P, Laurberg S, et al. Sensitivity and specificity of indocyanine green near-infrared fluorescence imaging in detection of

metastatic lymph nodes in colorectal cancer: Systematic review and meta-analysis. J Surg Oncol. 2017;116(6):730-40.

81. Liberale G, Bohlok A, Bormans A, Bouazza F, Galdon MG, El Nakadi I, et al. Indocyanine green fluorescence imaging for sentinel lymph node detection in colorectal cancer: A systematic review. Eur J Surg Oncol. 2018;44(9):1301-6.
82. Tuech JJ, Pessaux P, Regenet N, Bergamaschi R, Colson A. Sentinel lymph node mapping in colon cancer. Surg Endosc. 2004;18(12):1721-9.
83. Nakagoe T, Sawai T, Tsuji T, Jibiki M, Ohbatake M, Nanashima A, et al. Surgical treatment and subsequent outcome of patients with carcinoma of the splenic flexure. Surg Today. 2001;31(3):204-9.
84. Watanabe J, Ota M, Suwa Y, Ishibe A, Masui H, Nagahori K. Evaluation of lymph flow patterns in splenic flexural colon cancers using laparoscopic real-time indocyanine green fluorescence imaging. Int J Colorectal Dis. 2017;32(2):201-7.
85. Kobayashi H, Choyke PL. Target-cancer-cell-specific activatable fluorescence imaging probes: rational design and in vivo applications. Acc Chem Res. 2011;44(2):83-90.
86. Kaushal S, McElroy MK, Luiken GA, Talamini MA, Moossa AR, Hoffman RM, et al. Fluorophore-conjugated anti-CEA antibody for the intraoperative imaging of pancreatic and colorectal cancer. J Gastrointest Surg. 2008;12(11):1938-50.
87. van Dam GM, Themelis G, Crane LM, Harlaar NJ, Pleijhuis RG, Kelder W, et al. Intraoperative tumor-specific fluorescence imaging in ovarian cancer by folate receptor-alpha targeting: first in-human results. Nat Med. 2011;17(10):1315-9.
88. Nguyen QT, Olson ES, Aguilera TA, Jiang T, Scadeng M, Ellies LG, et al. Surgery with molecular fluorescence imaging using activatable cell-penetrating peptides decreases residual cancer and improves survival. Proc Natl Acad Sci U S A. 2010;107(9):4317-22.
89. Tringale KR, Pang J, Nguyen QT. Image-guided surgery in cancer: A strategy to reduce incidence of positive surgical margins. Wiley Interdiscip Rev Syst Biol Med. 2018;10(3):e1412.
90. Whitley MJ, Cardona DM, Lazarides AL, Spasojevic I, Ferrer JM, Cahill J, et al. A mouse-human phase 1 co-clinical trial of a protease-activated fluorescent probe for imaging cancer. Sci Transl Med. 2016;8(320):320ra4.
91. Boogerd LSF, Hoogstins CES, Schaap DP, Kusters M, Handgraaf HJM, van der Valk MJM, et al. Safety and effectiveness of SGM-101, a fluorescent antibody targeting carcinoembryonic antigen, for intraoperative detection of colorectal

cancer: a dose-escalation pilot study. Lancet Gastroenterol Hepatol. 2018;3(3):181-91.

92. Schindelin J, Arganda-Carreras I, Frise E, Kaynig V, Longair M, Pietzsch T, et al. Fiji: an open-source platform for biological-image analysis. Nat Methods. 2012;9(7):676-82.
93. National Institute of Health. Fiji Analyze Menu 2004 [Available from: https://imagej.nih.gov/ij/docs/menus/analyze.html.
94. European Medicines Agency. Guideline for good clinical practice E6(R2) 2017 [Available from: https://www.ema.europa.eu/documents/scientific-guideline/ich-e-6-r1-guideline-good-clinical-practice-step-5_en.pdf.
95. McCulloch P, Altman DG, Campbell WB, Flum DR, Glasziou P, Marshall JC, et al. No surgical innovation without evaluation: the IDEAL recommendations. Lancet. 2009;374(9695):1105-12.
96. Frober R. Surgical anatomy of the ureter. BJU Int. 2007;100(4):949-65.
97. Delacroix SE, Jr., Winters JC. Urinary tract injures: recognition and management. Clin Colon Rectal Surg. 2010;23(2):104-12.
98. da Silva G, Boutros M, Wexner SD. Role of prophylactic ureteric stents in colorectal surgery. Asian J Endosc Surg. 2012;5(3):105-10.
99. Kyzer S, Gordon PH. The prophylactic use of ureteral catheters during colorectal operations. Am Surg. 1994;60(3):212-6.
100. Janssen PF, Brolmann HA, Huirne JA. Causes and prevention of laparoscopic ureter injuries: an analysis of 31 cases during laparoscopic hysterectomy in the Netherlands. Surg Endosc. 2013;27(3):946-56.
101. St Lezin MA, Stoller ML. Surgical ureteral injuries. Urology. 1991;38(6):497-506.
102. Halabi WJ, Jafari MD, Nguyen VQ, Carmichael JC, Mills S, Pigazzi A, et al. Ureteral injuries in colorectal surgery: an analysis of trends, outcomes, and risk factors over a 10-year period in the United States. Dis Colon Rectum. 2014;57(2):179-86.
103. Mahendran HA, Praveen S, Ho C, Goh EH, Tan GH, Zuklifli MZ. Iatrogenic ureter injuries: eleven years experience in a tertiary hospital. Med J Malaysia. 2012;67(2):169-72.
104. Palaniappa NC, Telem DA, Ranasinghe NE, Divino CM. Incidence of iatrogenic ureteral injury after laparoscopic colectomy. Arch Surg. 2012;147(3):267-71.

105. Al-Awadi K, Kehinde EO, Al-Hunayan A, Al-Khayat A. Iatrogenic ureteric injuries: incidence, aetiological factors and the effect of early management on subsequent outcome. Int Urol Nephrol. 2005;37(2):235-41.
106. Tebala GD. The "Left Ureteral Triangle" as an Anatomic Landmark for the Identification of the Left Ureter in Laparoscopic Distal Colectomies. Surg Laparosc Endosc Percutan Tech. 2016;26(5):e100-e2.
107. Nam YS, Wexner SD. Clinical value of prophylactic ureteral stent indwelling during laparoscopic colorectal surgery. J Korean Med Sci. 2002;17(5):633-5.
108. Coakley KM, Kasten KR, Sims SM, Prasad T, Heniford BT, Davis BR. Prophylactic Ureteral Catheters for Colectomy: A National Surgical Quality Improvement Program-Based Analysis. Dis Colon Rectum. 2018;61(1):84-8.
109. Merola J, Arnold B, Luks V, Ibarra C, Resio B, Davis KA, et al. Prophylactic Ureteral Stent Placement vs No Ureteral Stent Placement During Open Colectomy. JAMA Surg. 2018;153(1):87-90.
110. Senagore AJ, Luchtefeld M. An initial experience with lighted ureteral catheters during laparoscopic colectomy. J Laparoendosc Surg. 1994;4(6):399-403.
111. Tsujinaka S, Wexner SD, DaSilva G, Sands DR, Weiss EG, Nogueras JJ, et al. Prophylactic ureteric catheters in laparoscopic colorectal surgery. Tech Coloproctol. 2008;12(1):45-50.
112. Bothwell WN, Bleicher RJ, Dent TL. Prophylactic ureteral catheterization in colon surgery. A five-year review. Dis Colon Rectum. 1994;37(4):330-4.
113. Boyan WP, Jr., Lavy D, Dinallo A, Otero J, Roding A, Hanos D, et al. Lighted ureteral stents in laparoscopic colorectal surgery; a five-year experience. Ann Transl Med. 2017;5(3):44.
114. Lee Z, Moore B, Giusto L, Eun DD. Use of indocyanine green during robot-assisted ureteral reconstructions. Eur Urol. 2015;67(2):291-8.
115. Park H, Farnam RW. Novel Use of Indocyanine Green for Intraoperative, Real-time Localization of Ureter During Robot-Assisted Excision of Endometriosis. J Minim Invasive Gynecol. 2015;22(6s):S69.
116. Lee Z, Simhan J, Parker DC, Reilly C, Llukani E, Lee DI, et al. Novel use of indocyanine green for intraoperative, real-time localization of ureteral stenosis during robot-assisted ureteroureterostomy. Urology. 2013;82(3):729-33.
117. Siddighi S, Yune JJ, Hardesty J. Indocyanine green for intraoperative localization of ureter. Am J Obstet Gynecol. 2014;211(4):436.e1-2.

118. Dip FD, Nahmod M, Anzorena FS, Moreira A, Sarotto L, Ampudia C, et al. Novel technique for identification of ureters using sodium fluorescein. Surg Endosc. 2014;28(9):2730-3.
119. Tanaka E, Ohnishi S, Laurence RG, Choi HS, Humblet V, Frangioni JV. Real-time intraoperative ureteral guidance using invisible near-infrared fluorescence. J Urol. 2007;178(5):2197-202.
120. Korb ML, Huh WK, Boone JD, Warram JM, Chung TK, de Boer E, et al. Laparoscopic Fluorescent Visualization of the Ureter With Intravenous IRDye800CW. J Minim Invasive Gynecol. 2015;22(5):799-806.
121. Verbeek FP, van der Vorst JR, Schaafsma BE, Swijnenburg RJ, Gaarenstroom KN, Elzevier HW, et al. Intraoperative near infrared fluorescence guided identification of the ureters using low dose methylene blue: a first in human experience. J Urol. 2013;190(2):574-9.
122. Yeung TM, Volpi D, Tullis ID, Nicholson GA, Buchs N, Cunningham C, et al. Identifying Ureters In Situ Under Fluorescence During Laparoscopic and Open Colorectal Surgery. Ann Surg. 2016;263(1):e1-2.
123. Kim K, Schwaitzberg S, Onel E. An infrared ureteral stent to aid in laparoscopic retroperitoneal lymph node dissection. J Urol. 2001;166(5):1815-6.
124. Reedy EA, Colombo-Burke KL, Resau JH. Discrimination of cell types in primary transitional cell carcinoma by monoclonal anti-cytokeratin antibodies. Pathobiology. 1990;58(6):304-11.
125. Mahalingam SM, Dip F, Castillo M, Roy M, Wexner SD, Rosenthal RJ, et al. Intraoperative Ureter Visualization Using a Novel Near-Infrared Fluorescent Dye. Mol Pharm. 2018;15(8):3442-7.
126. Cha J, Nani RR, Luciano MP, Kline G, Broch A, Kim K, et al. A chemically stable fluorescent marker of the ureter. Bioorg Med Chem Lett. 2018;28(16):2741-5.
127. Moore K, Dalley A. Clinically oriented anatomy. 4th ed. ed. Baltimore, Maryland: Lippincott Williams and Wilkins; 1999.
128. Kneist W, Stelzner S, Aigner F, Fürst A, Wedel T. Urethral injury in body donor TaTME training. coloproctology. 2017;39(3):179-83.
129. Westwood DA, Cuda TJ, Hamilton AER, Clark D, Stevenson ARL. Transanal total mesorectal excision for rectal cancer: state of the art. Tech Coloproctol. 2018;22(9):649-55.
130. Jeong SY, Park JW, Nam BH, Kim S, Kang SB, Lim SB, et al. Open versus laparoscopic surgery for mid-rectal or low-rectal cancer after neoadjuvant

chemoradiotherapy (COREAN trial): survival outcomes of an open-label, non-inferiority, randomised controlled trial. Lancet Oncol. 2014;15(7):767-74.

131. Stevenson AR, Solomon MJ, Lumley JW, Hewett P, Clouston AD, Gebski VJ, et al. Effect of Laparoscopic-Assisted Resection vs Open Resection on Pathological Outcomes in Rectal Cancer: The ALaCaRT Randomized Clinical Trial. JAMA. 2015;314(13):1356-63.
132. Fleshman J, Branda M, Sargent DJ, Boller AM, George V, Abbas M, et al. Effect of Laparoscopic-Assisted Resection vs Open Resection of Stage II or III Rectal Cancer on Pathologic Outcomes: The ACOSOG Z6051 Randomized Clinical Trial. JAMA. 2015;314(13):1346-55.
133. Spinelli A, D'Hoore A, Panis Y, Bemelman WA, Jayne DG, Fürst AJc. Critical appraisal of two randomized clinical trials on pathologic outcomes. 2017;39(4):277-.
134. Sylla P, Rattner DW, Delgado S, Lacy AM. NOTES transanal rectal cancer resection using transanal endoscopic microsurgery and laparoscopic assistance. Surg Endosc. 2010;24(5):1205-10.
135. Simillis C, Hompes R, Penna M, Rasheed S, Tekkis PP. A systematic review of transanal total mesorectal excision: is this the future of rectal cancer surgery? Colorectal Dis. 2016;18(1):19-36.
136. Atallah S. Transanal total mesorectal excision: full steam ahead. Tech Coloproctol. 2015;19(2):57-61.
137. Marecik SJ, Pai A, Sheikh T, Park JJ, Prasad LM. Transanal Total Mesorectal Excision: Save the Nerves and Urethra. Dis Colon Rectum. 2016;59(7):e410-4.
138. Althumairi AA, Efron JE. Genitourinary Considerations in Reoperative and Complex Colorectal Surgery. Clin Colon Rectal Surg. 2016;29(2):145-51.
139. Penna M, Hompes R, Arnold S, Wynn G, Austin R, Warusavitarne J, et al. Transanal Total Mesorectal Excision: International Registry Results of the First 720 Cases. Ann Surg. 2016.
140. Rouanet P, Mourregot A, Azar CC, Carrere S, Gutowski M, Quenet F, et al. Transanal endoscopic proctectomy: an innovative procedure for difficult resection of rectal tumors in men with narrow pelvis. Dis Colon Rectum. 2013;56(4):408-15.
141. Burke JP, Martin-Perez B, Khan A, Nassif G, de Beche-Adams T, Larach SW, et al. Transanal total mesorectal excision for rectal cancer: early outcomes in 50 consecutive patients. Colorectal Dis. 2016;18(6):570-7.

142. Atallah S, Mabardy A, Volpato AP, Chin T, Sneider J, Monson JRT. Surgery beyond the visible light spectrum: theoretical and applied methods for localization of the male urethra during transanal total mesorectal excision. Tech Coloproctol. 2017:1-12.
143. Atallah S, Larach SW, Monson JR. Stereotactic navigation for TAMIS-TME. Minim Invasive Ther Allied Technol. 2016;25(5):271-7.
144. McBride TO, Pogue BW, Gerety ED, Poplack SB, Osterberg UL, Paulsen KD. Spectroscopic diffuse optical tomography for the quantitative assessment of hemoglobin concentration and oxygen saturation in breast tissue. Appl Opt. 1999;38(25):5480-90.
145. Allison RR. The electromagnetic spectrum: current and future applications in oncology. Future Oncol. 2013;9(5):657-67.
146. Tabatabai H, Oliver DE, Rohrbaugh JW, Papadopoulos C. Novel Applications of Laser Doppler Vibration Measurements to Medical Imaging. Sens Imaging. 2013;14:13-28.
147. Burchfield TR, Venkatesan S. Accelerometer-based human abnormal movement detection in wireless sensor networks. Proceedings of the 1st ACM SIGMOBILE international workshop on Systems and networking support for healthcare and assisted living environments; San Juan, Puerto Rico. 1248073: ACM; 2007. p. 67-9.
148. Yujiri L, Shoucri M, Moffa P. Passive millimeter wave imaging. IEE Microwave Magazine. 2003;4(3):39-50.
149. Andrade M, Jacomo A. Anatomy of the Human Lymphatic System. In: Leong S.P.L, editor. Cancer Metastasis And The Lymphovascular System: Basis For Rational Therapy. 135. Boston: Springer; 2007.
150. Phang K, Bowman M, Phillips A, Windsor J. Review of thoracic duct anatomical variations and clinical implications. Clin Anat. 2014;27(4):637-44.
151. Akcali O, Kiray A, Ergur I, Tetik S, Alici E. Thoracic duct variations may complicate the anterior spine procedures. Eur Spine J. 2006;15(9):1347-51.
152. Cuesta MA, van der Wielen N, Weijs TJ, Bleys RL, Gisbertz SS, van Duijvendijk P, et al. Surgical anatomy of the supracarinal esophagus based on a minimally invasive approach: vascular and nervous anatomy and technical steps to resection and lymphadenectomy. Surg Endosc. 2017;31(4):1863-70.
153. Weijs TJ, Goense L, van Rossum PS, Meijer GJ, van Lier AL, Wessels FJ, et al. The peri-esophageal connective tissue layers and related compartments: visualization by histology and magnetic resonance imaging. J Anat. 2017;230(2):262-71.

154. Hagens ERC, van Berge Henegouwen MI, Cuesta MA, Gisbertz SS. The extent of lymphadenectomy in esophageal resection for cancer should be standardized. J Thorac Dis. 2017;9(Suppl 8):S713-S23.
155. Schurink B, Defize IL, Mazza E, Ruurda JP, Brosens LAA, Roeling TAP, et al. Two-Field Lymphadenectomy During Esophagectomy: The Presence of Thoracic Duct Lymph Nodes. Ann Thorac Surg. 2018;106(2):435-9.
156. Udagawa H, Ueno M, Shinohara H, Haruta S, Lee S, Momose K, et al. Should lymph nodes along the thoracic duct be dissected routinely in radical esophagectomy? 2014;11(3):204-10.
157. Matsuda S, Takeuchi H, Kawakubo H, Shimada A, Fukuda K, Nakamura R, et al. Clinical outcome of transthoracic esophagectomy with thoracic duct resection: Number of dissected lymph node and distribution of lymph node metastasis around the thoracic duct. Medicine (Baltimore). 2016;95(24):e3839.
158. Rao DV, Chava SP, Sahni P, Chattopadhyay TK. Thoracic duct injury during esophagectomy: 20 years experience at a tertiary care center in a developing country. Dis Esophagus. 2004;17(2):141-5.
159. Kranzfelder M, Gertler R, Hapfelmeier A, Friess H, Feith M. Chylothorax after esophagectomy for cancer: impact of the surgical approach and neoadjuvant treatment: systematic review and institutional analysis. Surg Endosc. 2013;27(10):3530-8.
160. Brinkmann S, Schroeder W, Junggeburth K, Gutschow CA, Bludau M, Hoelscher AH, et al. Incidence and management of chylothorax after Ivor Lewis esophagectomy for cancer of the esophagus. J Thorac Cardiovasc Surg. 2016;151(5):1398-404.
161. Shackcloth MJ, Poullis M, Lu J, Page RD. Preventing of chylothorax after oesophagectomy by routine pre-operative administration of oral cream. Eur J Cardiothorac Surg. 2001;20(5):1035-6.
162. McGrath EE, Blades Z, Anderson PB. Chylothorax: aetiology, diagnosis and therapeutic options. Respir Med. 2010;104(1):1-8.
163. Ashitate Y, Tanaka E, Stockdale A, Choi HS, Frangioni JV. Near-infrared fluorescence imaging of thoracic duct anatomy and function in open surgery and video-assisted thoracic surgery. J Thorac Cardiovasc Surg. 2011;142(1):31-8 e1-2.
164. Kamiya K, Unno N, Konno H. Intraoperative indocyanine green fluorescence lymphography, a novel imaging technique to detect a chyle fistula after an esophagectomy: report of a case. Surg Today. 2009;39(5):421-4.

165. Kaburagi T, Takeuchi H, Oyama T, Nakamura R, Takahashi T, Wada N, et al. Intraoperative fluorescence lymphography using indocyanine green in a patient with chylothorax after esophagectomy: report of a case. Surg Today. 2013;43(2):206-10.
166. Chang TI, Chen YS, Huang SC. Intraoperative indocyanine green fluorescence lymphography to detect chylous leakage sites after congenital heart surgery. J Thorac Cardiovasc Surg. 2014;148(2):739-40.
167. Matsutani T, Hirakata A, Nomura T, Hagiwara N, Matsuda A, Yoshida H, et al. Transabdominal approach for chylorrhea after esophagectomy by using fluorescence navigation with indocyanine green. Case Rep Surg. 2014;2014:464017.
168. Miao L, Zhang Y, Hu H, Ma L, Shun Y, Xiang J, et al. Incidence and management of chylothorax after esophagectomy. Thorac Cancer. 2015;6(3):354-8.
169. Steffey MA, Mayhew PD. Use of direct near-infrared fluorescent lymphography for thoracoscopic thoracic duct identification in 15 dogs with chylothorax. Vet Surg. 2018;47(2):267-76.
170. Yang F, Zhou J, Li H, Yang F, Xiao R, Chi C, et al. Near-infrared fluorescence-guided thoracoscopic surgical intervention for postoperative chylothorax. Interact Cardiovasc Thorac Surg. 2018;26(2):171-5.
171. Hall PA, Coates PJ, Ansari B, Hopwood D. Regulation of cell number in the mammalian gastrointestinal tract: the importance of apoptosis. J Cell Sci. 1994;107 (Pt 12):3569-77.
172. van der Flier LG, Clevers H. Stem cells, self-renewal, and differentiation in the intestinal epithelium. Annu Rev Physiol. 2009;71:241-60.
173. van Es JH, van Gijn ME, Riccio O, van den Born M, Vooijs M, Begthel H, et al. Notch/gamma-secretase inhibition turns proliferative cells in intestinal crypts and adenomas into goblet cells. Nature. 2005;435(7044):959-63.
174. Jensen J, Pedersen EE, Galante P, Hald J, Heller RS, Ishibashi M, et al. Control of endodermal endocrine development by Hes-1. Nat Genet. 2000;24(1):36-44.
175. Chang WW, Leblond CP. Renewal of the epithelium in the descending colon of the mouse. I. Presence of three cell populations: vacuolated-columnar, mucous and argentaffin. Am J Anat. 1971;131(1):73-99.
176. Karam SM. Lineage commitment and maturation of epithelial cells in the gut. Front Biosci. 1999;4:D286-98.
177. Pelaseyed T, Bergstrom JH, Gustafsson JK, Ermund A, Birchenough GM, Schutte A, et al. The mucus and mucins of the goblet cells and enterocytes provide the first

defense line of the gastrointestinal tract and interact with the immune system. Immunol Rev. 2014;260(1):8-20.

178. Velcich A, Yang W, Heyer J, Fragale A, Nicholas C, Viani S, et al. Colorectal cancer in mice genetically deficient in the mucin Muc2. Science. 2002;295(5560):1726-9.
179. Ambort D, Johansson ME, Gustafsson JK, Nilsson HE, Ermund A, Johansson BR, et al. Calcium and pH-dependent packing and release of the gel-forming MUC2 mucin. Proc Natl Acad Sci U S A. 2012;109(15):5645-50.
180. Johansson ME, Phillipson M, Petersson J, Velcich A, Holm L, Hansson GC. The inner of the two Muc2 mucin-dependent mucus layers in colon is devoid of bacteria. Proc Natl Acad Sci U S A. 2008;105(39):15064-9.
181. Karlsson NG, Johansson ME, Asker N, Karlsson H, Gendler SJ, Carlstedt I, et al. Molecular characterization of the large heavily glycosylated domain glycopeptide from the rat small intestinal Muc2 mucin. Glycoconj J. 1996;13(5):823-31.
182. Hollingsworth MA, Swanson BJ. Mucins in cancer: protection and control of the cell surface. Nat Rev Cancer. 2004;4(1):45-60.
183. Johansson ME, Ambort D, Pelaseyed T, Schutte A, Gustafsson JK, Ermund A, et al. Composition and functional role of the mucus layers in the intestine. Cell Mol Life Sci. 2011;68(22):3635-41.
184. Johansson ME, Larsson JM, Hansson GC. The two mucus layers of colon are organized by the MUC2 mucin, whereas the outer layer is a legislator of host-microbial interactions. Proc Natl Acad Sci U S A. 2011;108 Suppl 1:4659-65.
185. Arike L, Holmen-Larsson J, Hansson GC. Intestinal Muc2 mucin O-glycosylation is affected by microbiota and regulated by differential expression of glycosyltranferases. Glycobiology. 2017;27(4):318-28.
186. Bennett EP, Mandel U, Clausen H, Gerken TA, Fritz TA, Tabak LA. Control of mucin-type O-glycosylation: a classification of the polypeptide GalNAc-transferase gene family. Glycobiology. 2012;22(6):736-56.
187. Kim YS, Ho SB. Intestinal goblet cells and mucins in health and disease: recent insights and progress. Curr Gastroenterol Rep. 2010;12(5):319-30.
188. Atuma C, Strugala V, Allen A, Holm L. The adherent gastrointestinal mucus gel layer: thickness and physical state in vivo. Am J Physiol Gastrointest Liver Physiol. 2001;280(5):G922-9.
189. Sonnenburg JL, Xu J, Leip DD, Chen CH, Westover BP, Weatherford J, et al. Glycan foraging in vivo by an intestine-adapted bacterial symbiont. Science. 2005;307(5717):1955-9.

190. Gilgunn S, Conroy PJ, Saldova R, Rudd PM, O'Kennedy RJ. Aberrant PSA glycosylation--a sweet predictor of prostate cancer. Nat Rev Urol. 2013;10(2):99-107.
191. Zurawski VR, Jr., Orjaseter H, Andersen A, Jellum E. Elevated serum CA 125 levels prior to diagnosis of ovarian neoplasia: relevance for early detection of ovarian cancer. Int J Cancer. 1988;42(5):677-80.
192. Ebeling FG, Stieber P, Untch M, Nagel D, Konecny GE, Schmitt UM, et al. Serum CEA and CA 15-3 as prognostic factors in primary breast cancer. Br J Cancer. 2002;86(8):1217-22.
193. Gion M, Boracchi P, Dittadi R, Biganzoli E, Peloso L, Mione R, et al. Prognostic role of serum CA15.3 in 362 node-negative breast cancers. An old player for a new game. Eur J Cancer. 2002;38(9):1181-8.
194. Safi F, Schlosser W, Kolb G, Beger HG. Diagnostic value of CA 19-9 in patients with pancreatic cancer and nonspecific gastrointestinal symptoms. J Gastrointest Surg. 1997;1(2):106-12.
195. Goldstein MJ, Mitchell EP. Carcinoembryonic antigen in the staging and follow-up of patients with colorectal cancer. Cancer Invest. 2005;23(4):338-51.
196. Dube DH, Bertozzi CR. Glycans in cancer and inflammation--potential for therapeutics and diagnostics. Nat Rev Drug Discov. 2005;4(6):477-88.
197. Brockhausen I. Mucin-type O-glycans in human colon and breast cancer: glycodynamics and functions. EMBO Rep. 2006;7(6):599-604.
198. Kufe DW. Mucins in cancer: function, prognosis and therapy. Nat Rev Cancer. 2009;9(12):874-85.
199. Itzkowitz SH, Bloom EJ, Lau TS, Kim YS. Mucin associated Tn and sialosyl-Tn antigen expression in colorectal polyps. Gut. 1992;33(4):518-23.
200. Boyd WC, Shapleigh E. Antigenic relations of blood group antigens as suggested by tests with lectins. J Immunol. 1954;73(4):226-31.
201. Boyd WC, Shapleigh E. Diagnosis by subgroups of blood groups A and AB by use of plant agglutinins (lectins). J Lab Clin Med. 1954;44(2):235-7.
202. Lis H, Sharon N. Lectins as molecules and as tools. Annu Rev Biochem. 1986;55:35-67.
203. Nagata Y, Burger MM. Wheat germ agglutinin. Isolation and crystallization. J Biol Chem. 1972;247(7):2248-50.

204. Bird-Lieberman EL, Neves AA, Lao-Sirieix P, O'Donovan M, Novelli M, Lovat LB, et al. Molecular imaging using fluorescent lectins permits rapid endoscopic identification of dysplasia in Barrett's esophagus. Nat Med. 2012;18(2):315-21.
205. Rex DK, Johnson DA, Anderson JC, Schoenfeld PS, Burke CA, Inadomi JM, et al. American College of Gastroenterology guidelines for colorectal cancer screening 2009 [corrected]. Am J Gastroenterol. 2009;104(3):739-50.
206. Winawer SJ, Zauber AG, Ho MN, O'Brien MJ, Gottlieb LS, Sternberg SS, et al. Prevention of colorectal cancer by colonoscopic polypectomy. The National Polyp Study Workgroup. N Engl J Med. 1993;329(27):1977-81.
207. Zhao ZY, Guan YG, Li BR, Shan YQ, Yan FH, Gao YJ, et al. Detection and miss rates of autofluorescence imaging of adenomatous and polypoid lesions during colonoscopy: a systematic review and meta-analysis. Endosc Int Open. 2015;3(3):E226-35.
208. Aniwan S, Orkoonsawat P, Viriyautsahakul V, Angsuwatcharakon P, Pittayanon R, Wisedopas N, et al. The Secondary Quality Indicator to Improve Prediction of Adenoma Miss Rate Apart from Adenoma Detection Rate. Am J Gastroenterol. 2016.
209. Rex DK, Cutler CS, Lemmel GT, Rahmani EY, Clark DW, Helper DJ, et al. Colonoscopic miss rates of adenomas determined by back-to-back colonoscopies. Gastroenterology. 1997;112(1):24-8.
210. Robertson DJ, Greenberg ER, Beach M, Sandler RS, Ahnen D, Haile RW, et al. Colorectal cancer in patients under close colonoscopic surveillance. Gastroenterology. 2005;129(1):34-41.
211. van Rijn JC, Reitsma JB, Stoker J, Bossuyt PM, van Deventer SJ, Dekker E. Polyp miss rate determined by tandem colonoscopy: a systematic review. Am J Gastroenterol. 2006;101(2):343-50.
212. Rex DK, Schoenfeld PS, Cohen J, Pike IM, Adler DG, Fennerty MB, et al. Quality indicators for colonoscopy. Gastrointest Endosc. 2015;81(1):31-53.
213. Robertson DJ, Lieberman DA, Winawer SJ, Ahnen DJ, Baron JA, Schatzkin A, et al. Colorectal cancers soon after colonoscopy: a pooled multicohort analysis. Gut. 2014;63(6):949-56.
214. Corley DA, Jensen CD, Marks AR, Zhao WK, Lee JK, Doubeni CA, et al. Adenoma detection rate and risk of colorectal cancer and death. N Engl J Med. 2014;370(14):1298-306.

215. Fayad NF, Kahi CJ. Colonoscopy quality assessment. Gastrointest Endosc Clin N Am. 2015;25(2):373-86.
216. Kaminski MF, Regula J, Kraszewska E, Polkowski M, Wojciechowska U, Didkowska J, et al. Quality indicators for colonoscopy and the risk of interval cancer. N Engl J Med. 2010;362(19):1795-803.
217. Trivedi PJ, Braden B. Indications, stains and techniques in chromoendoscopy. QJM. 2013;106(2):117-31.
218. Jang JY. The Past, Present, and Future of Image-Enhanced Endoscopy. Clin Endosc. 2015;48(6):466-75.
219. Schiller W. Early diagnosis of carcinoma of the cervix. In: Mayo W, editor. Surg Gynecol Obstet. 56. Chicago: Surgical Publishing Co.; 1933. p. 210-22.
220. Voegeli R. Schiller's iodine test in the diagnosis of esophageal diseases. Preliminary report. Pract Otorhinolaryngol (Basel). 1966;28(3):230-9.
221. Ngamruengphong S, Sharma VK, Das A. Diagnostic yield of methylene blue chromoendoscopy for detecting specialized intestinal metaplasia and dysplasia in Barrett's esophagus: a meta-analysis. Gastrointest Endosc. 2009;69(6):1021-8.
222. Kiesslich R, Fritsch J, Holtmann M, Koehler HH, Stolte M, Kanzler S, et al. Methylene blue-aided chromoendoscopy for the detection of intraepithelial neoplasia and colon cancer in ulcerative colitis. Gastroenterology. 2003;124(4):880-8.
223. Repici A, Di Stefano AF, Radicioni MM, Jas V, Moro L, Danese S. Methylene blue MMX tablets for chromoendoscopy. Safety tolerability and bioavailability in healthy volunteers. Contemp Clin Trials. 2012;33(2):260-7.
224. Brown SR, Baraza W. Chromoscopy versus conventional endoscopy for the detection of polyps in the colon and rectum. Cochrane Database Syst Rev. 2010(10):CD006439.
225. Beg S, Ragunath K. Image-enhanced endoscopy technology in the gastrointestinal tract: what is available? Best Pract Res Clin Gastroenterol. 2015;29(4):627-38.
226. Lopez-Ceron M, Sanabria E, Pellise M. Colonic polyps: is it useful to characterize them with advanced endoscopy? World J Gastroenterol. 2014;20(26):8449-57.
227. Dinesen L, Chua TJ, Kaffes AJ. Meta-analysis of narrow-band imaging versus conventional colonoscopy for adenoma detection. Gastrointest Endosc. 2012;75(3):604-11.

228. Nagorni A, Bjelakovic G, Petrovic B. Narrow band imaging versus conventional white light colonoscopy for the detection of colorectal polyps. Cochrane Database Syst Rev. 2012;1:CD008361.
229. Pasha SF, Leighton JA, Das A, Harrison ME, Gurudu SR, Ramirez FC, et al. Comparison of the yield and miss rate of narrow band imaging and white light endoscopy in patients undergoing screening or surveillance colonoscopy: a meta-analysis. Am J Gastroenterol. 2012;107(3):363-70; quiz 71.
230. Sabbagh LC, Reveiz L, Aponte D, de Aguiar S. Narrow-band imaging does not improve detection of colorectal polyps when compared to conventional colonoscopy: a randomized controlled trial and meta-analysis of published studies. BMC Gastroenterol. 2011;11:100.
231. Rex DK, Clodfelter R, Rahmani F, Fatima H, James-Stevenson TN, Tang JC, et al. Narrow-band imaging versus white light for the detection of proximal colon serrated lesions: a randomized, controlled trial. Gastrointest Endosc. 2016;83(1):166-71.
232. Kim JJ, Hong KS, Kim JS, Jung HC. A Randomized Controlled Clinical Study Comparing the Diagnostic Accuracy of the Histologic Prediction for Colorectal Polyps Depending on the Use of Either Magnified or Nonmagnified Narrow Band Imaging. Clin Endosc. 2015;48(6):528-33.
233. Izuishi K, Tajiri H, Fujii T, Boku N, Ohtsu A, Ohnishi T, et al. The histological basis of detection of adenoma and cancer in the colon by autofluorescence endoscopic imaging. Endoscopy. 1999;31(7):511-6.
234. Hoetker MS, Goetz M. Molecular imaging in endoscopy. United European Gastroenterol J. 2013;1(2):84-92.
235. Klenske E, Neurath MF, Atreya R, Rath T. Molecular imaging in gastroenterology: A route for personalized endoscopy. Dig Liver Dis. 2018;50(9):878-85.
236. Keller R, Winde G, Terpe HJ, Foerster EC, Domschke W. Fluorescence endoscopy using a fluorescein-labeled monoclonal antibody against carcinoembryonic antigen in patients with colorectal carcinoma and adenoma. Endoscopy. 2002;34(10):801-7.
237. Goetz M, Hoetker MS, Diken M, Galle PR, Kiesslich R. In vivo molecular imaging with cetuximab, an anti-EGFR antibody, for prediction of response in xenograft models of human colorectal cancer. Endoscopy. 2013;45(6):469-77.
238. Liu J, Zuo X, Li C, Yu T, Gu X, Zhou C, et al. In vivo molecular imaging of epidermal growth factor receptor in patients with colorectal neoplasia using confocal laser endomicroscopy. Cancer Lett. 2013;330(2):200-7.

239. Zhou J, Joshi BP, Duan X, Pant A, Qiu Z, Kuick R, et al. EGFR Overexpressed in Colonic Neoplasia Can be Detected on Wide-Field Endoscopic Imaging. Clin Transl Gastroenterol. 2015;6:e101.
240. Wu AM, Olafsen T. Antibodies for molecular imaging of cancer. Cancer J. 2008;14(3):191-7.
241. Chen K, Chen X. Design and development of molecular imaging probes. Curr Top Med Chem. 2010;10(12):1227-36.
242. Burggraaf J, Kamerling IM, Gordon PB, Schrier L, de Kam ML, Kales AJ, et al. Detection of colorectal polyps in humans using an intravenously administered fluorescent peptide targeted against c-Met. Nat Med. 2015;21(8):955-61.
243. Hsiung PL, Hardy J, Friedland S, Soetikno R, Du CB, Wu AP, et al. Detection of colonic dysplasia in vivo using a targeted heptapeptide and confocal microendoscopy. Nat Med. 2008;14(4):454-8.
244. Richman PI, Bodmer WF. Monoclonal antibodies to human colorectal epithelium: markers for differentiation and tumour characterization. Int J Cancer. 1987;39(3):317-28.
245. Campbell AP, Merrett MN, Kettlewell M, Mortensen NJ, Jewell DP. Expression of colonic antigens by goblet and columnar epithelial cells in ileal pouch mucosa: their association with inflammatory change and faecal stasis. J Clin Pathol. 1994;47(9):834-8.
246. Liu H. Goblet cell differentiation in human colorectal cancer cell lines: University of Oxford; 2017.
247. Domon-Dell C, Schneider A, Moucadel V, Guerin E, Guenot D, Aguillon S, et al. Cdx1 homeobox gene during human colon cancer progression. Oncogene. 2003;22(39):7913-21.
248. Jones MF, Hara T, Francis P, Li XL, Bilke S, Zhu Y, et al. The CDX1-microRNA-215 axis regulates colorectal cancer stem cell differentiation. Proc Natl Acad Sci U S A. 2015;112(13):E1550-8.
249. Guo RJ, Huang E, Ezaki T, Patel N, Sinclair K, Wu J, et al. Cdx1 inhibits human colon cancer cell proliferation by reducing beta-catenin/T-cell factor transcriptional activity. J Biol Chem. 2004;279(35):36865-75.
250. John R, El-Rouby NM, Tomasetto C, Rio MC, Karam SM. Expression of TFF3 during multistep colon carcinogenesis. Histol Histopathol. 2007;22(7):743-51.

251. Yusup A, Huji B, Fang C, Wang F, Dadihan T, Wang HJ, et al. Expression of trefoil factors and TWIST1 in colorectal cancer and their correlation with metastatic potential and prognosis. World J Gastroenterol. 2017;23(1):110-20.
252. Babyatsky M, Lin J, Yio X, Chen A, Zhang JY, Zheng Y, et al. Trefoil factor-3 expression in human colon cancer liver metastasis. Clin Exp Metastasis. 2009;26(2):143-51.
253. Panarelli NC, Yantiss RK, Yeh MM, Liu Y, Chen YT. Tissue-specific cadherin CDH17 is a useful marker of gastrointestinal adenocarcinomas with higher sensitivity than CDX2. Am J Clin Pathol. 2012;138(2):211-22.
254. Su MC, Yuan RH, Lin CY, Jeng YM. Cadherin-17 is a useful diagnostic marker for adenocarcinomas of the digestive system. Mod Pathol. 2008;21(11):1379-86.
255. Baptistella AR, Salles Dias MV, Aguiar S, Jr., Begnami MD, Martins VR. Heterogeneous expression of A33 in colorectal cancer: possible explanation for A33 antibody treatment failure. Anticancer Drugs. 2016;27(8):734-7.
256. Wong N, Adamczyk LA, Evans S, Cullen J, Oniscu A, Oien KA. A33 shows similar sensitivity to but is more specific than CDX2 as an immunomarker of colorectal carcinoma. Histopathology. 2017;71(1):34-41.
257. Garinchesa P, Sakamoto J, Welt S, Real F, Rettig W, Old L. Organ-specific expression of the colon cancer antigen A33, a cell surface target for antibody-based therapy. Int J Oncol. 1996;9(3):465-71.
258. Welt S, Divgi CR, Real FX, Yeh SD, Garin-Chesa P, Finstad CL, et al. Quantitative analysis of antibody localization in human metastatic colon cancer: a phase I study of monoclonal antibody A33. J Clin Oncol. 1990;8(11):1894-906.
259. Yeung TM, Gandhi SC, Wilding JL, Muschel R, Bodmer WF. Cancer stem cells from colorectal cancer-derived cell lines. Proc Natl Acad Sci U S A. 2010;107(8):3722-7.
260. Ashley N, Yeung TM, Bodmer WF. Stem cell differentiation and lumen formation in colorectal cancer cell lines and primary tumors. Cancer Res. 2013;73(18):5798-809.
261. Sabates-Bellver J, Van der Flier LG, de Palo M, Cattaneo E, Maake C, Rehrauer H, et al. Transcriptome profile of human colorectal adenomas. Mol Cancer Res. 2007;5(12):1263-75.
262. Sheffer M, Bacolod MD, Zuk O, Giardina SF, Pincas H, Barany F, et al. Association of survival and disease progression with chromosomal instability: a genomic exploration of colorectal cancer. Proc Natl Acad Sci U S A. 2009;106(17):7131-6.

263. Heiskanen M. caArray_notte-00422: Molecular Dissection of Colon Cancer 2015 [Available from: https://www.ncbi.nlm.nih.gov/geo/query/acc.cgi?acc=GSE68468.
264. Nishihara R, Wu K, Lochhead P, Morikawa T, Liao X, Qian ZR, et al. Long-term colorectal-cancer incidence and mortality after lower endoscopy. N Engl J Med. 2013;369(12):1095-105.
265. Hartmans E, Tjalma JJJ, Linssen MD, Allende PBG, Koller M, Jorritsma-Smit A, et al. Potential Red-Flag Identification of Colorectal Adenomas with Wide-Field Fluorescence Molecular Endoscopy. Theranostics. 2018;8(6):1458-67.
266. Rath T, Kiesslich R, Neurath MF, Atreya R. Molecular imaging within the lower gastrointestinal tract: From feasibility to future. Dig Endosc. 2018.
267. Joshi BP, Dai Z, Gao Z, Lee JH, Ghimire N, Chen J, et al. Detection of Sessile Serrated Adenomas in the Proximal Colon Using Wide-Field Fluorescence Endoscopy. Gastroenterology. 2017;152(5):1002-13 e9.
268. Endlicher E, Gelbmann CM, Knuchel R, Furst A, Szeimies RM, Golder SK, et al. Hexaminolevulinate-induced fluorescence endoscopy in patients with rectal adenoma and cancer: a pilot study. Gastrointest Endosc. 2004;60(3):449-54.
269. Williams BB, Tebbutt NC, Buchert M, Putoczki TL, Doggett K, Bao S, et al. Glycoprotein A33 deficiency: a new mouse model of impaired intestinal epithelial barrier function and inflammatory disease. Dis Model Mech. 2015;8(8):805-15.
270. Welt S, Divgi CR, Kemeny N, Finn RD, Scott AM, Graham M, et al. Phase I/II study of iodine 131-labeled monoclonal antibody A33 in patients with advanced colon cancer. J Clin Oncol. 1994;12(8):1561-71.
271. Welt S, Scott AM, Divgi CR, Kemeny NE, Finn RD, Daghighian F, et al. Phase I/II study of iodine 125-labeled monoclonal antibody A33 in patients with advanced colon cancer. J Clin Oncol. 1996;14(6):1787-97.
272. Bendell JC, Lenz HJ, Ryan T, El-Rayes BF, Marshall JL, Modiano MR, et al. Phase 1/2 study of KRN330, a fully human anti-A33 monoclonal antibody, plus irinotecan as second-line treatment for patients with metastatic colorectal cancer. Invest New Drugs. 2014;32(4):682-90.
273. Diao S, Blackburn JL, Hong GS, Antaris AL, Chang JL, Wu JZ, et al. Fluorescence Imaging In Vivo at Wavelengths beyond 1500 nm. Angewandte Chemie-International Edition. 2015;54(49):14758-62.
274. Ding F, Chen S, Zhang W, Tu Y, Sun Y. UPAR targeted molecular imaging of cancers with small molecule-based probes. Bioorg Med Chem. 2017;25(20):5179-84.

275. Smith AM, Mancini MC, Nie SM. BIOIMAGING Second window for in vivo imaging. Nature Nanotechnology. 2009;4(11):710-1.
276. Hong GS, Lee JC, Robinson JT, Raaz U, Xie LM, Huang NF, et al. Multifunctional in vivo vascular imaging using near-infrared II fluorescence. Nat Med. 2012;18(12):1841-+.
277. Zhang XD, Wang HS, Antaris A, Li LL, Diao S, Ma R, et al. In Vivo Vascular Imaging of Traumatic Brain Injury in the Second near-Infrared Window. J Neurotrauma. 2016;33(13):A48-A.
278. Ding F, Zhan Y, Lu X, Sun Y. Recent advances in near-infrared II fluorophores for multifunctional biomedical imaging. Chem Sci. 2018;9(19):4370-80.
279. Liu Y, Bauer AQ, Akers WJ, Sudlow G, Liang K, Shen D, et al. Hands-free, wireless goggles for near-infrared fluorescence and real-time image-guided surgery. Surgery. 2011;149(5):689-98.

APPENDIX 1: ADVERSE EVENTS FOR IRDYE 800BK

AE No	Onset	Days post IMP	End	SAE Classification	Brief Description	Severity	Relationship
IRU-CRR-01_1	16/04/18	5	25/05/18	N/A	Deranged liver function tests.	Mild	Unrelated
IRU-CRR-01_2	15/04/18	4	08/05/18	N/A	Increased stoma output	Mild	Unrelated
IRU-CRR-02_1	24/04/18	0	24/04/18	Medically Important Event	Difficulty ventilating after intubation (before IMP administration)	Severe	Unrelated
IRU-CRR-02_2	25/04/18	1	26/04/18	N/A	Rash on face and arms resolved with antihistamine	Mild	Possibly Related
IRU-CRR-02_3	27/04/18	3	27/05/18	N/A	Post-operative ileus	Moderate	Unrelated
IRU-CRR-03_1	24/04/18	1	26/04/18	N/A	Nausea, vomiting and abdominal pain	Mild	Unrelated
IRU-CRR-05_1	30/04/18	0	05/01/18	N/A	Drowsy and poor respiratory effort post-operatively with CO2 retention. Thought to be due to opioid overdose	Moderate	Unrelated
IRU-CRR-05_3	06/05/18	6	24/05/18	N/A	Deranged liver function tests.	Mild	Possibly Related
IRU-CRR-06_1	26/05/18	1	18/06/18	N/A	Abdominal pain	Mild	Unrelated
IRU-CRR-07_1	20/05/18	2	23/05/18	N/A	Post-operative ileus	Mild	Unrelated
IRU-CRR-07_3	18/06/18	31		N/A	Abdominal pain & dysuria.	Mild	Unrelated
IRU-CRR-07_4	24/05/18	6	19/09/18	N/A	Deranged liver function tests.		Possibly Related
IRU-CRR-08_1	22/05/18	1		N/A	Odorous urine	Mild	Possibly Related
IRU-CRR-09_1	11/06/18	0	11/06/18	N/A	Blood pressure drop following IMP administration but at same time as pneumoperitoneum	Mild	Unrelated

AE No	Onset	Days post IMP	End	SAE Classification	Brief Description	Severity	Relationship
IRU-CRR-09_2	12/06/18	1	22/06/18	N/A	Abdominal pain	Mild	Unrelated
IRU-CRR-10_1	09/06/18	5		N/A	Right sided hip pain	Mild	Unrelated
IRU-CRR-11_1	06/06/18	1	06/06/18	N/A	Spike temperature to 38.2 degrees	Mild	Unrelated
IRU-CRR-11_2	07/06/18	2	19/06/18	N/A	Vomiting	Mild	Possibly Related
IRU-CRR-12_1	04/07/18	8		N/A	Dysuria, urgency and reduced urinary frequency. Testicular pain. Abdominal pain.	Mild	Unrelated
IRU-CRR-13_1	13/06/18	5	03/09/18	N/A	Deranged liver function tests.	Mild	Possibly Related
IRU-CRR-14_1	30/06/18	1	01/07/18	N/A	Post-operative delirium. History of post-operative delirium. Resolved on ceasing opioids.	Mild	Unrelated
IRU-CRR-14_2	05/07/18	6		N/A	Abdominal pain		Unrelated
IRU-CRR-14_3	27/07/18	28	05/06/18	N/A	Altered urine colour	Mild	Possibly Related
IRU-CRR-15_1	05/07/18	15		N/A	Abdominal pain	Mild	Unrelated
IRU-CRR-16_1	24/06/18	6		N/A	Abdominal pain, dysuria and frequency.	Mild	Unrelated
IRU-CRR-18_1	07/07/18	5	10/08/18	N/A	Deranged liver function tests.	Mild	Possibly Related
IRU-CRR-20_1	04/07/18	0	04/07/18	Life Threatening	Respiratory arrest following extubation. Re-intubated and further successful extubation.	Severe	Unrelated
IRU-CRR-21_1	07/08/18	1	08/08/18	N/A	PR bleeding	Moderate	Unrelated

AE No	Onset	Days post IMP	End	SAE Classification	Brief Description	Severity	Relationship
IRU-CRR-21_2	09/08/18	3	12/08/18	Subject Died	PR bleed, anastomotic leak, return to theatre and take down of anastomosis, post-operative sepsis secondary to extensive peristomal necrotising fasciitis extending across back and buttock, not appropriate for surgical intervention.	Severe	Unrelated
IRU-CRR-27_1	30/07/18	5	19/09/18	N/A	Urinary frequency and urgency.	Mild	Unrelated
IRU-CRR-29_1	03/09/18	5		N/A	Dysuria.	Mild	Unrelated
IRU-CRR-32_1	04/09/18	7		N/A	Abdominal pain	Mild	Unrelated
IRU-CRR-37_1	14/08/18	1		N/A	Back and hip pain. Dysuria and perianal pain on defaecation.	Mild	Unrelated
IRU-CRR-40_1	24/08/18	4	29/08/18	N/A	PR mucus and dysuria	Mild	Unrelated
IRU-CRR-41_1	18/09/18	28		N/A	Urinary tract infection	Mild	Unrelated